Biogeosciences, 19, 3537–3557, 2022
https://doi.org/10.5194/bg-19-3537-2022

Biogeosciences Open Access EGU

Ocean alkalinity enhancement – avoiding runaway $CaCO_3$ precipitation during quick and hydrated lime dissolution

Charly A. Moras[1], Lennart T. Bach[2], Tyler Cyronak[3], Renaud Joannes-Boyau[1], and Kai G. Schulz[1]

[1]Faculty of Science and Engineering, Southern Cross University, Lismore, NSW, Australia
[2]Ecology & Biodiversity, Institute for Marine and Antarctic Studies, University of Tasmania, Hobart, TAS, Australia
[3]Department of Marine and Environmental Sciences, Nova Southeastern University, Fort Lauderdale, FL, USA

Correspondence: Charly A. Moras (c.moras.10@student.scu.edu.au)

Received: 8 December 2021 – Discussion started: 10 December 2021
Revised: 19 June 2022 – Accepted: 26 June – Published: 1 August 2022

Abstract. Ocean alkalinity enhancement (OAE) is a method that can remove carbon dioxide (CO_2) from the atmosphere and counteract ocean acidification through the dissolution of alkaline minerals. Currently, critical knowledge gaps exist regarding the dissolution of different minerals suitable for OAE in natural seawater. Of particular importance is to understand how much alkaline mineral can be dissolved before secondary precipitation of calcium carbonate ($CaCO_3$) occurs, since secondary $CaCO_3$ precipitation reduces the atmospheric CO_2 uptake potential of OAE. Using two types of mineral proposed for OAE, quick lime (CaO) and hydrated lime ($Ca(OH)_2$), we show that both (<63 µm of diameter) dissolved in seawater within a few hours. No $CaCO_3$ precipitation occurred at a saturation state (Ω_A) of ∼ 5, but $CaCO_3$ precipitation in the form of aragonite occurred above an Ω_A value of 7. This limit is lower than expected for typical pseudo-homogeneous precipitation, i.e. in the presence of colloids and organic matter. Secondary precipitation at low Ω_A (∼ 7) was the result of heterogeneous precipitation onto mineral surfaces, most likely onto the added CaO and $Ca(OH)_2$ particles. Most importantly, runaway $CaCO_3$ precipitation was observed, a condition where significantly more total alkalinity (TA) was removed than initially added. Such runaway precipitation could reduce the OAE CO_2 uptake efficiency from ∼ 0.8 mol of CO_2 per mole of added TA down to 0.1 mol of CO_2 per mole of TA. Runaway precipitation appears to be avoidable by dilution below the critical Ω_A threshold of 5, ideally within hours of the mineral additions to minimise initial $CaCO_3$ precipitation. Finally, OAE simulations suggest that for the same Ω_A threshold, the amount of TA that can be added to seawater would be more than 3 times higher at 5 °C than at 30 °C. The maximum TA addition could also be increased by equilibrating the seawater to atmospheric CO_2 levels (i.e. to a pCO_2 of ∼ 416 µatm) during addition. This would allow for more TA to be added in seawater without inducing $CaCO_3$ precipitation, using OAE at its CO_2 removal potential.

1 Introduction

Modern climate change is considered one of the greatest threats to humankind (Hoegh-Guldberg et al., 2019; IPCC, 2021; The Royal Society and Royal Academy of Engineering, 2018). Global mean temperature has increased by 1.0 °C since pre-industrial times and could reach +1.2–1.9 °C in the next 20 years and +2.1–5.7 °C by the end of this century (IPCC, 2021). Furthermore, about 26 % of all anthropogenic carbon dioxide (CO_2) emissions were taken up by the ocean through air–sea gas exchange between 1750 and 2020 (Friedlingstein et al., 2022). This has led to a decrease in the average open-ocean pH by 0.1 units in a process termed ocean acidification – OA (Bates et al., 2012; Canadell et al., 2007; Carter et al., 2019; Cyronak et al., 2014; Doney et al., 2009; Hoegh-Guldberg et al., 2007).

The aim of the 2015 Paris Agreement is to minimise the negative impacts of global warming and OA by limiting global warming to less than +2.0 °C, ideally below +1.5 °C, by the end of this century (Goodwin et al., 2018). However, the current and pledged reductions will likely not be enough, and additional CO_2 mitigation strategies are needed, such as ocean alkalinity enhancement – OAE (Gattuso et

al., 2015; GESAMP, 2019; Lenton and Vaughan, 2009; The Royal Society and Royal Academy of Engineering, 2018). OAE could be an efficient approach for CO_2 removal (current emissions of 40 Gt yr^{-1}), with models suggesting a potential of 165 to 790 Gt (1 Gt = 10^{15} g) of atmospheric CO_2 removed by the year 2100 on a global scale if OAE were implemented today (Burt et al., 2021; Feng et al., 2017; IPCC, 2021; Keller et al., 2014; Köhler et al., 2013; Lenton et al., 2018). However, empirical data on OAE efficacies are limited, and safe thresholds for mineral dissolution are particularly lacking (National Academies of Sciences and Medicine, 2022).

OAE typically relies on the dissolution of alkaline minerals in seawater, releasing alkalinity similarly to natural rock-weathering processes (Kheshgi, 1995). Suitable candidates are magnesium-rich minerals such as brucite, periclase or forsterite and calcium-rich minerals such as quick and hydrated lime (Renforth and Henderson, 2017). Quick lime and hydrated lime are of particular interest due to their high solubility in seawater and rapid dissolution. Quick lime, i.e. calcium oxide (CaO), is obtained by the calcination of limestone, composed primarily of calcium carbonate ($CaCO_3$), which is present in large quantities within the earth's crust. Once heated to temperatures of $\sim 1200\,^{\circ}C$, each molecule of $CaCO_3$ breaks down into one molecule of CaO and one molecule of CO_2 (Ilyina et al., 2013; Kheshgi, 1995). Hence, for maximum OAE potential, carbon capture during calcination and subsequent storage would be necessary (Bach et al., 2019; Ilyina et al., 2013; Kheshgi, 1995; Renforth et al., 2013; Renforth and Kruger, 2013). CaO can be hydrated into calcium hydroxide ($Ca(OH)_2$), also known as hydrated lime. The addition of either CaO or $Ca(OH)_2$ to seawater leads to the dissociation of $Ca(OH)_2$ into one calcium Ca^{2+} and two hydroxyl ions OH^- (Feng et al., 2017; Harvey, 2008). Ignoring the non-linearities of the seawater carbonate system (i.e. changes in total alkalinity, TA, and dissolved inorganic carbon, DIC, are not 1 : 1), the chemical reaction of CO_2 and $Ca(OH)_2$ dissolution and the subsequent uptake of atmospheric CO_2 can be written as

$$(CaO + H_2O \rightleftharpoons Ca(OH)_2) + 2CO_2 \rightarrow Ca^{2+} + 2HCO_3^-. \quad (1)$$

The dissolution of CaO and $Ca(OH)_2$ and the subsequent addition of TA increase the pH of seawater, which changes the carbonate chemistry speciation (Zeebe and Wolf-Gladrow, 2001). DIC can be approximated as the sum of HCO_3^- and CO_3^{2-} (ignoring the small contribution by CO_2). Similarly, TA can be approximated as the sum of HCO_3^- and 2 CO_3^{2-} (ignoring the smaller contributions by boric and silicic acids and other minor components). Combining both DIC and TA equations reveals that CO_3^{2-} concentrations can be expressed as $[CO_3^{2-}] = TA - DIC$. Hence, increasing TA at a constant DIC, e.g. by dissolving CaO or $Ca(OH)_2$, increases $[CO_3^{2-}]$, shifting the carbonate chemistry speciation towards a higher pH (Fig. A1) (Dickson et al., 2007; Wolf-Gladrow et al., 2007; Zeebe and Wolf-Gladrow, 2001). The subsequent shift in DIC speciation leads to a decrease in dissolved CO_2 concentrations, reducing the partial pressure of CO_2 (pCO_2) in seawater and increasing its atmospheric CO_2 uptake potential.

Depending on the amount of TA added and the initial seawater pCO_2, the TA-enriched seawater would either take up CO_2 from the atmosphere or reduce outgassing of CO_2. Factoring in the non-linearities of the carbonate system, about 1.6 mol of atmospheric CO_2 could be taken up per mole of dissolved CaO or $Ca(OH)_2$ (Köhler et al., 2010). Furthermore, dissolving CaO and $Ca(OH)_2$ can also counteract ocean acidification. During the dissolution of alkaline minerals, both pH and the $CaCO_3$ saturation state of seawater (Ω) increase through increasing Ca^{2+} and CO_3^{2-} concentrations. This makes OAE a dual solution for removing atmospheric CO_2 and mitigating OA (Feng et al., 2017; GESAMP, 2019; Harvey, 2008). However, there are important knowledge gaps in our understanding surrounding basic mineral dissolution in seawater (Feng et al., 2016; González and Ilyina, 2016; Mongin et al., 2021; Renforth and Henderson, 2017).

One knowledge gap is the critical Ω threshold beyond which $CaCO_3$ starts to precipitate inorganically. Such secondary precipitation constitutes the opposite of alkaline mineral dissolution and would decrease pH and Ω while simultaneously increasing the CO_2 concentration in seawater. This would decrease the ocean uptake's capacity for atmospheric CO_2, causing the opposite of the intended effect. Additionally, if all added alkalinity were precipitated, only 1 mol of atmospheric CO_2 per mole of Ca^{2+} would be removed, instead of ~ 1.6 mol in the absence of $CaCO_3$ precipitation. If even more $CaCO_3$ precipitated, the efficiency of OAE would be further reduced. Under typical seawater conditions, $CaCO_3$ precipitation does not occur due to the absence of mineral-phase precipitation nuclei and the presence of precipitation inhibitors such as dissolved organic compounds, magnesium (Mg) or phosphate (Chave and Suess, 1970; De Choudens-Sanchez and Gonzalez, 2009; Pytkowicz, 1965; Rushdi et al., 1992; Simkiss, 1964). There are three types of $CaCO_3$ precipitation, (1) homogeneous (in the absence of any precipitation nuclei), (2) heterogeneous (in the presence of mineral phases) and (3) pseudo-homogeneous (in the presence of colloids and organic materials) (Marion et al., 2009; Morse and He, 1993). For pseudo-homogeneous precipitation, the critical threshold at which calcite precipitates spontaneously is at a calcite saturation state (Ω_C) of ~ 18.8 (at a salinity of 35 and at a temperature of 21 °C) (Marion et al., 2009). Assuming typical open-ocean carbonate chemistry (e.g. TA $\sim 2350\,\mu mol\,kg^{-1}$ and DIC $\sim 2100\,\mu mol\,kg^{-1}$), this threshold would be reached through an increase in TA of $\sim 810\,\mu mol\,kg^{-1}$. This corresponds to a critical threshold for Ω with respect to aragonite, i.e. Ω_A, of ~ 12.3. The two other types of precipitation (i.e. homogeneous and heterogeneous) are more poorly constrained (Marion et al., 2009). Importantly, at current dissolved Mg and Ca concentrations

in seawater, the $CaCO_3$ polymorph that is favoured during inorganic precipitation is aragonite rather than calcite (Morse et al., 1997; Pan et al., 2021). Therefore, aragonite saturation state Ω_A may be a more important determinant of critical runaway precipitation thresholds. No matter what mineral phase is precipitating, a better understanding of $CaCO_3$ precipitation under conditions relevant to OAE is needed.

To gain a better understanding of the consequences of CaO and $Ca(OH)_2$ dissolution for OAE, we conducted several dissolution experiments with CaO and $Ca(OH)_2$ to determine (1) how much alkaline material can be dissolved without inducing $CaCO_3$ precipitation, (2) what causes secondary $CaCO_3$ precipitation and (3) how secondary precipitation can be avoided.

2 Material and methods

2.1 Experimental setup

Two different calcium minerals were used, CaO powder from Ajax Finechem (CAS no. 1305-78-8) and industrial $Ca(OH)_2$ powder (hydrated lime 20 kg, Dingo). The elemental compositions of these powders were analysed using an Agilent 7700 inductively coupled plasma mass spectrometer (ICP-MS), coupled to a laser ablation unit (NWR213, Electro Scientific Industries, Inc). Samples were embedded in resin and instrument readings calibrated against standard reference materials, batch nos. 610 and 612, from the National Institute of Standards and Technology.

All dissolution experiments were conducted in natural seawater. The seawater was collected between September 2020 and June 2021, about 200 to 300 m from the shore, avoiding suspended sand or silt, at Broken Head, New South Wales, Australia (28°42′12″ S, 153°37′03″ E). Seawater was stored for up to 14 d at 4 °C in the dark to slow bacterial metabolic activity and allow for all suspended particles to settle on the bottom before being sterile-filtered using a peristaltic pump, connected to a 0.2 µm Whatman Polycap 75 AS filter. For salinity measurements, about 200 mL of seawater was placed in a gas-tight polycarbonate container and allowed to equilibrate to room temperature overnight. The sample's conductivity and temperature were then measured with a Metrohm cell (6.017.080), connected to a 914 pH/Conductometer. The conductivity was recorded in millisiemens per centimetre ($mS\,cm^{-1}$) and the temperature in degrees Celsius (°C). Salinity was calculated according to Lewis and Perkin (1981) on the 1978 practical salinity scale. The salinity in each experiment is reported in Table A1.

2.2 OAE experiments

For each experiment, seawater was accurately weighed (in grams to 2 decimal places) into high-quality 2 L borosilicate 3.3 Schott DURAN beakers, and the temperature was controlled via a Tank chiller line TK-1000 set at 21 °C, feeding a re-circulation water jacket (Fig. A2). A magnetic stir bar was placed in the beaker, and the natural seawater was constantly stirred at ∼ 200 rpm. To minimise gas exchange, a floating lid with various sampling ports was placed on top. Finally, after 1 h of equilibration, calculated quantities of weighed-in calcium alkaline compounds were added. Upon addition, samples for DIC and TA were taken at increasing time intervals to fully capture the dissolution kinetics and check for potential secondary precipitation. Furthermore, the pH was monitored at a frequency of 1 Hz for the first hour before alkalinity addition and over 4 h after addition to determine when alkalinity was fully released. Once the pH plateaued (corresponding to maximum TA release), the content of the beaker was carefully transferred to a clean Schott bottle to ensure that evaporation would not alter the DIC or TA concentrations. Bottles were kept in the dark for the duration of each experiment, i.e. up to 48 d, with the same constant stirring of ∼ 200 rpm at 21 °C. Each bottle was exposed to UV light for at least 30 min after each sampling to inhibit bacterial growth.

2.2.1 CaO and $Ca(OH)_2$ dissolution

Following the beaker setup as described in Sect. 2.2, TA was added by sieving CaO and $Ca(OH)_2$ through a 63 µm mesh to avoid the formation of larger CaO or $Ca(OH)_2$ aggregates. The mesh was placed in a clean 50 mL upside-down Falcon tube cap to minimise the loss of material smaller than 63 µm, and the overall weight was recorded in milligrams. Then, the mesh was placed above the Schott bottle, and the mineral was added by gently tapping the side of the sieve. Finally, the sieve was placed in the same upside-down Falcon tube cap and weighed once again, thereby making sure that the desired amount had been added to the beaker. The weighing steps were carefully performed to avoid material loss between the bottle and the balance and were achieved in less than 5 min. Two alkalinity additions, +250 and +500 $\mu mol\,kg^{-1}$ with each calcium mineral powder, were performed (Table 1).

2.2.2 Na_2CO_3 alkalinity, particles additions and filtration

Three further experiments assessed the role of mineral phases during secondary $CaCO_3$ precipitation observed in the previous experiments. The first experiment used a 1 M solution of sodium carbonate (Na_2CO_3, CAS number 497-19-8), freshly prepared on the day to limit CO_2 ingassing. Ultrapure Na_2CO_3 was accurately weighed (in mg with 2 decimal places) into a clean 100 mL Schott bottle and made up to 100 g with Milli-Q (18.2 MΩ). The solution was then sonicated for 15 min, with gentle mixing every 5 min. The amount of Na_2CO_3 to be added to seawater was calculated so that a similar maximum Ω_A would be reached, i.e. ∼ 7.7, as in the previous experiments with the highest addition of CaO and $Ca(OH)_2$. This required about twice

Table 1. Summary of experimental conditions. Please note that for comparability, more TA was added in the liquid than the sieved approaches to match the theoretical increases in calcium carbonate saturation state (see "Materials and methods" section for details).

TA agent	TA target ($\mu mol\,kg^{-1}$)	Comments	Amount added in mg (or mL*)	Amount of natural seawater in kg	mg kg^{-1} (or mL kg^{-1}*)	Theoretical TA addition ($\mu mol\,kg^{-1}$)	Recorded TA addition ($\mu mol\,kg^{-1}$)	Experiment duration	Additional samples apart from TA and DIC
Sieved calcium minerals experiments									
CaO	250	Sieved in	15.50	2.0159	7.69	274.21	216.49	47 d	n/a
CaO	500	Sieved in	30.60	2.0045	15.27	544.42	410.70	47 d	TPC, POC and SEM samples
$Ca(OH)_2$	250	Sieved in	19.90	2.0019	9.94	268.34	221.96	28 d	n/a
$Ca(OH)_2$	500	Sieved in	37.40	2.0042	18.66	503.73	440.19	42 d	TPC, POC and SEM samples
Na_2CO_3, particles and filtration experiments									
Na_2CO_3	1050	1 M Na_2CO_3 solution	1.05*	2.0006	0.52*	1050.32	1057.41	42 d	n/a
Na_2CO_3	1050	1 M Na_2CO_3 solution, plus quartz powder after 2 d	1.05*	2.0003	0.50*	1050.16	1073.92	48 d	TPC, POC and SEM samples
$Ca(OH)_2$	500	Sieved in, filtered after 4 h	39.30	2.0043	19.61	529.30	470.79	48 d	n/a
Dilution experiments									
$Ca(OH)_2$	500	1 : 1 dilution after 10 min, 1 h, 1 d and 1 week	101.60	5.1325	19.80	534.36	452.65	14 d	TPC, POC and SEM samples
$Ca(OH)_2$	2000	1 : 7 dilution after 10 min, 1 h, 1 d and 1 week	155.90	2.0038	77.80	2100.21	724.04	48 d	TPC, POC and SEM samples

n/a: not applicable.

the alkalinity increase as before (Table 1) because Na_2CO_3 additions concomitantly increase DIC when dissociating in two sodium ions and one CO_3^{2-} ion, making the Ω_A increase smaller. All carbonate chemistry calculations were performed in CO2SYS (see below).

In another experiment similar to the Na_2CO_3 addition, quartz powder was added after 2 d. Quartz powder was chosen as it does not dissolve on the timescales relevant for this study (Montserrat et al., 2017). The addition of quartz powder was similar to the sieved CaO and $Ca(OH)_2$ additions, i.e. through a 63 µm mesh. The mass of quartz particles added (in mg with 2 decimal places) was determined to provide the same mineral surface area as for the $Ca(OH)_2$ experiments with a TA increase of 500 $\mu mol\,kg^{-1}$. It was calculated using densities and masses of $Ca(OH)_2$ and quartz, assuming spherical particles with a diameter of 63 µm.

The third experiment followed the same experimental setup as described in Sect. 2.2.1. Here, $Ca(OH)_2$ was added to first increase TA by $\sim$ 500 $\mu mol\,kg^{-1}$ (Table 1). After 4 h of reaction, the entire content of the 2 L Schott beaker was filtered through a Nylon Captiva EconoFilter (25 mm) with a pore size of 0.45 µm into a clean 1 L Schott bottle using a peristaltic pump. The bottle was filled from bottom to top, with overflow to minimise gas exchange.

2.2.3 Dilution experiments

In a last set of experiments, alkalinity-enriched seawater was diluted with natural seawater to test if secondary precipitation could be avoided or stopped. $Ca(OH)_2$ powder was added to reach final alkalinity enrichments of 500 and 2000 $\mu mol\,kg^{-1}$, and dilutions were carried out at several time intervals.

For the experiment with a targeted TA increase of 500 $\mu mol\,kg^{-1}$, a larger quantity of TA-enriched seawater was required to perform all dilutions and sampling in comparison to the previous experiments. Therefore, two 5 L Schott bottles were filled with 5 kg of natural seawater and placed on a magnetic stirring platform. Calculated weighed-in masses of $Ca(OH)_2$ were added to the first bottle, as described in Sect. 2.2.1, using the 63 µm sieve, while the natural seawater in the second bottle was kept for subsequent dilutions. Both bottles were kept on the same bench under the same conditions, stirring at a rate of $\sim$ 200 rpm, for the duration of the experiment.

Following the $Ca(OH)_2$ addition, 1 : 1 dilutions (500 g TA-enriched seawater : 500 g natural seawater) were performed in clean 1 L Schott bottles that were kept in the dark and placed on a magnetic platform at a stirring rate of $\sim$ 200 rpm. After each sampling time, the bottles were exposed to UV light for at least 30 min. The second dilution experiment was

set up like the first one, the only difference being that the targeted TA increase was 2000 µmol kg^{-1}. The dilution ratio was 1 : 7 to reduce the targeted TA increase again to 250 µmol kg^{-1}. All dilutions were performed 10 min, 1 h, 1 d and 1 week after $Ca(OH)_2$ addition, leading to two TA-enriched and eight diluted treatments.

2.3 Carbonate chemistry measurements

Samples for TA and DIC measurements were filtered through a Nylon Captiva EconoFilter (0.45 µm) using a peristaltic pump into 100 mL borosilicate 3.3 Schott DURAN glass stopper bottles. The bottles were gently filled from the bottom to top, using a 14-gauge needle as described in Schulz et al. (2017), with at least half of their volume allowed to overflow, corresponding to ∼ 150 mL of seawater sampled per time point. After filling, 50 µL of saturated mercuric chloride solution was added to each sample before being stored without headspace in the dark at 4 °C.

TA was analysed in duplicate via potentiometric titrations by a Metrohm 848 Titrino plus coupled to an 869 Compact Sample Changer using 0.05 M HCl, with the ionic strength adjusted to 0.72 mol kg^{-1} using NaCl, corresponding to a salinity of 35. Titrations and calculations followed the open-cell titration protocols by Dickson et al. (2007). DIC was measured in triplicate using an Automated Infra-Red Inorganic Carbon Analyzer (AIRICA, Marianda) coupled to a LI-COR LI-7000 infra-red detector as described in Gafar and Schulz (2018). Measured values of TA and DIC were corrected using an internal standard prepared as described in Dickson (2010), calibrated against certified reference materials, batch nos. 175 and 190.

The overall instrument uncertainty for TA and DIC was calculated as follows. For each measurement, a standard deviation was calculated, from duplicates of TA and triplicates of DIC. The samples and reference material standard deviations were averaged, and an error propagation on these values were used to estimate average measurement uncertainty, i.e. ± 1.0 µmol kg^{-1} and DIC at ± 0.8 µmol kg^{-1}, for TA and DIC, respectively.

2.4 Particulate inorganic carbon and scanning electron microscopy (SEM)

In cases where TA and DIC decreases were observed, indicative of $CaCO_3$ precipitation, samples were taken at the end of the experiments for total particulate carbon (TPC), particulate organic carbon (POC) and scanning electron microscopy (SEM) analyses. TPC and POC samples were collected in duplicates on pre-combusted (450 °C) GF/F filters and stored frozen until analysis. Before analysis, POC filters were fumed with HCl for 2 h before drying overnight at 60 °C while TPC filters were dried untreated (Gafar and Schulz, 2018). The filters were wrapped in tin capsules and pressed into small 5 mm diameter balls. TPC and POC were quantified on a Thermo Fisher Flash Elemental Analyzer, coupled to a Delta V Plus isotope ratio mass spectrometer. Particulate inorganic carbon (PIC), or $CaCO_3$, was calculated based on the difference between TPC and POC. The results are reported in µmol kg^{-1} of seawater with an uncertainty estimate by an error propagation of the square root of the sum of the squared standard deviations for TPC and POC.

For SEM analysis, 10 to 15 mL of the sample water was collected on polycarbonate Whatman Cyclopore filters with a 0.2 µm pore size and rinsed with 50 mL of Milli-Q. The filters were dried at 60 °C overnight and kept in a desiccator until analysis on a tabletop Hitachi TM4000 Plus scanning electron microscope. The microscope was coupled to an energy-dispersive X-ray (EDX) analyser, allowing us to identify the $CaCO_3$ polymorph and elemental composition of precipitates. Finally, CaO and $Ca(OH)_2$ powders were analysed for their carbon content. This analysis aimed to identify the presence and estimate the amount of particulate carbon, most likely $CaCO_3$, in the respective mineral powders.

2.5 Carbonate chemistry calculations

Measured DIC, TA, temperature and salinity were used to calculate the remaining carbonate chemistry parameters with the CO2SYS script for MATLAB® (MathWorks) (Sharp et al., 2021). The borate-to-salinity relationship and boric acid dissociation constant from Uppstrom (1974) and the carbonic acid dissociation constants of Lueker et al. (2000) were used. With two measured carbonate chemistry parameters, i.e. DIC and TA, the others can be derived. An important difference in our experiments was that the dissolution of CaO and $Ca(OH)_2$ changed the calcium concentration, and hence the salinity-based Ω calculated by CO2SYS is underestimated. Ω is defined by the solubility product of $CaCO_3$ as

$$\Omega = \frac{\left[Ca^{2+}\right] \times \left[CO_3^{2-}\right]}{K_{sp}}, \tag{2}$$

where $[Ca^{2+}]$ and $[CO_3^{2-}]$ denote seawater concentrations of Ca^{2+} and CO_3^{2-} and K_{sp} is the solubility product for calcite or aragonite at the appropriate salinity and temperature. To calculate saturation states, the correct calcium concentration $[Ca^{2+}]_{Corr}$ was estimated from measured salinity (Riley and Tongudai, 1967) and half the alkalinity concentration change, ΔTA, generated during CaO or $Ca(OH)_2$ dissolution or loss due to $CaCO_3$ precipitation:

$$\left[Ca^{2+}\right]_{Corr} = \frac{0.01028}{35} \times \text{salinity} + \frac{\Delta TA}{2}, \tag{3}$$

where 0.01028 is the molar Ca^{2+} concentration at a salinity of 35. K_{sp} was calculated from in situ temperature and salinity according to Mucci (1983). The correct Ω_C and Ω_A were then calculated according to Eq. (2). Please note that we have opted to report Ω_A rather than Ω_C since aragonite

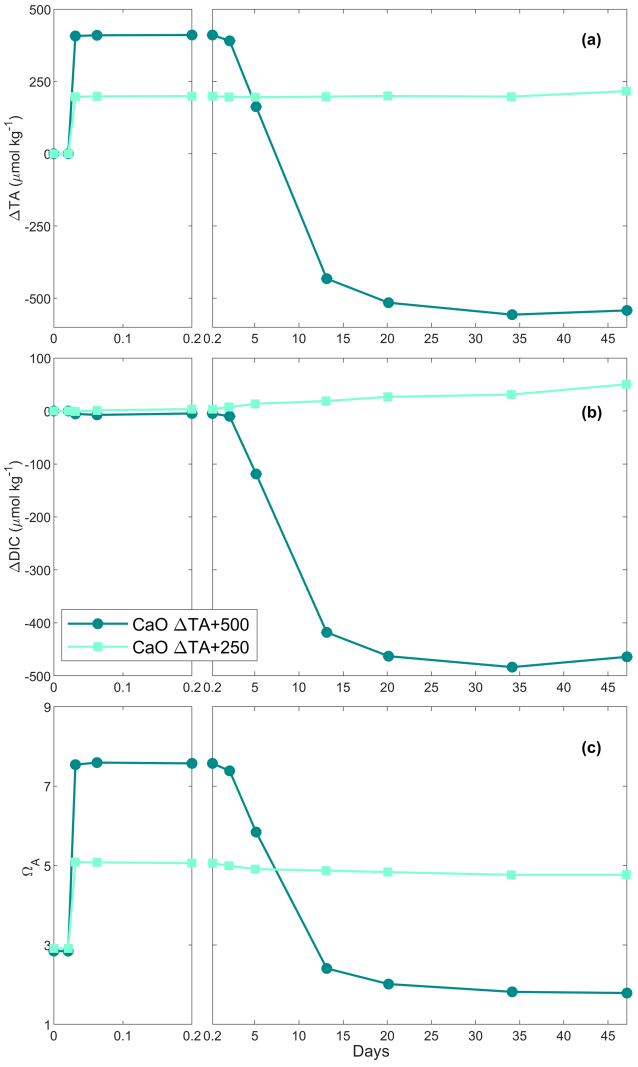

Figure 1. Changes in TA **(a)**, DIC **(b)** and Ω_A **(c)** over time following two CaO additions.

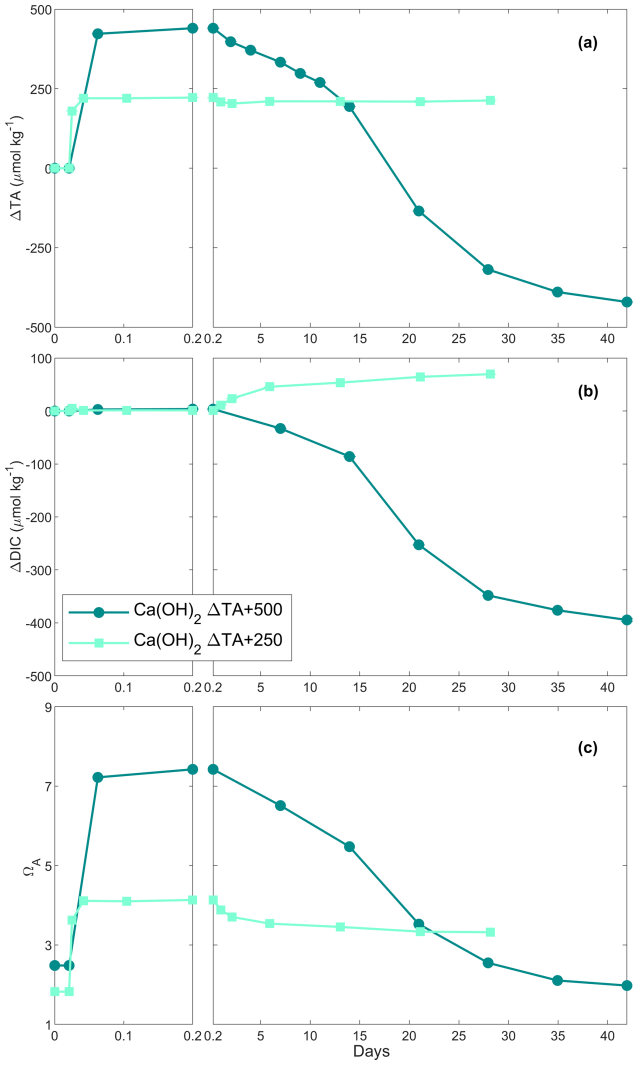

Figure 2. Changes in TA **(a)**, DIC **(b)** and Ω_A **(c)** of the samples over time following two $Ca(OH)_2$ additions.

is more likely to be precipitated in natural modern seawater (Morse et al., 1997).

2.6 OAE simulations

CO2SYS and the results from the various dissolution experiments were used to simulate three OAE scenarios (Table 3). Three alkalinity additions were simulated, +250, +500 and +1000 µmol kg^{-1}. The starting parameters were TA = 2350 µmol kg^{-1}, DIC = 2100 µmol kg^{-1}, salinity = 35 and temperature = 19 °C, using the same acid–base equilibrium constants as described in Sect. 2.5. In the first scenario, for all three additions, no $CaCO_3$ precipitation was assumed. We then estimated the amount of CO_2 taken up by the seawater after atmospheric re-equilibration, i.e. until a pCO_2 of ∼ 416 ppm. For the +500 and +1000 µmol kg^{-1} TA increases, two additional simulations were performed. First, we assumed that as much $CaCO_3$ precipitated as TA was added; e.g. after increasing the TA by 500 µmol kg^{-1}, we assumed a loss of 500 µmol kg^{-1} of TA and 250 µmol kg^{-1} of DIC. We then simulated atmospheric re-equilibration until a pCO_2 of ∼ 416 ppm and recorded the changes in the carbonate chemistry parameters. Second, we assumed that $CaCO_3$ precipitated down to an Ω_A of ∼ 2 as observed in our experiments. After calculating full carbonate chemistry speciation in these various scenarios, the amount of CO_2 taken up after atmospheric re-equilibration was determined using the same approach as described above.

3 Results

3.1 Chemical composition of CaO and $Ca(OH)_2$

The bulk chemical compositions of the CaO and $Ca(OH)_2$ powders were analysed. These consisted primarily of calcium, with minor contributions of magnesium and silicon (see Table A2 for a more comprehensive list). Furthermore, CaO and $Ca(OH)_2$ contained about 9.4 ± 0.1 and $18.0 \pm 0.2\,mg\,g^{-1}$ of particulate carbon, respectively, i.e. $\sim 0.9\,\%$ and $\sim 1.8\,\%$ by weight.

3.2 CaO dissolution in filtered natural seawater

In the first CaO experiment with a targeted $250\,\mu mol\,kg^{-1}$ TA addition, TA increased by $\sim 200\,\mu mol\,kg^{-1}$ within the first 4 h (Fig. 1a). Following this increase, TA was stable over time. In contrast, DIC increased slowly, at about $1\,\mu mol\,kg^{-1}\,d^{-1}$, reaching about $+50\,\mu mol\,kg^{-1}$ on day 47 of the experiment (Fig. 1b). Ω_A reflected the trend observed for ΔTA, increasing from ~ 2.9 to ~ 5.1 within the first 4 h before slowly decreasing to 5.0 on day 47 (Fig. 1c).

In the second CaO experiment with a targeted $500\,\mu mol\,kg^{-1}$ TA addition, TA increased by $\sim 410\,\mu mol\,kg^{-1}$ within the first 4 h before slowly decreasing on day 3 (Fig. 1a). This was followed by a rapid decrease over the following week, eventually reaching a steady state on day 20 at a final ΔTA of about $-540\,\mu mol\,kg^{-1}$. This corresponds to a total loss of TA of $\sim 950\,\mu mol\,kg^{-1}$, between the maximum measured TA and the final recorded TA. A small decrease in DIC of $\sim 10\,\mu mol\,kg^{-1}$ was observed over the first 2 d before a more significant reduction in the following week. Finally, ΔDIC levelled off at about $-465\,\mu mol\,kg^{-1}$ (Fig. 1b). Ω_A rapidly increased during the first 4 h of the experiment from 2.8 up to 7.6 (Fig. 1c). Following this quick increase, Ω_A decreased by 0.3 units by day 3. Afterwards, Ω_A dropped quickly to 2.4 on day 13, and reached ~ 1.8 on day 47, corresponding to a reduction of 1.0 compared to the starting seawater value.

3.3 $Ca(OH)_2$ dissolution in filtered natural seawater

In the first $Ca(OH)_2$ experiment with a targeted TA addition of $250\,\mu mol\,kg^{-1}$, TA increased by $\sim 220\,\mu mol\,kg^{-1}$ after 4 h of reaction, before stabilising at a ΔTA of $\sim 210\,\mu mol\,kg^{-1}$ for the rest of the experiment (Fig. 2a). The DIC concentration increased quickly over the first 6 d after the TA addition before slowing down, reaching about $+70\,\mu mol\,kg^{-1}$ by the end of the experiment (Fig. 2b). Finally, Ω_A reached ~ 4.1 after 4 h, slightly decreasing over time, reaching 3.3 on day 28 (Fig. 2c).

In the second $Ca(OH)_2$ experiment with a targeted TA addition of $500\,\mu mol\,kg^{-1}$, TA increased by $\sim 440\,\mu mol\,kg^{-1}$ within the first 4 h (Fig. 2a). This was followed by a steady decrease of $\sim 18\,\mu mol\,kg^{-1}\,d^{-1}$ over the next 2 weeks, after which the decrease accelerated to $\sim 28\,\mu mol\,kg^{-1}\,d^{-1}$ until day 35. Then, it levelled off at a ΔTA of about $-420\,\mu mol\,kg^{-1}$ towards the end of the experiment. Overall, $\sim 860\,\mu mol\,kg^{-1}$ of TA was lost compared to the highest TA recorded. The overall DIC concentration decreased in a similar fashion to TA, reaching a ΔDIC of about $-395\,\mu mol\,kg^{-1}$ compared to the initial DIC concentration (Fig. 2b). Ω_A increased from 2.5 to 7.4 in the first 4 h before decreasing, similarly to TA and DIC, reaching ~ 2.0 on day 42 (Fig. 2c).

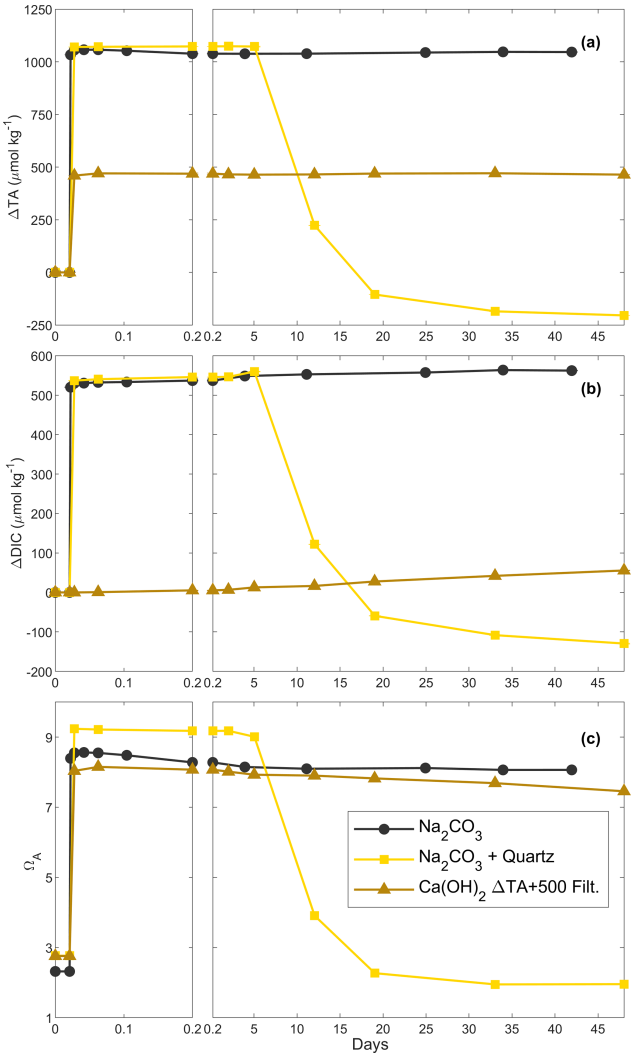

Figure 3. Changes in TA **(a)**, DIC **(b)** and Ω_A **(c)** over time following additions of Na_2CO_3, Na_2CO_3 plus quartz particles and $Ca(OH)_2$ followed by a filtration step (see "Material and methods" for details).

3.4 Na_2CO_3, particle addition and filtration

Three experiments assessed the influence of particles on $CaCO_3$ precipitation. In the first one, $\sim 1050\,\mu mol\,kg^{-1}$ of TA was added using a 1 M Na_2CO_3 solution, designed to obtain a similar maximum Ω_A to the previous experiments when TA decreased (Table 1). Upon addition, TA increased

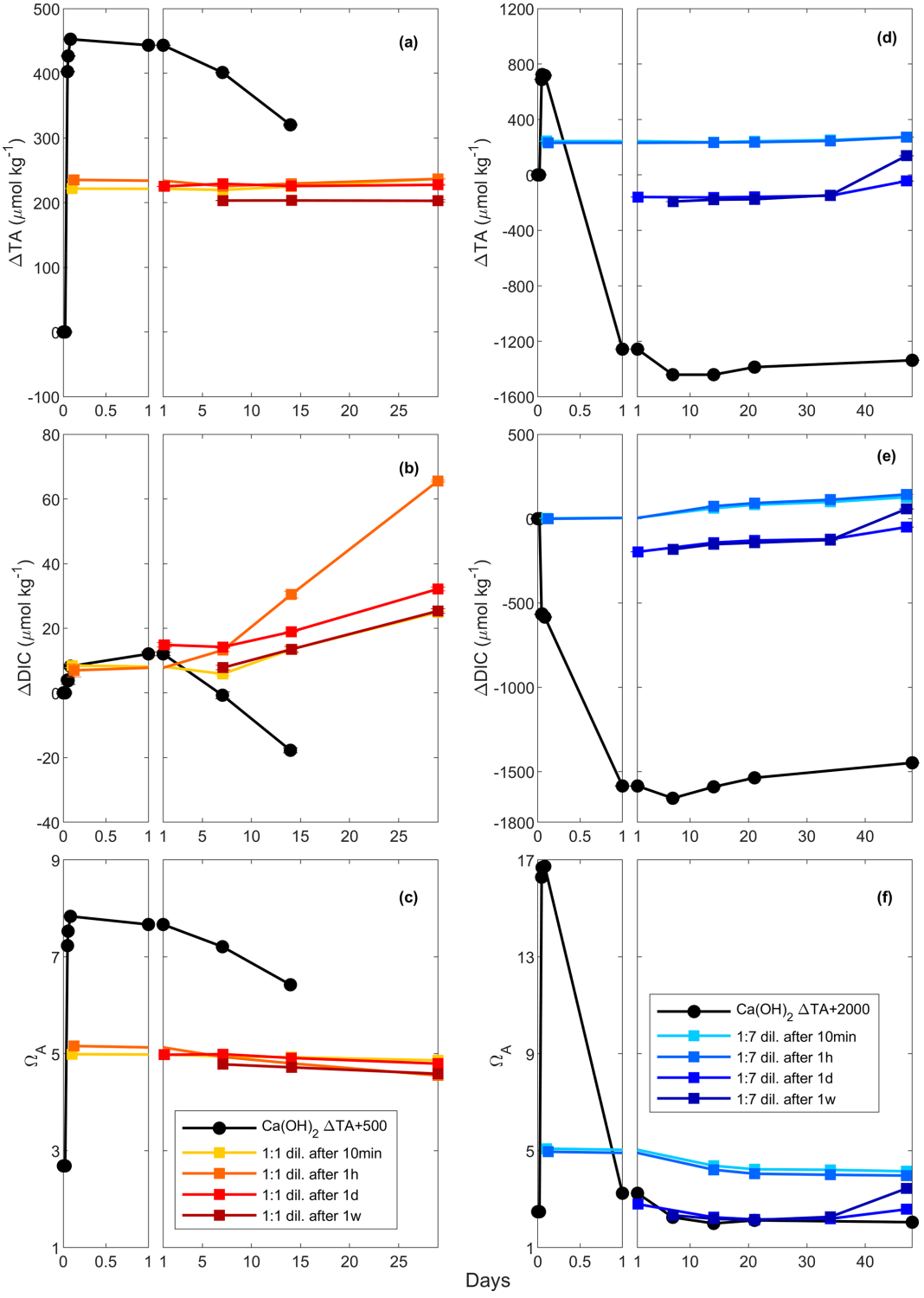

Figure 4. Changes in TA (**a** and **d**), DIC (**b** and **e**) and Ω_A (**c** and **f**) following a TA addition of 500 and 2000 µmol kg^{-1}, respectively, by $Ca(OH)_2$ (black line), as well as following a 1 : 1 dilution for the 500 µmol kg^{-1} TA addition (red and yellow lines) and a 1 : 7 dilution for the 2000 µmol kg^{-1} TA addition (blue lines). The dilutions were performed after 10 min, 1 h, 1 d and 1 week, and earlier dilutions are represented by lighter colours.

Table 2. Comparison between the estimated particulate inorganic carbon (PIC) based on half the TA change between the theoretical maximum TA increase upon full dissolution of the alkaline material added and the measured TA at the end of the experiment (Table 1), the estimated PIC based on half the TA changes between the measured maximum TA increase and the measured TA at the end of the experiment, and the measured PIC from the particulate carbon analysis.

Experiment	PICΔTA$_{\text{Theo}}$ (μmol kg^{-1})	PICΔTA (μmol kg^{-1})	Measured PIC (μmol kg^{-1})
500 TA–CaO	543.24	476.38	491.82 ± 39.18
500 TA–$Ca(OH)_2$	462.28	430.51	550.87 ± 71.32
1050 TA–1 M Na_2CO_3+ quartz particles	627.20	639.07	397.37 ± 24.03
500 TA–$Ca(OH)_2$ dilution	107.05	66.20	89.51 ± 4.27
2000 TA–$Ca(OH)_2$ dilution	1718.83	1030.74	1331.48 ± 50.73

by $\sim 1060\,\mu$mol kg^{-1} and DIC by $\sim 530\,\mu$mol kg^{-1} within minutes. For the remainder of the experiment, ΔTA was fairly constant between 1060 and 1040 μmol kg^{-1} (Fig. 3a). In contrast, DIC slightly increased over 42 d from a ΔDIC of $\sim 530\,\mu$mol kg^{-1} on day 1 to $\sim 560\,\mu$mol kg^{-1} on day 42 (Fig. 3b). Ω_A increased from ~ 2.3 to ~ 8.5 within minutes of the Na_2CO_3 addition and slightly decreased to ~ 8.1 after 42 d of the experiment (Fig. 3c).

In the second experiment, the addition of 1 M Na_2CO_3 solution (Table 1) increased TA by 1070 μmol kg^{-1}, while DIC increased by $\sim 540\,\mu$mol kg^{-1} within minutes and remained stable (Fig. 3a, b). After 2 d, quartz particles were added. Whereas ΔTA and ΔDIC remained invariant after 1 d, ΔTA decreased to $\sim 220\,\mu$mol kg^{-1} and ΔDIC dropped to $\sim 120\,\mu$mol kg^{-1} between day 5 and 12 (Fig. 3a, b). Over the next month, ΔTA and ΔDIC continued to decrease, although at a slowing rate, reaching about -200 and $-110\,\mu$mol kg^{-1}, respectively, on day 42. Ω_A followed a similar trend, with an increase from ~ 2.8 up to ~ 9.2 within the first 1.5 h and a significant decline to ~ 3.9 between day 5 and day 12, before stabilising at around ~ 2.0 at the end of the experiment on day 48.

In the last experiment, $Ca(OH)_2$ was added, aiming for a TA increase of 500 μmol kg^{-1} (Table 1), a level at which a significant TA decrease had been observed previously (Fig. 2a). In contrast to the previous experiment, after reaching $\sim 470\,\mu$mol kg^{-1} at the 4 h mark, the content of the bottle was filtered and ΔTA remained relatively constant between 465 and 470 μmol kg^{-1} over the following 48 d of the experiment (Fig. 3a). Meanwhile, ΔDIC increased from ~ 5 to 55 μmol kg^{-1} after filtration (Fig. 3b). Ω_A increased from ~ 2.8 to ~ 8.2 within the first 1.5 h after $Ca(OH)_2$ addition and then slightly decreased to ~ 7.5 over the 48 d of the experiment (Fig. 3c).

3.5 Dilution experiments

3.5.1 The 500 μmol kg^{-1} addition

In these experiments with a targeted TA increase of 500 μmol kg^{-1} by $Ca(OH)_2$ addition, ΔTA increased to $\sim 450\,\mu$mol kg^{-1} after 2 h (Fig. 4). These changes in TA were followed by a decline to $\sim 320\,\mu$mol kg^{-1} after 14 d, although the latter was a slightly slower decrease than previously (Figs. 2, 4a). After a first increase in ΔDIC by $\sim 10\,\mu$mol kg^{-1} on day 1, ΔDIC steadily decreased to about $-20\,\mu$mol kg^{-1} after 2 weeks (Fig. 4b). Finally, Ω_A increased from ~ 2.7 to ~ 7.8 after 2 h, before steadily decreasing to ~ 6.4 on day 14 (Fig. 4c).

In the diluted treatments, ΔTA remained relatively stable over time, until the end of the experiments on day 29, regardless of dilution time (Fig. 4a). Upon dilution, ΔTA was reduced, values of which were similar for the 10 min, 1 h and 1 d dilutions. Overall, in the 1-week dilution, ΔTA was slightly lower, i.e. $\sim 205\,\mu$mol kg^{-1} instead of $\sim 230\,\mu$mol kg^{-1} on average. In all dilutions, ΔDIC increased over time, ranging between ~ 20 and $\sim 60\,\mu$mol kg^{-1}, independently of dilution timing. Finally, Ω_A showed similar trends to ΔTA, reaching between ~ 4.8 and ~ 5.2 and slightly decreasing over time until the end of the experiment.

3.5.2 The 2000 μmol kg^{-1} addition

This set of experiments aimed for a TA increase of 2000 μmol kg^{-1} by $Ca(OH)_2$ addition. However, TA only increased to approximately one-third of the targeted value, i.e. $\sim 725\,\mu$mol kg^{-1} within the first 2 h (Fig. 4d). Following this increase, TA rapidly decreased during the first day, reaching a ΔTA of about -1260 and then $-1440\,\mu$mol kg^{-1} in the following week (Fig. 4d). Over the second week of the experiment, TA appeared to stabilise before increasing until day 21. In contrast, ΔDIC decreased by $\sim 580\,\mu$mol kg^{-1} within the first 2 h, before rapidly dropping to about $-1590\,\mu$mol kg^{-1} on day 1 and $-1660\,\mu$mol kg^{-1} after 7 d (Fig. 4e). Over the remaining 41 d, ΔDIC increased by $\sim 210\,\mu$mol kg^{-1}, remaining $\sim 1450\,\mu$mol kg^{-1} below the starting DIC concentration. Ω_A increased to ~ 16.7 after 2 h, followed by a rapid drop to ~ 3.2 on day 1 and ~ 2.0 on day 14 and slightly increasing over the following 34 d, varying between 2.0 and 2.1 (Fig. 4f).

With respect to ΔTA, ΔDIC and Ω_A, the 10 min and 1 h dilutions showed similar responses, as did the 1 d and 1-week dilutions. Upon dilution, ΔTA reached values of $\sim 240\,\mu mol\,kg^{-1}$ after the 10 min and 1 h dilutions and about -160 to $-190\,\mu mol\,kg^{-1}$ after the 1 d and 1-week dilutions. With the exception of one data point in the 1-week dilution data, ΔTA remained relatively constant throughout all dilution experiments (Fig. 4d). DIC changes were similar to the TA changes, slowly increasing over time between 0.6 and $2.5\,\mu mol\,kg^{-1}\,d^{-1}$, with very similar values reached for the 10 min and 1 h dilutions, as opposed to the 1 d and 1-week dilutions (Fig. 4e). Finally, Ω_A dropped from ~ 5.0–5.1 to ~ 4.0–4.1 over time in the 10 min and 1 h dilutions, while it decreased from ~ 2.3–2.8 to ~ 2.1–2.2 until day 21 in the 1 d and 1-week dilutions before increasing to ~ 2.6–3.4 towards the end of the experiments (Fig. 4f).

3.6 Particulate inorganic carbon

With the exception of the $\sim 1050\,\mu mol\,kg^{-1}$ TA addition by Na_2CO_3 and quartz particles, measured PIC in experiments was always higher than estimates from measured ΔTA (Table 2). Furthermore, PIC estimated from the theoretical maximum TA increase upon full mineral dissolution, ΔTA_{Theo}, was always higher than estimated PIC from ΔTA, by about 7 % to 14 % in the $\sim 500\,\mu mol\,kg^{-1}$ TA additions with $Ca(OH)_2$ and CaO, respectively, and up to 67 % in the experiment with $\sim 2000\,\mu mol\,kg^{-1}$ TA additions.

4 Discussion

This study presents the first results investigating the dissolution of CaO and $Ca(OH)_2$ in natural seawater in the context of OAE. In experiments with at least $500\,\mu mol\,kg^{-1}$ TA increase, secondary precipitation was detected through observed TA and DIC decreases, as well as PIC increases. More specifically, at TA additions leading to an Ω_A higher than 7 (in the +500 and $+1000\,\mu mol\,kg^{-1}$ TA treatments), "runaway $CaCO_3$ precipitation" was observed, meaning that not only was the added TA completely removed but significant portions of residual seawater TA were as well, until a new steady state was reached. This vastly reduces the desired CO_2 removal potential by OAE and should therefore be avoided. In a subsequent set of experiments, we simulated ocean mixing to estimate the timescales required to avoid and/or stop secondary $CaCO_3$ precipitation for applications that initially have TA additions above the critical threshold.

4.1 Identifying $CaCO_3$ precipitation, the problem of unmeasured precipitation, CO_2 gas exchange

$CaCO_3$ precipitation can occur via three pathways, i.e. heterogeneous, homogeneous and pseudo-homogeneous nucleation and precipitation (Chen et al., 2005; Marion et al., 2009; Wolf et al., 2008). Heterogeneous precipitation relies on the presence of existing solid mineral surfaces. This differs from homogeneous precipitation, characterised by the formation of $CaCO_3$ crystals from Ca^{2+} and CO_3^{2-} ions in the absence of any nucleation surfaces (Chen et al., 2005; Wolf et al., 2008). Finally, the last type of precipitation, termed pseudo-homogeneous, is similar to homogeneous nucleation, but it occurs on nuclei other than solid minerals such as colloids, organic particles or glassware in a laboratory setting (Marion et al., 2009). Concerning the Ω thresholds above which $CaCO_3$ precipitation is expected, the lowest threshold would be for heterogeneous and the highest for homogeneous, with pseudo-homogeneous nucleation in between. This is because nucleation sites effectively lower the activation energy required for $CaCO_3$ precipitation (Morse et al., 2007).

When 1 mol of $CaCO_3$ is precipitated, the TA of the solution decreases by 2 mol due to the removal of 1 mol of CO_3^{2-} ions, accounting for 2 mol of TA (Zeebe and Wolf-Gladrow, 2001). Simultaneously, the loss of 1 mol of CO_3^{2-} ions decreases the DIC concentration by 1 mol. Hence, any loss of TA and DIC following a 2 : 1 ratio can be linked to $CaCO_3$ precipitation (Zeebe and Wolf-Gladrow, 2001). Additionally, when $CaCO_3$ precipitation was suspected in our experiments, SEM and particulate inorganic carbon samples were taken to confirm the presence of $CaCO_3$ and to identify which polymorphs were predominant. In the $+250\,\mu mol\,kg^{-1}$ TA additions by CaO and $Ca(OH)_2$, both appeared to fully dissolve without inducing $CaCO_3$ precipitation as TA and Ω_A quickly increased within minutes, similarly to what has been described in the literature (Chave and Suess, 1970; Rushdi et al., 1992), until reaching their respective maxima after about a day and remaining stable over weeks (Figs. 1a and c, 2a and c). A slight increase in DIC was observed over time as expected since atmospheric CO_2 was absorbed from the bottle headspace, created when 150 to 200 mL of solution was withdrawn at each sampling point. The measured TA increase was slightly below the theoretically expected increase, which is assumed to be due to a combination of impurities present (in the case of CaO, a significant fraction could be hydrated) and any loss of the finely ground material during the process of weighing and sieving. On average, ~ 23 % of alkalinity added was not detected in the experiments with CaO and about 14 % for the experiments using $Ca(OH)_2$ (Table 1, Figs. 1 and 2).

In contrast, in the $+500\,\mu mol\,kg^{-1}$ TA additions by CaO and $Ca(OH)_2$, TA started decreasing after about 1 d following the observed initial increase. If this TA loss was through $CaCO_3$ precipitation, DIC should be reduced by half this amount. The measured TA and DIC losses were very close to this 2 : 1 ratio for both the CaO and the $Ca(OH)_2$ experiments with a TA addition of $500\,\mu mol\,kg^{-1}$ (950 : 465 and 860 : 395 for CaO and $Ca(OH)_2$, respectively). This suggests that TA precipitated in the form of $CaCO_3$. The slight offset can be explained by ingassing of CO_2 from the headspace which lowers the TA : DIC ratio, becoming visi-

ble only when precipitation ceases towards the end (Fig. 1b). Another caveat is that the maximum increase in TA from full dissolution of CaO or $Ca(OH)_2$ cannot be measured in the presence of concurrent $CaCO_3$ precipitation. This is mostly evident in the $+2000\,\mu mol\,kg^{-1}$ TA addition (Fig. 4), where DIC decreases due to $CaCO_3$ precipitation yet TA increases due to higher $Ca(OH)_2$ dissolution rates. This also explains why estimated PIC calculated from measured TA changes is generally smaller than measured PIC concentrations (Table 2). In the experiment with 1 M Na_2CO_3 and quartz particles, the measured TA-based PIC estimates were larger than the measured PIC. This difference is difficult to explain and could be possibly linked to the observed white layer on the bottle walls, indicative of $CaCO_3$ precipitation. In any case, while being a laboratory artefact, this has no practical consequences as in a natural setting the TA would eventually precipitate in the water column. In summary, trying to estimate $CaCO_3$ precipitation from measured changes in TA, without knowing how much TA was actually generated by full mineral dissolution or actual PIC measurements, might underestimate total precipitation.

4.2 The presence of mineral phases triggers runaway $CaCO_3$ precipitation

An important finding in our experiments was that whenever $CaCO_3$ precipitation was observed, it continued even if the solution dropped below an Ω_A of $\sim$4–5, levels at which no precipitation was observed in the $+250\,\mu mol\,kg^{-1}$ TA addition experiments. Furthermore, in all these experiments, precipitation decreased and seemingly ceased at an Ω_A of $\sim$1.8–2.0. Therefore, it appears that when $CaCO_3$ is initially precipitated, $CaCO_3$ continues to precipitate in a runaway fashion, even if Ω_A drops below levels where precipitation would not be initiated in natural seawater. This is to be expected as $CaCO_3$ precipitates onto $CaCO_3$ mineral surfaces at any saturation state above 1, and the initial precipitation at high-saturation states provides new nucleation sites (Morse et al., 2003, 2007; Zhong and Mucci, 1989). The precipitation rate is directly proportional to Ω, decreasing exponentially until reaching zero at an Ω value of 1 (Fig. A4). However, the question of why precipitation occurred at a much lower Ω than anticipated, i.e. $\Omega \sim 7.5$ vs. ~ 12.3, remains (Marion et al., 2009).

It is known that the presence of particles in suspension can initiate and accelerate $CaCO_3$ precipitation (Millero et al., 2001; Morse et al., 2003; Wurgaft et al., 2021). It is unlikely that the presence of $CaCO_3$ impurities in CaO (less than 1 % carbon) and $Ca(OH)_2$ (less than 2 % carbon) from imperfect calcination would have caused precipitation as the presence of $CaCO_3$ mineral phases should have caused precipitation at any saturation state above 1, i.e. also in the $+250\,\mu mol\,kg^{-1}$ TA addition experiments. Furthermore, modelling precipitation using experimentally determined Ω_A and surface-area-dependent aragonite precipitation rates onto $CaCO_3$ mineral phases (Zhong and Mucci, 1989) suggests that once precipitation becomes analytically detectable, it should proceed very rapidly before levelling off (Fig. A5). Furthermore, while we expected $CaCO_3$ precipitation to stop at $\Omega_A \sim 1$, we observed it to stop at $\Omega_A \sim 2$. The presence of dissolved organic carbon and soluble reactive phosphate could have slowed down if not stopped $CaCO_3$ precipitation at an Ω_A higher than 1 (Chave and Suess, 1970; Pan et al., 2021). We also observed that the bulk of precipitation occurred over a period of at least a week, after which an equilibration was reached with apparent differences between the different dissolving minerals (i.e. CaO, $Ca(OH)_2$ and quartz, although it is acknowledged that the experiments were not replicated).

Another explanation for $CaCO_3$ precipitation is heterogeneous precipitation on not-yet-dissolved CaO and $Ca(OH)_2$ particles (or other impurities), leading to $CaCO_3$ crystal formation and initiating runaway precipitation. The Ω_A threshold for this process would depend on lattice compatibility of the mineral phases (Tang et al., 2020). For instance, $CaCO_3$ precipitation has been observed at any saturation state above 1 when introducing $CaCO_3$ seed particles. In contrast, Lioliou et al. (2007) did not report $CaCO_3$ precipitation onto quartz particles at an Ω_A lower than 3.5, and in order to trigger $CaCO_3$ precipitation onto quartz particles, Ω_A would need to be further increased. Here, we observed $CaCO_3$ precipitation on quartz particles at an Ω_A of $\sim$9.2 (Fig. 3). The reason for initially slower but then more rapid precipitation could be a combination of exponentially increasing $CaCO_3$ surface area while increasing lattice compatibility (Lioliou et al., 2007; Pan et al., 2021). The filtration of TA-enriched seawater supports this idea since not-yet-dissolved mineral phases that could facilitate early nucleation were removed, preventing runaway $CaCO_3$ precipitation (Fig. 3).

Needle-shaped aragonite precipitation onto quartz particles (Fig. 5c and d) was observed by SEM imaging. EDX analyses identified the larger mineral to be rich in silicon, a key characteristic of quartz, and the needle-shaped particles were composed of carbon, oxygen and calcium, indicative of $CaCO_3$ (Chang et al., 2017; Ni and Ratner, 2008; Pan et al., 2021). In contrast, direct aragonite precipitation onto not-yet-dissolved CaO and $Ca(OH)_2$ in the $+500\,\mu mol\,kg^{-1}$ TA addition is difficult to prove as EDX analyses revealed the presence of Ca and O in both the mineral feedstocks and aragonite (Fig. 5a and b). Finally, in some situations (Fig. 5b), round crystals were also observed, suggesting the presence of vaterite (Chang et al., 2017). Nevertheless, aragonite crystals represented the majority of $CaCO_3$ observed by SEM.

4.3 Impacts of $CaCO_3$ precipitation on OAE potential

From an OAE perspective, $CaCO_3$ precipitation is an important chemical reaction that needs to be avoided. During $CaCO_3$ precipitation, dissolved $[CO_3^{2-}]$ and Ω decrease and $[CO_2]$ increases, which reduces the ocean's uptake capacity for atmospheric CO_2, hence impacting the OAE potential.

Table 3. Simulations of the changes in TA, DIC, Ω_A, pCO_2 and pH_T (total scale) after TA increases of 250, 500 and 1000 µmol kg^{-1}, assuming complete mineral dissolution without precipitation, a complete dissolution followed by as much $CaCO_3$ precipitated as the amount of TA added and a complete dissolution followed by $CaCO_3$ precipitation until reaching an Ω_A of 2.0, before CO_2 re-equilibration to initial pCO_2. For each scenario, the number of moles of CO_2 absorbed per mole of TA added has been calculated for comparison. The 500 µmol kg^{-1} TA addition simulation is shown in Fig. A3 in the Appendix.

			TA + 500 µmol kg^{-1}			TA + 1000 µmol kg^{-1}		
	Starting conditions (salinity = 35, 19 °C)	TA + 250 µmol kg^{-1} No $CaCO_3$ precipitation	No $CaCO_3$ Prec.	$CaCO_3$ Prec. = TA added	$CaCO_3$ Prec. until Ω_A of 2	No $CaCO_3$ Prec.	$CaCO_3$ Prec. = TA added	$CaCO_3$ Prec. until Ω_A of 2
TA (µmol kg^{-1})	2350	2600	2850	2350	1748	3350	2350	1320
DIC (µmol kg^{-1})	2100	2100	2100	1850	1549	2100	1600	1085
Ω_A	2.80	5.53	8.45	5.34	2.00	14.57	7.89	2.00
pCO_2 (µatm)	416.2	175.1	91.5	135.6	319.2	29.6	48.2	144.8
pH_T	8.04	8.38	8.61	8.42	8.02	8.97	8.73	8.20
After re-equilibration, i.e. pCO_2 ~416 µatm								
Final TA (µmol kg^{-1})	2350	2600	2850	2350	1748	3350	2350	1320
Final DIC (µmol kg^{-1})	2100	2309	2517	2100	1588	2927	2100	1216
Final Ω_A	2.80	3.34	3.90	2.80	1.66	5.14	2.80	1.00*
Final pH_T	8.04	8.08	8.11	8.04	7.93	8.17	8.04	7.82
CO_2 uptake (mol mol^{-1} TA)	n/a	0.84	0.83	0.50	0.08	0.83	0.50	0.13

* Note the value for Ω_A is rounded to 1.00 but calculated at 0.997. n/a: not applicable.

Considering typical open-ocean TA and DIC concentrations of 2350 and 2100 µmol kg^{-1}, respectively, at a salinity of 35 and a temperature of 19 °C, this water mass would have a pCO_2 close to atmospheric equilibrium of 416 µatm, a pH_T value (total scale) of 8.04 and an Ω_A of 2.80. Without $CaCO_3$ precipitation, an addition of 500 µmol kg^{-1} TA would lower pCO_2 to ~92 µatm while increasing pH_T and Ω_A to about 8.61 and 8.45, respectively. If fully re-equilibrated with the atmosphere, DIC would increase by about 420 µmol kg^{-1}, leading to a pH_T and Ω_A 0.07 and 1.10 higher, respectively, than prior to the addition (Table 3). The resulting OAE efficiency would be 0.83 mol of atmospheric CO_2 absorbed per mole of TA added, very similar to estimates by Köhler et al. (2010). Considering that $CaCO_3$ is the source material for CaO and $Ca(OH)_2$ and that 2 mol of TA is produced per mole of CaO or $Ca(OH)_2$ mineral dissolution, ~0.7 t of CO_2 could be captured per tonne of source material, assuming CO_2 capture during the calcination process. At a global scale, using all available ship capacity and assuming a slow discharge of 1.7 to 4.0 Gt of $Ca(OH)_2$ per year (Caserini et al., 2021), between 1.2 and 2.8 Gt of CO_2 per year could be absorbed by the ocean. Including direct coastal TA discharge at a constant addition of $Ca(OH)_2$ of 10 Gt yr^{-1} (Feng et al., 2016), we could expect to absorb an additional 7 Gt of CO_2 per year. To put these model-derived numbers into perspective, the global cement industry currently produces about 4.1 Gt of cement per year (Statista, 2021). Depending on whether hydraulic ($4CaO \cdot Al_2O_3 \cdot Fe_2O_3$) or non-hydraulic ($Ca(OH)_2$) cement is being produced and assuming a molar Ca^{2+}-to-CO_2 sequestration potential of 1.6, up to 3.9 Gt of atmospheric CO_2 could be captured per year. This is within the range required over the next 30 years to keep global warming below the 2 °C target, as in the Representative Concentration Pathway (RCP) 2.6 scenario (Huppmann et al., 2018).

The above numbers can only be achieved if CaO or $Ca(OH)_2$ dissolution is complete without $CaCO_3$ precipitation. Hypothetically, when as much $CaCO_3$ precipitates as TA is added, i.e. 100 µmol kg^{-1} of $CaCO_3$ precipitates after a TA increase of 100 µmol kg^{-1}, only 1 instead of 1.6 mol of DIC can be absorbed per 2 mol of TA, after equilibration with atmospheric pCO_2 (Table 3). This represents a decrease by nearly 40 % in OAE potential. Similarly, runaway $CaCO_3$ precipitation until an Ω_A of 2.0, as observed here, decreases the OAE potential further by almost 90 %. Consequently, only ~0.1 mol of DIC would be absorbed per mole of TA added (Table 3). Furthermore, secondary $CaCO_3$ precipitation higher than TA addition will lead to pH_T and Ω levels lower than the initial ones. For instance, runaway

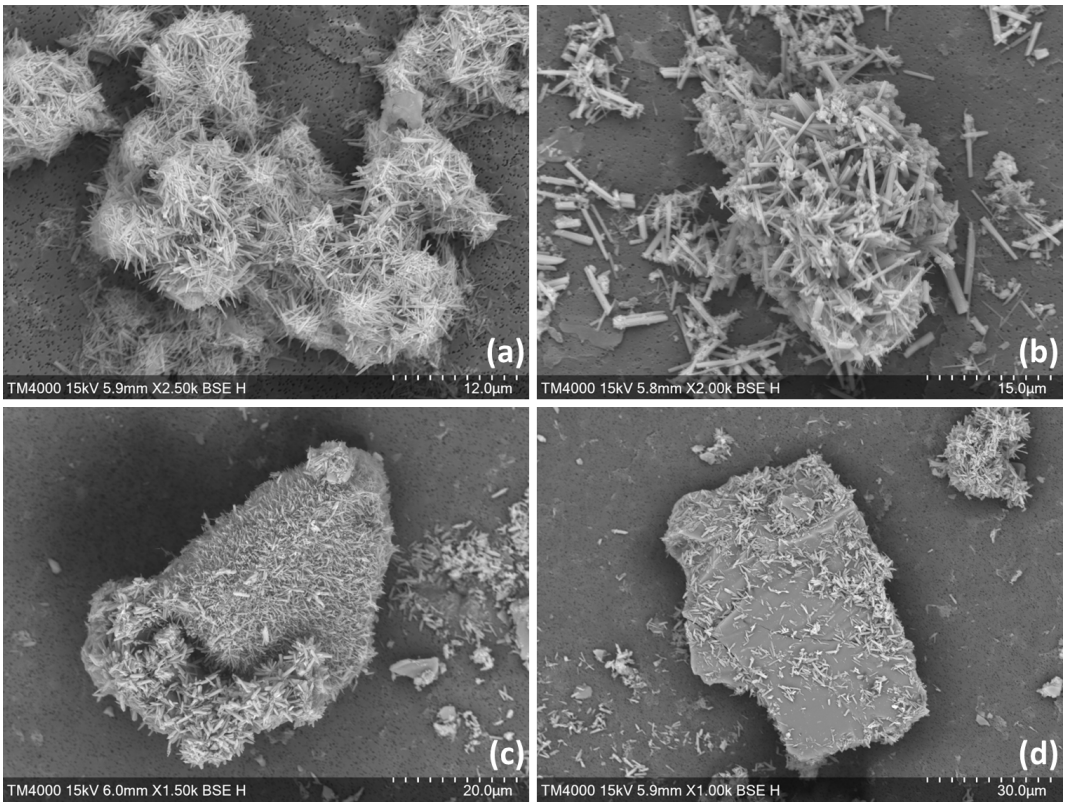

Figure 5. SEM images from experiments with an increase in TA of $\sim 500\,\mu mol\,kg^{-1}$ by CaO **(a)** and $Ca(OH)_2$ **(b)** and with a TA increase of $\sim 1050\,\mu mol\,kg^{-1}$ by 1 M Na_2CO_3, followed by quartz particles addition (**c** and **d**).

precipitation for a TA addition of $500\,\mu mol\,kg^{-1}$ will see pH_T drop by about 0.1 from 8.04 to 7.93 and Ω_A from 2.80 to 1.66, significantly enhancing ongoing ocean acidification (Table 3). Runaway $CaCO_3$ precipitation for a TA addition of $1000\,\mu mol\,kg^{-1}$ (assumed to cease at an Ω_A of 2 as observed here) would see a further drop in Ω_A, i.e. to below 1, upon CO_2 re-equilibration with the atmosphere (Table 3). Under such conditions, aragonite would start to dissolve, impacting various marine organisms, especially carbonate-secreting organisms, e.g. sessile corals, benthic molluscs and planktonic pteropods (Riebesell et al., 2011; Zeebe and Wolf-Gladrow, 2001). In summary, runaway $CaCO_3$ precipitation in OAE must be avoided as it will not only reduce CO_2 uptake efficiency significantly but also enhance ocean acidification. Keeping track of OAE efficiency from changes in TA concentrations can be challenging as $CaCO_3$ precipitation can be underestimated as described earlier, requiring new and clever monitoring strategies.

4.4 Avoiding $CaCO_3$ precipitation by dilution and other TA addition strategies

An important aspect when it comes to avoiding $CaCO_3$ precipitation is the dilution that would occur in the wake of ships releasing TA in the ocean or by natural mixing of TA-enriched water with surrounding seawater (Caserini et al., 2021; Feng et al., 2017; Mongin et al., 2021). In our experiments, a 1 : 1 dilution appeared to seemingly inhibit $CaCO_3$ precipitation in seawater, even if performed only after 1 week for the $+500\,\mu mol\,kg^{-1}$ TA addition. At a first glance, this comes as a surprise since precipitation nuclei would only be diluted by half, reducing surface area and precipitation rates by a factor of 2. However, as Ω_A is simultaneously reduced, precipitation rates are further reduced by a factor of 10 (see Fig. A4). Hence, the overall precipitation rate would see a reduction by a factor of 20. This should slow down precipitation initiated upon the alkalinity addition if on $CaCO_3$ particles but not completely inhibit it (Zhong and Mucci, 1989). A possible explanation could be that dilution lowers Ω_A below the critical threshold, overcoming the lattice mismatch, as most of the aragonite precipitation appears to be on the original seed mineral itself rather than on the newly formed aragonite (compare Fig. 5c and d).

Overall, $CaCO_3$ precipitation can be avoided if the $TA + 500\,\mu mol\,kg^{-1}$ enriched seawater is diluted 1 : 1, reaching an Ω_A of ~ 5.0. The more quickly dilution takes place, the less $CaCO_3$ would precipitate prior to dilution. Similar results were found for a TA addition of $+2000\,\mu mol\,kg^{-1}$, i.e. the ability to stop precipitation at an Ω_A of ~ 5.0, after a 1 : 7 dilution. However, only the 10 min

and 1 h dilutions seem to be suitable in an OAE context as rapid aragonite precipitation at a higher initial Ω_A of about 16.7 would significantly reduce the CO_2 uptake efficiency. Furthermore, the difficulty in monitoring precipitation from simple TA measurements (as described above) would also mean that quantification of CO_2 removal is not straightforward. Therefore, in order to assign carbon credits, TA additions have to be done in a way that rule out or at least minimise secondary $CaCO_3$ precipitation. This is true for any type of TA addition and is not specific to additions of quick and hydrated lime.

Adding TA from land, as modelled by Feng et al. (2017), shows that as more TA is added, higher coastal Ω_A would be reached. By staying well below the Ω_A threshold identified here, i.e. limiting coastal Ω_A to only 3.2, up to ~ 550 Gt of carbon in the form of CO_2 could be removed from the atmosphere between 2020 and 2100, corresponding to a reduction by about 260 ppm (Feng et al., 2017). The critical Ω_A threshold beyond which secondary $CaCO_3$ precipitation occurs could be higher for other alkaline minerals of interest for OAE, theoretically allowing for higher TA additions. However, it has to be kept in mind that in waters with high sediment load, often found in coastal settings, $CaCO_3$ could precipitate onto mineral particles other than those added to increase TA. This has been observed in river plumes (Wurgaft et al., 2021), on resuspended sediments of the Bahama Banks (Bustos-Serrano et al., 2009), and in the Red Sea following flash flood deposition of resuspended sediments and particles (Wurgaft et al., 2016). Even with minerals allowing for higher TA additions, an Ω_A threshold of 5 might be safer to adopt. Atmospheric CO_2 removal could be increased if TA were also added to the open ocean, e.g. on ships of opportunity. Here, additions could be much higher as ship movement and rapid mixing within a ship's wake would significantly dilute added TA as opposed to coastal point sources (Caserini et al., 2021; Köhler et al., 2013).

Finally, another option to increase atmospheric CO_2 uptake would be to keep the seawater equilibrated with air or CO_2-enriched flue gases, during mineral dissolution. Firstly, an Ω_A of 3.3 would be reached as opposed to 5 in the $+250\,\mu mol\,kg^{-1}$ TA scenario (Table 3), when equilibration occurs during instead of after the dissolution process. Secondly, when reaching an Ω_A of 5 with CO_2 equilibration, nearly 1000 instead of $250\,\mu mol\,kg^{-1}$ of TA could be added, allowing for almost 4 times the amount of atmospheric CO_2 to be removed (this number is highly sensitive to temperature and ranges between ~ 3 and ~ 6 between 30 and 5 °C). Unfortunately, this requires an extra step, which appears to be far more time-consuming and costly than a simple mineral addition. It should also be kept in mind that for the same Ω_A threshold, the amount of TA that can be added will increase at lower temperatures because of higher CO_2 solubility and, hence, naturally lower Ω_A in colder waters. Based on our Ω_A threshold of 5, at a salinity of 35 and at 5 °C, about 3 times as much TA can be dissolved than at 30 °C.

5 Conclusions

OAE is a negative-emission technology with large potential for atmospheric CO_2 removal (Caserini et al., 2021; Feng et al., 2016; Köhler et al., 2010). In order to maximise CO_2 uptake efficiency, secondary $CaCO_3$ precipitation has to be avoided. Here we show that an increase in TA by $500\,\mu mol\,kg^{-1}$ led to aragonite precipitation, reducing the CO_2 uptake potential from about $0.8\,mol\,mol^{-1}$ of TA added to nearly 0.1 mol. Precipitation most likely occurred on the CaO and $Ca(OH)_2$ mineral surfaces prior to their full dissolution. In contrast, an addition of $250\,\mu mol\,kg^{-1}$ of TA did not result in $CaCO_3$ precipitation, suggesting that an Ω_A of about 5 is a safe limit. This is probably the case for other minerals with even lower lattice compatibility for $CaCO_3$ since $CaCO_3$ could precipitate onto naturally present mineral phases in coastal settings, such as resuspended sediments. Safely increasing the amount of TA that could be added to the ocean could be achieved by (1) allowing for major mixing and dilution of enriched seawater by coastal tides or in the wake of ships, (2) equilibrating the seawater to atmospheric CO_2 levels prior to the addition during mineral dissolution, and/or (3) targeting low- rather than high-temperature regions.

Appendix A

Table A1. Seawater salinity in each experiment and phosphate concentrations in one of the batches.

Alkaline mineral	TA increase (in µmol kg^{-1})	Experiment details	Seawater salinity	Phosphate (in µmol kg^{-1})
CaO	250	n/a	36.52	Not measured
	500	n/a	36.52	Not measured
$Ca(OH)_2$	250	n/a	36.91	Not measured
	500	N/A	36.91	Not measured
	500	For dilutions	35.46	Not measured
	500	For filtration	36.52	Not measured
	2000	For dilution	36.74	0.32 ± 0.03
Na_2CO_3	1050	n/a	36.91	Not measured
	1050	With quartz particles	36.52	Not measured

n/a: not applicable.

Table A2. Main chemical composition of the CaO and $Ca(OH)_2$ feedstocks used for the TA increase experiments determined by ICP-MS analysis (expressed in mg g^{-1}, with the corresponding standard deviation, SD).

CaO powder			$Ca(OH)_2$ powder		
Element	mg g^{-1}	SD	Element	mg g^{-1}	SD
Calcium	545.15	70.92	Calcium	529.79	117.30
Magnesium	2.10	0.23	Magnesium	6.87	1.98
Silicon	2.02	1.79	Silicon	2.70	1.12
Aluminium	0.50	0.19	Aluminium	1.98	0.77
Iron	0.32	0.10	Iron	0.91	0.34
Manganese	0.11	0.01	Potassium	0.43	0.23
Potassium	0.03	0.00	Titanium	0.07	0.03
Phosphorus	0.02	0.02	Manganese	0.05	0.01
Titanium	0.02	0.01	Phosphorus	0.04	0.01
Chromium	0.01	0.01	Bromine	0.03	0.01

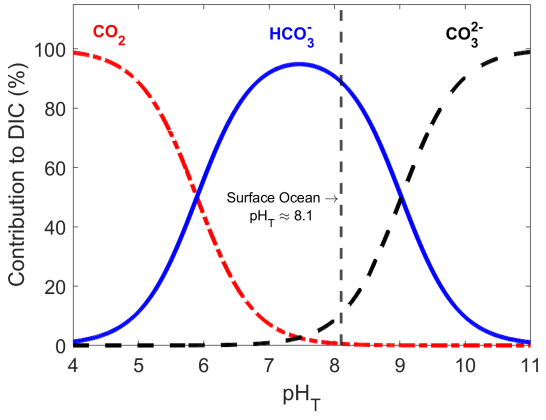

Figure A1. Relative contribution of dissolved CO_2, HCO_3^- and CO_3^{2-} to total dissolved inorganic carbon in seawater as a function of pH_T (total scale), also known as a Bjerrum plot (based on the carbonic acid equilibrium constant from Mehrbach et al., 1973, and refitted by Dickson and Millero, 1987), at 25 °C and a salinity of 35, with the current surface ocean pH average represented by the dashed vertical line ($pH_T \sim 8.1$).

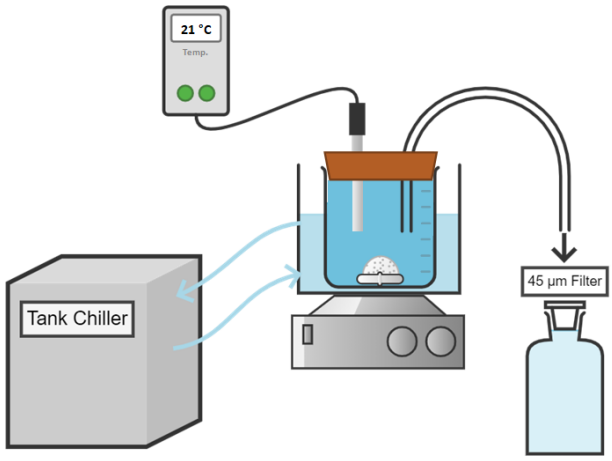

Figure A2. Conceptual diagram of the experimental setup used for the dissolution of alkaline minerals.

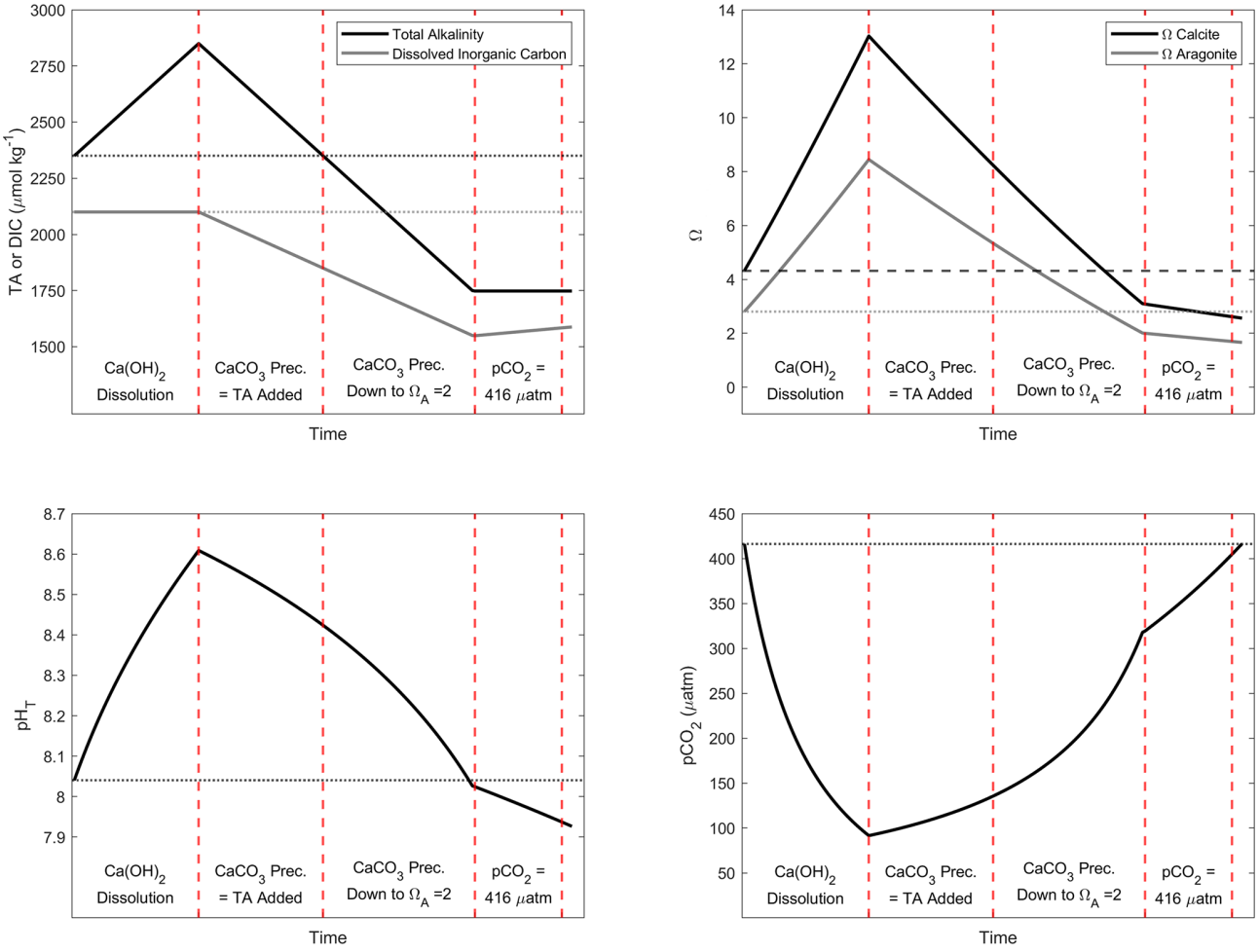

Figure A3. Simulation of the changes in TA, DIC, Ω_C, Ω_A, pCO_2 and pH_T after addition of 500 µmol kg^{-1} of alkalinity. Four important steps are presented: first, assuming the complete $Ca(OH)_2$ dissolution without $CaCO_3$ precipitation; second, assuming as much $CaCO_3$ precipitation as the amount of TA added; third, assuming $CaCO_3$ precipitation happening until reaching an Ω_A of 2; and fourth, CO_2 uptake until equilibrium is reached between atmosphere and seawater at a pCO_2 of ∼ 416 µ atm.

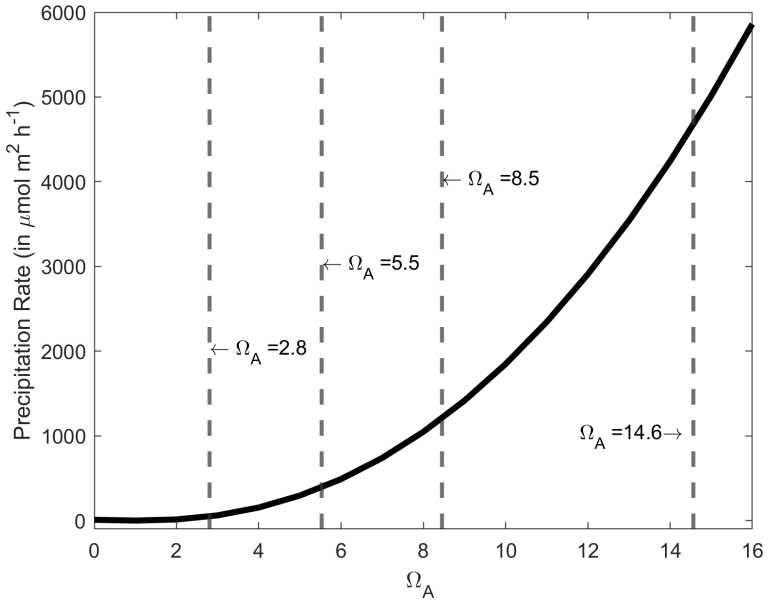

Figure A4. $CaCO_3$ precipitation rate onto aragonite seed crystals in µmol m^{-2} h^{-1} as a function of Ω_A, based on the measurements of Zhong and Mucci (1989) at 25 °C and for a salinity of 35. The Ω_A values for the starting conditions and following a +250, +500 and +1000 µmol kg^{-1} TA increase are presented by the dashed grey lines, i.e. 2.8, 5.5, 8.5 and 14.6, respectively.

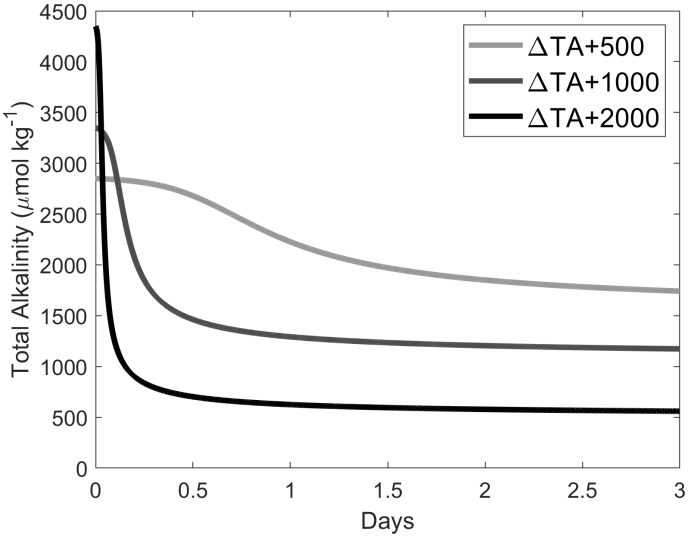

Figure A5. Simulations of TA loss due to aragonite precipitation after a TA addition of 500, 1000 and 2000 µmol kg^{-1}, based on Ω_A and surface-area-dependent precipitation rates shown in Fig. A4, assuming the initial presence of 2 % of $CaCO_3$ in our samples, i.e. ∼ 0.37, ∼ 0.74 and ∼ 1.48 mg kg^{-1} for ΔTA + 500, ΔTA + 1000 and ΔTA + 2000 µmol kg^{-1}, respectively. $CaCO_3$ mass was converted to a surface area as described in Zhong and Mucci (1989). The starting conditions were TA = 2300 µmol kg^{-1}, DIC = 2100 µmol kg^{-1}, salinity = 35 and temperature = 21 °C.

Data availability. All data regarding the changes in TA and DIC were collected by Charly A. Moras and were publicly published on the 15 July 2022 by the Australian Ocean Data Network (AODN) under the name "Quick and hydrated lime dissolution for Ocean Alkalinity Enhancement" and can be found at https://doi.org/10.26198/8znv-e436 (Moras, 2022).

Author contributions. CM and KS designed the initial experiments. LB, TC and RJB contributed to designing the follow-up experiments after observing unexpected $CaCO_3$ precipitation. CM and RJB conducted the ICP-MS analyses of the various materials and, with the help of KS and TC, the identification and analyses of $CaCO_3$ using the SEM. CM and KS mainly wrote the paper, with inputs from all co-authors and specific inputs from LB for carbonate chemistry and TC for $CaCO_3$.

Competing interests. At least one of the (co-)authors is a member of the editorial board of *Biogeosciences*. The peer-review process was guided by an independent editor, and the authors also have no other competing interests to declare.

Disclaimer. Publisher's note: Copernicus Publications remains neutral with regard to jurisdictional claims in published maps and institutional affiliations.

Acknowledgements. We would like to thank Marian Bailey for her help with ICP-MS sample preparation, as well as Nick Ward for his help with preliminary X-ray diffraction analyses of the calcium powders. We are also thankful to Matheus Carvalho de Carvalho for the particulate carbon analyses and Nadia Toppler for her help arranging the use of the SEM.

Financial support. This research is part of the PhD project of Charly A. Moras that is funded by a Cat. 5 – SCU Grad School scholarship from the Southern Cross University, Lismore, Australia. The ICP-MS analyses were made possible by Australian Research Council grants to Renaud Joannes-Boyau and Kai G. Schulz (grant no. LE200100022) and to Renaud Joannes-Boyau (grant no. LE120100201).

Review statement. This paper was edited by Jean-Pierre Gattuso and reviewed by Daniel Burt and one anonymous referee.

References

Bach, L. T., Gill, S., Rickaby, R., Gore, S., and Renforth, P.: CO_2 removal with enhanced weathering and ocean alkalinity enhancement: Potential risks and co-benefits for marine pelagic ecosystems, Front. Clim., 1, 7, https://doi.org/10.3389/fclim.2019.00007, 2019.

Bates, N. R., Best, M. H. P., Neely, K., Garley, R., Dickson, A. G., and Johnson, R. J.: Detecting anthropogenic carbon dioxide uptake and ocean acidification in the North Atlantic Ocean, Biogeosciences, 9, 2509–2522, https://doi.org/10.5194/bg-9-2509-2012, 2012.

Burt, D. J., Fröb, F., and Ilyina, T.: The sensitivity of the marine carbonate system to regional ocean alkalinity enhancement, Front. Clim., 3, 624075, https://doi.org/10.3389/fclim.2021.624075, 2021.

Bustos-Serrano, H., Morse, J. W., and Millero, F. J.: The formation of whitings on the Little Bahama Bank, Mar. Chem., 113, 1–8, 2009.

Canadell, J. G., Le Quéré, C., Raupach, M. R., Field, C. B., Buitenhuis, E. T., Ciais, P., Conway, T. J., Gillett, N. P., Houghton, R., and Marland, G.: Contributions to accelerating atmospheric CO_2 growth from economic activity, carbon intensity, and efficiency of natural sinks, P. Natl. Acad. Sci. USA, 104, 18866–18870, 2007.

Carter, B. R., Feely, R. A., Wanninkhof, R., Kouketsu, S., Sonnerup, R. E., Pardo, P. C., Sabine, C. L., Johnson, G. C., Sloyan, B. M., and Murata, A.: Pacific anthropogenic carbon between 1991 and 2017, Global Biogeochem. Cy., 33, 597–617, 2019.

Caserini, S., Pagano, D., Campo, F., Abbà, A., De Marco, S., Righi, D., Renforth, P., and Grosso, M.: Potential of Maritime Transport for Ocean Liming and Atmospheric CO_2 Removal, Frontiers in Climate, 3, 575900, https://doi.org/10.3389/fclim.2021.575900, 2021.

Chang, R., Kim, S., Lee, S., Choi, S., Kim, M., and Park, Y.: Calcium carbonate precipitation for CO_2 storage and utilization: a review of the carbonate crystallization and polymorphism, Frontiers in Energy Research, 5, 17, https://doi.org/10.3389/fenrg.2017.00017, 2017.

Chave, K. E. and Suess, E.: Calcium Carbonate Saturation in Seawater: Effects of Dissolved Organic Matter 1, Limnol. Oceanogr., 15, 633–637, 1970.

Chen, T., Neville, A., and Yuan, M.: Calcium carbonate scale formation – assessing the initial stages of precipitation and deposition, J. Petrol. Sci. Eng., 46, 185–194, 2005.

Cyronak, T., Schulz, K. G., Santos, I. R., and Eyre, B. D.: Enhanced acidification of global coral reefs driven by regional biogeochemical feedbacks, Geophys. Res. Lett., 41, 5538–5546, 2014.

De Choudens-Sanchez, V. and Gonzalez, L. A.: Calcite and aragonite precipitation under controlled instantaneous supersaturation: elucidating the role of $CaCO_3$ saturation state and Mg/Ca ratio on calcium carbonate polymorphism, J. Sediment. Res., 79, 363–376, 2009.

Dickson, A. G.: Standards for ocean measurements, Oceanography, 23, 34–47, 2010.

Dickson, A. G. and Millero, F. J.: A comparison of the equilibrium constants for the dissociation of carbonic acid in seawater media, Deep-Sea Res., 34, 1733–1743, 1987.

Dickson, A. G., Sabine, C. L., and Christian, J. R.: Guide to best practices for ocean CO_2 measurements, PICES Special Publication 3, IOCCP Report 8, Sidney, British Columbia, North Pacific Marine Science Organization, 191 pp., https://doi.org/10.25607/OBP-1342, 2007.

Doney, S. C., Fabry, V. J., Feely, R. A., and Kleypas, J. A.: Ocean acidification: the other CO_2 problem, Annual Rev. Mar. Sci., 1, 169–192, 2009.

Feng, E. Y., Keller, D. P., Koeve, W., and Oschlies, A.: Could artificial ocean alkalinization protect tropical coral ecosystems from ocean acidification?, Environ. Res. Lett., 11, 074008, https://doi.org/10.1088/1748-9326/11/7/074008, 2016.

Feng, E. Y., Koeve, W., Keller, D. P., and Oschlies, A.: Model-Based Assessment of the CO_2 Sequestration Potential of Coastal Ocean Alkalinization, Earth's Future, 5, 1252–1266, 2017.

Friedlingstein, P., Jones, M. W., O'Sullivan, M., Andrew, R. M., Bakker, D. C. E., Hauck, J., Le Quéré, C., Peters, G. P., Peters, W., Pongratz, J., Sitch, S., Canadell, J. G., Ciais, P., Jackson, R. B., Alin, S. R., Anthoni, P., Bates, N. R., Becker, M., Bellouin, N., Bopp, L., Chau, T. T. T., Chevallier, F., Chini, L. P., Cronin, M., Currie, K. I., Decharme, B., Djeutchouang, L. M., Dou, X., Evans, W., Feely, R. A., Feng, L., Gasser, T., Gilfillan, D., Gkritzalis, T., Grassi, G., Gregor, L., Gruber, N., Gürses, Ö., Harris, I., Houghton, R. A., Hurtt, G. C., Iida, Y., Ilyina, T., Luijkx, I. T., Jain, A., Jones, S. D., Kato, E., Kennedy, D., Klein Goldewijk, K., Knauer, J., Korsbakken, J. I., Körtzinger, A., Landschützer, P., Lauvset, S. K., Lefèvre, N., Lienert, S., Liu, J., Marland, G., McGuire, P. C., Melton, J. R., Munro, D. R., Nabel, J. E. M. S., Nakaoka, S.-I., Niwa, Y., Ono, T., Pierrot, D., Poulter, B., Rehder, G., Resplandy, L., Robertson, E., Rödenbeck, C., Rosan, T. M., Schwinger, J., Schwingshackl, C., Séférian, R., Sutton, A. J., Sweeney, C., Tanhua, T., Tans, P. P., Tian, H., Tilbrook, B., Tubiello, F., van der Werf, G. R., Vuichard, N., Wada, C., Wanninkhof, R., Watson, A. J., Willis, D., Wiltshire, A. J., Yuan, W., Yue, C., Yue, X., Zaehle, S., and Zeng, J.: Global Carbon Budget 2021, Earth Syst. Sci. Data, 14, 1917–2005, https://doi.org/10.5194/essd-14-1917-2022, 2022.

Gafar, N. A. and Schulz, K. G.: A three-dimensional niche comparison of *Emiliania huxleyi* and *Gephyrocapsa oceanica*: reconciling observations with projections, Biogeosciences, 15, 3541–3560, https://doi.org/10.5194/bg-15-3541-2018, 2018.

Gattuso, J.-P., Magnan, A., Billé, R., Cheung, W. W., Howes, E. L., Joos, F., Allemand, D., Bopp, L., Cooley, S. R., and Eakin, C. M.: Contrasting futures for ocean and society from different anthropogenic CO_2 emissions scenarios, Science, 349, aac4722, https://doi.org/10.1126/science.aac4722, 2015.

GESAMP: High level review of a wide range of proposed marine geoengineering techniques, edited by: Boyd, P. W. and Vivian, C. M. G., IMO/FAO/UNESCO-IOC/UNIDO/WMO/IAEA/UN/UN Environment/UNDP/ISA Joint Group of Experts on the Scientific Aspects of Marine Environmental Protection, GESAMP, Rep. Stud. GESAMP No. 98, 144, 1020–4873, 2019.

González, M. F. and Ilyina, T.: Impacts of artificial ocean alkalinization on the carbon cycle and climate in Earth system simulations, Geophys. Res. Lett., 43, 6493–6502, 2016.

Goodwin, P., Brown, S., Haigh, I. D., Nicholls, R. J., and Matter, J. M.: Adjusting mitigation pathways to stabilize climate at 1.5 °C and 2.0 °C rise in global temperatures to year 2300, Earth's Future, 6, 601–615, 2018.

Harvey, L.: Mitigating the atmospheric CO_2 increase and ocean acidification by adding limestone powder to upwelling regions, J. Geophys. Res.-Oceans, 113, C04028, https://doi.org/10.1029/2007JC004373, 2008.

Hoegh-Guldberg, O., Mumby, P. J., Hooten, A. J., Steneck, R. S., Greenfield, P., Gomez, E., Harvell, C. D., Sale, P. F., Edwards, A. J., and Caldeira, K.: Coral reefs under rapid climate change and ocean acidification, Science, 318, 1737–1742, 2007.

Hoegh-Guldberg, O., Jacob, D., Taylor, M., Bolaños, T. G., Bindi, M., Brown, S., Camilloni, I., Diedhiou, A., Djalante, R., and Ebi, K.: The human imperative of stabilizing global climate change at 1.5 °C, Science, 365, eaaw6974, https://doi.org/10.1126/science.aaw6974, 2019.

Huppmann, D., Kriegler, E., Krey, V., Riahi, K., Rogelj, J., Rose, S. K., Weyant, J., Bauer, N., Bertram, C., and Bosetti, V.: IAMC 1.5 °C Scenario Explorer and Data hosted by IIASA, International Institute for Applied Systems Analysis & Integrated Assessment Modeling Consortium, https://doi.org/10.22022/SR15/08-2018.15429, 2018.

Ilyina, T., Wolf-Gladrow, D., Munhoven, G., and Heinze, C.: Assessing the potential of calcium-based artificial ocean alkalinization to mitigate rising atmospheric CO_2 and ocean acidification, Geophys. Res. Lett., 40, 5909–5914, 2013.

IPCC: Summary for Policymakers, in: Climate Change 2021: The Physical Science Basis. Contribution of Working Group I to the Sixth Assessment Report of the Intergovernmental Panel on Climate Change, edited by: Masson-Delmotte, V., Zhai, P., Pirani, A., Connors, S. L., Péan, C., Berger, S., Caud, N., Chen, L., Goldfarb, M. I., Gomis, M., Huang, K., Leitzell, E., Lonnoy, J. B. R., Matthews, Y., Maycock, T. K., Waterfield, T., Yelekçi, O., Yu, R., and Zhou, B., Cambridge University Press, Cambridge University Press, Cambridge, United Kingdom and New York, NY, USA, 3−-32, https://www.ipcc.ch/report/ar6/wg1/downloads/report/IPCC_AR6_WGI_SPM.pdf, https://doi.org/10.1017/9781009157896.001, 2021.

Keller, D. P., Feng, E. Y., and Oschlies, A.: Potential climate engineering effectiveness and side effects during a high carbon dioxide-emission scenario, Nat. Commun., 5, 1–11, 2014.

Kheshgi, H. S.: Sequestering atmospheric carbon dioxide by increasing ocean alkalinity, Energy, 20, 915–922, 1995.

Köhler, P., Hartmann, J., and Wolf-Gladrow, D. A.: Geoengineering potential of artificially enhanced silicate weathering of olivine, P. Natl. Acad. Sci. USA, 107, 20228–20233, 2010.

Köhler, P., Abrams, J. F., Völker, C., Hauck, J., and Wolf-Gladrow, D. A.: Geoengineering impact of open ocean dissolution of olivine on atmospheric CO_2, surface ocean pH and marine biology, Environ. Res. Lett., 8, 014009, https://doi.org/10.1088/1748-9326/8/1/014009, 2013.

Lenton, T. M. and Vaughan, N. E.: The radiative forcing potential of different climate geoengineering options, Atmos. Chem. Phys., 9, 5539–5561, https://doi.org/10.5194/acp-9-5539-2009, 2009.

Lenton, A., Matear, R. J., Keller, D. P., Scott, V., and Vaughan, N. E.: Assessing carbon dioxide removal through global and regional ocean alkalinization under high and low emission pathways, Earth Syst. Dynam., 9, 339–357, https://doi.org/10.5194/esd-9-339-2018, 2018.

Lewis, E. and Perkin, R.: The practical salinity scale 1978: conversion of existing data, Deep-Sea Res., 28, 307–328, 1981.

Lioliou, M. G., Paraskeva, C. A., Koutsoukos, P. G., and Payatakes, A. C.: Heterogeneous nucleation and growth of calcium carbonate on calcite and quartz, J. Colloid Interf. Sci., 308, 421–428, 2007.

Lueker, T. J., Dickson, A. G., and Keeling, C. D.: Ocean pCO_2 calculated from dissolved inorganic carbon, alkalinity, and equations for K1 and K2: validation based on laboratory measurements of CO_2 in gas and seawater at equilibrium, Mar. Chem., 70, 105–119, 2000.

Marion, G. M., Millero, F. J., and Feistel, R.: Precipitation of solid phase calcium carbonates and their effect on application of seawater $S_A - T - P$ models, Ocean Sci., 5, 285–291, https://doi.org/10.5194/os-5-285-2009, 2009.

Mehrbach, C., Culberson, C., Hawley, J., and Pytkowicx, R.: Measurement of the apparent dissociation constants of carbonic acid in seawater at atmospheric pressure 1, Limnol. Oceanogr., 18, 897–907, 1973.

Millero, F., Huang, F., Zhu, X., Liu, X., and Zhang, J.-Z.: Adsorption and desorption of phosphate on calcite and aragonite in seawater, Aquat. Geochem., 7, 33–56, 2001.

Mongin, M., Baird, M. E., Lenton, A., Neill, C., and Akl, J.: Reversing ocean acidification along the Great Barrier Reef using alkalinity injection, Environ. Res. Lett., 16, 064068, https://doi.org/10.1088/1748-9326/ac002d, 2021.

Montserrat, F., Renforth, P., Hartmann, J., Leermakers, M., Knops, P., and Meysman, F. J.: Olivine dissolution in seawater: implications for CO_2 sequestration through enhanced weathering in coastal environments, Environ. Sci. Technol., 51, 3960–3972, 2017.

Moras, C. A.: Quick and hydrated lime dissolution for Ocean Alkalinity Enhancement, Australian Ocean Data Network [data set], https://doi.org/10.26198/8znv-e436, 2022.

Morse, J. W. and He, S.: Influences of T, S and pCO_2 on the pseudohomogeneous precipitation of $CaCO_3$ from seawater: implications for whiting formation, Mar. Chem., 41, 291–297, 1993.

Morse, J. W., Wang, Q., and Tsio, M. Y.: Influences of temperature and Mg: Ca ratio on $CaCO_3$ precipitates from seawater, Geology, 25, 85–87, 1997.

Morse, J. W., Gledhill, D. K., and Millero, F. J.: $CaCO_3$ precipitation kinetics in waters from the great Bahama bank: Implications for the relationship between bank hydrochemistry and whitings, Geochim. Cosmochim. Ac., 67, 2819–2826, 2003.

Morse, J. W., Arvidson, R. S., and Lüttge, A.: Calcium carbonate formation and dissolution, Chem. Rev., 107, 342–381, 2007.

Mucci, A.: The solubility of calcite and aragonite in seawater at various salinities, temperatures, and one atmosphere total pressure, Am. J. Sci., 283, 780–799, 1983.

National Academies of Sciences, Engineering, and Medicine: A Research Strategy for Ocean-based Carbon Dioxide Removal and Sequestration, The National Academies Press, Washington, DC, 322 pp., https://doi.org/10.17226/26278, 2022.

Ni, M. and Ratner, B. D.: Differentiating calcium carbonate polymorphs by surface analysis techniques – an XPS and TOF-SIMS study, Surf. Interface Anal., 40, 1356–1361, 2008.

Pan, Y., Li, Y., Ma, Q., He, H., Wang, S., Sun, Z., Cai, W.-J., Dong, B., Di, Y., and Fu, W.: The role of Mg^{2+} in inhibiting $CaCO_3$ precipitation from seawater, Mar. Chem., 237, 104036, https://doi.org/10.1016/j.marchem.2021.104036, 2021.

Pytkowicz, R. M.: Rates of inorganic calcium carbonate nucleation, The Journal of Geology, 73, 196–199, 1965.

Renforth, P. and Henderson, G.: Assessing ocean alkalinity for carbon sequestration, Rev. Geophys., 55, 636–674, 2017.

Renforth, P. and Kruger, T.: Coupling mineral carbonation and ocean liming, Energ. Fuel., 27, 4199–4207, 2013.

Renforth, P., Jenkins, B., and Kruger, T.: Engineering challenges of ocean liming, Energy, 60, 442–452, 2013.

Riebesell, U., Fabry, V. J., Hansson, L., and Gattuso, J.-P.: Guide to best practices for ocean acidification research and data reporting, Office for Official Publications of the European Communities, Luxembourg, 258 pp., https://doi.org/10.2777/66906, 2011.

Riley, J. and Tongudai, M.: The major cation/chlorinity ratios in sea water, Chem. Geol., 2, 263–269, 1967.

Rushdi, A., Pytkowicz, R., Suess, E., and Chen, C.: The effects of magnesium-to-calcium ratios in artificial seawater, at different ionic products, upon the induction time, and the mineralogy of calcium carbonate: a laboratory study, Geol. Rundsch., 81, 571–578, 1992.

Schulz, K. G., Bach, L. T., Bellerby, R. G., Bermúdez, R., Büdenbender, J., Boxhammer, T., Czerny, J., Engel, A., Ludwig, A., and Meyerhöfer, M.: Phytoplankton blooms at increasing levels of atmospheric carbon dioxide: experimental evidence for negative effects on prymnesiophytes and positive on small picoeukaryotes, Frontiers in Marine Science, 4, https://doi.org/10.3389/fmars.2017.00064, 2017.

Sharp, J. D., Pierrot, D., Humphreys, M. P., Epitalon, J.-M., Orr, J. C., Lewis, E. R., and Wallace, D. W. R.: CO2SYSv3 for MATLAB (Version v3.2.0), Zenodo, https://doi.org/10.5281/zenodo.3950562, 2021.

Simkiss, K.: The inhibitory effects of some metabolites on the precipitation of calcium carbonate from artificial and natural sea water, ICES J. Mar. Sci., 29, 6–18, 1964.

Statista: Global cement industry – Statistics & Facts, https://www.statista.com/topics/8700/cement-industry-worldwide/ (last access: 28 March 2022), 2021.

Tang, H., Wu, X., Xian, H., Zhu, J., Wei, J., Liu, H., and He, H.: Heterogeneous Nucleation and Growth of $CaCO_3$ on Calcite (104) and Aragonite (110) Surfaces: Implications for the Formation of Abiogenic Carbonate Cements in the Ocean, Minerals, 10, 294, https://doi.org/10.3390/min10040294, 2020.

The Royal Society and Royal Academy of Engineering: Greenhouse Gas Removal, https://royalsociety.org/-/media/policy/projects/greenhouse-gas-removal/royal-society-greenhouse-gas-removal-report-2018.pdf (last access: 7 May 2022), 2018.

Uppstrom, L.: The boron/chlorinity ratio of deep-sea water from the Pacific Ocean, Deep-Sea Res., 21, 161–162, 1974.

Wolf-Gladrow, D. A., Zeebe, R. E., Klaas, C., Körtzinger, A., and Dickson, A. G.: Total alkalinity: The explicit conservative expression and its application to biogeochemical processes, Mar. Chem., 106, 287–300, 2007.

Wolf, S. E., Leiterer, J., Kappl, M., Emmerling, F., and Tremel, W.: Early homogenous amorphous precursor stages of calcium carbonate and subsequent crystal growth in levitated droplets, J. Am. Chem. Soc., 130, 12342–12347, 2008.

Wurgaft, E., Steiner, Z., Luz, B., and Lazar, B.: Evidence for inorganic precipitation of $CaCO_3$ on suspended solids in the open water of the Red Sea, Mar. Chem., 186, 145–155, 2016.

Wurgaft, E., Wang, Z., Churchill, J., Dellapenna, T., Song, S., Du, J., Ringham, M., Rivlin, T., and Lazar, B.: Particle triggered reactions as an important mechanism of alkalinity and inorganic carbon removal in river plumes, Geophys. Res. Lett., 48, e2021GL093178, https://doi.org/10.1029/2021GL093178, 2021.

Zeebe, R. E. and Wolf-Gladrow, D.: CO_2 in seawater: equilibrium, kinetics, isotopes, 65, Gulf Professional Publishing, 360 pp, ISBN 9780444509468, 2001.

Zhong, S. and Mucci, A.: Calcite and aragonite precipitation from seawater solutions of various salinities: Precipitation rates and overgrowth compositions, Chem. Geol., 78, 283–299, 1989.

Biogeosciences, 19, 5375–5399, 2022
https://doi.org/10.5194/bg-19-5375-2022

Biogeosciences Open Access EGU

Assessing the influence of ocean alkalinity enhancement on a coastal phytoplankton community

Aaron Ferderer[1], **Zanna Chase**[1], **Fraser Kennedy**[1], **Kai G. Schulz**[2], **and Lennart T. Bach**[1]

[1]Ecology and Biodiversity, Institute for Marine and Antarctic Studies, University of Tasmania, Hobart, TAS, Australia
[2]Centre for Coastal Biogeochemistry, School of Environment, Science and Engineering, Southern Cross University, Lismore, NSW, Australia

Correspondence: Aaron Ferderer (aaron.ferderer@utas.edu.au)

Received: 17 January 2022 – Discussion started: 21 January 2022
Revised: 25 October 2022 – Accepted: 5 November 2022 – Published: 1 December 2022

Abstract. Ocean alkalinity enhancement (OAE) is a proposed method to counteract climate change by increasing the alkalinity of the surface ocean and thus the chemical storage capacity of seawater for atmospheric CO_2. The impact of OAE on marine ecosystems, including phytoplankton communities which make up the base of the marine food web, is largely unknown. To investigate the influence of OAE on phytoplankton communities, we enclosed a natural plankton community from coastal Tasmania for 22 d in nine microcosms during a spring bloom. Microcosms were split into three groups, (1) the unperturbed control, (2) the unequilibrated treatment where alkalinity was increased ($+495 \pm 5.2\,\mu mol\,kg^{-1}$) but seawater CO_2 was not in equilibrium with atmospheric CO_2, and (3) the equilibrated treatment where alkalinity was increased ($+500 \pm 3.2\,\mu mol\,kg^{-1}$) and seawater CO_2 was in equilibrium with atmospheric CO_2. Both treatments have the capacity to increase the inorganic carbon sink of seawater by 21 %. We found that simulated OAE had significant but generally moderate effects on various groups in the phytoplankton community and on heterotrophic bacteria. More pronounced effects were observed for the diatom community where silicic acid drawdown and biogenic silica build-up were reduced at increased alkalinity. Observed changes in phytoplankton communities affected the temporal trends of key biogeochemical parameters such as the organic matter carbon-to-nitrogen ratio. Interestingly, the unequilibrated treatment did not have a noticeably larger impact on the phytoplankton (and heterotrophic bacteria) community than the equilibrated treatment, even though the changes in carbonate chemistry conditions were much more severe. This was particularly evident from the occurrence and peak of the phytoplankton spring bloom during the experiment, which was not noticeably different from the control. Altogether, the inadvertent effects of increased alkalinity on the coastal phytoplankton communities appear to be rather limited relative to the enormous climatic benefit of increasing the inorganic carbon sink of seawater by 21 %. We note, however, that more detailed and widespread investigations of plankton community responses to OAE are required to confirm or dismiss this first impression.

1 Introduction

Keeping global warming below 2 °C requires drastic and rapid emission reductions. In addition, a portfolio of carbon dioxide removal (CDR) methods is required to extract several hundred gigatonnes of CO_2 from the atmosphere and store it safely in other carbon reservoirs for thousands of years (Rogelj et al., 2018). However, few CDR methods have been proven to work at this scale, and all have potential side effects for the Earth system (Fuss et al., 2018).

One potential method of CDR from the marine portfolio is ocean alkalinity enhancement (OAE). The idea behind OAE is to increase the chemical storage capacity of the ocean for atmospheric CO_2 by adding proton-neutralizing substances to the surface ocean (Kheshgi, 1995). This is measurable as an enhancement of seawater alkalinity, the name-giving process behind OAE. Enhanced alkalinity causes a shift in the inorganic carbon speciation in seawater, from carbon dioxide (CO_2) to bicarbonate (HCO_3^-) and carbonate (CO_3^{2-}),

thereby making new space for additional atmospheric CO_2 to be absorbed (Hartmann et al., 2013). In addition to generating CDR, the absorption of protons through OAE counteracts ocean acidification (OA), which is considered an environmental threat for a range of marine ecosystems (Doney et al., 2020).

OAE can be achieved through a variety of approaches (Renforth and Henderson, 2017). Most of these approaches are either directly or indirectly linked to the chemical weathering of minerals, which neutralize protons when they dissolve. The simplest approach is to extract suitable minerals via mining, grind those minerals into a powder, and distribute them over land or ocean surfaces where they can dissolve in aqueous media over days to decades (Feng et al., 2017; Taylor et al., 2016). When applied on humid land surfaces, this CDR method is usually referred to as "enhanced weathering" (Schuiling and Krijgsman, 2006). Here, alkalinity and other mineral dissolution products associated with the ground minerals such as dissolved silicate or trace metals would primarily affect terrestrial ecosystems but ultimately wash into the oceans via rivers (Köhler et al., 2010). When ground minerals are added directly to the surface ocean (OAE), dissolution products, such as trace metals, affect ocean biota immediately (Bach et al., 2019). In both cases, the release of alkalinity and other dissolution products is highly dependent on the applied source mineral (Renforth and Henderson, 2017). Mineral weathering can be further accelerated when ground minerals are dissolved in electrolysis cells for hydrogen production (Rau et al., 2013). Here, hydrogen serves as a valuable co-product to CDR, with alkalinity and other dissolution products still being formed and requiring deposition in the environment where they potentially affect biota. Another approach is the electrodialytic separation of water into acid and alkalinity (de Lannoy et al., 2018). Here, alkalinity (in the form of hydroxide) is maintained in the surface ocean, enabling CDR (de Lannoy et al., 2018). The acid can be utilized commercially (e.g. as hydrochloric acid), stored in geological reservoirs underground, or pumped into the deep ocean where it is partially neutralized through the dissolution of carbonate sediments (Tyka et al., 2022). The advantage of this approach is that it does not directly depend on mineral weathering so that mineral supply chains become redundant and no dissolution co-products (e.g. trace metals) are released into the environment (Tyka et al., 2022).

It is currently not possible to predict which of the approaches described above will be implemented in the future. Furthermore, it is unclear how ocean ecosystems would be affected by OAE, as each method differs in the quality and quantity of released dissolution products. However, what all approaches have in common is the intentional change in carbonate chemistry via the addition of alkalinity. It is therefore an important first step to assess if increased seawater alkalinity constitutes a threat to the environment or not (Bach et al., 2019).

This study investigates, for the first time, if and how the changes in carbonate chemistry due to OAE influences coastal phytoplankton communities. More explicitly, we compared the effects of two different alkalinity addition scenarios. Scenario one assumes that the surface ocean is in equilibrium with the overlying atmosphere so that the fugacity of CO_2 (fCO_2) in seawater is equal to that in the overlying atmosphere (the equilibrated treatment). Scenario two assumes that alkalinity is added but atmospheric CO_2 has not yet been absorbed by the perturbed seawater (the unequilibrated treatment). This second scenario is highly relevant because CO_2 equilibration can take months to years (Jones et al., 2014), and carbonate chemistry changes are substantially more pronounced in this unequilibrated transient state that occurs after the alkalinity addition (Bach et al., 2019).

The treatments were tested with a natural plankton community from coastal Tasmania and compared to an unperturbed control. The communities were enclosed in nine identical microcosms in late winter with high nutrient concentrations naturally available. Our goal was to study OAE effects during the spring bloom, an ecologically and biogeochemically important event in the seasonal cycle with the highest biomass accumulation rates during the year.

2 Methods

2.1 Microcosm setup and mixing methods

This experiment made use of Kegland® Fermzilla conical unitank fermenters as microcosms for the monitoring of coastal phytoplankton communities (Fig. 1c). Each microcosm consisted of a $\sim$55 L PET conical tank and a butterfly dump valve connected to a 1 L collection container (sediment collection cup) (Fig. 1c). Microcosms were heated from the base of the conical tank using two 30 W heat belts to induce convective mixing. This prevented the plankton community from sinking out of the water column in a non-invasive way (i.e. without a stirrer; Fig. 1c). To test the efficiency of the convective mixing, we filled eight microcosms with $\sim$50 L of seawater sourced from the Derwent Estuary and placed them in a temperature-controlled room set to 8 °C. This temperature was selected so that, once heating was applied, the water temperature in microcosms would be within the range observed in the Derwent Estuary during late winter (12–14 °C). Once the enclosed seawater had reached thermal equilibrium, the heating on four of the microcosms was turned off. Thirty minutes later, 2.5 mL of blue dye (food colouring) was added to all eight microcosms – four with no heating and four with heating applied (Fig. 1e). The blue dye was added with a pipette to the uppermost $\sim$5 cm of seawater enclosed in microcosms. The rate of mixing within microcosms was then assessed by regularly measuring the absorbance of water samples taken from each microcosm in a spectrophotometer at 630 nm. Samples were carefully taken

from the top of each microcosm using a pipette at a depth of ∼ 5 cm below the water surface. After 3 h, all microcosms were manually mixed with a plastic stirrer to ensure homogeneity. After mixing, the absorbance was measured an additional three times and used as a reference for a homogeneously mixed solution.

Microcosms that had the convection system switched on were well mixed after approximately 30 min (Fig. 1d). In contrast, the no-convection microcosms where the convection system was switched off remained relatively un-mixed, expressed as variable dye concentrations measured with the spectrophotometer (Fig. 1d). The variability in absorbance was consistent with our observations, as filaments of high dye concentration were observed inside the no-convection microcosms until they were manually mixed (Video supplement 1). It is important to note that there was residual convective mixing within the no-convection microcosms, as the convection system was switched off only 30 min before the experiment, allowing residual heat to enter the system (Video supplement 1). The rapid mixing induced via convection as observed in the dye experiment was confirmed by observations during the experiment, with large aggregates suspended in the water column failing to sink into the sediment trap (Fig. 1f, Video supplement 2). Thus, the convection mechanism used here is an effective and non-invasive method to keep plankton in suspension and prevent the unrealistic sinking of particles.

Nevertheless, despite some potential advantages, we acknowledge and are fully aware that our microcosm setup cannot reproduce the full physical (or chemical/biological) complexity of nature (Carpenter, 1996). Enclosures of any type will very likely induce so-called bottle effects (Bach and Taucher, 2019), which can alter the observed community succession and therefore affect the transferability of the outcome to natural (non-enclosed) communities (Carpenter, 1996). While this is a general limitation of these kinds of experimental studies, we stress that bottle effects would occur in all replicates so that the comparison between control and treatments (as done in our study) is valid.

2.2 Enclosure of phytoplankton communities, treatment manipulation, and initiation of the experiment

Nine microcosms were filled with seawater from the Derwent Estuary (August 2021) outside the University of Tasmania Institute for Marine and Antarctic Studies building (42.53095° S, 147.20101° E; Fig. 1a). We refrained from pumping the water into the microcosms as this may harm organisms and alter the plankton community composition. Instead, microcosms were gently filled from the base up (similar to a Niskin sampler) by lowering microcosms one at a time into the water, approximately 5 m out from the edge of the wharf (Fig. 1a). Water was filtered through a 2 mm mesh screen attached to the top and base of microcosms prior to filling. The base of each microcosm was submerged to a depth of ∼ 1 m below the surface and the base closed using a rope attached to the valve handle. Sediment collection cups were then attached to all microcosms with the valve closed. The filling procedure lasted less than 30 min, ensuring enclosure of similar water masses. All microcosms were weighed separately before and after the filling procedure and contained volumes ranging between 55.2 and 55.9 L.

Microcosms were then transported to a temperature-controlled room set to 8 °C (± 2 °C) and heat belts attached as per the methods outlined in Sect. 2.1 (Fig. 1b, c). To simulate natural light conditions, 10 LED light strips were installed in the room, providing a cool white light source with approximately 200 µmol photons m^{-2} s^{-1} inside each microcosm on a 12 : 12 light : dark cycle. Light intensity was measured in the centre of each microcosm with a quantum light meter (LI-COR Biosciences, Lincoln, USA). Due to slight variations in temperature and irradiance throughout the room, microcosms were rotated around the room once a day at ∼ 11:00 (Fig. 1b). The temperature of the room was lowered from 8–6.5 °C over the course of the experiment to ensure temperature stability within the microcosms at 12–14 °C (Fig. 2). This was necessary because the reduced volume of water within microcosms due to sampling caused an increase in heat input per volume via the heat belts so that the cooling from outside had to be increased. Salinity of the seawater enclosed was 34.5 as measured with a 914 Metrohm salinometer.

Microcosms were split into three groups: a control (M1, M4, M7), which received no alkalinity manipulation; the unequilibrated group (M2, M5, M8) enriched with 500 µL of NaOH (Merck, Titripur) per litre; and the equilibrated group (M3, M6, M9) enriched with 423 µL of 1 M $NaHCO_3$ solution (prepared by dissolving 8.401 g of $NaHCO_3$ (Sigma-Aldrich) in 100 mL of double-deionized water) per litre and 77 µL of NaOH (Merck, Titripur) per litre. The mixing ratio of $NaHCO_3$ and NaOH in the equilibrated group was determined with the carbonate chemistry calculation software seacarb (Gattuso et al., 2021) prior to the manipulation, assuming that the collected seawater had a total alkalinity of 2280 µmol kg^{-1} and the fCO_2 was in equilibrium with the atmosphere (∼ 410 µatm). A more detailed description of the calculation of carbonate chemistry conditions is provided in Sect. 2.4. The whole procedure lasted 4 h, and we consider the end of the manipulation as the beginning of the experiment.

2.3 Seawater sampling and particulate matter analyses

Samples were extracted from all microcosms between 07:00–09:00; however, sampling intervals varied depending upon the parameter as indicated in Fig. 2. Prior to sampling, each microcosm was gently mixed in a circular motion five times, using a 60 cm plastic stirrer to ensure no sedimentation bias was introduced in the sampling (this was carried out as

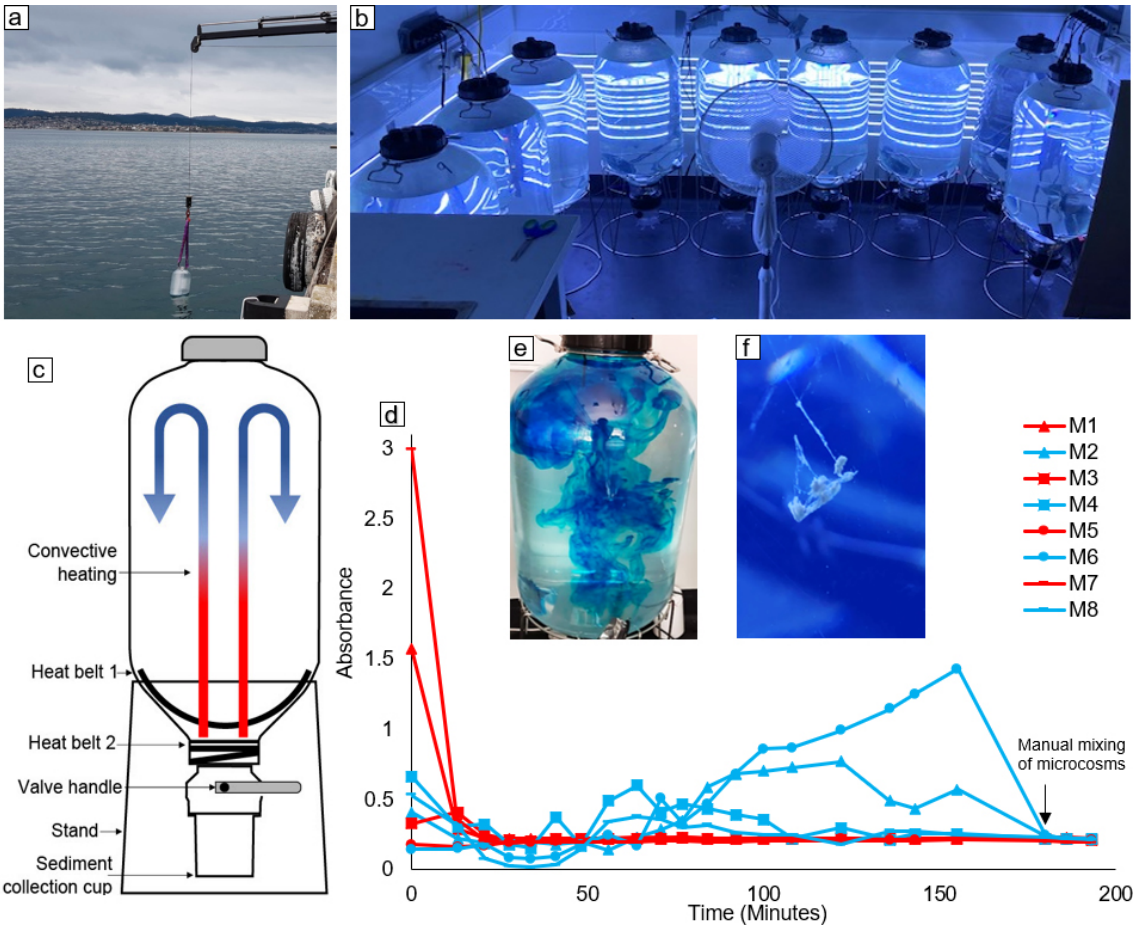

Figure 1. **(a)** Method and location of microcosm filling, **(b)** experimental setup, **(c)** schematic diagram of the microcosms used in this study, **(d)** results of the convective mixing test (microcosms with convective mixing are indicated by red lines and no-convection microcosms indicated by blue lines), **(e)** microcosm with dye addition for assessment of convective mixing, and **(f)** formation of an aggregate within a microcosm.

a precaution, even though preliminary tests with flow cytometry illustrated that homogenization was achieved with convective mixing alone; data not shown). Seawater was sampled from the microcosms using either a silicon tube (particulate matter) or a Tygon tube (nutrients, total alkalinity, flow cytometry) and pumped directly into clean bottles (pre-rinsed with sample). Sampled volumes ranged between 125–1250 mL, depending on the parameters assessed. Samples for dissolved inorganic nutrients (nitrate + nitrite, phosphate, and silicate) and total alkalinity were filtered through a syringe filter (0.2 µm, Millipore) to minimize biological processes. Nutrient concentrations were analysed within 5 h after sampling (Sect. 2.4). Total alkalinity samples were stored at 6 °C in the dark for 0–14 d until analysis (analyses described in Sect. 2.4).

Samples for chlorophyll *a*, biogenic silica (BSi), total particulate carbon (TPC), and total particulate nitrogen (TPN) were taken by filtration of 150–240 mL at a mild vacuum pressure of −200 mbar relative to the atmosphere. Blank filters (placed onto the filtration rack without filtering particles onto them) were prepared for all four parameters during each sampling day. TPC and TPN were filtered on pre-combusted (6 h at 450 °C) quartz fibre (QMA, Whatman) filters (nominal pore-size = 2.2 µm) and stored at −4 °C in pre-combusted (6 h at 450 °C) glass petri dishes for 3–25 d. Prior to analysis, filters were dried at 60 °C for 2 h, packaged into tin foil, and analysed using a Thermo Finnigan EA 1112 Series Flash Elemental Analyser. Combustion of the pressed tin cups was achieved in high-purity oxygen at 1000 °C using tungstic oxide on alumina as an oxidizing agent followed by copper wires as a reducing agent. The results were calibrated using a certified sulfanilamide standard. Please note that we conducted flow-cytometric test measurements where we filtered samples from the microcosms through the QMA filters to test if pico-phytoplankton (0.2–2 µm) would be retained on the filters. These measurements revealed that pico-phytoplankton did not pass through the QMA filters; thus, the entire phytoplankton community was sampled (Fig. A1).

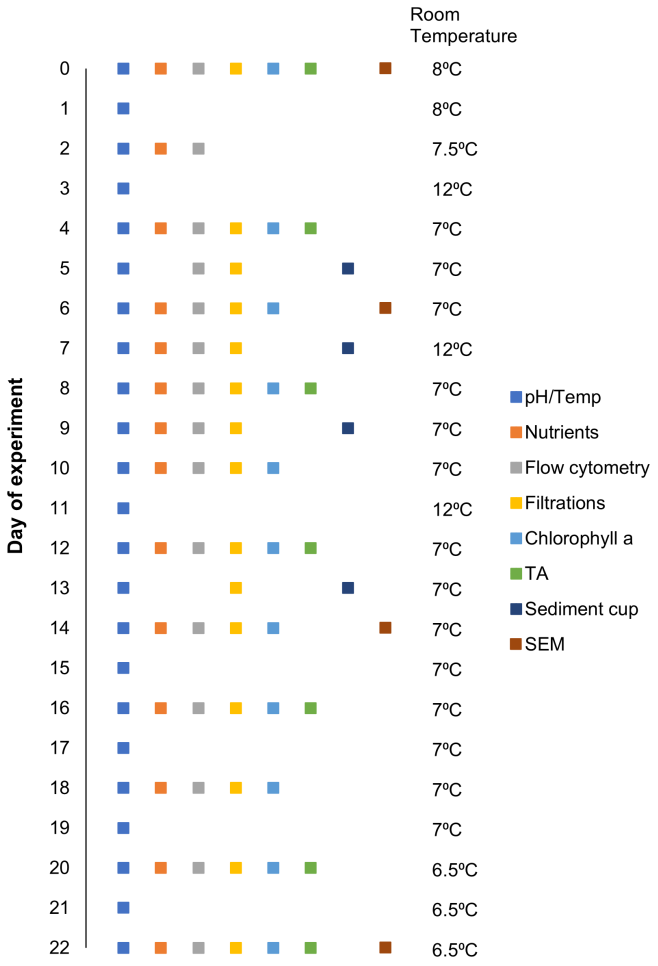

Figure 2. Sampling schedule for given parameters and room temperature on a given day (0–22) over the experimental period.

BSi was filtered on 3 µm nitrocellulose membrane filters which were then stored in plastic petri dishes for 51–73 d at −4 °C until samples were analysed. For the analysis, BSi first needed to be converted into silicic acid. For this, filters were put into 60 mL polypropylene vials filled with 0.1 M NaOH solution; the vials were then firmly closed and heated for 135 min at 80 °C in a temperature-controlled bath. Afterward, the vials were allowed to cool down to room temperature, and the silicic acid concentration was measured photometrically following Hansen and Koroleff (1999).

Chlorophyll *a* samples were filtered through glass fibre filters (GF/F, nominal pore size = 0.7 µm). After filtration, filters were carefully folded, placed in 15 mL polypropylene tubes wrapped in aluminium foil, and immediately frozen and stored at −80 °C. After extraction with 10 mL of methanol (100 %) for 14 h, samples were analysed fluorometrically on a Turner fluorometer following the acidification method outlined by Evans et al. (1987).

Samples for scanning electron microscopy (SEM) were taken by filtration of 30 mL at a mild vacuum pressure of −200 mbar relative to the atmosphere through 0.2 µm polycarbonate filters and dried for 2 h at 60 °C in a desiccator. Prior to analysis, samples were glued onto aluminium stubs and sputtered with gold–palladium. Samples were analysed in a Hitachi SU-70 analytical field emission scanning electron microscope.

2.4 Nutrient and carbonate chemistry analyses

Dissolved nutrient concentrations were determined via spectrophotometric methods developed by Hansen and Koroleff (1999). Nitrate + nitrite (NO_x^-) was determined by first briefly running samples through a peristaltic pump, mixing samples with an ammonium-chloride buffer before being passed through a cadmium reductor to reduce nitrate to nitrite. The reduced sample was mixed with sulfanilamide and *N*-1-naphthyl-ethylenediamine-dihydrochloride, and absorption was measured in a spectrophotometer at 542 nm. Dissolved inorganic phosphate was determined by mixing samples with ascorbic acid and a mixed reagent containing 4.5 M H_2SO_4, ammonium-molybdate solution, and potassium antimony tartrate solution, forming blue heteropoly acid. The absorption of the solution was measured at 882 nm. Dissolved silicate was determined by mixing a mixed reagent containing equal amounts of molybdate solution and 3.6 M H_2SO_4 with the sample, followed by ascorbic acid and oxalic acid. Sample absorbance was then measured at 810 nm. Nutrient concentrations were calibrated with standards of known nitrate, phosphate, and silicate concentrations. The performance of the cadmium reductor and methods used for nutrient analysis were monitored by analysing the same calibration series for each sample day and recording the absorbance and slopes of the calibration series over time. Each sample was measured in duplicate to assess technical variability between measurements. Differences were on average 0.061, 0.001, and 0.122 µmol L^{-1} for NO_x^-, phosphate, and silicate concentrations, respectively

The carbonate chemistry conditions were determined based on potentiometric pH and total alkalinity measurements. pH was measured daily at ∼07:00 inside each microcosm with a Metrohm 914 pH meter and a Metrohm Aquatrode Plus coupled glass and reference electrode, which also includes a PT1000 temperature sensor. We recorded voltage for subsequent pH calculations (see below) and temperature after observed readings had stopped drifting. This was achieved by carefully stirring the electrode for ∼2–5 min in the upper 10 cm of the water column. pH was calibrated to the total scale (pH_T) using the certified Tris buffer provided by Andrew Dickson's laboratory at Scripps Institution of Oceanography as described in SOP6a by Dickson et al. (2007). The calibration was conducted by cooling the Tris buffer to ∼4 °C and measuring voltage in the buffer while it was gradually warmed to 25 °C. That way, we generated a temperature vs. voltage correlation (26 steps along the temperature gradient), and we used the fitted equation

($R^2 = 0.999$) to obtain a reference voltage (required for the pH_T calculation with Eq. 3 in SOP6a of Dickson et al., 2007) for every possible temperature in the microcosms. We omitted the step described by Dickson et al. (2007) that involves the use of AMP buffer to test for ideal Nernst behaviour of the electrode, but we note that we used a new, high-quality electrode for our measurements. Repeat measurements in buffers on different days during the experiment were within ± 0.005 pH units, suggesting limited drift and comparatively high precision.

Total alkalinity (TA) was determined every fourth day with an open-cell titration following SOP3b in Dickson et al. (2007) using a Metrohm 862 Compact Titrosampler coupled with an Aquatrode Plus with PT1000 temperature sensor. Between 52–61 g of sample was added to plastic beakers (weighed using a Mettler Toledo balance with a precision of ± 0.02 mg) and acclimated to room temperature. The samples were titrated in a two-step procedure: an initial increment of 2.5 mL of ~ 0.05 M HCl (dissolved in double deionized water enriched with 0.6 mol kg^{-1} NaCl) was added to the beaker, followed by a 300 s waiting period with constant stirring. Afterward, the titration continued with additions of 0.1 mL per time step (30–60 s between additions depending on drift). The titration curves were evaluated following Dickson et al. (2007) using the "calkulate" script within PyCO2sys by Humphreys et al. (2022). Certified reference material (CRM, batch 192) provided by Dickson were included in some analytical runs for accuracy control. In the runs where no CRMs were included, we included internal seawater standards (0.02 % $HgCl_2$ poisoned), which were thoroughly referenced against Dickson's CRMs. Although such a procedure is clearly not recommended, this was unavoidable due to the Coronavirus pandemic and CRM supply shortage. We note, however, that in analytical runs where both CRMs and internal standards were included, we calculated almost identical TAs, regardless of whether we used CRMs or internal standards for accuracy control. The deviation between duplicate measurements was usually below ± 3 µmol kg^{-1} and rarely above ± 5 µmol kg^{-1}, suggesting reasonable precision of the measurement.

Carbonate chemistry conditions were calculated from measured pH_T, TA, phosphate, silicate, salinity, and temperature, with equilibrium constants recommended by Orr et al (2015) (e.g. K1 and K2 from Lueker et al., 2000), using the "SIR_full" function in the carbonate chemistry software "seacarb" for R (Gattuso et al., 2021).

2.5 Flow cytometry sampling and analyses

Flow cytometry samples for phytoplankton (3.5 mL) and bacteria (1 mL) were collected with pipettes from the bottles used for particulate matter sample collection (see Sect. 2.3). Care was taken to gently mix the bottles before sub-sampling to avoid sedimentation bias. During the main phytoplankton bloom (days 4–10), we collected additional samples in between regular sampling days to achieve daily resolution. These samples were collected directly from the microcosms using pipettes (~ 5 cm below surface) after carefully stirring the microcosms as described in Sect. 2.3. Samples were immediately fixed with 100 µL of a formalin/hexamine mixture for phytoplankton and 20 µL glutaraldehyde for bacteria, stored at 4 °C for 25 min, and then flash-frozen in liquid nitrogen and stored at −80 °C until analysis 1–5 weeks later. For the measurements, samples were thawed at 37 °C, and then 500 µL for phytoplankton and 30 µL for bacteria were immediately analysed with the CYTEK Aurora flow cytometer. Phytoplankton populations were distinguished by encircling phytoplankton populations on the cytogram plots (also known as "gating") based on the signal strength of the forward light scatter (FSC) and several fluorescence colours (Fig. A2). Bacterial DNA was stained with SYBR Green I (diluted in dimethylsulfoxide) and added to samples in a final ratio of 1 : 10 000 (SYBR Green I : sample) prior to analysis. This allowed us to distinguish them from other particles in the size range of bacteria (Fig. A2). Small phytoplankton were distinguished from bacteria by excluding all particles with chlorophyll autofluorescence from the bacteria gate.

We used the FSC signal strength to estimate how much each phytoplankton group contributed to the total phytoplankton community during each day. For this calculation, we multiplied the abundance of each group within a given gate by the mean "FSC-area" signal strength measured for that group. Please note that "area" in FSC area refers to the integrated area below the FSC emission peak of each particle. We assume "area" to be the better metric for biomass estimates than the height of the FSC peak because elongated particles (e.g. diatom chains) will have a more-stretched-out FSC peak with a lower peak height.

2.6 Sediment traps

The butterfly valves at the bottom of the microcosms were initially closed so that no material could sink into the sediment collection cups. On day 4 we opened the butterfly valves, allowing water from the microcosms to enter the collection cups. This was done to enable the sedimentation of the large aggregates which had begun to flocculate within the microcosms (Fig. 1f, Video supplement 2). Due to the high effectiveness of our convection mixing mechanism, which kept large aggregates in suspension, we assisted the sedimentation process by turning off the heating and setting the room temperature to 12 °C for 24 h. On day 5 the butterfly valves were closed and the sediment collection cups were removed to take samples for flow cytometry and filtrations. Fifty millilitres of water containing sedimented material was collected with a 50 mL pipette from the base of each cup. These samples were collected in small plastic beakers and carefully homogenized before filtering TPC/TPN and BSi samples. Filtrations followed the same procedure as described above, with reduced volumes ranging between 0.5–

1 mL due to the increased concentrations of organic matter in the sediment slurry. After sampling, the cups were reattached to the corresponding microcosm, butterfly valves were opened, heating belts were turned on, and the room temperature returned to 7 °C. The same process was repeated on days 6–7 and 8–9, with the exception that the traps were emptied entirely and cleaned on day 9 before being reattached with the valves closed. Finally on day 12, the traps were reopened and any remaining aggregates allowed to drop out of suspension before sampling and removal of the traps from the microcosms for the remainder of the experiment. (Please note that the cleaning of collection cups during the last two samplings was conducted because the major sedimentation of organic material from the bloom was complete by day 9, and we wanted to avoid the leakage of nutrients from the collection cups back into the water column.)

2.7 Statistical analysis

We used generalized additive mixed models (GAMMs) to assess statistically significant differences in phytoplankton growth (abundance and biomass) as well as nutrient and particulate matter concentrations over the experimental period. GAMMs were fitted using R v. 1.4.1717 (RStudio Team, 2022), and the package "mgcv" (Wood, 2015). Prior to fitting the GAMMs, nutrient and particulate matter concentrations were $\log10(x)$ transformed and phytoplankton count data square root transformed. Four different models were fitted to explore the potential changes in temporal trends and absolute values of each parameter as a result of alkalinity treatments (Fig. 3). All models allowed temporal trends to occur with either no difference between treatments (model 1), differences in temporal trends between treatments but no difference in absolute values (model 2), differences in absolute values between treatments but not in temporal trends (model 3), or differences in both temporal trends and absolute values as a result of the treatments (model 4). Individual microcosms were fitted as a random intercept in each model to account for any unknown differences between the individual microcosms. In addition, heteroscedasticity and temporal autocorrelation of the residuals within models was visually assessed to ensure model assumptions were satisfied. Models were then compared by means of the Akaike information criterion (AIC), with lower AIC values indicating preferred models with an improved ratio between the explained variance and number of variables. Predictor variables included in the preferred models were considered to have a statistically significant influence on the assessed parameter. Plots with fitted smoothers and corresponding confidence intervals were produced using the models with the lowest AIC value. The occurrence of significant differences between the treatments and the control could then be visually assessed by the absence of overlapping smooths and their confidence intervals between the treatments.

3 Results

3.1 Carbonate chemistry and dissolved inorganic nutrients

The addition of NaOH (for the unequilibrated treatment) and NaOH and $NaHCO_3$ (for the equilibrated treatment) resulted in an increase in total alkalinity (TA) from $2164.6 \pm 3.1\,\mu mol\,kg^{-1}$ in the controls to $2660.1 \pm 8.4\,\mu mol\,kg^{-1}$ in the unequilibrated and $2665.2 \pm 2.2\,\mu mol\,kg^{-1}$ in the equilibrated microcosms (Fig. 4a). TA remained relatively constant at these levels, apart from minor increases within the first 8 d of $\sim 5\,\mu mol\,kg^{-1}$ likely due to the uptake of NO_x^- during the phytoplankton bloom. The addition of $NaHCO_3$ in the equilibrated treatment increased dissolved inorganic carbon (DIC) to $2406.1 \pm 2.1\,\mu mol\,kg^{-1}$, approximately $400\,\mu mol\,kg^{-1}$ more than the control (2019.1 ± 4.1) and the unequilibrated treatment (2007.9 ± 9.4) (Fig. 4c). DIC decreased during the bloom with the most pronounced decline in the control, consistent with the highest build-up of TPC (Figs. 4c, 5b). DIC gradually increased in all microcosms after bloom collapse, due to biomass respiration. CO_2 uptake from the atmosphere could have only had a small influence on DIC as the microcosms were tightly sealed and only opened for ~ 20 min per sampling day through a 2 cm opening. The different scenarios of alkalinity enrichment increased pH_T to 8.128 ± 0.009 (equilibrated) and 8.662 ± 0.005 (unequilibrated) relative to 7.945 ± 0.007 in the control (Fig. 4b). Changes in pH_T reflect the phytoplankton bloom with increasing pH_T until the peak of the bloom and gradually decreasing pH_T thereafter. The amplitude of the pH_T change during the bloom was mitigated by increased TA (Fig. 4b). However, the mitigation of the amplitude is obscured by the logarithmic nature of the pH scale, as it is important to consider absolute changes in the free proton ($[H^+]_F$) concentration as this reflects what organisms experience (Fassbender et al., 2021), Fig. 4d). fCO_2 was initially 489.2 ± 9.5 (control), 373.1 ± 8.4 (equilibrated), and 76.6 ± 0.9 µatm (unequilibrated) (Fig. 4e). The temporal trends were driven by the phytoplankton bloom and largely resembled those of $[H^+]_F$. Finally, the saturation state of the calcium carbonate ($CaCO_3$) mineral calcite ($\Omega_{calcite}$) was greatly elevated in the unequilibrated treatment with an initial value of 11.06 ± 0.03 in comparison to 2.59 ± 0.02 in the control and 4.61 ± 0.03 in the equilibrated treatment (Fig. 4f). $\Omega_{calcite}$ increased further during the bloom but gradually declined thereafter. Inorganic precipitation of $CaCO_3$ was not observed.

The water enclosed within microcosms was rich in dissolved inorganic nutrients due to winter mixing. This allowed a phytoplankton spring bloom to occur without further additions of nutrients. Initial nutrient concentrations were $6.39 \pm 0.19\,\mu mol\,L^{-1}$ for NO_x^-, $0.78 \pm 0.01\,\mu mol\,L^{-1}$ for PO_4^{3-}, and $9.65 \pm 0.39\,\mu mol\,L^{-1}$ for $Si(OH)_4$. Nutri-

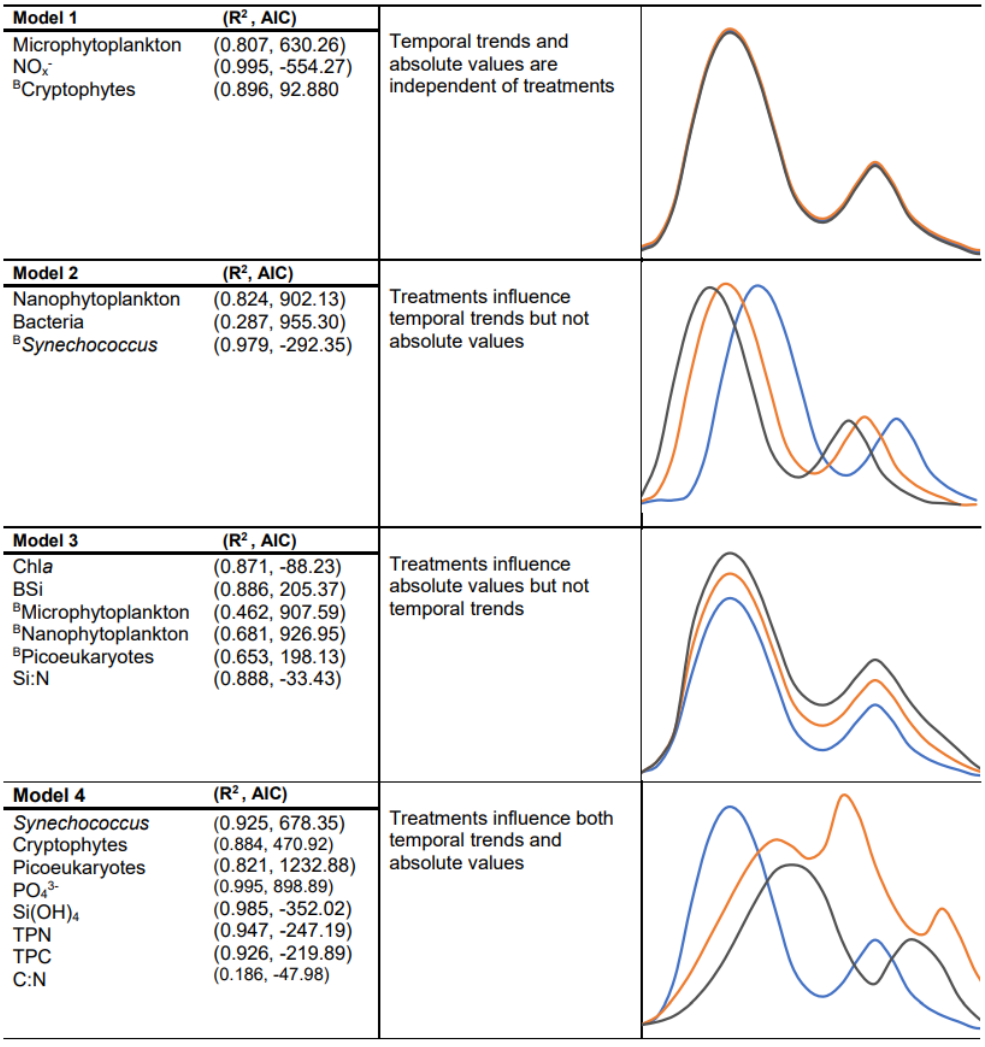

Figure 3. GAMM results (AIC and R^2) from the preferred model for each parameter with descriptive plots indicating the hypothesized smoothers for each model (phytoplankton biomass indicated with a ^{B} for each group). All smoothers had a p value < 0.05, indicating smoothers were significantly different from a straight line. For a given dependent variable, the model with the lowest AIC was considered to best represent the temporal trends during the experiment and is present in the figure above.

ent drawdown occurred from the onset of the experiment, with the most rapid drawdown occurring between days 4–7 (Fig. 4g, i). Statistical analysis of dissolved inorganic nutrient concentrations revealed the drawdown of PO_4^{3-} and $Si(OH)_4$ varied significantly between the control and treatments, whereas NO_x^- did not (Fig. 3g, h, i). Visual inspection of the PO_4^{3-} trends indicates that drawdown occurred slightly later in the unequilibrated and equilibrated treatments when compared to the control, although differences were small (Fig. 4h). The equilibrated treatment displayed elevated PO_4^{3-} values between days 10 and 14, although again the difference was small. The drawdown of $Si(OH)_4$ was slightly delayed and considerably slower in the unequilibrated treatment and even more so in the equilibrated treatment (Fig. 4i). In the controls, $Si(OH)_4$ was fully depleted on day 8 while depletion continued gradually in the equilibrated and unequilibrated treatments after the bloom but did not show complete depletion until the end of the experiment (Fig. 4i).

3.2 Particulate matter and chlorophyll *a* dynamics

The drawdown of inorganic nutrients early in the experiment coincided with increasing Chl *a*, TPC, TPN, and BSi concentrations (Figs. 5a–d). After the peak of the phytoplankton bloom on day 6, Chl *a*, TPC, TPN, and BSi declined relatively quickly until day 8–10 and continued to decline at a slower rate until the end of the experiment. The alkalinity treatments had a significant influence on the temporal trends and absolute values of TPC and TPN while they only influenced the absolute values of Chl *a* and BSi (Figs. 3, 5a–

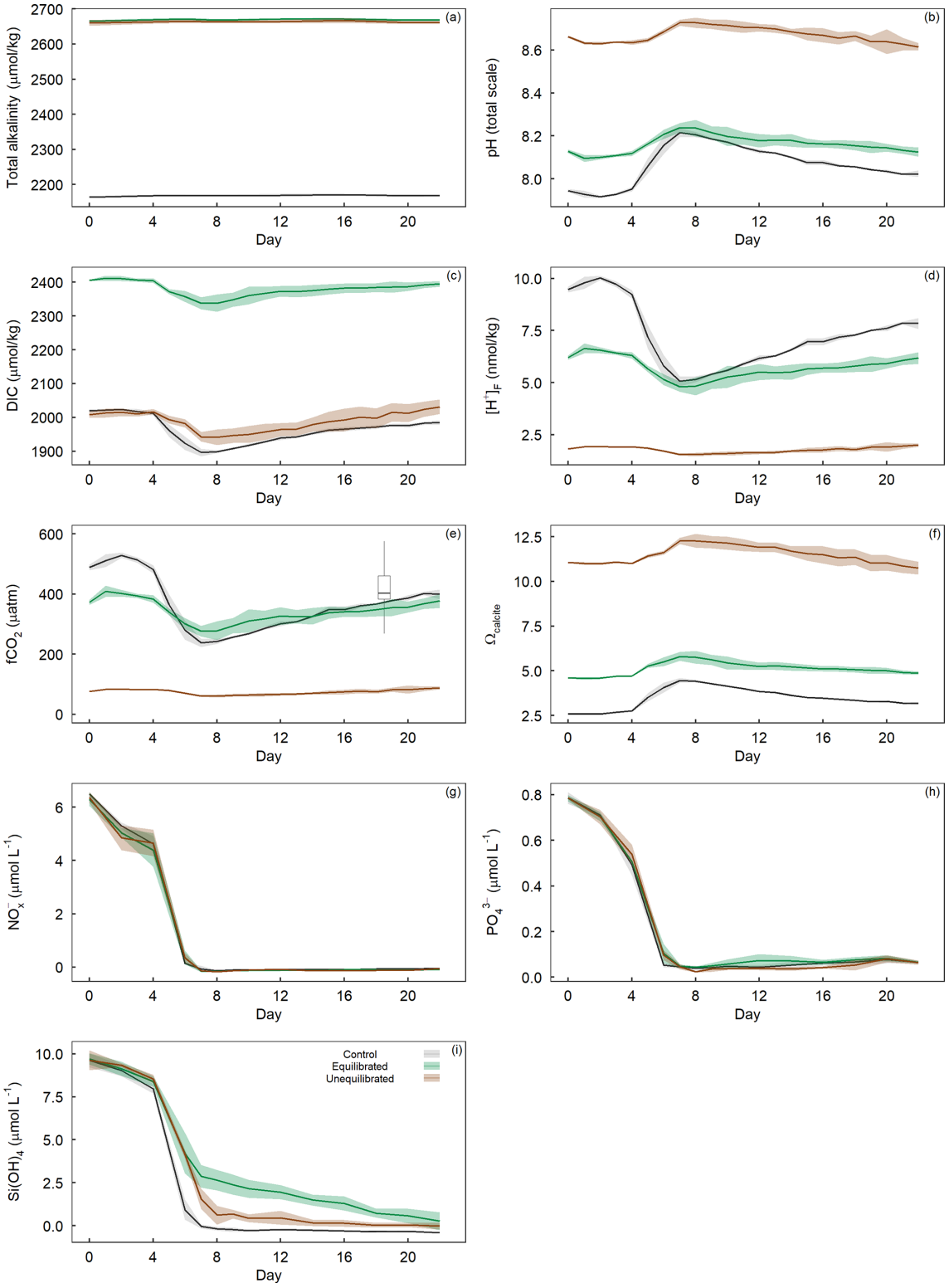

Figure 4. Temporal variation in measured **(a)** total alkalinity, **(b)** pH_T, and calculated **(c)** dissolved inorganic carbon, **(d)** proton concentration on the free scale ($[H^+]_F$), **(e)** fCO_2 with overlaid boxplot illustrating the range of fCO_2 observed in the Derwent/Storm Bay area, Tasmania (42.84–43.10° S, 147.46–147.31° E), based on 10 857 measurements between 1993–2019 (Bakker et al., 2016), **(f)** $\Omega_{calcite}$, as well as dissolved inorganic **(g)** nitrate + nitrite concentrations, **(h)** phosphate concentration, and **(i)** silicate concentration within the treatment groups. Coloured shading around the respective means represents standard deviation within a treatment group.

d). Visual inspection of the data revealed similar trends in TPC and TPN, with control microcosms displaying greater concentrations after the bloom phase for both parameters (Fig. 5b, c). Differences between the treatments were less apparent for Chl *a*, with visual inspection of the trends revealing minimal differences (Fig. 5a). In contrast, BSi trends supported the significant difference observed in the model selection process as well as the silicate trend, with control microcosms displaying elevated levels of BSi across most of the experimental period (Fig. 5d).

Stoichiometric ratios

The molar ratio of TPC to TPN (C : N) varied both temporally and in absolute values as a result of the alkalinity treatments. C : N declined from the initiation of the experiment until the bloom phase, with the ratio of C : N then rising rapidly in the control when compared to the alkalinity treatments, which displayed a delayed increase and lower absolute C : N value (Fig. 5e). After the bloom phase, the C : N ratio was more variable between microcosms, with the control and unequilibrated treatment having a higher C : N in comparison to the equilibrated treatment. Differences in the drawdown of inorganic nutrients, particularly PO_4^3 and $Si(OH)_4$ (Fig. 4), may have enabled or amplified differences in organic matter stoichiometry, which developed in the post-bloom period. However, it is important to keep in mind that such developments (when significant) were ultimately caused by the treatments, even if they are indirectly induced by direct effects on nutrient drawdown that occurred earlier in the experiment. Similar trends in the ratio of C : N between the treatments were also visible in the sediment collection cups, with discernibly greater values in the control and unequilibrated treatment, compared to the equilibrated treatment (Fig. 5g). The ratio of BSi to TPN (Si : N) declined rapidly from the onset of the experiment, with two small increases on day 8 and 15 (Fig. 5f). Statistical analysis of the trend revealed the control to have a marginally higher Si : N despite the unequilibrated treatment being the greatest at the two peaks. There was no discernible difference between treatments for Si : N ratios of organic matter from the sediment collection cups (Fig. 5h).

3.3 Changes in the phytoplankton community determined via flow cytometry

The GAMM analyses of flow cytometry count data revealed microphytoplankton to be unaffected by alkalinity enrichment, while nanophytoplankton and bacteria showed a shift in temporal trends and *Synechococcus*, cryptophytes, and picoeukaryotes exhibited a shift in both temporal and absolute counts (Fig. 3). In contrast, relative biomass contributions by cryptophytes were unaffected by alkalinity treatments, whereas contributions by *Synechococcus* displayed shifts in temporal trends, and those by picoeukaryotes, nanophytoplankton, and microphytoplankton displayed shifts in absolute biomass (Fig. 3). *Synechococcus* was initially abundant, but due to their small size their contribution to total biomass was only $\sim 4\,\%$ (Fig. 6a, b). *Synechococcus* abundance declined from the start of the experiment in both alkalinity treatments, while the decline occurred 2 d later in the control (Fig. 6a). There were also significant temporal differences between treatments in *Synechococcus* biomass, with an earlier decline in the equilibrated treatment followed by the control and then unequilibrated treatment (Figs. 3, 6b). After day 8, *Synechococcus* abundance remained close to the detection limit and provided minimal contribution to the plankton community biomass thereafter (Fig. 6a, b). Picoeukaryote abundance and biomass showed little variation between the control and equilibrated treatment throughout the experiment but was significantly smaller and slightly delayed in the unequilibrated treatment during the bloom (Fig. 6c). This trend was reflected in the biomass contribution of picoeukaryotes, which was notably lower in the unequilibrated treatment during the bloom (Fig. 6d). Cryptophytes contributed up to 20 % to the total plankton biomass with no temporal or absolute difference between treatments (Fig. 3). Cryptophyte abundance was significantly elevated and peaked earlier in the control compared to the two alkalinity treatments. After the bloom, cryptophyte abundance declined close to or below the detection limit in all treatments and did not contribute significantly to total phytoplankton biomass thereafter (Fig. 6e, f). Nanophytoplankton abundance increased during the bloom phase of the experiment, but there was no significant difference observed between the treatments. However, during the post-bloom phase, abundances were significantly elevated in the unequilibrated treatment (Fig. 6g). The nanophytoplankton group initially contributed $\sim 60\,\%$ to phytoplankton biomass, with marginally greater biomass in the unequilibrated treatment in comparison to the equilibrated treatment over the extent of the experimental period (Fig. 6h). Microphytoplankton abundances increased during the bloom and peaked on day 6, but as analysis revealed model 1 to be the preferred model, we conclude that there were no statistically significant differences between the treatments (Figs. 3, 6i). However, there was a significant trend in microphytoplankton contribution to total biomass, with a peak of $\sim 35\,\%$ during the bloom phase before dropping to $\sim 1\,\%$–$25\,\%$ for the remainder of the experiment (Fig. 5j). Microphytoplankton contributed marginally but significantly more biomass in the control microcosms during the last 6 d of the study (Fig. 5j). Finally, bacteria showed variations in temporal trends as a result of the treatments with a greater abundance in high-alkalinity treatments during the phytoplankton bloom and more constant abundances throughout the experiment, whereas abundances in the control were low during the bloom but increased rapidly thereafter (Fig. 5k).

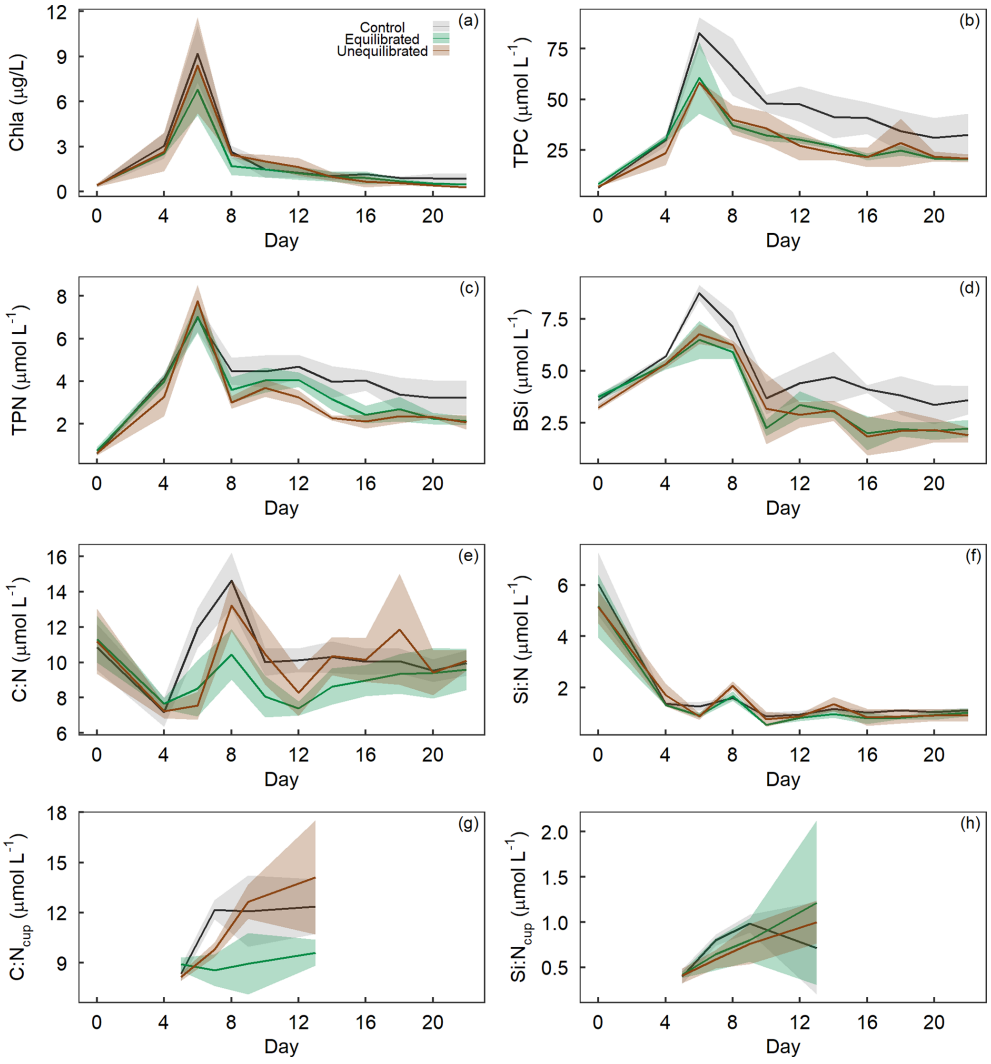

Figure 5. Temporal trends of **(a)** chlorophyll *a*, **(b)** total particulate carbon, **(c)** total particulate nitrogen, and **(d)** biogenic silica concentrations, as well as molar ratios of **(e)** TPC to TPN and **(f)** BSi to TPN within microcosms and molar ratios of **(g)** TPC to TPN and **(h)** BSi to TPN within sediment collection cups, denoted by "C : N_{cup}" or "SI : N_{cup}". Coloured shading around the respective means represents the standard deviation.

4 Discussion

Alkalinity had a noticeable influence on the characteristics of the phytoplankton bloom and associated succession of the phytoplankton community. However, finding unequivocal explanations for how alkalinity altered succession patterns is very difficult in this form of community experiment due to the numerous degrees of freedom in complex food webs. Therefore, we use the discussion henceforth to present potential explanations, which we believe to be particularly plausible while emphasizing that none of these can be exclusively proven or excluded. This leads to many speculations with regards to data interpretation as the reader will likely notice in the text below. However, our observations are still highly valuable as they reveal important patterns and any strong effects of alkalinity on components of the phytoplankton community that can then be investigated in more targeted future studies.

4.1 Treatment effects on chlorophyll *a*, carbon, nitrogen, and silicon dynamics

4.1.1 Build-up of chlorophyll *a* during the phytoplankton bloom

A significant difference in chlorophyll *a* of $\sim 3\,\mu g\,L^{-1}$ was observed between the control and equilibrated treatments during the peak of the phytoplankton bloom, while no significant differences were observed between the control and unequilibrated treatment. The lower peak chlorophyll *a* in the equilibrated treatment was unexpected as CO_2 and H^+,

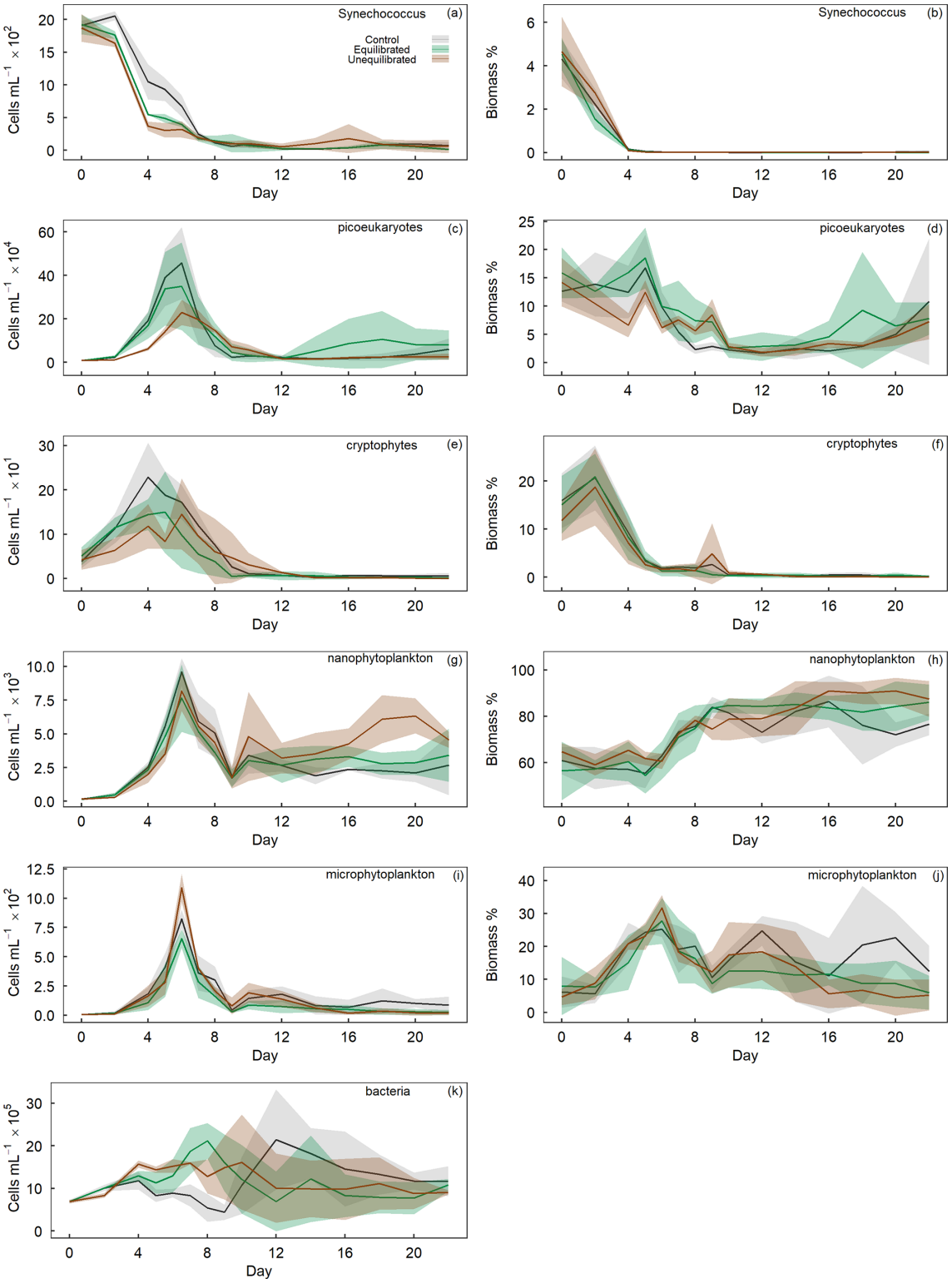

Figure 6. Temporal trends of phytoplankton group abundance (left column) and percent biomass contribution (right column) determined by flow cytometry. Group names provided in the top right of each plot. Coloured shading around the respective means represents standard deviation within a treatment group.

two carbonate chemistry parameters believed to drive phytoplankton growth (Paul and Bach, 2020), were relatively similar to the control and within natural ranges (Fig. 4d, e). We suspect the low peak in chlorophyll *a* concentration may be due to differences in the predominant species driving chlorophyll *a* build-up. This is supported by careful inspection of the raw flow cytometry data where we noticed that different types of phytoplankton occurred within the flow cytometry gate denoted as nanophytoplankton (Fig. A3). The majority of the population was closer to the upper edge of the nanophytoplankton gate in the equilibrated treatment in comparison to the control on day 6. Although speculative, lower concentrations of chlorophyll *a* could also be due to increased grazing in the equilibrated treatment. However, the influence of grazing was not assessed in this study.

In contrast, and even more unexpected, there was no significant difference in peak chlorophyll *a* between the control/equilibrated and the unequilibrated treatment. The fCO_2 was as low as $\sim 70\,\mu atm$ in the unequilibrated treatment, which is substantially lower than what is encountered by phytoplankton in coastal Tasmania over the course of a season (Figs. 4e, A4; see also Pardo et al., 2019). Previous studies have revealed that growth rates of phytoplankton are relatively unaffected by low CO_2, as long as CO_2 concentrations are only mildly reduced (Riebesell et al., 1993, Wolf-Gladrow et al. 1999). However, rapid declines in growth were frequently observed once CO_2 concentrations fell below species-specific thresholds, with such thresholds usually being well above 70 µatm (Riebesell et al., 1993; Chen et al., 1994; Hinga, 2002; Berge et al., 2010; Paul and Bach, 2020). Based on these studies, we expected a delay in the peak of the phytoplankton bloom and/or reduced bloom intensity. The fact that neither of these occurred suggests (1) that the phytoplankton species growing during the bloom were unaffected by (i.e. well adapted to) low CO_2 or (2) that certain species within the community were adapted to low CO_2 and could compensate for less well-adapted species. While our data do not provide a definitive answer to this, there are two arguments that favour the second explanation. First, BSi build-up and corresponding $Si(OH)_4$ drawdown strongly suggest that the alkalinity treatments affected the diatom community during the bloom. Second, there were significant differences in picoeukaryote and cryptophyte abundances during the bloom, with lower abundance and contribution to biomass in the unequilibrated treatment (see Sect. 4.3 for further discussion on picoeukaryote responses). Together, these observations suggest that the addition of alkalinity without immediate CO_2 equilibration with the atmosphere may have less of an impact on phytoplankton bloom dynamics than previously thought. However, phytoplankton species composition may still be affected, with implications for energy transfer to higher trophic levels and biogeochemical fluxes, both of which are strongly dependent on phytoplankton species composition (Mallin and Paerl, 1994; Wassmànn, 1997).

4.1.2 Carbon and nitrogen dynamics

TPC, TPN, and the C : N ratio were all significantly greater in the control compared to the high-alkalinity treatments during the phytoplankton bloom (days 4–8). In contrast, minor differences were observed between the two alkalinity treatments during this period. Previous experiments have shown that carbonate chemistry conditions can affect the build-up and stoichiometric relationship of organic carbon and nitrogen, but the effect is highly variable and dependent on the composition of the plankton community (Taucher et al., 2020). The key outcome reported by Taucher et al. (2020) was that heterotrophic processes seem to have an important influence on C : N stoichiometries. Consistent with their observation, we observed significant increases in TPC and C : N in the control during the bloom, while bacterial abundances remained relatively low (compare Figs. 5e, 6k). In contrast, bacterial abundances were significantly higher in the alkalinity treatments, indicative of higher respiratory activity, which may have limited the build-up of TPC (Figs. 5e, 6k). Furthermore, differences in diatom growth and/or community composition between the control and the alkalinity treatments (discussed in Sect. 4.1.3) can also offer a direct explanation for the differences in TPC build-up and C : N ratios observed during the bloom. Diatoms often dominate phytoplankton blooms where they exude DOC, which partially aggregates to form "transparent exopolymer particles" (TEPs) (Passow, 2002). TEPs have high C : N ratios which commonly exceed the Redfield ratio (Engel and Passow, 2001) and would be part of the TPC pool measured in our study. The production of TEPs has been found to vary significantly between diatom species, with a laboratory study revealing four species to produce significantly different concentrations of TEPs per cell volume (Fukao et al., 2010; Passow, 2002). As such it is plausible that alkalinity treatments altered the abundance and/or composition of the diatom community (see Sect. 4.1.3.), leading to fewer TEPs, measurable as higher TPC build-up and C : N.

Diatoms are between a few micrometres to a few millimetres in size (Armbrust, 2009). The largest diatom cells in our experiment were roughly 50 µm, and we did not find any diatoms smaller than 3 µm (determined from SEM). Thus, all diatom cells are most likely found in the nano- and microphytoplankton groups in flow cytometry data. Although not statistically significant, visual inspection of microphytoplankton abundance during the peak of the bloom (day 6) revealed greater abundances in the unequilibrated treatment followed by the control and then equilibrated treatment. This indicates differences in the phytoplankton communities between the treatments and the control with potential influence on TPC build-up and C : N ratios. In addition, significant differences in the build-up of BSi and drawdown of $Si(OH)_4$ between the control and treatments strongly suggests that the alkalinity treatments influenced the diatom communities.

In summary, the evidence provided herein suggests that the altered carbonate chemistry conditions due to elevated alkalinity caused changes in the autotrophic and heterotrophic communities which collectively altered TPC build-up and C : N ratios. Accordingly, anthropogenic increase in ocean alkalinity may have the capacity to influence ecological processes, with implications for biogeochemical processes. Crucial next steps are to confirm such impacts in community studies, other environments, and to reveal the underlying mechanism(s) responsible for triggering the observed community changes in response to alkalinity additions.

4.1.3 Biogenic silica and dissolved inorganic silicate drawdown

Scanning electron microscopy investigations of samples taken before, during, and after the phytoplankton bloom revealed that diatoms were the only silicifiers detected in the plankton community. Therefore, the drawdown of $Si(OH)_4$ and build-up of BSi within microcosms can be attributed to the diatom community. BSi increased during the peak bloom before declining and remaining rather constant from day ~ 12 onwards, with significantly higher concentrations in the control than in the alkalinity treatments (Fig. 5d). The greater concentration of BSi in the control is consistent with a more complete drawdown in $Si(OH)_4$ (Figs. 4i, 5d). There was no significant difference observed in the build-up of BSi between the two alkalinity treatments even though the drawdown of $Si(OH)_4$ was significantly greater in the unequilibrated treatment. There are two Si pools that were not quantified in our study where the additional Si consumed in the unequilibrated treatment could have gone. These are (i) the walls of the microcosms where benthic diatoms may have grown and consumed Si or (ii) the sediment traps where relatively more BSi from sinking diatoms may have been collected (please note that we quantified elemental ratios of sinking organic matter collected in the sediment traps but not total mass flux as this requires sampling of all collected material for which we did not have the capacity).

The significant and pronounced differences in $Si(OH)_4$ drawdown and BSi build-up between the control and the alkalinity treatments are arguably one of the most striking observations in this experiment. It suggests that alkalinity enhancements and associated changes in carbonate chemistry can have considerable effects on diatom communities. Carbonate chemistry changes invoked by simulated ocean acidification have been shown to have a significant influence on BSi content, silicate metabolism, growth, and diatom silicification (Milligan et al., 2004; Hervé et al., 2012; Petrou et al., 2019) albeit the sign and magnitude of diatom responses were species-specific and dependent on the communities investigated (Pedersen and Hansen, 2003; Bach and Taucher, 2019; Petrou et al., 2019). To the best of our knowledge, there is currently no established mechanistic framework that can explain the variable responses of diatoms to carbonate chemistry, although useful concepts exist that link the carbonate chemistry sensitivity to diatom size (Flynn et al., 2012; Wolf-Gladrow and Riebesell, 1997; Wu et al., 2014). The observation is also remarkable because the differences in BSi occur between the control and both alkalinity treatments even though differences in CO_2 and $[H^+]_F$ are much larger between the equilibrated and unequilibrated alkalinity treatments (Fig. 4d, e). This suggests (i) that an unexpected factor in the carbonate chemistry drove the diatom response or (ii) that the carbonate chemistry effect on diatoms was indirect, e.g. transmitted through altered grazing pressure. The second scenario could for example be caused by the additions of acid and base in the treatments, which may have harmed the grazers and affected the grazing pressure. Either of these (or other) physiological and/or ecological explanations for the treatment effects on $Si(OH)_4$ drawdown and BSi build-up should be visible as a change in the diatom abundance and/or community composition. For example, there could be a shift in the diatom community towards smaller, less heavily silicified species and/or a higher fraction of non-silicifying phytoplankton. To explore this possibility, we analysed the diatom community at peak bloom (day 6) via scanning electron microscopy. However, there were no clear differences in composition or biovolume of the diatom community between the control and alkalinity treatments on day 6 (Fig. A5). Furthermore, ratios of carbon to silica did not differ between treatments across the experimental period supporting SEM count data (Fig. A6). Thus, although we suspect that shifts within the diatom community were responsible for the observed differences in silicon dynamics, we are currently unable to provide a definitive mechanism for these observations.

4.2 Treatment effects on the phytoplankton community determined via flow cytometry

The aim of this experiment was to assess the influence of alkalinity enhancement on the various stages of a spring bloom. This included periods at which nutrients were in excess, declining, and depleted. The effect of nutrient depletion on the phytoplankton community in the absence of enhanced alkalinity was observable in the control treatment. However, it is possible that OAE treatments affected nutrient drawdown during the bloom so that differential nutrient concentrations in the post-bloom phase amplified the emerging differences between the control and OAE treatments. Alkalinity treatments were found to significantly influence the abundance and biomass of five out of the six phytoplankton groups assessed via flow cytometry and analysed using GAMMs (Fig. 3). The majority of the detected differences were in absolute values during the peak bloom and small temporal shifts between treatments.

Comparatively pronounced differences between treatments and the control were identified within the groups *Synechococcus*, cryptophytes, and picoeukaryotes, where alkalinity treatments negatively influenced abundance during the

bloom phase and/or delayed the peak bloom. The unequilibrated treatment had the greatest influence on these groups, suggesting that the significantly lower concentration of CO_2 and/or increased pH negatively affected these groups. Previous micro- and mesocosm research on ocean acidification has found variable responses of *Synechococcus* and cryptophytes, indicating that their responses to carbonate chemistry may be (i) population-specific, thus varying between experiments, or (ii) transmitted indirectly through food web interactions, which also vary across experimental communities (Sala et al., 2016; Schulz et al., 2017; Bach et al., 2017).

The response of picoeukaryotes to ocean acidification (i.e. increasing CO_2, declining pH) has been remarkably consistent through experiments in various climatic and experimental settings (Thomson et al., 2016; Maugendre et al., 2015; Sala et al., 2016; Schulz et al., 2017; Davidson et al., 2016; Hoppe et al., 2018; Newbold et al., 2012; Schaum et al., 2012; White et al., 2020). Our results are consistent with these findings as we reveal the opposite trend occurred when carbonate chemistry changes were reversed; i.e. when we decrease CO_2 and increase pH, we observe a reduction in picoeukaryote abundance. This is illustrated by the equilibrated treatment where relatively small differences in CO_2 and pH result in little to no differences in picoeukaryote abundance, whereas large differences between the control and unequilibrated treatment had a pronounced effect on picoeukaryote abundance (Fig. 6c). It has been speculated that the influence of CO_2 on picoeukaryotes is due to their increased reliance on diffusive CO_2 entry in comparison to other functional groups which rely more heavily on carbon concentrating mechanisms (CCMs) and the substantially larger HCO_3^- pool (Crawfurd et al., 2016; Meakin and Wyman, 2011; Engel et al., 2008). The operation of CCMs is energetically costly; however, larger cells have been revealed to be more efficient at transporting carbon using CCMs with a reduction in CO_2 leakage as a function of size (Engel et al., 2008; Malerba et al., 2021). Within this framework, smaller cells such as picoeukaryotes would be at a disadvantage at lower CO_2 concentrations in comparison to larger cells (Malerba et al., 2021; Meakin and Wyman, 2011). Our results support this as picoeukaryotes were apparently more sensitive to low CO_2 or high pH than the larger phytoplankton groups such as microphytoplankton (discussed below).

Differences between the treatments were less apparent for the nanophytoplankton group, with no differences during the bloom phase and slightly greater abundance during the post-bloom phase for the unequilibrated treatment. The nanophytoplankton group contributed the largest proportion to total biomass of all the assessed groups, increasing from 55 %–65 % at the initiation of the experiment up to 95 % at the end. The nanophytoplankton cluster in the flow cytometer is usually variable across or within treatments as there are many species in this approximate size range that could be captured. It is therefore possible, if not likely, that there was a succession towards different nanophytoplankton species between the control and treatments, which may explain different succession patterns. Treatment-specific differences in nanophytoplankton abundances are usually hard to interpret as it is mostly unclear what species are contributing to the cluster and what physiological/ecological responses to perturbation we can expect.

The microphytoplankton group did not display statistically significant differences in absolute abundances or temporal shifts for cell counts. However, as discussed in Sect. 4.1.2, we argue that there may have been higher microphytoplankton abundances in the unequilibrated treatment during the peak of the phytoplankton bloom (Fig. 6i), but this was too short to be detected as a significant difference in the statistical analysis. The absence of a negative effect of low CO_2 and high pH in the unequilibrated treatment was surprising as theory predicts more pronounced constraints on diffusive CO_2 uptake of larger phytoplankton species (Wolf-Gladrow and Riebesell, 1997; Flynn et al., 2012). Our experimental approach does not reveal how this absence of an effect could be explained. As argued in Sect. 4.1.2 and 4.1.3, we speculate that the most likely explanation is a shift in the species composition where species that are more capable at low-CO_2 and high-pH conditions may have compensated for those with reduced capacity. This important observation warrants further investigation.

4.3 Implications of the environmental assessment of ocean alkalinity enhancement

The amount of alkalinity added in our experiment increases the capacity of seawater to store atmospheric CO_2 by 21 %. It is crucial to understand that this is a massive enhancement of the inorganic carbon sink of seawater. For example, 21 % of all DIC in the ocean equals ~ 8000 GtC, > 10 times more than all carbon emissions since 1750 (Friedlingstein et al., 2019). The inadvertent effect of a 21 % sink enhancement on the phytoplankton community seems justifiable in our experiments in relation to the substantial benefits such permanent ($>>1000$ years) CO_2 storage would have for the climate. Other marine CO_2 removal methods such as ocean iron fertilization are likely associated with at least equally pronounced perturbations of the phytoplankton community (Quéguiner, 2013), for the benefit of an approximately 1 % non-permanent (< 100 years) enhancement of the marine carbon sink observed during mesoscale iron fertilization experiments in the Southern Ocean (Bakker et al., 2005).

One particularly interesting observation was that the unequilibrated alkalinity treatment was not noticeably more affected by the perturbation than the equilibrated treatment (Figs. 5, 6), despite substantially larger differences in carbonate chemistry relative to the control (Fig. 4). This is of significant importance as equilibrated alkalinity additions will likely be associated with additional costs, due to engineering efforts and energetic requirements of equilibrating sys-

tems (e.g. CO_2 bubbling and associated pumping). However, the release of alkalinity into the marine environment without a controlled influx of atmospheric CO_2 leads to verification challenges as it remains unclear where and when the CO_2 influx will occur (Orr and Sarmiento, 1992; Gnanadesikan and Marinov, 2008; Bach et al., 2021). Verification is important to refinance and incentivize CO_2 removal efforts (Hepburn et al., 2019; Rickels et al., 2021). Thus, if not for environmental reasons, an engineered and controlled influx of atmospheric CO_2 after alkalinity additions as tested in the equilibrated treatment may still be important for economic reasons.

One limitation of our experimental microcosm setup was the consistently high alkalinity ($+498 \pm 5.2\,\mu mol\,kg^{-1}$) in the treatments for the entire 22 d experiment. In real-world OAE applications, alkalinity-enriched seawater from point sources (e.g. electrochemical facilities, de Lannoy et al., 2018) or mineral-powder-enriched surface ocean areas (Renforth and Henderson, 2017) will be diluted over time with surrounding seawater of lower alkalinity. The degree of dilution with unperturbed water is site-specific and depends on the type of application (e.g. more dilution for a small point source in a system with high mixing rates). It can be expected that the dilution of alkalinity-enriched seawater would weaken the impact of alkalinity on the plankton community because of decreasing changes in carbonate chemistry relative to the non-perturbed state. Thus, our experimental setup simulated a relatively high intensity of perturbation as any impact mitigation through dilution is excluded.

OAE can be achieved through a variety of approaches, ranging from distributing pulverized minerals onto the sea surface to splitting water into acid and base using electrochemistry (Renforth and Henderson, 2017). All methods seek to increase surface ocean alkalinity, but the by-products generated in the various processes are highly variable. In this study, we utilized laboratory grade NaOH to increase the alkalinity of microcosms, a perturbation scenario representative of OAE via the electrochemical splitting of water (de Lannoy et al., 2018). Here, no other chemicals than strong acid (HCl) and base (NaOH) are generated, and only the base is released into the surface ocean (de Lannoy et al., 2018; Tyka et al., 2022). OAE approaches associated with the release of other bioactive components such as trace metals could have more substantial effects on the plankton community. We emphasize this aspect to stress that our observations of relatively moderate impacts of equilibrated and unequilibrated alkalinity perturbations cannot be generalized for all OAE approaches. From this perspective, our simulated perturbation arguably tested a mild version of OAE. The environmental assessment of OAE needs to remain in close contact with geochemical research in order to anticipate which OAE approaches have the greatest chance for upscaling. This will allow for a targeted assessment of the perturbations associated with the OAE approaches most likely to be implemented in the future.

5 Conclusion and outlook

This study is the first study to report on the effects of OAE on a coastal plankton community. Our key findings are the following.

1. Two different scenarios of alkalinity enhancement (CO_2 equilibrated with the atmosphere and unequilibrated) had a significant influence on the succession of the phytoplankton community and heterotrophic bacteria.
2. There were pronounced effects of alkalinity enhancement on diatoms even though dissolved Si concentrations were not manipulated in this study.
3. Consistent with previous research on ocean acidification, we found that low-CO_2/high-pH conditions are detrimental for picoeukaryote phytoplankton.
4. Surprisingly, the unequilibrated alkalinity treatment did not have a noticeably greater effect on the phytoplankton community than the equilibrated treatment, despite much larger changes in physiologically important carbonate chemistry parameters.

Altogether our findings suggest that sudden increases in alkalinity leave a noticeable imprint on the succession of the phytoplankton community. However, as highlighted in the concluding sentence of the abstract, the environmental effects investigated here appeared to be moderate when compared to the enormous climatic benefit of increasing the inorganic carbon sink of seawater by 21 %.

It is generally problematic to quantify changes in plankton communities as positive or negative as this depends on the perspective. More than two decades of ocean acidification research have shown that there will be winners and losers in plankton communities when carbonate chemistry is perturbed (Schulz et al., 2017; Alvarez-Fernandez et al., 2018; Taucher et al., 2020). These shifts were often perceived as negative (Falkenberg et al., 2020; le Quesne et al., 2012; Doney et al., 2020) but occasionally also as positive (Sswat et al., 2018; le Quesne et al., 2012). Mixed (or perspective-dependent) outcomes can also be expected for the assessment of OAE. From a human perspective, plankton community shifts affecting trophic transfer and ultimately fish production are comparatively easy to quantify as positive or negative. Our dataset did not provide insights on this aspect as we focussed only on the lowest trophic level. It is possible that the seemingly moderate effects of alkalinity observed at the lowest trophic level could have been amplified in higher trophic levels. Future studies should aim for a comprehensive assessment of higher trophic levels to better understand how lower trophic level change affects upper trophic levels and also to reveal potential top-down effects of OAE. Furthermore, other pelagic and benthic ecosystems, from arctic to tropical, need to be investigated to gather a reliable and comprehensive assessment of OAE effects on marine ecosystems. This study can therefore only be seen as a small first step.

Appendix A

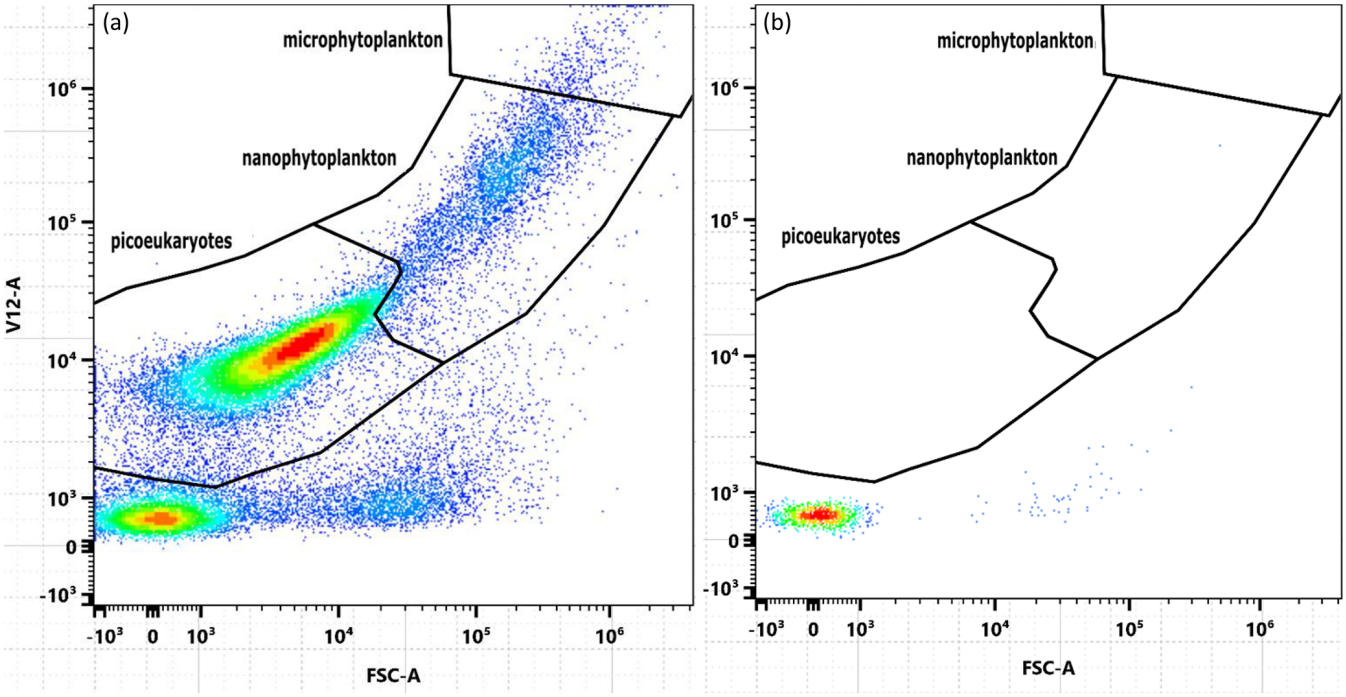

Figure A1. Cytograms used to determine the size of particles filtered by QMA filters used in TPC and TPN analysis. Plot **(a)** depicts a water sample filtered through a QMA filter (2.2 µm) and plot **(b)** an unfiltered sample. Both plots were produced using the same sample from microcosm M4 on day 6.

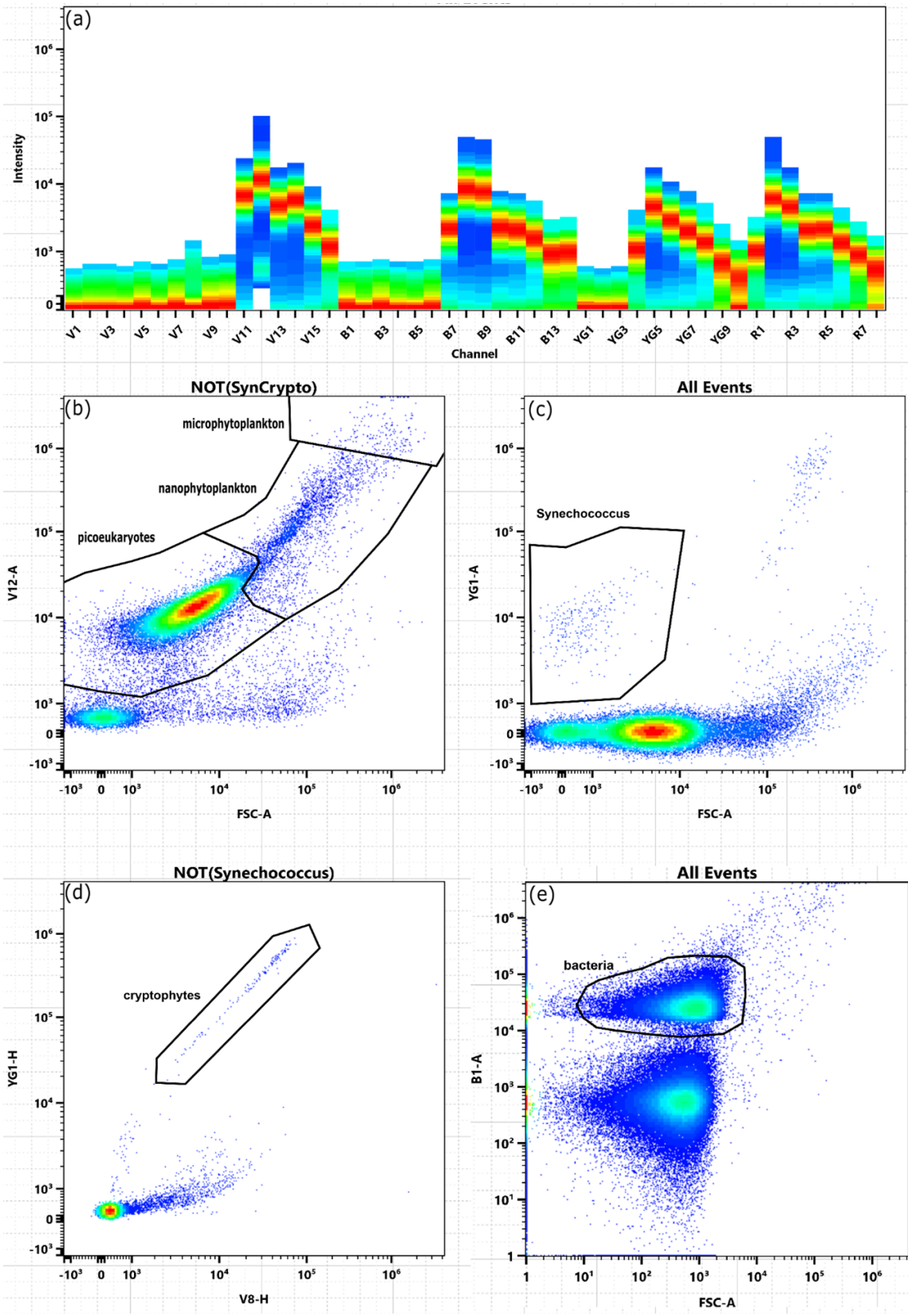

Figure A2. Gating strategy when analysing data via flow cytometry. Plot **(a)** illustrates the intensity of fluorescence for each channel in the total sample. Plots **(b)**–**(d)** show gates for picoeukaryotes, nanophytoplankton, microphytoplankton, *Synechococcus*, and cryptophytes in microcosm M3 on day 5. Plot **(e)** shows the gate for bacteria in microcosm M4 on day 12.

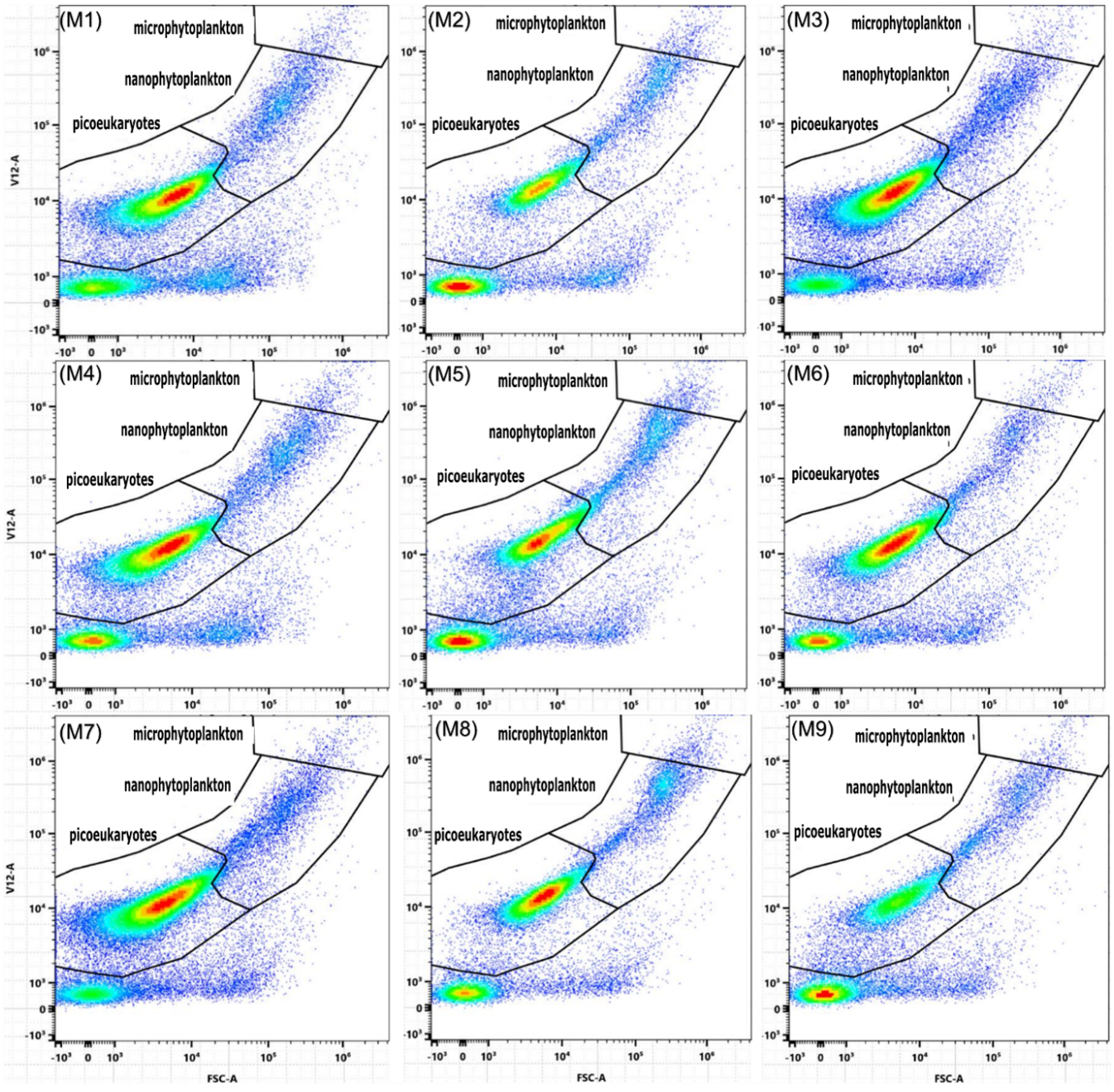

Figure A3. Cytograms depicting differences within gates, between treatments. Plots are labelled according to corresponding microcosms so that M1, M4, and M7 represent the unperturbed control; M2, M5, and M8 represent the unequilibrated treatment; and M3, M6, and M9 represent the equilibrated treatment. All plots are from samples taken during the peak bloom on day 6.

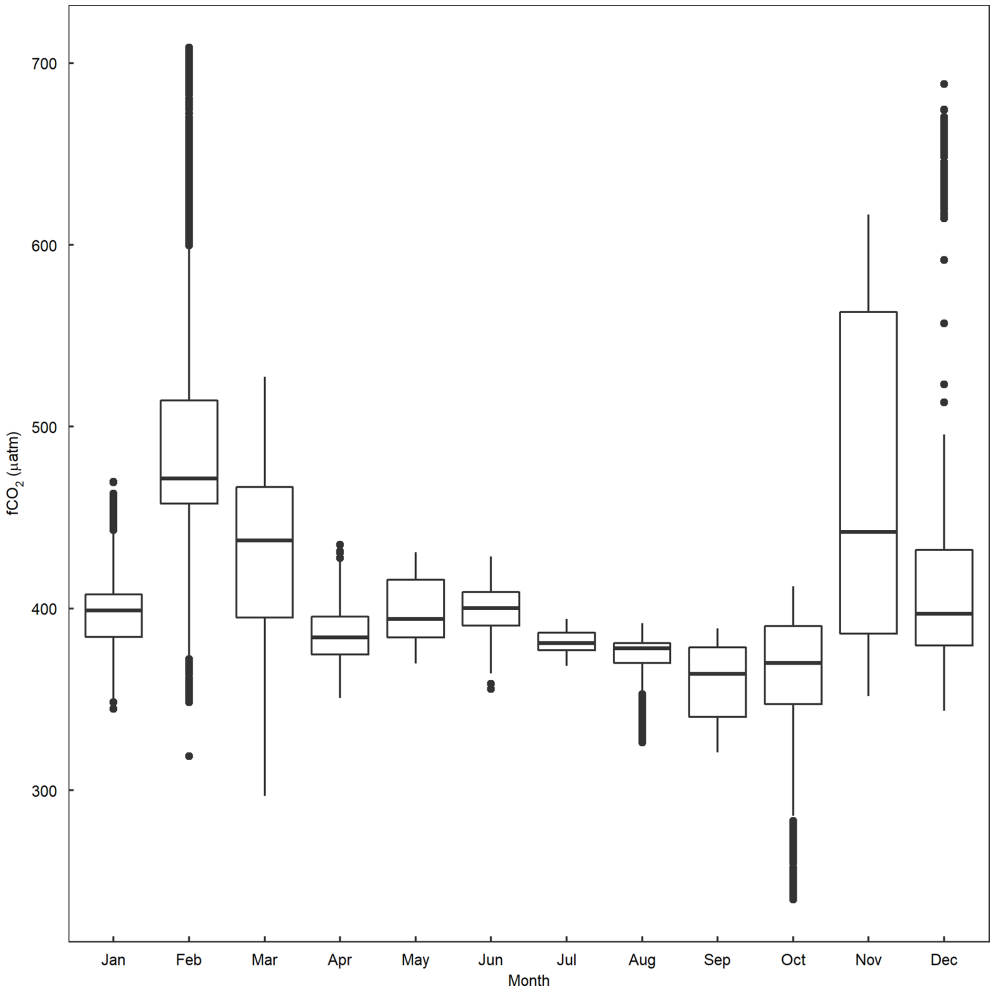

Figure A4. Boxplot depicting seasonal values of fCO_2 recorded between 1993–2019 at Storm Bay (43.1–42.8442° S, 147.307–147.46° E), Tasmania (Bakker et al., 2016).

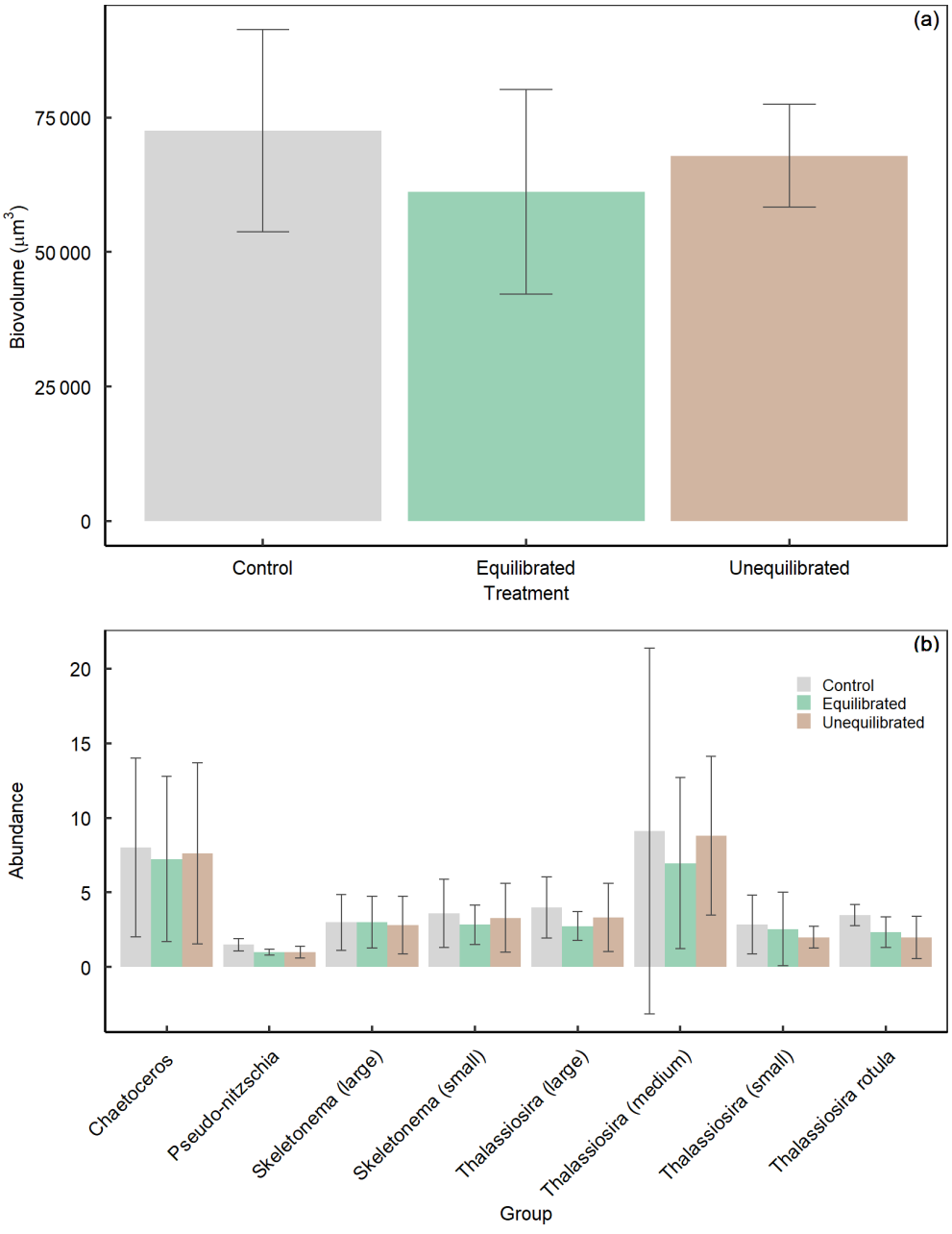

Figure A5. Average diatom **(a)** biovolume and **(b)** abundance, during the peak bloom (day 6) within treatments determined via SEM. Data are presented as mean values ± SD.

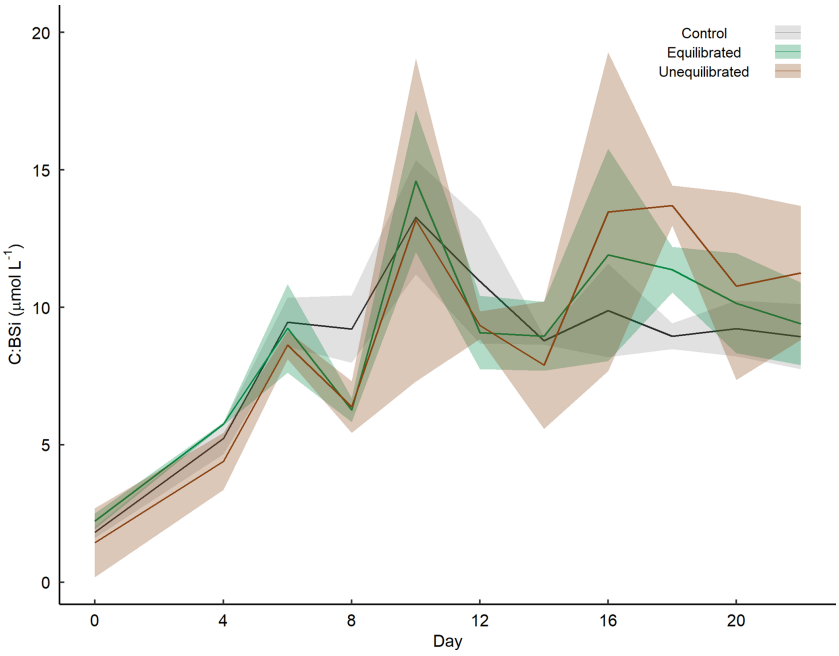

Figure A6. Temporal variation in the molar ratios of TPC to BSi within microcosms. Coloured shading around the respective means represents the standard deviation.

Data availability. Data are available from the Institute for Marine and Antarctic Studies (IMAS) data catalogue, University of Tasmania (UTAS) (https://doi.org/10.25959/8PEA-SW88, Federer, 2021a).

Video supplement. Video supplement 1 contains a time lapse of the convective mixing test described in Sect. 2.1, taken on 3 August 2021. The video can be accessed online at https://doi.org/10.5446/55861 (Federer, 2021b). Video supplement 2 contains a time lapse depicting aggregate formation and suspension within a microcosm as a result of convective mixing, taken on 15 August 2021. The video can be accessed online at https://doi.org/10.5446/55860 (Federer, 2021c).

Author contributions. LTB designed the experiment. AF was responsible for the investigation with the help of LTB and FK. AF was also responsible for the data curation, formal analysis, and writing. LTB and FK supervised data collection. AF wrote the manuscript with contributions from LTB, FK, ZC, and KGS.

Competing interests. The contact author has declared that none of the authors has any competing interests.

Disclaimer. Publisher's note: Copernicus Publications remains neutral with regard to jurisdictional claims in published maps and institutional affiliations.

Acknowledgements. We would like to thank Sandrin Feig, Thomas Rodemann, and Terry Pinfold for support on scanning electron microscopy, particulate organic matter, and flow cytometry measurements. This research was funded by a Future Fellowship (FT200100846) by the Australian Research Council awarded to LTB. This research was also conducted while Aaron Ferderer was in receipt of an Australian Government Research Training Program (RTP) scholarship.

Financial support. This research has been supported by the Australian Research Council (grant no. FT200100846).

Review statement. This paper was edited by Carol Robinson and reviewed by Alex Poulton and two anonymous referees.

References

Alvarez-Fernandez, S., Bach, L. T., Taucher, J., Riebesell, U., Sommer, U., Aberle, N., Brussaard, C. P. D., and Boersma, M.: Plankton responses to ocean acidification: The role of nutrient limitation, Prog. Oceanogr., 165, 11–18, https://doi.org/10.1016/J.POCEAN.2018.04.006, 2018.

Armbrust, E.: The life of diatoms in the world's oceans, Nature, 459, 185–192, https://doi.org/10.1038/nature08057, 2009.

Bach, L. T. and Taucher, J.: CO_2 effects on diatoms: a synthesis of more than a decade of ocean acidification experiments with natural communities, Ocean Sci., 15, 1159–1175, https://doi.org/10.5194/os-15-1159-2019, 2019.

Bach, L. T., Alvarez-Fernandez, S., Hornick, T., Stuhr, A., and Riebesell, U.: Simulated ocean acidification reveals winners and losers in coastal phytoplankton, PLoS One, 12, e0188198, https://doi.org/10.1371/JOURNAL.PONE.0188198, 2017.

Bach, L. T., Gill, S. J., Rickaby, R. E. M., Gore, S., and Renforth, P.: CO_2 Removal With Enhanced Weathering and Ocean Alkalinity Enhancement: Potential Risks and Co-benefits for Marine Pelagic Ecosystems, Front. Clim., 1, 7, https://doi.org/10.3389/fclim.2019.00007, 2019.

Bach, L. T., Tamsitt, V., Gower, J., Hurd, C. L., Raven, J. A., and Boyd, P. W.: Testing the climate intervention potential of ocean afforestation using the Great Atlantic Sargassum Belt, Nat. Commun., 12, 1–10, https://doi.org/10.1038/s41467-021-22837-2, 2021.

Bakker, D. C. E., Bozec, Y., Nightingale, P. D., Goldson, L., Messias, M. J., de Baar, H. J. W., Liddicoat, M., Skjelvan, I., Strass, V., and Watson, A. J.: Iron and mixing affect biological carbon uptake in SOIREE and EisenEx, two Southern Ocean iron fertilisation experiments, Deep-Sea Res. Pt. I, 52, 1001–1019, https://doi.org/10.1016/J.DSR.2004.11.015, 2005.

Bakker, D. C. E., Pfeil, B., Landa, C. S., Metzl, N., O'Brien, K. M., Olsen, A., Smith, K., Cosca, C., Harasawa, S., Jones, S. D., Nakaoka, S., Nojiri, Y., Schuster, U., Steinhoff, T., Sweeney, C., Takahashi, T., Tilbrook, B., Wada, C., Wanninkhof, R., Alin, S. R., Balestrini, C. F., Barbero, L., Bates, N. R., Bianchi, A. A., Bonou, F., Boutin, J., Bozec, Y., Burger, E. F., Cai, W.-J., Castle, R. D., Chen, L., Chierici, M., Currie, K., Evans, W., Featherstone, C., Feely, R. A., Fransson, A., Goyet, C., Greenwood, N., Gregor, L., Hankin, S., Hardman-Mountford, N. J., Harlay, J., Hauck, J., Hoppema, M., Humphreys, M. P., Hunt, C. W., Huss, B., Ibánhez, J. S. P., Johannessen, T., Keeling, R., Kitidis, V., Körtzinger, A., Kozyr, A., Krasakopoulou, E., Kuwata, A., Landschützer, P., Lauvset, S. K., Lefèvre, N., Lo Monaco, C., Manke, A., Mathis, J. T., Merlivat, L., Millero, F. J., Monteiro, P. M. S., Munro, D. R., Murata, A., Newberger, T., Omar, A. M., Ono, T., Paterson, K., Pearce, D., Pierrot, D., Robbins, L. L., Saito, S., Salisbury, J., Schlitzer, R., Schneider, B., Schweitzer, R., Sieger, R., Skjelvan, I., Sullivan, K. F., Sutherland, S. C., Sutton, A. J., Tadokoro, K., Telszewski, M., Tuma, M., van Heuven, S. M. A. C., Vandemark, D., Ward, B., Watson, A. J., and Xu, S.: A multi-decade record of high-quality fCO_2 data in version 3 of the Surface Ocean CO_2 Atlas (SOCAT), Earth Syst. Sci. Data, 8, 383–413, https://doi.org/10.5194/essd-8-383-2016, 2016.

Berge, T., Daugbjerg, N., Andersen, B. B., and Hansen, P. J.: Effect of lowered pH on marine phytoplankton growth rates, Mar. Ecol. Prog. Ser., 416, 79–91, https://doi.org/10.3354/MEPS08780, 2010.

Carpenter, S. R.: Microcosm experiments have limited relevance for community and ecosystem ecology, Ecology, 77, 677–680, https://doi.org/10.2307/2265490, 1996.

Chen, C. Y. and Durbin, E. G.: Effects of pH on the growth and carbon uptake of marine phytoplankton, Mar. Ecol. Prog. Ser., 109, 83–94, https://doi.org/10.3354/meps109083, 1994.

Crawfurd, K. J., Riebesell, U., and Brussaard, C. P. D.: Shifts in the microbial community in the Baltic Sea with increasing CO_2, Biogeosciences Discuss., 1–51, https://doi.org/10.5194/bg-2015-606, 2016.

Davidson, A. T., McKinlay, J., Westwood, K., Thomson, P. G., van den Enden, R., de Salas, M., Wright, S., Johnson, R., and Berry, K.: Enhanced CO_2 concentrations change the structure of Antarctic marine microbial communities, Mar. Ecol. Prog. Ser., 552, 93–113, https://doi.org/10.3354/MEPS11742, 2016.

de Lannoy, C. F., Eisaman, M. D., Jose, A., Karnitz, S. D., DeVaul, R. W., Hannun, K., and Rivest, J. L. B.: Indirect ocean capture of atmospheric CO_2: Part I. Prototype of a negative emissions technology, Int. J. Greenhouse Gas Con., 70, 243–253, https://doi.org/10.1016/J.IJGGC.2017.10.007, 2018.

Dickson, A. G., Sabine, C. L., and Christian, J. R. (Eds.): Guide to Best Practice for Ocean CO_2 Measurements, PICES Special Publication, 3, 191 pp., 2007.

Doney, S. C., Busch, D. S., Cooley, S. R., and Kroeker, K. J.: The Impacts of Ocean Acidification on Marine Ecosystems and Reliant Human Communities, Ann. Rev. Environ. Resour., 45, 83–112, https://doi.org/10.1146/annurev-environ-012320-083019, 2020.

Engel, A. and Passow, U.: Carbon and nitrogen content of transparent exopolymer particles (TEP) in relation to their Alcian Blue adsorption, Mar. Ecol. Prog. Ser., 219, 1–10, https://doi.org/10.3354/MEPS219001, 2001.

Engel, A., Schulz, K. G., Riebesell, U., Bellerby, R., Delille, B., and Schartau, M.: Effects of CO_2 on particle size distribution and phytoplankton abundance during a mesocosm bloom experiment (PeECE II), Biogeosciences, 5, 509–521, https://doi.org/10.5194/bg-5-509-2008, 2008.

Evans, C. A., O'Reilly, J. E., and Thomas, J. P.: A handbook for the measurement of chlorophyll *a* and primary production, College Station, College Station, Texas, USA, A&M Univ., ISBN 0948277076, 1987.

Falkenberg, L. J., Bellerby, R. G. J., Connell, S. D., Fleming, L. E., Maycock, B., Russell, B. D., Sullivan, F. J., and Dupont, S.: Ocean Acidification and Human Health, Int. J. Env. Res. Pub. He., 17, 4563, https://doi.org/10.3390/IJERPH17124563, 2020.

Fassbender, A. J., Orr, J. C., and Dickson, A. G.: Technical note: Interpreting pH changes, Biogeosciences, 18, 1407–1415, https://doi.org/10.5194/bg-18-1407-2021, 2021.

Ferderer, A.: Assessing the influence of ocean alkalinity enhancement on a coastal phytoplankton community – manuscript data, Institute for Marine and Antarctic Studies (IMAS), University of Tasmania (UTAS), IMAS Metadata [data set], https://doi.org/10.25959/8PEA-SW88, 2021a.

Ferderer, A.: Convective mixing vs no mixing inside two microcosms, TIB [video supplement], https://doi.org/10.5446/55861, 2021b.

Ferderer, A.: Aggregates suspended in microcosm, TIB [video supplement], https://doi.org/10.5446/55860, 2021c.

Feng, E. Y., Koeve, W., Keller, D. P., and Oschlies, A.: Model-Based Assessment of the CO_2 Sequestration Potential of Coastal Ocean Alkalinization, Earth's Future, 5, 1252–1266, https://doi.org/10.1002/2017EF000659, 2017.

Flynn, K. J., Blackford, J. C., Baird, M. E., Raven, J. A., Clark, D. R., Beardall, J., Brownlee, C., Fabian, H., and Wheeler, G. L.: Changes in pH at the exterior surface of plankton with ocean acidification, Nat. Clim. Change, 2, 510–513, https://doi.org/10.1038/nclimate1489, 2012.

Friedlingstein, P., Jones, M. W., O'Sullivan, M., Andrew, R. M., Hauck, J., Peters, G. P., Peters, W., Pongratz, J., Sitch, S., Le Quéré, C., Bakker, D. C. E., Canadell, J. G., Ciais, P., Jackson, R. B., Anthoni, P., Barbero, L., Bastos, A., Bastrikov, V.,

Becker, M., Bopp, L., Buitenhuis, E., Chandra, N., Chevallier, F., Chini, L. P., Currie, K. I., Feely, R. A., Gehlen, M., Gilfillan, D., Gkritzalis, T., Goll, D. S., Gruber, N., Gutekunst, S., Harris, I., Haverd, V., Houghton, R. A., Hurtt, G., Ilyina, T., Jain, A. K., Joetzjer, E., Kaplan, J. O., Kato, E., Klein Goldewijk, K., Korsbakken, J. I., Landschützer, P., Lauvset, S. K., Lefèvre, N., Lenton, A., Lienert, S., Lombardozzi, D., Marland, G., McGuire, P. C., Melton, J. R., Metzl, N., Munro, D. R., Nabel, J. E. M. S., Nakaoka, S.-I., Neill, C., Omar, A. M., Ono, T., Peregon, A., Pierrot, D., Poulter, B., Rehder, G., Resplandy, L., Robertson, E., Rödenbeck, C., Séférian, R., Schwinger, J., Smith, N., Tans, P. P., Tian, H., Tilbrook, B., Tubiello, F. N., van der Werf, G. R., Wiltshire, A. J., and Zaehle, S.: Global Carbon Budget 2019, Earth Syst. Sci. Data, 11, 1783–1838, https://doi.org/10.5194/essd-11-1783-2019, 2019.

Fukao, T., Kimoto, K., and Kotani, Y.: Production of transparent exopolymer particles by four diatom species, Fish. Sci., 76, 755–760, 2010.

Fuss, S., Lamb, W. F., Callaghan, M. W., Hilaire, J., Creutzig, F., Amann, T., Beringer, T., de Oliveira Garcia, W., Hartmann, J., Khanna, T., Luderer, G., Nemet, G. F., Rogelj, J., Smith, P., Vicente, J. V., Wilcox, J., del Mar Zamora Dominguez, M., and Minx, J. C.: Negative emissions – Part 2: Costs, potentials and side effects, Environ.l Res. Lett., 13, 063002, https://doi.org/10.1088/1748-9326/AABF9F, 2018.

Gattuso, J., Epitalon, J., Lavigne, H., Orr, J., Gentili, B., Hagens, M., Hofman, A., Mueller, J., Proye, A., Rae, J., and Soetaert, K.: Seacarb: seawater carbonate chemistry, R package version 3.3.0, https://CRAN.R-project.org/package=seacarb, last access: 15 December 2021.

Gnanadesikan, A. and Marinov, I.: Export is not enough: nutrient cycling and carbon sequestration, Mar. Ecol. Prog. Ser., 364, 289–294, https://doi.org/10.3354/MEPS07550, 2008.

Hansen, H. P. and Koroleff, F.: Determination of nutrients, in: Methods of Seawater Analysis, John Wiley & Sons, Ltd., 159–228, https://doi.org/10.1002/9783527613984.ch10, 1999.

Hartmann, J., West, A. J., Renforth, P., Köhler, P., Rocha, C. L. D. la, Wolf-Gladrow, D. A., Dürr, H. H., and Scheffran, J.: Enhanced chemical weathering as a geoengineering strategy to reduce atmospheric carbon dioxide, supply nutrients, and mitigate ocean acidification, Rev. Geophys., 51, 113–149, https://doi.org/10.1002/ROG.20004, 2013.

Hepburn, C., Adlen, E., Beddington, J., Carter, E. A., Fuss, S., mac Dowell, N., Minx, J. C., Smith, P., and Williams, C. K.: The technological and economic prospects for CO_2 utilization and removal, Nature, 575, 87–97, https://doi.org/10.1038/s41586-019-1681-6, 2019.

Hervé, V., Derr, J., Douady, S., Quinet, M., Moisan, L., and Lopez, P. J.: Multiparametric Analyses Reveal the pH-Dependence of Silicon Biomineralization in Diatoms, PLoS One, 7, e46722, https://doi.org/10.1371/JOURNAL.PONE.0046722, 2012.

Hinga, K. R.: Effects of pH on coastal marine phytoplankton, Mar. Ecol. Prog. Ser., 238, 281–300, https://doi.org/10.3354/meps238281, 2002.

Hoppe, C. J. M., Flintrop, C. M., and Rost, B.: The Arctic picoeukaryote *Micromonas pusilla* benefits synergistically from warming and ocean acidification, Biogeosciences, 15, 4353–4365, https://doi.org/10.5194/bg-15-4353-2018, 2018.

Humphreys, M. P., Lewis, E. R., Sharp, J. D., and Pierrot, D.: PyCO2SYS v1.8: marine carbonate system calculations in Python, Geosci. Model Dev., 15, 15–43, https://doi.org/10.5194/gmd-15-15-2022, 2022.

Jones, J.-P., Prakash, G. K. S., and Olah, G. A.: Electrochemical CO_2 Reduction: Recent Advances and Current Trends, Israel J. Chem., 54, 1451–1466, https://doi.org/10.1002/IJCH.201400081, 2014.

Kheshgi, H. S.: Sequestering atmospheric carbon dioxide by increasing ocean alkalinity, Energy, 20, 915–922, https://doi.org/10.1016/0360-5442(95)00035-F, 1995.

Köhler, P., Hartmann, J., and Wolf-Gladrow, D. A.: Geoengineering potential of artificially enhanced silicate weathering of olivine, P. Natl. Acad. Sci. USA, 107, 20228–20233, https://doi.org/10.1073/PNAS.1000545107, 2010.

le Quesne, W. J. F. and Pinnegar, J. K.: The potential impacts of ocean acidification: Scaling from physiology to fisheries, Fish Fish., 13, 333–344, https://doi.org/10.1111/J.1467-2979.2011.00423.x, 2012.

Lueker, T. J., Dickson, A. G., and Keeling, C. D.: Ocean pCO2 calculated from dissolved inorganic carbon, alkalinity, and equations for K1 and K2: validation based on laboratory measurements of CO_2 in gas and seawater at equilibrium, Mar. Chem., 70, 105–119, https://doi.org/10.1016/S0304-4203(00)00022-0, 2000.

Malerba, M. E., Marshall, D. J., Palacios, M. M., Raven, J. A., and Beardall, J.: Cell size influences inorganic carbon acquisition in artificially selected phytoplankton, New Phytol., 229, 2647–2659, https://doi.org/10.1111/NPH.17068, 2021.

Mallin, M. A. and Paerl, H. W.: Planktonic Trophic Transfer in an Estuary: Seasonal, Diel, and Community Structure Effects, Ecology, 75, 2168–2184, https://doi.org/10.2307/1940875, 1994.

Maugendre, L., Gattuso, J. P., Louis, J., de Kluijver, A., Marro, S., Soetaert, K., and Gazeau, F.: Effect of ocean warming and acidification on a plankton community in the NW Mediterranean Sea, ICES J. Mar. Sci., 72, 1744–1755, https://doi.org/10.1093/ICESJMS/FSU161, 2015.

Meakin, N. G. and Wyman, M.: Rapid shifts in picoeukaryote community structure in response to ocean acidification, ISME J., 5, 1397–1405, https://doi.org/10.1038/ismej.2011.18, 2011.

Milligan, A. J., Varela, D. E., Brzezinski, M. A., and Morel, F. M. M.: Dynamics of silicon metabolism and silicon isotopic discrimination in a marine diatomas a function of pCO_2, Limnol. Oceanogr., 49, 322–329, https://doi.org/10.4319/LO.2004.49.2.0322, 2004.

Newbold, L. K., Oliver, A. E., Booth, T., Tiwari, B., Desantis, T., Maguire, M., Andersen, G., van der Gast, C. J., and Whiteley, A. S.: The response of marine picoplankton to ocean acidification, Environ. Microbiol., 14, 2293–2307, https://doi.org/10.1111/J.1462-2920.2012.02762.X, 2012.

Orr, J. C. and Sarmiento, J. L.: Potential of marine macroalgae as a sink for CO_2: Constraints from a 3-D general circulation model of the global ocean, Water Air Soil Pollut., 64, 405–421, https://doi.org/10.1007/BF00477113, 1992.

Orr, J. C., Epitalon, J.-M., and Gattuso, J.-P.: Comparison of ten packages that compute ocean carbonate chemistry, Biogeosciences, 12, 1483–1510, https://doi.org/10.5194/bg-12-1483-2015, 2015.

Pardo, P., Tilbrook, B., van Ooijen, E., Passmore, A., Neill, C., Jansen, P., Sutton, A. J., and Trull, T. W.: Surface ocean carbon dioxide variability in South Pacific boundary currents and Subantarctic waters, Nature, 9, 7592, https://doi.org/10.1038/s41598-019-44109-2, 2019.

Passow, U.: Production of transparent exopolymer particles (TEP) by phyto- and bacterioplankton, Mar. Ecol. Prog. Ser., 236, 1–12, https://doi.org/10.3354/MEPS236001, 2002.

Paul, A. J. and Bach, L. T.: Universal response pattern of phytoplankton growth rates to increasing CO_2, New Phytol., 228, 1710–1716, https://doi.org/10.1111/NPH.16806, 2020.

Pedersen, M. F. and Hansen, P. J.: Effects of high pH on a natural marine planktonic community, Mar. Ecol. Prog. Ser., 260, 19–31, https://doi.org/10.3354/MEPS260019, 2003.

Petrou, K., Baker, K. G., Nielsen, D. A., Hancock, A. M., Schulz, K. G., and Davidson, A. T.: Acidification diminishes diatom silica production in the Southern Ocean, Nat. Clim. Change, 9, 781–786, https://doi.org/10.1038/s41558-019-0557-y, 2019.

Quéguiner, B.: Iron fertilization and the structure of planktonic communities in high nutrient regions of the Southern Ocean, Deep-Sea Res. Pt. II, 90, 43–54, https://doi.org/10.1016/J.DSR2.2012.07.024, 2013.

Rau, G. H., Carroll, S. A., Bourcier, W. L., Singleton, M. J., Smith, M. M., and Aines, R. D.: Direct electrolytic dissolution of silicate minerals for air CO_2 mitigation and carbon-negative H_2 production, Earth Atmos. Planet. Sc., 110, 10095–10100, 2013.

Renforth, P. and Henderson, G.: Assessing ocean alkalinity for carbon sequestration, Rev. Geophys., 55, 636–674, https://doi.org/10.1002/2016RG000533, 2017.

Rickels, W., Proelß, A., Geden, O., Burhenne, J., and Fridahl, M.: Integrating Carbon Dioxide Removal Into European Emissions Trading, Front. Clim., 3, 690023, https://doi.org/10.3389/FCLIM.2021.690023, 2021.

Riebesell, U., Wolf-Gladrow, D. A., and Smetacek, V.: Carbon dioxide limitation of marine phytoplankton growth rates, Nature, 361, 249–251, https://doi.org/10.1038/361249a0, 1993.

Rogelj, J., Popp, A., Calvin, K. v., Luderer, G., Emmerling, J., Gernaat, D., Fujimori, S., Strefler, J., Hasegawa, T., Marangoni, G., Krey, V., Kriegler, E., Riahi, K., van Vuuren, D. P., Doelman, J., Drouet, L., Edmonds, J., Fricko, O., Harmsen, M., Havlík, P., Humpenöder, F., Stehfest, E., and Tavoni, M.: Scenarios towards limiting global mean temperature increase below 1.5 °C, Nat. Clim. Change, 8, 325–332, https://doi.org/10.1038/s41558-018-0091-3, 2018.

RStudio Team: RStudio: Integrated Development for R, http://www.rstudio.com/ (last access: 28 December 2021), 2022.

Sala, M. M., Aparicio, F. L., Balagué, V., Boras, J. A., Borrull, E., Cardelús, C., Cros, L., Gomes, A., López-Sanz, A., Malits, A., Martínez, R. A., Mestre, M., Movilla, J., Sarmento, H., Vázquez-Domínguez, E., Vaqué, D., Pinhassi, J., Calbet, A., Calvo, E., Gasol, J. M., Pelejero, C., and Marrasé, C.: Contrasting effects of ocean acidification on the microbial food web under different trophic conditions, ICES J. Mar. Sci., 73, 670–679, https://doi.org/10.1093/ICESJMS/FSV130, 2016.

Schaum, E., Rost, B., Millar, A. J., and Collins, S.: Variation in plastic responses of a globally distributed picoplankton species to ocean acidification, Nat. Clim. Change, 3, 298–302, https://doi.org/10.1038/nclimate1774, 2012.

Schuiling, R. D. and Krijgsman, P.: Enhanced Weathering: An Effective and Cheap Tool to Sequester CO_2, Climatic Change, 74, 349–354, https://doi.org/10.1007/S10584-005-3485-Y, 2006.

Schulz, K. G., Bach, L. T., Bellerby, R. G. J., Bermúdez, R., Büdenbender, J., Boxhammer, T., Czerny, J., Engel, A., Ludwig, A., Meyerhöfer, M., Larsen, A., Paul, A. J., Sswat, M., and Riebesell, U.: Phytoplankton Blooms at Increasing Levels of Atmospheric Carbon Dioxide: Experimental Evidence for Negative Effects on Prymnesiophytes and Positive on Small Picoeukaryotes, Front Mar. Sci., 4, 64, https://doi.org/10.3389/FMARS.2017.00064, 2017.

Sswat, M., Stiasny, M. H., Taucher, J., Algueró-Muñiz, M., Bach, L. T., Jutfelt, F., Riebesell, U., and Clemmesen, C.: Food web changes under ocean acidification promote herring larvae survival, Nat. Ecol. Evol., 2, 836–840, https://doi.org/10.1038/s41559-018-0514-6, 2018.

Taucher, J., Boxhammer, T., Bach, L. T., Paul, A. J., Schartau, M., Stange, P., and Riebesell, U.: Changing carbon-to-nitrogen ratios of organic-matter export under ocean acidification, Nat. Clim. Change, 11, 52–57, https://doi.org/10.1038/s41558-020-00915-5, 2020.

Taylor, L. L., Quirk, J., Thorley, R. M. S., Kharecha, P. A., Hansen, J., Ridgwell, A., Lomas, M. R., Banwart, S. A., and Beerling, D. J.: Enhanced weathering strategies for stabilizing climate and averting ocean acidification, Nat. Clim. Change, 6, 402–406, https://doi.org/10.1038/nclimate2882, 2016.

Thomson, P. G., Davidson, A. T., and Maher, L.: Increasing CO_2 changes community composition of pico- and nano-sized protists and prokaryotes at a coastal Antarctic site, Mar. Ecol. Prog. Ser., 554, 51–69, https://doi.org/10.3354/MEPS11803, 2016.

Tyka, M. D., Arsdale, C. van, and Platt, J. C.: CO_2 capture by pumping surface acidity to the deep ocean, Energ. Environ. Sci., 15, 786–798, https://doi.org/10.1039/D1EE01532J, 2022.

Wassmànn, P.: Retention versus export food chains: processes controlling sinking loss from marine pelagic systems, Hydrobiologia, 363, 29–57, https://doi.org/10.1023/A:1003113403096, 1997.

White, E., Hoppe, C. J. M., and Rost, B.: The Arctic picoeukaryote Micromonas pusilla benefits from ocean acidification under constant and dynamic light, Biogeosciences, 17, 635–647, https://doi.org/10.5194/bg-17-635-2020, 2020.

Wolf-Gladrow, D. and Riebesell, U.: Diffusion and reactions in the vicinity of plankton: A refined model for inorganic carbon transport, Mar. Chem., 59, 17–34, https://doi.org/10.1016/S0304-4203(97)00069-8, 1997.

Wood, S.: Mixed GAM computation vehicle with automatic smoothness estimation, CRAN, https://cran.r-project.org/web/packages/mgcv/mgcv.pdf (last access: 10 December 2021), 2015.

Wu, Y., Campbell, D. A., Irwin, A. J., Suggett, D. J., and Finkel, Z. v.: Ocean acidification enhances the growth rate of larger diatoms, Limnol. Oceanogr., 59, 1027–1034, https://doi.org/10.4319/LO.2014.59.3.1027, 2014.

Biogeosciences, 21, 2859–2876, 2024
https://doi.org/10.5194/bg-21-2859-2024

Biogeosciences Open Access EGU

Assessing the impact of CO_2-equilibrated ocean alkalinity enhancement on microbial metabolic rates in an oligotrophic system

Laura Marín-Samper[1], Javier Arístegui[1], Nauzet Hernández-Hernández[1], Joaquín Ortiz[1], Stephen D. Archer[3], Andrea Ludwig[2], and Ulf Riebesell[2]

[1]Instituto de Oceanografía y Cambio Global, Universidad de Las Palmas de Gran Canaria, 35017 Telde, Spain
[2]GEOMAR Helmholtz Centre for Ocean Research Kiel, 24148 Kiel, Germany
[3]Bigelow Laboratory for Ocean Sciences, 60 Bigelow Dr., P.O. Box 380, East Boothbay, Maine 04544, USA

Correspondence: Laura Marín-Samper (laura.marin@ulpgc.es) and Javier Arístegui (javier.aristegui@ulpgc.es)

Received: 17 October 2023 – Discussion started: 18 October 2023
Revised: 8 May 2024 – Accepted: 17 May 2024 – Published: 13 June 2024

Abstract. Ocean alkalinity enhancement (OAE) is a negative emissions technology (NET) that shows significant potential for climate change mitigation. By increasing the bicarbonate ion concentration in ocean water, OAE could enhance long-term carbon storage and mitigate ocean acidification. However, the side effects and/or potential co-benefits of OAE on natural planktonic communities remain poorly understood. To address this knowledge gap, a mesocosm experiment was conducted in the oligotrophic waters of Gran Canaria. A CO_2-equilibrated total alkalinity (TA) gradient was employed in increments of 300 µmol L^{-1}, ranging from ∼ 2400 to ∼ 4800 µmol L^{-1}. This study represents the first attempt to evaluate the potential impacts of OAE on planktonic communities under natural conditions. The results show that net community production (NCP), gross production (GP), community respiration (CR) rates, and the metabolic balance (GP : CR) did not exhibit a linear response to the whole alkalinity gradient. Instead, significant polynomial and linear regression models were observed for all rates up to ΔTA 1800 µmol L^{-1}, in relation to the dissolved inorganic carbon (DIC) concentrations. Notably, the ΔTA 1500 and 1800 µmol L^{-1} treatments showed peaks in NCP shifting from a heterotrophic to an autotrophic state, with NCP values of 4 and 8 µmol O_2 kg^{-1} d^{-1}, respectively. These peaks and the optimum curve were also reflected in the nanoplankton abundance, size-fractionated chlorophyll *a*, and ^{14}C uptake data. Furthermore, abiotic precipitation occurred in the highest treatment after day 21, but no impact on the measured parameters was detected. Overall, a damaging effect of CO_2-equilibrated OAE in the range applied here on phytoplankton primary production, community metabolism, and composition could not be inferred. In fact, a potential co-benefit to OAE was observed in the form of the positive curvilinear response to the DIC gradient up to the ΔTA 1800 treatment. Further experimental research at this scale is key to gain a better understanding of the short- and long-term effects of OAE on planktonic communities.

1 Introduction

Limiting global warming to between 1.5 and 2 °C relative to preindustrial times, as stipulated in the 2015 Paris Agreement, will be necessary to avoid long-term, dangerous climatic consequences. Out of all the scenarios outlined in the fifth IPCC Assessment Report that meet this temperature target, 87 % require extensive deployment of technologies to remove and sequester carbon dioxide (CO_2) from the atmosphere (Burns and Corbett, 2020). Similarly, the Shared Socio-Economic Pathways that assume net-zero CO_2 emissions being reached by 2050 and negative emissions for the rest of this century are the only ones in which the temperature increase is *more likely than not* bounded to below 2 °C (Canadell et al., 2021). Besides, an estimated 26 % of the anthropogenic CO_2 emitted between 1750 and 2020 has been taken up by the ocean through sea–gas exchange (Friedlingstein et al., 2022), subsequently altering its chemistry (Feely et al., 1985; Orr et al., 2005), a process that is commonly known as ocean acidification (OA). This phenomenon is notorious for being a threat to a wide range of marine taxa in

terms of overall survival, calcification, growth, development, and abundance (Kroeker et al., 2013, 2010; Wittmann and Pörtner, 2013; Hendriks and Duarte, 2010). The implementation of carbon dioxide removal (CDR) strategies will thus be crucial to timely offset the hard-to-abate emissions (Haszeldine et al., 2018; National Academies of Sciences, Engineering, and Medicine, 2018; Renforth et al., 2013). Yet most approaches remain understudied, particularly those focused on ocean-based CDR (Gattuso et al., 2021, 2018; Rau et al., 2012).

Ocean alkalinity enhancement (OAE) is one of the ocean-based negative emissions technologies (NETs) that is presently being considered. It consists of atmospheric CO_2 removal by enhancing the ocean's carbon uptake capacity through mineral weathering (Kheshgi, 1995). It involves the dissolution of carbonate- or silicate-based alkaline or alkali compounds/minerals in seawater, which consumes protons, altering the carbonate chemistry equilibrium by pushing it towards the carbonate and bicarbonate ion species. Thereby dissolved CO_2 concentration is reduced, counteracting OA while allowing for additional CO_2 uptake from the atmosphere. Model studies indicate that OAE could potentially remove between 3 and 10 Gt of atmospheric CO_2 per year (Feng et al., 2017; Harvey, 2008). Given the urgency to remove, capture, and store atmospheric CO_2 (Haszeldine et al., 2018; Canadell et al., 2021) and the ocean's potential to do so (Burns and Corbett, 2020), the evaluation of OAE applicability is of vital importance. Its implementation will depend on its scalability and on its environmental safety.

There are many proposed approaches for OAE deployment, for example, the supply of ground-up minerals to coastal environments, the injection of alkaline solutions to or dispersal of alkaline particles over the surface ocean, and the electrochemical acid removal from seawater (Eisaman et al., 2023; Renforth and Henderson, 2017). In the present study we simulated a carbonate-based alkalinity addition to the open-ocean surface, using a mesocosm approach. The waters off the coast of Gran Canaria were selected due to their oligotrophic nature (Fig. S1 in the Supplement)

There are many model-based studies that focused on evaluating the feasibility, scalability and efficacy of this OAE approach (Butenschön et al., 2021; Caserini et al., 2021; González and Ilyina, 2016; Ilyina et al., 2013; Kheshgi, 1995; Lenton et al., 2018). But although conceptually it shows potential to mitigate OA and CDR at global and regional scales, all the model simulations are based on a series of assumptions that remain poorly understood (Hartmann et al., 2023). This is due to the lack of focused experimental work under natural conditions.

Choosing a suitable approach to employ OAE is essential and complex. The maintenance of high alkalinity levels and thus the avoidance of alkalinity consumption through abiotic carbonate precipitation are key to ensure its CDR potential (Hartmann et al., 2023). Additionally, the type of source mineral (Bach et al., 2019), grinding fineness, whether it is added in its particulate form or in solution, and if the latter is CO_2 equilibrated prior to addition or not can all influence its potential environmental impacts. Also, precipitation occurrence may depend on the targeted TA level, especially if CO_2 sequestration is not undertaken prior to addition, but also on the presence of biogenic (Enmar et al., 2000; Nassif et al., 2005) or abiotic particles in seawater (Moras et al., 2022). Therefore, the latter may all impact its CDR efficiency.

The simplest OAE deployment strategy is the direct dispersal of ground-up minerals to the surface ocean (Harvey, 2008; Köhler et al., 2013). This method, however, may facilitate abiotic precipitation by supplying substrate for carbonate formation in an already supersaturated medium (Wurgaft et al., 2021). Additionally, if silicate-based (through the use of, for instance, dunite, an olivine-rich mineral), it may cause the release of potentially harmful dissolution by-products such as trace metals (Bach et al., 2019; Ferderer et al., 2022; Montserrat et al., 2017; Meysman and Montserrat, 2017). Thus, despite being the simplest, it may not be the most suitable approach. The impacts on biota of different OAE strategies may also depend on the associated changes to the carbonate chemistry. This is especially true for non-CO_2-equilibrated OAE deployment scenarios where pCO_2 would be decreased and thus pH more heavily altered than when employing an equilibrated approach (Bach et al., 2019; Paul and Bach, 2020; Chen et al., 1994; Giordano et al., 2005; Riebesell et al., 1993).

As a first attempt to evaluate OAE at a mesocosm scale, specifically to test the effect of the associated increment in total alkalinity (TA) and dissolved inorganic carbon (DIC), as well as to examine TA stability, we deployed an air-equilibrated alkalinity gradient with carbonate-based solutions. Therefore, our TA manipulation did not contain any associated and potentially harmful dissolution by-products, nor was the pCO_2 decreased, in this way simulating the alkalinity levels reached as one gradually moves away from a hypothetical OAE point source in oligotrophic conditions under a best-case scenario. Changes in metabolic rates, primary production, chlorophyll *a* concentration, and community composition, associated with the alkalinity gradient applied, were monitored. The goal was thus to detect possible environmental impacts and alkalinity thresholds. No major effects were expected since the carbonate chemistry parameters that are believed to drive phytoplankton growth, and CO_2 and H^+ concentration (Paul and Bach, 2020) remained unaltered and moderately decreased, respectively.

2 Materials and methods

2.1 Experimental design and sampling

The experiment (KOSMOS Gran Canaria 2021) was set up at the Oceanic Platform of the Canary Islands' (PLOCAN) pier in the Taliarte harbor, Gran Canaria (Canary Islands, Spain),

Table 1. Averages ± the standard errors for the whole experiment after the total alkalinity (TA) manipulation (day > 4) of the measured (italics) TA and dissolved inorganic carbon (DIC) and of the theoretical values obtained through the CO2SYS v2.1 software for the rest of the carbonate system parameters, per mesocosm (MK), where "*n*" corresponds to the sample size. The TA, DIC, bicarbonate (HCO_3^-), and carbonate (CO_3^{2-}) concentrations are reported in µmol L^{-1}; pCO_2 is in µatm; and pH is conveyed using the seawater scale.

MK	TA	DIC	pH_{sw}	pCO_2	HCO_3^-	CO_3^{2-}	Ω_{Ca}	Ω_{Ar}
5 $n = 15$	*2427.7 ± 4.31*	*2119.6 ± 2.92*	8.03 ± 0.003	417.7 ± 2.87	1889.6 ± 2.59	219.4 ± 1.48	5.2 ± 0.03	3.4 ± 0.02
1 $n = 15$	*2706.4 ± 10.24*	*2348.5 ± 3.27*	8.06 ± 0.012	435.6 ± 15.94	2078.6 ± 5.44	257.0 ± 6.02	6.1 ± 0.14	4.0 ± 0.09
7 $n = 15$	*3003.7 ± 7.59*	*2593.6 ± 4.73*	8.10 ± 0.006	427.7 ± 6.34	2271.0 ± 5.60	310.0 ± 3.94	7.3 ± 0.09	4.8 ± 0.06
4 $n = 15$	*3297.4 ± 4.45*	*2829.8 ± 4.53*	8.14 ± 0.007	429.8 ± 7.82	2456.2 ± 8.07	361.0 ± 4.49	8.5 ± 0.11	5.6 ± 0.07
9 $n = 15$	*3603.9 ± 7.27*	*3079.6 ± 4.95*	8.16 ± 0.005	438.2 ± 5.40	2654.1 ± 6.18	412.6 ± 4.03	9.8 ± 0.09	6.4 ± 0.06
3 $n = 15$	*3881.7 ± 8.23*	*3295.7 ± 6.65*	8.19 ± 0.007	435.2 ± 8.58	2814.8 ± 10.89	468.1 ± 6.55	11.1 ± 0.15	7.3 ± 0.10
6 $n = 14$	*4165.4 ± 7.77*	*3507.0 ± 6.43*	8.22 ± 0.007	429.7 ± 8.13	2969.3 ± 11.40	528.5 ± 6.92	12.5 ± 0.16	8.2 ± 0.10
2 $n = 15$	*4458.0 ± 7.42*	*3752.3 ± 6.72*	8.23 ± 0.005	443.7 ± 6.26	3160.9 ± 9.72	578.4 ± 5.21	13.7 ± 0.12	9.0 ± 0.08
8 $n = 15$	*4655.8 ± 22.09*	*3920.4 ± 13.53*	8.23 ± 0.007	461.7 ± 8.53	3299.0 ± 9.99	607.8 ± 9.15	14.4 ± 0.22	9.4 ± 0.15

from 14 September to 16 October 2021. Nine mesocosms were deployed. They were supported by floating frames with joined flexible bags of 4 m in length that were suspended and enclosed at the bottom with a conical sediment trap (Goldenberg et al., 2022; Fig. S2). Mesocosms were simultaneously filled up on 10 September 2021, with pre-filtered (3 mm) seawater pumped from nearby offshore waters (from the integrated water column going from 2–12 m depth) with a peristaltic pump (14 $m^3 h^{-1}$, KUNZ SPF60, Flexodamp FD-50). Seawater was distributed equally across all mesocosms using a digital flow meter. The attained final volumes ranged between 8001–8051 L.

To examine the effects of an increment in TA, we applied a CO_2-equilibrated nine-step alkalinity gradient in increments of 300 µmol L^{-1}, with Na_2CO_3 and $NaHCO_3$ stock solutions. The latter were prepared by adding 22 kg of each salt separately to 22 kg of deionized water. The volume containing the difference in TA between the ambient and the target levels was added to each mesocosm. The applied gradient is displayed in Table 1. The averages of the measured (see Sect. 2.2) TA and DIC are shown in italics and were used to calculate the rest of the carbonate chemistry parameters using CO2SYS v2.1 software (Lewis and Wallace, 1998). Lueker et al.'s (2000) carbonate dissociation constants (K_1 and K_2) and the boron from Uppström (1974) were the constants employed for the mentioned calculation. The measured nutrient concentrations (Fig. S1) and in situ salinity were also used.

Mesocosms were placed in order from one to nine along the Taliarte pier; thus the actual TA treatments (from ΔTA 0–2400 µmol L^{-1}, Table 1) were set out in random order. Custom-made samplers, constructed with 2.5 m long polypropylene tubing with a valve at each end and a 5 L internal volume, were used to collect depth-integrated samples. These were collected every 2 d for a 33 d period. For further details on all activities conducted throughout the experiment including conductivity, temperature, and depth (CTD) and net tows, sediment trap pumping, mesocosm cleaning, and overall maintenance, refer to Fig. S3.

2.2 TA and DIC measurements

TA and DIC samples were collected directly from the custom-made samplers into 250 mL glass flasks, allowing for substantial overflow and no headspace to avoid contamination. The samples were sterile-filtered (0.2 µm, SARSTEDT, Nümbrecht, Germany) with a peristaltic pump. TA concentrations were determined by potentiometric titration using a Metrohm 862 Compact Titrosampler with HCl 0.05 M as the titrant and Aquatrode Plus (Pt1000) and 907 Titrando unit as in Chen et al. (2022). DIC concentrations were measured using an AIRICA system (Marianda, Kiel, Germany; see Gafar and Schulz, 2018, and Taucher et al., 2017) with a differen-

tial gas analyzer (LI-7000, Li-cor Biosciences GmbH, Bad Homburg, Germany) at room temperature and within 12 h.

2.3 Metabolic rates through oxygen production and consumption

Gross production (GP), net community production (NCP), and community respiration (CR) rates were determined by oxygen production and consumption in calibrated 125 mL nominal volume soda lime glass bottles following the Winkler method and the recommendations from Bryan et al. (1976), Carpenter and Carritt (1966), and Grasshof et al. (1999). Polycarbonate bottles were filled with 4.5 L of seawater per mesocosm on each sampling day and brought to the lab. Out of these samples, 12 soda lime bottles per mesocosm were first rinsed with sample water and then randomly filled, allowing ample overflow, using a silicone tube with an attached 280 µm mesh on one end. The lids were then carefully placed, and each individual bottle was checked to be bubble free. Four subsamples per mesocosm were fixed at the moment of collection, "initials", through the addition of 1 mL of a manganese sulfate ($MnSO_4$) solution and 1 mL of a sodium iodide (NaI)-based alkaline solution, in this order. They were later covered with a blackout piece of fabric and stored in a rack underwater. Another four bottles were incubated in the "dark", and the remaining four were incubated under "light" conditions. The "dark" ones were set inside light-proof bags, which were then placed in an opaque black box. The "light" ones were randomly distributed inside clear methacrylate boxes, which were covered with a blue foil (172 Lagoon Blue foil, LEE Filters, Burbank, USA) to better simulate the light spectrum of the water column. The boxes containing the light and dark bottles and the rack with the initials were placed in an outside pool found in the Parque Científico Tecnológico Marino of Taliarte, fed with a constant flow of seawater from the Taliarte pier. Data loggers (HOBO UA-002-64, Australia/New Zealand) were put inside the incubators to monitor the temperature (approximately 24.3 and 23.8 °C during the day and night, respectively) and light (ranging from 0.25 to approximately 2313.15 µmol photons $m^{-2}\,s^{-1}$) conditions throughout the experiment. After an incubation period of 24 h, all samples were fixed and left to sediment for at least 2 h. Finally, samples were acidified with 1 mL of 5 M sulfuric acid (H_2SO_4) right before being analyzed with an automated titration system, with colorimetric end-point detection (dissolved oxygen analyzer, SIS, Schwentinental, Germany), using a 0.25 M sodium thiosulfate solution ($Na_2S_2O_3 \cdot 5\,H_2O$) as the titrant. The mean of each set of four replicates was used to calculate CR, NCP, and GP rates, using the following Eqs. (1)–(3), respectively:

$$\mathrm{CR}\ [\mu\mathrm{mol\,L^{-1}\,h^{-1}}] = \frac{\mathrm{Conc_I} - \mathrm{Conc_D}}{h_\mathrm{D}}, \quad (1)$$

$$\mathrm{NCP}\ [\mu\mathrm{mol\,L^{-1}\,h^{-1}}] = \frac{\mathrm{Conc_L} - \mathrm{Conc_I}}{h_\mathrm{L}}, \quad (2)$$

$$\mathrm{GP}\ [\mu\mathrm{mol\,L^{-1}\,h^{-1}}] = \mathrm{CR} + \mathrm{NCP}, \quad (3)$$

where $\mathrm{Conc_I}$, $\mathrm{Conc_D}$, and $\mathrm{Conc_L}$ correspond to the mean oxygen concentration of the initial, dark, and light samples, respectively. h_L and h_D stand for incubation time in hours under light and dark conditions, respectively. The metabolic balance was later calculated by dividing the obtained GP by CR.

2.4 Size-fractionated primary production through ^{14}C uptake

Samples from each mesocosm were taken in 10 L high density polyethylene (HDPE) canisters and transported to the GOB laboratories every 2 sampling days. Primary production (PP) in pico (0.2–2 µm), nano (2–20 µm), and micro (20–280 µm) size fractions were measured following a modified version of the approach by Cermeño et al. (2012). Four culture flasks (Sarstedt TC Flask d15, Nümbrecht, Germany) per mesocosm were filled up to the bottle neck (70 mL) and spiked with 80 µL (0.296 MBq) of a ^{14}C-labeled sodium bicarbonate ($NaH^{14}CO_3$, Perkin Elmer, Waltham, USA) stock solution (3.7 MBq mL^{-1}). Prior to ^{14}C inoculation, samples were prefiltered through a 280 µm mesh to exclude most of the zooplankton fraction. Each flask was then closed and gently homogenized. All culture flasks were incubated for 24 h in an environmental chamber (Aralab FitoClima 600 Bio Chamber, Lisbon, Portugal) at in situ light (12 h light–dark cycle with a mean daily PAR intensity of ~ 500 µmol photons $m^{-2}\,s^{-1}$) and temperature (21–24 °C depending on the temperature in the mesocosms on each sampling day). One out of the four culture flasks per mesocosm was incubated inside a light-proof bag to prevent photosynthesis.

After incubation, all samples were sequentially filtered on a circular filtration manifold (Oceomic, Fuerteventura, Spain) under low vacuum pressure (< 200 mbar) through polycarbonate membrane filters with pore sizes of 20 µm (top), 2 µm (middle), and 0.2 µm (bottom) (DHI GVS 20 µm, Hørsholm, Denmark; Whatman Nuclepore 2 and 0.2 µm, Maidstone, UK). The manifold allowed us to collect the filtrate in 120 mL HDPE bottles. The filters were placed in 5 mL scintillation vials (Sarstedt HDPE mini-vial, Nümbrecht, Germany), while 5 mL of the filtrates was transferred to 20 mL scintillation vials (Sarstedt HDPE scintillation vial, Nümbrecht, Germany) for dissolved organic carbon production ($\mathrm{PP_{DOC}}$) determination. To remove the remaining inorganic ^{14}C, all samples were acidified. To do so, the 5 mL vials with the filters were placed inside a desiccator and exposed to fuming hydrochloric acid (HCl 37 %) for 24 h, whilst 100 µL of hydrochloric acid (HCl 17.5 %) was added to the filtrate subsamples and placed on an orbital oscillator at 60 rpm, also for 24 h.

After acidifying, filters were pushed into the vials and 3.5 and 10 mL of scintillation cocktail (Ultima Gold XR, Perkin Elmer, Waltham, USA) was added to the filters and the liquid

samples, respectively. All vials were vigorously shaken and left for an additional 24 h in the dark before being measured with a scintillation counter (Beckman LS-6500, Brea, USA). The counted disintegrations per minute (DPM) were used to calculate primary production rates ($\mu g\,C\,L^{-1}\,h^{-1}$) using the following Eq. (4):

$$PP = \frac{V_S}{V_F} \cdot \frac{DIC \cdot (DPM_S - DPM_D)}{DPM_A \cdot t_i}, \quad (4)$$

where V_S is sample volume (L), V_F is filtered volume (L), DPM_S is sample disintegrations per minute, DPM_D is dark-incubated sample disintegrations per minute, DIC is dissolved inorganic carbon ($\mu mol\,C\,L^{-1}$), DPM_A is initially added ^{14}C in disintegrations per minute, and t_i is time of incubation (h).

The average of the triplicates was used to calculate the final PP rates. The three size fractions were summed up to calculate the particulate organic carbon production (PP_{POC}). Moreover, Eq. (5) below was utilized to calculate the percentage of extracellular organic carbon release (PER):

$$PER(\%) = \frac{PP_{DOC}}{PP_{POC} + PP_{DOC}} \cdot 100. \quad (5)$$

2.5 Size-fractionated chlorophyll *a*

Chlorophyll *a* (Chl *a*) samples for each mesocosm were collected in 500 mL dark bottles from the same 10 L canisters as PP. Samples were sequentially filtered through superimposed polycarbonate filters of 20 µm, 2, and 0.2 µm pore size (DHI GVS 20 µm, Hørsholm, Denmark, Whatman Nuclepore 2 and 0.2 µm, Maidstone, UK). The filters were stored at −20 °C while pending analysis. The pigment was extracted by submerging the filters in 10 mL of acetone (90 %) at −20 °C for 24 h. The extracts were analyzed using a benchtop fluorometer (Turner Design AU-10, San Jose, USA) as in Welschmeyer (1994). Total Chl *a* concentration was determined by adding up the three size fractions.

2.6 Prokaryotic and eukaryotic abundances

Duplicate flow cytometry samples were collected every 2 d and ran in vivo. A CytoSense (CytoBuoy, Woerden, Netherlands) flow cytometer was used, and the default software (CytoClus) was employed to differentiate the phytoplankton population clusters based on red, yellow, and green fluorescence as well as forward and side scatter, which are indicators of size and cell complexity (Dubelaar and Gerritzen, 2000). *Synechococcus* and picoeukaryotes fall within the same forward- and side-scatter range, but *Synechococcus* are distinguished due to their yellow fluorescence content. Picoeukaryotes and nanoeukaryotes both contain red fluorescence, but the latter group is larger in size and complexity. Thus, falling within distinct forward- and side-scatter ranges.

2.7 Data analysis

The experiment was divided into two phases (I: days 5–19; II: days 21–33; the reasons for this division are explained in the Results section). All parameters were analyzed in relation to the alkalinity gradient deployed using simple linear regressions. Additionally, in the parameters that showed a potential curvilinear trend in relation to the TA, and thus DIC gradient, linear and polynomial regression models were also fitted, excluding the two highest treatments. For these parameters, in order to avoid overfitting, cross validation was used to assess the polynomial model's performance to pick the best-fitting model order. DIC was chosen as the predictor variable for the latter. Averages of the response variables for each phase and for the entirety of the experiment, in both cases excluding the days prior to the TA addition, were used. Assumptions of normality were tested using Q–Q and Shapiro–Wilk tests on test residuals. Data analyses were performed using RStudio (2022.02.3 Build 492; package stats, ggplot2 v3.3.5; Wickham et al., 2016).

3 Results

3.1 Carbonate chemistry temporal development and phase determination

The TA gradient in increments of 300 $\mu mol\,L^{-1}$ was attained, and DIC and TA were stable up to day 21 (Fig. 1a). The experimental period up to that day, 5–19, was differentiated and designated as phase I (< 4 d after the TA addition), with phase II defined as the period starting on day 20 that coincided with an abrupt change in the biological response among the mesocosms. Additionally, in this second phase (> 14 d after the TA addition), indirect abiotic precipitation occurred in the highest treatment, $\Delta 2400\,\mu mol\,L^{-1}$. Precipitates were visibly forming on the mesocosm walls by day 28, a process that advanced quite rapidly during the 6 d after cleaning. The precipitation process lasted until the end of the experiment and led to a TA and DIC loss of ∼ 293.7 and 175.3 $\mu mol\,L^{-1}$, respectively (Fig. 1a and b).

After the alkalinity addition on day 4, the pH varied slightly according to the gradient applied, ranging from 8.03 in the control to almost 8.3 in the highest treatment (Fig. 1c). CO_2 partial pressure did not vary alongside the TA gradient due to the equilibrated nature of the alkalinity manipulation (Fig. 1d). However, the estimated pCO_2 in the highest treatment in phase II increased from ∼ 450 in phase I to a maximum of ∼ 550 µatm by day 33 due to the triggered calcification process ($\Delta TA\ 2400\,\mu mol\,L^{-1}$). It was ∼ 50 µatm higher than the rest of the treatments starting on day 27, increasing towards the end of the experiment, when it was ∼ 100 µatm greater than ambient levels (Fig. 1d). Because of the increase in pCO_2 in this treatment in phase II, pH dropped from 8.24

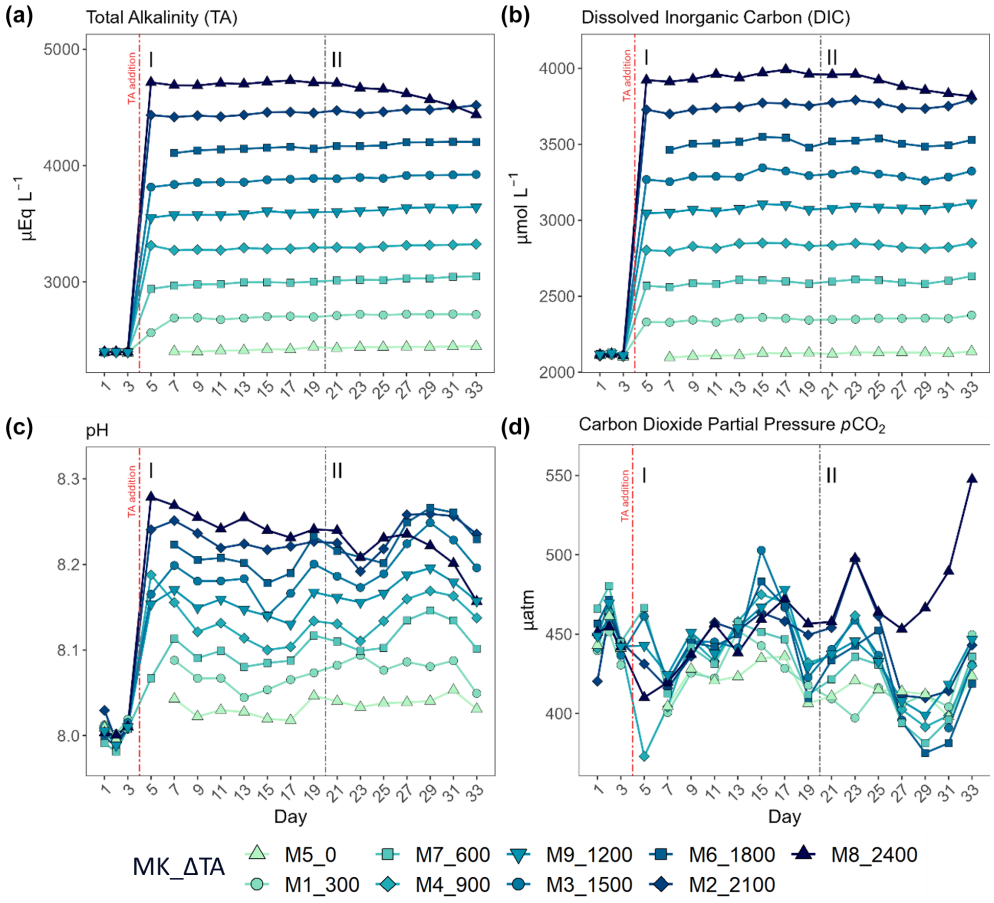

Figure 1. Temporal development of **(a)** total alkalinity (TA), **(b)** dissolved inorganic carbon (DIC), **(c)** pH (seawater scale), and **(d)** pCO_2 throughout the entire experiment for each mesocosm (MK) and treatment (ΔTA). The x axis represents the number of days elapsed since the beginning of the experiment.

on day 18 down to a minimum of 8.16 at the end of the experiment (Fig. 1c and d).

3.2 Primary production and metabolic balance

As previously mentioned, another reason for the delineation of the mentioned phases (I: days 5–19; II: days 21–33) is the observed increase in production and chlorophyll *a* concentration in specific intermediate treatments after day 20 when compared to phase I (Fig. 2). This division of the experimental period was chosen to facilitate the system's response interpretation. Overall, NCP, GP, and the metabolic balance (GP : CR) show similar developments. All metabolic rates behaved differently in the two phases (Fig. 2a–c). In the first phase, CR accounted for most of the GP, while NCP was for the most part negative (more respiration than oxygen production; Fig. 2b and d). In contrast, a peak in GP and NCP rates occurred at Δ1500 and Δ1800 during the second phase, showing 2- and 3-fold increased GP, respectively. Autotrophy was also observed in the Δ600 and Δ900 treatments during this phase although only for 2 d (Fig. 2b and d).

Phase-averaged linear regressions with the whole TA gradient revealed no significant treatment effect (alpha < 0.05) on NCP, GP, and CR rates as well as metabolic balance (GP : CR) (Fig. S4). Additionally, no impact of the abiotic precipitation in the highest treatment was observed regarding GP, NCP, CR, GP : CR (Fig. 2), ^{14}C primary production, and Chl *a* concentration (Figs. 3 and 4).

In terms of the relative contributions of pico, nano, and micro to total PP and Chl *a*, differences between phases, although they are not statistically significant, are only visually clear in the Δ600, Δ900, Δ1500, and Δ1800 treatments – those that showed autotrophy (Fig. 2d) in the second phase (Fig. 3). In these mesocosms, pico and in Δ900 micro also in terms of PP (Fig. 3, left) contributed the most in the first phase. However, in the second phase, nano became more dominant in these intermediate treatments, especially in Δ1500 and Δ1800. In Δ1200 the latter pattern is not clear. Instead, the micro fraction contributed more throughout the whole experiment when compared to all other treatments. Total PP and Chl *a* concentration data matched the spike in oxygen production observed in treatments Δ1500

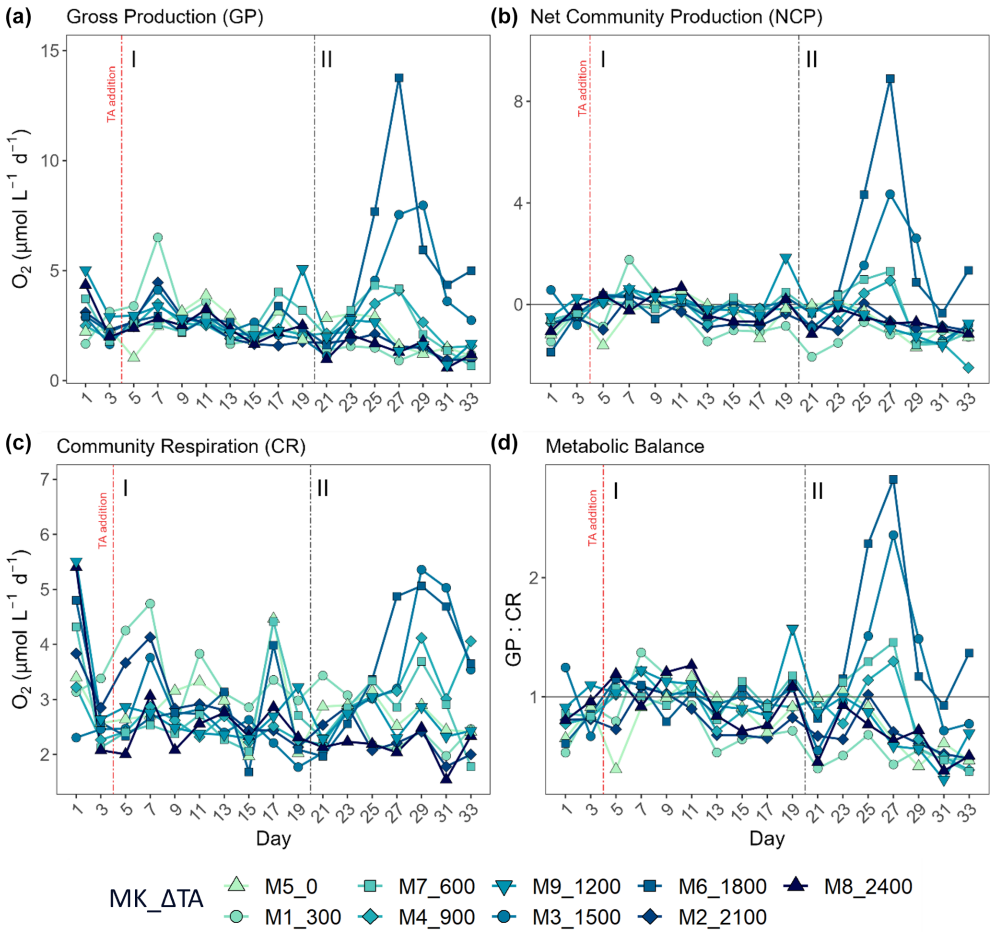

Figure 2. Results for metabolic rates measured through oxygen production and consumption showing the temporal development of **(a)** the gross production (GP), **(b)** the net community production (NCP), **(c)** the community respiration (CR), and **(d)** the metabolic balance (GCP over CR). In the legend, MK corresponds to mesocosm and ΔTA to Δtotal alkalinity. The *x* axis represents the number of days elapsed since the beginning of the experiment.

and Δ1800 and also the slight increases found in treatments Δ600 and Δ900 (Fig. 4). Data for PP on day 27, when oxygen production and Chl *a* concentration in Δ1800 were the highest of all values recorded throughout the entire experiment and for all mesocosms, were not collected, thus meaning that the peak in Δ1800 reflected by Chl *a* (Fig. 4a and b) and the gross community production (GCP) and NCP rates (Fig. 2) was excluded (Fig. 4c and d). This explains why the peak in production is lower in the Δ1800 treatment than in the Δ1500, particularly in Fig. 4d.

The increases in production observed in phase II were driven by nanoplankton growth (Figs. 3 and 4b, d). When considering all treatments, in phase I this size fraction showed a positive linear trend in relation to the alkalinity ($R^2 = 0.51$; $p = 0.031$) and the DIC ($R^2 = 0.50$; $p = 0.031$) gradients in terms of ^{14}C uptake. However, this significant relationship vanished by phase II.

Regarding percent of extracellular organic carbon release (PER), no statistically significant linear relationship with the whole DIC gradient, chosen since it likely was the driver behind a potential response in PP rather than TA, was found (Fig. 5). Moreover, and as is true for all other parameters presented in this study, PER behaved disparately during the two phases. For the intermediate treatments where there was autotrophy in the second phase, PER values dropped in comparison to the two highest and two lowest treatments, while Δ1200 stayed the same. Additionally, if the two highest treatments are excluded from the analysis, a significant negative relationship between the PER and the DIC gradient can be observed (Fig. 5).

3.3 Pico- and nanoeukaryote abundances

The second phase of the experiment was characterized by an increase in production and Chl *a* concentrations in all intermediate treatments below the two highest and above the two lowest treatments, except Δ1200, while phase I was distinguished by extremely low GP, NCP, PP rates, and Chl *a*

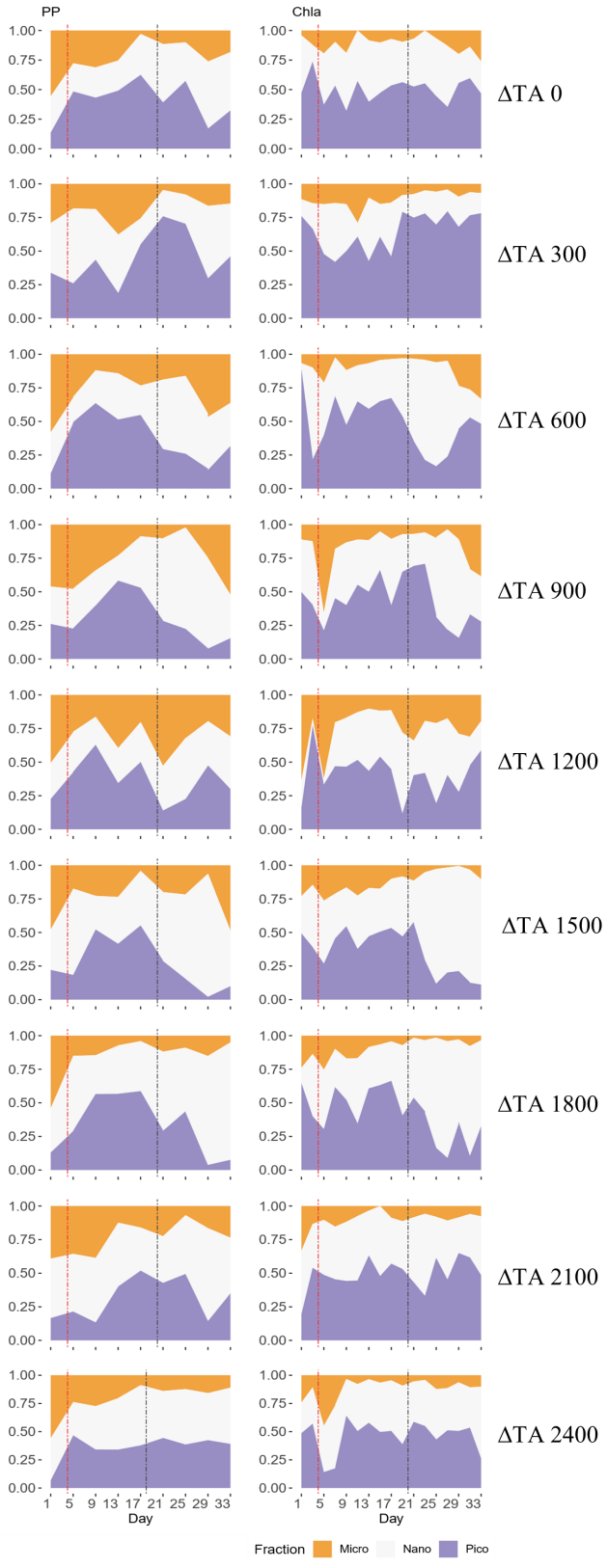

Figure 3. Temporal development of the three phytoplankton size fractions' (pico 0.2–2 µm, nano 2–20 µm, micro > 20 µm) relative contributions to primary production (PP) through ^{14}C uptake (left column) and chlorophyll *a* (Chl *a*) concentration (right column) for each treatment. The *x* axis represents the number of days elapsed since the beginning of the experiment.

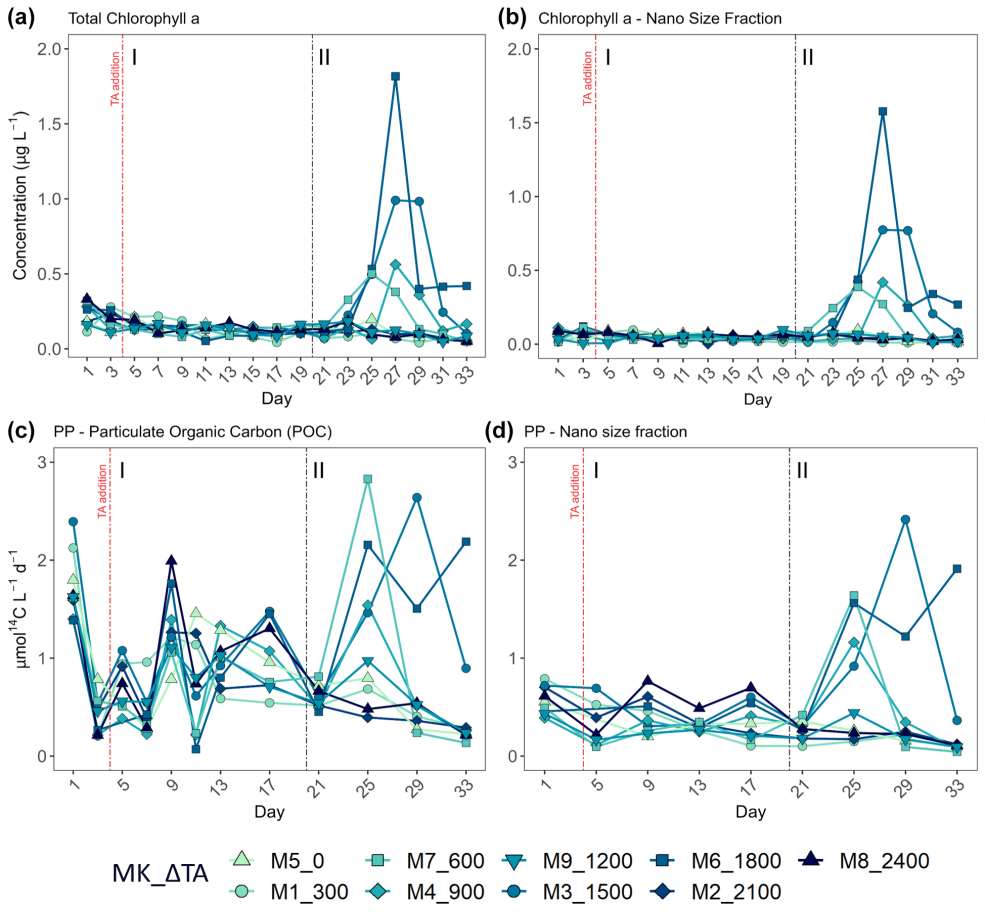

Figure 4. Temporal development of **(a)** total chlorophyll *a* (Chl *a*) concentration, **(b)** the nano-size fraction's (2–20 µm) contribution to the total Chl *a* concentration, **(c)** total particulate organic carbon production (where PP is primary production), and **(d)** the nano size fraction's (same size range as for the Chl *a*) contribution to total PP. MK corresponds to mesocosm and ΔTA to Δtotal alkalinity. The *x* axis represents the number of days elapsed since the beginning of the experiment.

throughout and across all mesocosms. Picoeukaryote abundance decreased during the first phase and picked back up 3-fold in the intermediate treatments going from Δ600 to Δ1800 (Fig. 6a). *Synechococcus* proliferated in phase II in the lower intermediate treatments (treatments Δ600 and Δ900) as seen in Fig. 6b. Two nanoeukaryote groups could be distinguished based on complexity and red fluorescence content. Nanoeukaryotes (2) were larger and contained more red fluorescence than the nanoeukaryotes (1), and they also held some yellow fluorescence. Nanoeukaryote (1) abundance, despite gradually dropping throughout the experiment (Fig. 6c), showed a positive linear relationship ($R^2 = 0.634$; $p = 0.01$) with TA across both phases. Nanoeukaryote (2) abundance drove GP, NCP, and PP rates and contributed the most to Chl *a* in the intermediate treatments, except Δ1200, during phase II (Figs. 4 and 6d). In addition, no impact of the indirect abiotic precipitation that occurred in the highest treatment during phase II was observed in any of the population abundances monitored (Fig. 6). In fact, abundances of all groups in the latter treatment are comparable to those observed in the control.

3.4 Nonlinear response vs. no response

TA and DIC, in an equilibrated OAE approach, vary together (as TA increases, so does DIC; Fig. S5), and, if a potential nonlinear response between the metabolic parameters listed in Table 2 were to be considered, the driver behind these relationships would most likely be DIC (key substrate for carbon fixation; Badger et al., 1998), not TA. The nonlinear response was detected for the longer-term phase, meaning the averaged-out values of phase II, but also for the entire duration of the experiment (Fig. 7). Average GP and NCP rates, GP : CR, total PP, particulate and dissolved organic carbon (POC and DOC) production, and Chl *a*, the nanoplankton contribution to the latter two, and the nanoeukaryote abundances all exhibited a gradual increase in the intermediate treatments and a decline beyond ΔTA 1800 µmol L^{-1}, during the mentioned time periods. Indeed, if the two highest

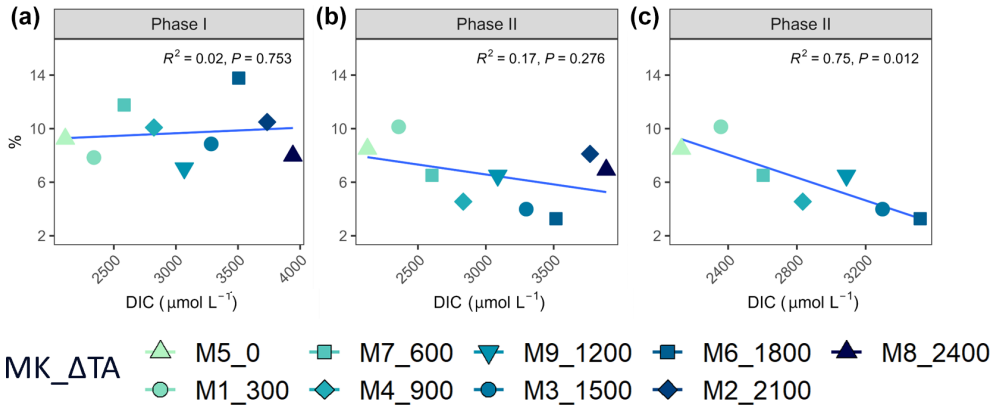

Figure 5. Linear regressions between ΔTA treatment and PER per phase (**a** phase I and **b** phase II) and **(c)** removing the two highest treatments in phase II. MK corresponds to mesocosm and ΔTA to Δtotal alkalinity.

Table 2. Summary tables showing the regression coefficient values of (left) second-order polynomial regression models; (middle) linear regression models, in both cases excluding the two highest treatments (Δ2100 and Δ2400 µmol L^{-1}); and (right) linear models excluding the two treatments that show the highest response (Δ1500 and Δ1800 µmol L^{-1}), fitted for gross and net community production (GP and NCP), metabolic balance (GP : CR), ^{14}C primary production (PP_total, POC, and DOC), the nanoplankton fraction contribution to PP_Total (PP_Nano), total Chl *a* concentration (Chl *a*), the nanoplankton fraction contribution to total Chl *a* concentration (Chl *a*_Nano), and the abundances of nanoeukaryotes (1) and (2) counted through flow cytometry in relation to DIC. The *p* values are indicated by the symbol to the right of each regression coefficient (see legend). All significant regressions are also marked in bold letters.

y	Polynomial without two highest treatments [$y \sim$ DIC + I (DIC^2)]			Linear without two highest treatments [$y \sim$ DIC]			Linear without Δ1500 and Δ1800 treatments [$y \sim$ DIC]		
	Phase I	Phase II	Throughout	Phase I	Phase II	Throughout	Phase I	Phase II	Throughout
GP	0.034	**0.834** *	**0.880** *	0.007	**0.630** *	**0.677** *	0.192	0.158	0.405
NCP	**0.729** ·	**0.857** *	**0.881** *	0.487	**0.614** *	**0.763** *	0.025	0.004	0.018
GP : CR	**0.758** ·	**0.812** *	**0.878** *	0.463	**0.616** *	**0.767** **	0.016	0.022	0.0005
PP_Total	0.527	**0.705** ·	**0.791** *	0.002	**0.618** *	**0.532** ·	0.091	0.130	0.001
PP_POC	0.538	**0.703** ·	**0.806** *	0.008	**0.620** *	**0.561** ·	0.085	0.118	0.005
PP_DOC	0.250	**0.792** *	**0.749** ·	0.160	**0.656** *	**0.528** ·	0.057	0.104	0.002
PP_Nano	0.588	**0.752** ·	**0.788** *	0.369	**0.644** *	**0.371** *	**0.474** ·	0.048	0.096
Chl *a*	0.176	**0.783** *	**0.782** *	0.128	**0.667** *	**0.668** *	0.110	0.039	0.029
Chl *a*_Nano	0.243	**0.779** *	**0.785** *	0.148	**0.653** *	**0.643** *	0.039	0.028	0.023
Nano (1)	0.132	**0.872** *	**0.687** ·	0.003	**0.598** *	**0.577** *	0.407	0.194	**0.623** *
Nano (2)	**0.723** ·	**0.658** ·	**0.696** ·	**0.683** *	**0.576** *	**0.623** *	0.015	0.0001	9.86×10^{-6}
***P* value**	0–0.001 ***	0.001–0.01 **	0.01–0.05 *	0.05–0.1 ·	0.1–1				

treatments are excluded from the model, significant linear relationships emerge between DIC and all the parameters listed above for both phase II and the entire experiment (Table 2). However, it is worth noting that these relationships yield stronger regression coefficients when second-order polynomial regression models are employed instead (Table 2). Furthermore, a significant relationship is observed in phase I between NCP, metabolic balance, and nanoeukaryote (2) abundance if the polynomial model is fitted (Table 2, left). Linear relationships also become evident for the latter parameter when analyzed independently (Table 2, middle).

However, when linear regressions are employed and the two treatments with the highest responses (Δ1500 and Δ1800 µmol L^{-1}) are excluded instead, the significance of all the previously described relationships is no longer observed (Table 2), although even when these two intermediate treatments are excluded, the nanoplankton contribution to PP in phase I and the nanoeukaryote (1) abundance throughout the experiment continue to exhibit a significant linear trend. This suggests that these specific relationships remain robust and significant, regardless of the exclusion of the highest-response treatments.

The cross-validation test results indicate that the second polynomial term of DIC is marginally significant (p value between 0.05 and 0.1), while the first polynomial term (the linear model) is statistically significant (p values < 0.05), although notably both of these terms have a positive coefficient, thus suggesting that, even though the second poly-

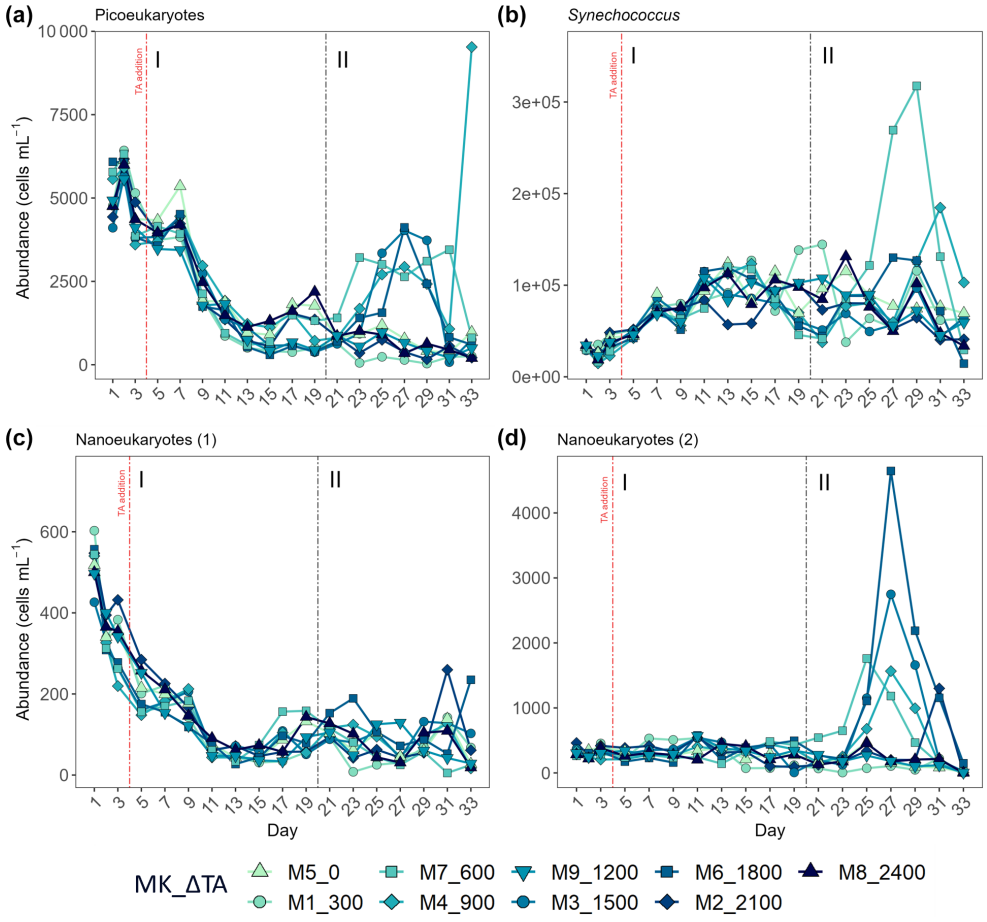

Figure 6. Abundance in cells mL^{-1} obtained through flow cytometry of **(a)** picoeukaryotes, **(b)** *Synechococcus*, **(c)** nanoeukaryote (1), and **(d)** nanoeukaryote (2). The two latter correspond to two different nanoeukaryote populations by both complexity/size and red fluorescence content. MK corresponds to mesocosm and ΔTA to Δtotal alkalinity. The *x* axis represents the number of days elapsed since the beginning of the experiment.

nomial term leads to higher regression coefficients, it may have a weaker although albeit potentially relevant effect (still > 90 % confidence level) on the response variable when compared to the linear model.

4 Discussion

The main goal of this study was to simulate a carbonate-based OAE scenario. As a first step, carbonate-based, CO_2-equilibrated solutions were used in order to simulate a best-case scenario. CO_2 equilibration, i.e., keeping pCO_2 levels constant, allows for greater alkalinity additions before the $CaCO_3$ saturation threshold is reached. The levels of exposure experienced by the microbial community (< 80 µm in the current study) at an alkalinity dispersal plume were simulated through the ΔTA gradient. The oligotrophic waters surrounding the Canary Islands were chosen as an open-ocean oligotrophic system analog in terms of nutrient availability and community composition.

A neutral response of the measured metabolic rates, PP, Chl *a*, and community composition, when taking the entire alkalinity range (from ambient to ∼ 4600 µmol kg^{-1}) applied here into account, was observed. These results are consistent with 4 d microcosm experiments carried out at sea with two natural microbial communities of the North Atlantic subtropical gyre (Subhas et al., 2022). In this case, only three alkalinity treatments were deployed, with the highest being ∼ 4500 µmol kg^{-1}, and also using $NaHCO_3$ and Na_2CO_3 stock solutions. No major effect on the estimated net primary production, minor effects on community composition, and no influence on net calcification rates were observed after 4 d, results that, followed by those obtained from the current longer-term study, suggest this OAE approach may not entail significant alterations to microbial communities in oligotrophic pelagic systems.

However, nutrient limitation (Fig. S1) may have concealed more apparent responses to the TA and DIC gradients. Research on OAE's potential impacts in oligotrophic systems

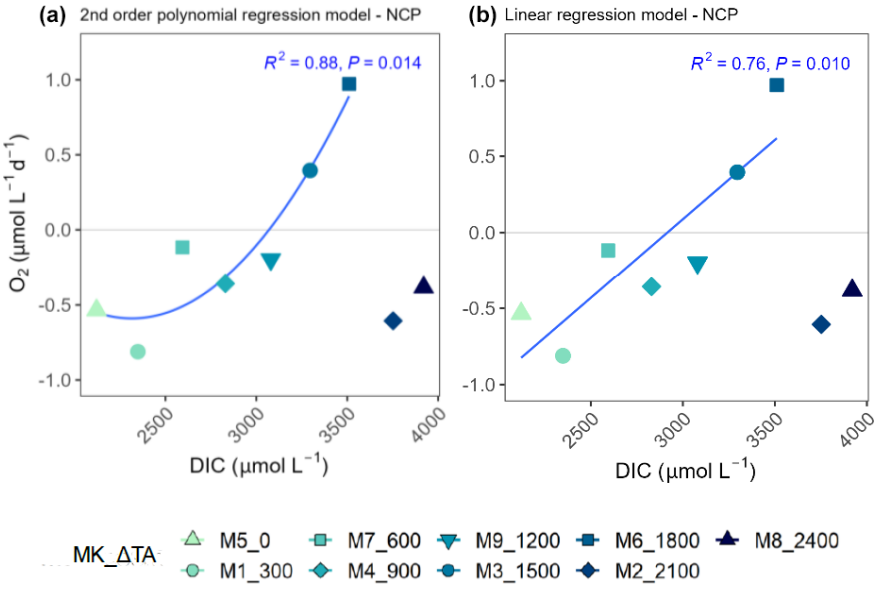

Figure 7. Second-order polynomial **(a)** and linear **(b)** regression models fitted to the treatments of up to ΔTA1800 µmol L^{-1} relating net community production (NCP) rates and the associated dissolved inorganic carbon (DIC) levels averaged out for the whole experiment. In the legend, MK corresponds to mesocosm and TA to total alkalinity.

at a comparable scale is non-existent. In eutrophic environments, a transient positive impact on calcifiers, if present at the time of deployment, has been hypothesized due to the provision of additional substrate for calcification in the form of carbonate ions (Bach et al., 2019), notably at and surrounding the alkalinity addition hotspot where the carbonate system is altered the most. Nevertheless, a recently published study showed no response of *Emiliania huxleyi* to a limestone-inspired alkalinity addition in a laboratory setting, with high nutrient availability, in terms of growth rates and elemental ratios after 6 d (Gately et al., 2023). Whether this is the case in a natural environment and for longer term exposure to such conditions is unknown. These results suggest that the effects of OAE on community structure and composition may be more complex than anticipated with the "green vs. white" ocean hypothesis (Bach et al., 2019). However, further experimental research is necessary to evaluate the consequences of, for instance, a silicate- vs. a carbonate-based OAE deployment but also of OAE in more eutrophic environments, more specifically regarding community structure, calcification, and silicification, but also primary production and metabolic balance, to address key knowledge gaps.

4.1 Potential for nonlinear effects of OAE on metabolic rates

In the current study, a linear short-term response was observed for the nano fraction's contribution to PP, and a positive relationship between nanoeukaryote (1) abundance and TA was detected when considering the averages for the whole experiment. These results are not entirely supported by those obtained by Ferderer et al. (2022). In their study, the water enclosed in ∼ 55 L microcosms for 25 d was rich in inorganic nutrients (PO_4^{3-} 0.79 ± 0.01 µM; NO_x 6.38 ± 0.19 µM; 9.65 ± 0.39 µM $Si(OH)_4$). The alkalinity addition in their equilibrated treatment was of roughly 500 µmol L^{-1}, which is comparable to the Δ600 µmol L^{-1} treatment in the present study which mildly responds in the second phase. They observed a significant difference in the Chl *a* concentrations, also driven by nanoplankton growth, between the control and their equilibrated alkalinity treatment, in which the latter was lower. They report on a short-term response to the initial nutrient concentrations after closure. In the current study, however, relationships with a gradient rather than differences between one treatment and another are reported on instead. Additionally, production and Chl *a* responses here occur in the long term, past day 27, and the significant linear trends stated at the beginning of this section are not with regard to Chl *a*. Furthermore, in the present study, no significant linear relationships with the whole TA gradient were found in any other parameter after a month-long exposure to such conditions.

Albeit at constant pCO_2, prolonged exposure to higher calcite and aragonite saturation states and moderate pH increases in an OAE dispersal plume has been hypothesized to lead to nonlinear and/or threshold-like responses in the long-term (Subhas et al., 2022). This pattern was noticed for the parameters listed in Table 2 in relation to DIC, suggesting there may in fact be an optimum-curve-like response and a threshold between Δ1800 and Δ2100 µmol L^{-1} treatments (Fig. 6). Indeed, if only the treatments below Δ2100 µmol L^{-1} are considered, positive significant relationships, described by polynomial (higher regression coef-

ficients) and linear regression models (Table 2 and Fig. 7), arise between DIC and NCP, GP, GP : CR, PP_total, POC and DOC production, PP_Nano, total Chl *a*, Chl *a*_Nano, and both nanoeukaryote clusters' abundances, in addition to the opposite pattern being reflected by the PER (Fig. 7). PER is known to be higher in oligotrophic than in eutrophic waters (Chróst, 1983; Teira et al., 2001). The observed significant decrease in the PER associated with the OAE treatment up to $\Delta 1800\,\mu mol\,L^{-1}$ in the second phase suggests there may have been a slight increase in inorganic nutrients in relation to the TA manipulation, potentially caused by enhanced nitrogen cycling. In fact, the latter process is known to be pH dependent (Beman et al., 2011; Fumasoli et al., 2017; Pommerening-Röser and Koops, 2005). The previous explanation may be further supported by the increase in NO_x ($NO_3 + NO_2$; in particular of nitrite, NO_2^-) concentrations (Fig. S1) observed in the second phase. Additionally, Paul et al. (2024) observed a positive relationship of particulate organic carbon to particulate organic nitrogen (POC : PON) ratios in the second phase and a negative relation of particulate organic nitrogen (PON) concentrations in the first phase, both with the OAE treatment during the same mesocosm study. Thus, considering that all the earlier described responses occurred in the second phase (designated as long term), the peak in production may have been possible due to a slight increase in heterotrophic turnover of organic nitrogen associated with the carbonate chemistry manipulation, which would explain the lag in the observed responses.

Actually, considering the nutrient-depleted nature of the system in all mesocosms, the occurrence of the peaks in production that drive the optimum-curve-like relationship was unexpected. All that is currently known about the species responsible for the increase in productivity observed in the four intermediate treatments (Fig. 6) is that it was a *Chrysochromulina* spp. after exemplary samples were analyzed via microscopy. In a study carried out from May to June 1988 in the Kattegat, *C. polylepis* was monitored prior to the decline of a bloom (Kaas et al., 1991). The authors measured its distribution, primary production, and nitrogen dynamics and found that *C. polylepis* showed high affinity for ammonia. It was its main nitrogen source and, as previously stated, the only nutrient that was not measured in the current study.

An alternative explanation could be that the protagonist in the intermediate treatments during the second phase of the experiment was *C. parkeae*, which is a life cycle stage of *Braarudosphaera bigelowii* (Suzuki et al., 2021). The latter is known to possess a nitrogen-fixing cyanobacterial endosymbiont (UCYN-A; Suzuki et al., 2021) that would have allowed it to adapt to the highly nutrient-depleted environment. In addition, *B. bigelowii* is a haptophyte that was found to perform extracellular calcification (Hagino et al., 2016) and thus, may have benefited from the increase in the calcite saturation state.

Taxon-specific, optimum-curve-like responses of phytoplankton growth to the combined effect of H^+ and CO_2 have previously been reported (Paul and Bach, 2020). CO_2 is usually considered the main source of carbon for primary production. However, most marine phytoplankton are capable of actively taking up bicarbonate thanks to carbon concentrating mechanisms (CCMs; Giordano et al., 2005; Price et al., 2008). Bicarbonate ions are accumulated in the cytosol and later converted to CO_2 prior to carboxylation (Price et al., 2008). In the present study DIC was increased according to an equilibrated (no reduction in CO_2) TA gradient. This manipulation was the main difference between the mesocosms. Thus, the bicarbonate availability levels attained in the intermediate treatments, where autotrophy was observed, may have been behind the detected peaks in production, alongside the potential relief of nutrient limitation explained above, meaning that, in the current experiment, a certain nanoplankton species with more evolved CCMs may have benefited from the higher DIC concentrations and slight pH increase, directly and indirectly, respectively.

Chi et al. (2014) studied different strains of microalgae and cyanobacteria as candidates for bicarbonate-based carbon capture for algae production (BICCAPS). Depending on the species, different growth rates and thresholds, and in some cases growth inhibition, were observed when these were cultured under varying bicarbonate concentrations. This is likely due to species-specific ionic strength tolerance, meaning their capacity to adapt and thrive in varied bicarbonate ion concentrations, potentially explaining the observed threshold.

However, whether the peaks observed in $\Delta 1500$ and $\Delta 1800\,\mu mol\,L^{-1}$, which drive the detected optimum curve (Table 2 and Fig. 7), occurred by random chance and were thus not caused by the carbonate chemistry conditions remains unclear. In fact, when removing $\Delta 1500$ and $\Delta 1800\,\mu mol\,L^{-1}$ from the model instead of the two highest treatments, these positive significant relationships with DIC vanish (Table 2), although these nutrient-decoupled peaks in production only occurred in mesocosms where TA, DIC, and, to a lesser extent, pH were increased. It is a novel sighting since a response of this magnitude has not been observed in previous experiments carried out under nutrient-depleted conditions and/or while testing ocean acidification in the Canary Islands (Paul et al., 2024). Consequently, and also considering the results from the cross-validation test, additional studies simulating the gradient applied here or similar, though with replicates, could further elucidate if such a threshold and the positive relation found below it hold. If the latter were further supported, long-term consequences in terms of microbial community metabolic functioning associated with said changes would need to be taken into consideration and further evaluated before OAE implementation.

4.2 Challenges and limitations of OAE studies

A limitation of this experimental setup that should also be mentioned is that mesocosm studies are limited to temporal

scales of weeks to months, precluding the study of potential longer-term effects. Additionally, secondary precipitation in the highest treatment likely occurred due to the substrate for nuclei formation provided by the mesocosm walls themselves, although it may not be the sole cause.

Hartmann et al. (2023) carried out CO_2-equilibrated alkalinity additions of up to $\Delta 2400\,\mu mol\,L^{-1}$ using the same stock solutions as in our experiment. Biotic incubations that included phytoplankton and particles smaller than 55 µm, which are a potential seed surface for nucleation, were set up. They observed no precipitates forming on the bottle walls and thus no TA consumption, after 4 d. However, in their long-term alkalinity stability experiment (up to 90 d), precipitation was observed in the "untreated mode" (or control, meaning no particle addition) 10 d after the TA increase. Hartmann et al. (2023) hypothesized that precipitation was potentially triggered by the wall effect since it was an abiotic treatment containing no particles larger than 0.2 µm. Furthermore, when precipitates from other experiments were added to the "treated mode" treatments, immediate and persistent precipitation was observed for both $\Delta 2100$ and $\Delta 2400\,\mu mol\,L^{-1}$. Additionally, Wurgaft et al. (2021) found that TA loss via abiotic precipitation occurred at lower levels in a natural system than in these experiments due to the sediment particles in river plumes.

Thus, the secondary precipitation observed in the present study, as previously stated, may have been due to a combination of the wall effect, including cleaning procedures that caused resuspension of particles present on the walls, but also to the existence of particles and cells in the water column. Whether carbonate formation would occur around the levels ($\sim 4500\,\mu mol\,L^{-1}$) observed in this study in a natural oligotrophic, open-ocean environment is still unclear. Actually, the theoretical aragonite saturation (Ω_{Ar}) threshold of 12.5 above which carbonate precipitation was expected to occur (Morse and He, 1993) was never surpassed (Table 1).

4.3 Implications for future OAE research

Further experimental research at this scale is essential to test the effects of non-equilibrated OAE approaches as well. These may be more viable considering the current infrastructure since large-scale equilibrated OAE application may require the use of reactors to CO_2-equilibrate the alkaline solutions prior to addition (Hartmann et al., 2023).

At the alkalinity point source, and depending on the alkalinity dispersal plume dynamics, the carbonate system perturbations associated with non-equilibrated OAE can be much stronger. Alkalinity loss would also be triggered at much lower levels than those observed for CO_2-equilibrated OAE (Hartmann et al., 2023). Besides, when precipitation is triggered, a process by which precipitation keeps progressing past reaching the aragonite saturation levels of 12.5–13.5 and even ambient levels, also known as "runaway precipitation" (Moras et al., 2022), may be induced.

The findings of the current study suggest that carbonate-based, CO_2-equilibrated OAE may be environmentally safe in terms of the metabolic processes measured here, in an oligotrophic environment, even if abiotic precipitation were triggered, although further research is required on the impacts of this phenomenon on other processes, i.e., on particle sinking due to ballasting. Moreover, uncertainty remains in the determination of responses to longer-term exposure to the conditions simulated in this study and in the levels at which abiotic precipitation may occur in the natural open ocean.

Several risks and co-benefits have been listed for this NET (Bach et al., 2019), although none have been really tested at a reasonable scale. This study concludes there may be a potential co-benefit to the addition of carbonates in solution, with CO_2 equilibration, where biological carbon sequestration is increased up to a certain threshold. Moreover, and as is true for ocean acidification, this response is species/group specific. In addition, past the mentioned threshold, production decreased but rates were comparable to those measured for the control and $\Delta 300\,\mu mol\,L^{-1}$ treatments. Therefore, no impact of equilibrated OAE past the $\sim 4000\,\mu mol\,L^{-1}$ TA threshold and of abiotic precipitation at $\sim 4300\,\mu mol\,L^{-1}$ on the measured metabolic rates can be inferred.

5 Conclusions

An ideal ocean alkalinity enhancement (OAE) deployment scenario was simulated under natural conditions. Total alkalinity (TA) was increased without the introduction of potentially harmful dissolution by-products, and CO_2 was chemically sequestered prior to the TA manipulation. The OAE approach employed within the specified TA range did not pose a threat to the pelagic microbial community in relation to the parameters monitored in the current study. Importantly, this held true even when abiotic precipitation occurred in the highest treatment. In fact, there is a potential co-benefit in the form of increased microbial community and primary production up to a specific threshold. This increase could be driven indirectly either by the rise in pH, enhancing nitrogen cycling and consequently inorganic nutrient availability, or by the carbonate chemistry conditions, specifically increased dissolved inorganic carbon (DIC) availability. Our discovery of a nonlinear, optimum-curve-like response in microbial production rates to the applied dissolved inorganic carbon (DIC) gradient (as shown in Table 2) is noteworthy. This finding is novel and warrants further investigation. Therefore, considering the substantial climatic benefits it could offer, additional research on carbon uptake efficiency and the effects of CO_2 but also non-CO_2-equilibrated OAE on natural microbial communities is of high priority.

Data availability. Datasets of the response variables presented in this study can be found in an online repository. The name of the

repository is PANGAEA, and the access link is https://doi.org/10.1594/PANGAEA.964537 (Marín-Samper et al., 2024). Biogeochemical data (nutrient concentrations and carbonate chemistry) will be made available in the same repository, without undue reservation.

Supplement. The supplement related to this article is available online at: https://doi.org/10.5194/bg-21-2859-2024-supplement.

Author contributions. Experimental concept and design: UR and JA. Execution of the experiment: all authors. Data analysis: LMS with input from NHH and JO. Original draft preparation: LMS. Review and editing: all authors.

Competing interests. The contact author has declared that none of the authors has any competing interests.

Disclaimer. Publisher's note: Copernicus Publications remains neutral with regard to jurisdictional claims made in the text, published maps, institutional affiliations, or any other geographical representation in this paper. While Copernicus Publications makes every effort to include appropriate place names, the final responsibility lies with the authors.

Special issue statement. This article is part of the special issue "Environmental impacts of ocean alkalinity enhancement". It is not associated with a conference.

Acknowledgements. The authors are grateful for the entire KOSMOS team of GEOMAR for all the logistical and technical work associated with the mesocosm campaign, coordinating all the onsite research activities, and for promoting fair data management and exchange. A special thank you goes to the biological oceanography group (GOB-ULPGC), in particular to Acorayda González, for helping with the oxygen measurements, and to Minerva Espino, Aja Trebec, Beatriz Fernández, Lucía Palacios, and Maria Fernanda Montero for carrying out a large volume of sample analyses. Also, we would like to acknowledge Levka Hansen (GEOMAR) for helping with the primary production through ^{14}C uptake measurements, Julieta Schneider (GEOMAR) for the carbonate chemistry measurements, and Allanah Paul for the interesting discussions on data interpretation. Finally, we want to thank the Oceanic Platform of the Canary Islands (PLOCAN) and the University of Las Palmas of Gran Canaria (ULPGC) for providing all the essential facilities to conduct this experiment.

Financial support. This research has been supported by the EU Horizon 2020 Research and Innovation Programme project OceanNETs ("Ocean-based Negative Emissions Technologies – analysing the feasibility, risks and co-benefits of ocean-based negative emission technologies for stabilizing the climate", grant no. 869357) and by the Helmholtz European Partnering project Ocean-CDR ("Ocean-based carbon dioxide removal strategies", project no.: PIE-0021). Additional funding was provided through the EU H2020-INFRAIA's project AQUACOSM ("AQUACOSM: Network of Leading European AQUAtic MesoCOSM Facilities Connecting Mountains to Oceans from the Arctic to the Mediterranean", project no. 731065). This work was co-financed by the "Agencia Canaria de Investigación, Innovación y Sociedad de la Información" (ACIISI) of the "Consejería de Economía, Conocimiento y Empleo" and by the "Fondo Social Europeo (FSE) Programa Operativo Integrado de Canarias 2014–2020, Eje 3 Tema Prioritario 74 (85 %)".

Review statement. This paper was edited by Lydia Kapsenberg and reviewed by Joana Barcelos e Ramos and one anonymous referee.

References

Bach, L. T., Gill, S. J., Rickaby, R. E. M., Gore, S., and Renforth, P.: CO_2 Removal With Enhanced Weathering and Ocean Alkalinity Enhancement: Potential Risks and Co-benefits for Marine Pelagic Ecosystems, Front. Clim., 1, 7, https://doi.org/10.3389/fclim.2019.00007, 2019.

Badger, M. R., Andrews, T. J., Whitney, S. M., Ludwig, M., Yellowlees, D. C., Leggat, W., and Price, G. D.: The diversity and coevolution of Rubisco, plastids, pyrenoids, and chloroplast-based CO_2-concentrating mechanisms in algae, Can. J. Bot., 76, 1052–1071, https://doi.org/10.1139/b98-074, 1998.

Beman, J. M., Chow, C. E., King, A. L., Feng, Y., Fuhrman, J. A., Andersson, A., Bates, N. R., Popp, B. N., and Hutchins, D. A.: Global declines in oceanic nitrification rates as a consequence of ocean acidification, P. Natl. Acad. Sci. USA, 108, 208–213, https://doi.org/10.1073/pnas.1011053108, 2011.

Bryan, J. R., Rlley, J. P., and Williams, P. J. L.: A winkler procedure for making precise measurements of oxygen concentration for productivity and related studies, J. Exp. Mar. Biol. Ecol., 21, 191–197, https://doi.org/10.1016/0022-0981(76)90114-3, 1976.

Burns, W. and Corbett, C. R.: Antacids for the Sea? Artificial Ocean Alkalinization and Climate Change, One Earth, 3, 154–156, https://doi.org/10.1016/j.oneear.2020.07.016, 2020.

Butenschön, M., Lovato, T., Masina, S., Caserini, S., and Grosso, M.: Alkalinization Scenarios in the Mediterranean Sea for Efficient Removal of Atmospheric CO_2 and the Mitigation of Ocean Acidification, Front. Clim., 3, 1–11, https://doi.org/10.3389/fclim.2021.614537, 2021.

Canadell, J. G., Monteiro, P. M. S., Costa, M. H., Cotrim da Cunha, L., Cox, P. M., Eliseev, A. V., Henson, S., Ishii, M., Jaccard, S., Koven, C., Lohila, A., Patra, P. K., Piao, S., Rogelj, J., Syampungani, S., Zaehle, S., and Zickfeld, K.: Global Carbon and other Biogeochemical Cycles and Feedbacks. In Climate Change 2021: The Physical Science Basis. Contribution of Working Group I to the Sixth Assessment Report of the Intergovernmental Panel on Climate Change, edited by: Masson-Delmotte, V., Zhai, P., Pirani, A., Connors, S. L., Péan, C., Berger, S., Caud, N., Chen, Y., Goldfarb, L., Gomis, M. I., Huang, M., Leitzell, K., Lonnoy, E., Matthews, J. B. R., Maycock, T. K., Waterfield, T., Yelekçi, O., Yu, R., and Zhou, B., Cambridge University Press,

Cambridge, United Kingdom and New York, NY, USA, 673–816, https://doi.org/10.1017/9781009157896.007, 2021.

Carpenter, J. and Carritt, D.: Modifications Employed of the Winkler Method for Determining Dissolved Oxygen in Seawater, A NASCO Report, 1966.

Caserini, S., Pagano, D., Campo, F., Abbà, A., De Marco, S., Righi, D., Renforth, P., and Grosso, M.: Potential of Maritime Transport for Ocean Liming and Atmospheric CO_2 Removal, Front. Clim., 3, 1–18, https://doi.org/10.3389/fclim.2021.575900, 2021.

Cermeño, P., Fernández, A., and Marañón, E.: Determinación de la producción primaria fraccionada por tamaños, in: Expedición de circunnavegación Malaspina 2010: cambio global y exploración de la biodiversidad del océano/Enrique Moreno Ostos (aut.), Carlos M. Duarte (aut.), 437–442, ISBN 978-84-00-09419-5, 2012.

Chen, C. Y., Durbin, E. G., Marine, S., Progress, E., and June, N.: Effects of pH on the growth and carbon uptake of marine phytoplankton, Mar. Ecol. Prog. Ser., 109, 83–94, https://doi.org/10.3354/meps109083, 1994.

Chen, S.-M., Riebesell, U., Schulz, K. G., von der Esch, E., Achterberg, E. P., and Bach, L. T.: Temporal dynamics of surface ocean carbonate chemistry in response to natural and simulated upwelling events during the 2017 coastal El Niño near Callao, Peru, Biogeosciences, 19, 295–312, https://doi.org/10.5194/bg-19-295-2022, 2022.

Chi, Z., Elloy, F., Xie, Y., Hu, Y., and Chen, S.: Selection of microalgae and cyanobacteria strains for bicarbonate-based integrated carbon capture and algae production system, Appl. Biochem. Biotech., 172, 447–457, https://doi.org/10.1007/s12010-013-0515-5, 2014.

Chróst, R. J.: Plankton photosynthesis, extracellular release and bacterial utilization of released dissolved organic carbon (RDOC) in lakes of different trophy, Acta Microbiol. Pol., 32, 275–287, 1983.

Dubelaar, G. B. J. and Gerritzen, P. L.: CytoBuoy: A step forward towards using flow cytometry in operational oceanography, Sci. Mar., 64, 255–265, https://doi.org/10.3989/scimar.2000.64n2255, 2000.

Eisaman, M. D., Geilert, S., Renforth, P., Bastianini, L., Campbell, J., Dale, A. W., Foteinis, S., Grasse, P., Hawrot, O., Löscher, C. R., Rau, G. H., and Rønning, J.: Assessing the technical aspects of ocean-alkalinity-enhancement approaches, in: Guide to Best Practices in Ocean Alkalinity Enhancement Research, edited by: Oschlies, A., Stevenson, A., Bach, L. T., Fennel, K., Rickaby, R. E. M., Satterfield, T., Webb, R., and Gattuso, J.-P., Copernicus Publications, State Planet, 2-oae2023, 3, https://doi.org/10.5194/sp-2-oae2023-3-2023, 2023.

Enmar, R., Stein, M., Bar-Matthews, M., Sass, E., Katz, A., and Lazar, B.: Diagenesis in live corals from the Gulf of Aqaba. I. The effect on paleo-oceanography tracers, Geochim. Cosmochim. Ac., 64, 3123–3132, https://doi.org/10.1016/S0016-7037(00)00417-8, 2000.

Feely, R. A., Sabine, C. L., Lee, K., Berelson, W., Kleypas, J., Fabry, V. J., and Millero, F. J.: Impact of Anthropogenic CO_2 on the $CaCO_3$ System in the Oceans, J. Agron. Educ., 14, 3–7, https://doi.org/10.2134/jae1985.0003, 1985.

Feng, E. Y., Koeve, W., Keller, D. P., and Oschlies, A.: Model-Based Assessment of the CO_2 Sequestration Potential of Coastal Ocean Alkalinization, Earths Future, 5, 1252–1266, https://doi.org/10.1002/2017EF000659, 2017.

Ferderer, A., Chase, Z., Kennedy, F., Schulz, K. G., and Bach, L. T.: Assessing the influence of ocean alkalinity enhancement on a coastal phytoplankton community, Biogeosciences, 19, 5375–5399, https://doi.org/10.5194/bg-19-5375-2022, 2022.

Friedlingstein, P., Jones, M. W., O'Sullivan, M., Andrew, R. M., Bakker, D. C. E., Hauck, J., Le Quéré, C., Peters, G. P., Peters, W., Pongratz, J., Sitch, S., Canadell, J. G., Ciais, P., Jackson, R. B., Alin, S. R., Anthoni, P., Bates, N. R., Becker, M., Bellouin, N., Bopp, L., Chau, T. T. T., Chevallier, F., Chini, L. P., Cronin, M., Currie, K. I., Decharme, B., Djeutchouang, L. M., Dou, X., Evans, W., Feely, R. A., Feng, L., Gasser, T., Gilfillan, D., Gkritzalis, T., Grassi, G., Gregor, L., Gruber, N., Gürses, Ö., Harris, I., Houghton, R. A., Hurtt, G. C., Iida, Y., Ilyina, T., Luijkx, I. T., Jain, A., Jones, S. D., Kato, E., Kennedy, D., Klein Goldewijk, K., Knauer, J., Korsbakken, J. I., Körtzinger, A., Landschützer, P., Lauvset, S. K., Lefèvre, N., Lienert, S., Liu, J., Marland, G., McGuire, P. C., Melton, J. R., Munro, D. R., Nabel, J. E. M. S., Nakaoka, S.-I., Niwa, Y., Ono, T., Pierrot, D., Poulter, B., Rehder, G., Resplandy, L., Robertson, E., Rödenbeck, C., Rosan, T. M., Schwinger, J., Schwingshackl, C., Séférian, R., Sutton, A. J., Sweeney, C., Tanhua, T., Tans, P. P., Tian, H., Tilbrook, B., Tubiello, F., van der Werf, G. R., Vuichard, N., Wada, C., Wanninkhof, R., Watson, A. J., Willis, D., Wiltshire, A. J., Yuan, W., Yue, C., Yue, X., Zaehle, S., and Zeng, J.: Global Carbon Budget 2021, Earth Syst. Sci. Data, 14, 1917–2005, https://doi.org/10.5194/essd-14-1917-2022, 2022.

Fumasoli, A., Bürgmann, H., Weissbrodt, D. G., Wells, G. F., Beck, K., Mohn, J., Morgenroth, E., and Udert, K. M.: Growth of Nitrosococcus-Related Ammonia Oxidizing Bacteria Coincides with Extremely Low pH Values in Wastewater with High Ammonia Content, Environ. Sci. Technol., 51, 6857–6866, https://doi.org/10.1021/acs.est.7b00392, 2017.

Gafar, N. A. and Schulz, K. G.: A three-dimensional niche comparison of *Emiliania huxleyi* and *Gephyrocapsa oceanica*: reconciling observations with projections, Biogeosciences, 15, 3541–3560, https://doi.org/10.5194/bg-15-3541-2018, 2018.

Gately, J. A., Kim, S. M., Jin, B., Brzezinski, M. A., and Iglesias-rodriguez, M. D.: Coccolithophores and diatoms resilient to ocean alkalinity enhancement: A glimpse of hope?, Science, 9, 6066, https://doi.org/10.1126/sciadv.adg6066, 2023.

Gattuso, J. P., Magnan, A. K., Bopp, L., Cheung, W. W. L., Duarte, C. M., Hinkel, J., Mcleod, E., Micheli, F., Oschlies, A., Williamson, P., Billé, R., Chalastani, V. I., Gates, R. D., Irisson, J. O., Middelburg, J. J., Pörtner, H. O., and Rau, G. H.: Ocean solutions to address climate change and its effects on marine ecosystems, Front. Mar. Sci., 5, 337, https://doi.org/10.3389/fmars.2018.00337, 2018.

Gattuso, J. P., Williamson, P., Duarte, C. M., and Magnan, A. K.: The Potential for Ocean-Based Climate Action: Negative Emissions Technologies and Beyond, Front. Clim., 2, 1–8, https://doi.org/10.3389/fclim.2020.575716, 2021.

Giordano, M., Beardall, J., and Raven, J. A.: CO_2 concentrating mechanisms in algae: Mechanisms, environmental modulation, and evolution, Annu. Rev. Plant Biol., 56, 99–131, https://doi.org/10.1146/annurev.arplant.56.032604.144052, 2005.

Goldenberg, S. U., Taucher, J., Fernández-Méndez, M., Ludwig, A., Arístegui, J., Baumann, M., Ortiz, J., Stuhr, A., and Riebesell, U.: Nutrient composition (Si : N) as driver of plankton com-

munities during artificial upwelling, Front. Mar. Sci., 9, 1–15, https://doi.org/10.3389/fmars.2022.1015188, 2022.

González, M. F. and Ilyina, T.: Impacts of artificial ocean alkalinization on the carbon cycle and climate in Earth system simulations, Geophys. Res. Lett., 43, 6493–6502, https://doi.org/10.1002/2016GL068576, 2016.

Grasshof, K., Kremling, K., and Ehrhard, M. (Eds.): Arsenic, antimony, and germanium, in: Methods of Seawater Analysis, edited, Wiley-VCH, Weinheim, 274–294, https://hdl.handle.net/11858/00-001M-0000-0014-9602-3 (last access: 11 June 2024), 1999.

Hagino, K., Tomioka, N., Young, J. R., Takano, Y., Onuma, R., and Horiguchi, T.: Extracellular calcification of *Braarudosphaera bigelowii* deduced from electron microscopic observations of cell surface structure and elemental composition of pentaliths, Mar. Micropaleontol., 125, 85–94, https://doi.org/10.1016/j.marmicro.2016.04.002, 2016.

Hartmann, J., Suitner, N., Lim, C., Schneider, J., Marín-Samper, L., Arístegui, J., Renforth, P., Taucher, J., and Riebesell, U.: Stability of alkalinity in ocean alkalinity enhancement (OAE) approaches – consequences for durability of CO_2 storage, Biogeosciences, 20, 781–802, https://doi.org/10.5194/bg-20-781-2023, 2023.

Harvey, L. D. D.: Mitigating the atmospheric CO_2 increase and ocean acidification by adding limestone powder to upwelling regions, J. Geophys. Res.-Oceans, 113, 1–21, https://doi.org/10.1029/2007JC004373, 2008.

Haszeldine, R. S., Flude, S., Johnson, G., and Scott, V.: Negative emissions technologies and carbon capture and storage to achieve the Paris Agreement commitments, Philos. T. R. Soc. A, 376, 20160447, https://doi.org/10.1098/rsta.2016.0447, 2018.

Hendriks, I. E. and Duarte, C. M.: Ocean acidification: Separating evidence from judgment – A reply to Dupont et al., Estuar. Coast. Shelf S., 89, 186–190, https://doi.org/10.1016/j.ecss.2010.06.007, 2010.

Ilyina, T., Wolf-Gladrow, D., Munhoven, G., and Heinze, C.: Assessing the potential of calcium-based artificial ocean alkalinization to mitigate rising atmospheric CO_2 and ocean acidification, Geophys. Res. Lett., 40, 5909–5914, https://doi.org/10.1002/2013GL057981, 2013.

Kaas, H., Larsen, J., Mohlenberg, F., and Richardson, K.: The Chrysochromulina polylepis bloom in the Kattegat (Scandinavia) May–June 1988. Distribution, primary production and nutrient dynamics in the late stage of the bloom, Mar. Ecol. Prog. Ser., 79, 151–161, https://doi.org/10.3354/meps079151, 1991.

Kheshgi, H. S.: Sequestering atmospheric carbon dioxide by increasing ocean alkalinity, Energy, 20, 915–922, https://doi.org/10.1016/0360-5442(95)00035-F, 1995.

Köhler, P., Abrams, J. F., Völker, C., Hauck, J., and Wolf-Gladrow, D. A.: Geoengineering impact of open ocean dissolution of olivine on atmospheric CO_2, surface ocean pH and marine biology, Environ. Res. Lett., 8, 014009, https://doi.org/10.1088/1748-9326/8/1/014009, 2013.

Kroeker, K. J., Kordas, R. L., Crim, R. N., and Singh, G. G.: Meta-analysis reveals negative yet variable effects of ocean acidification on marine organisms, Ecol. Lett., 13, 1419–1434, https://doi.org/10.1111/j.1461-0248.2010.01518.x, 2010.

Kroeker, K. J., Kordas, R. L., Crim, R., Hendriks, I. E., Ramajo, L., Singh, G. S., Duarte, C. M., and Gattuso, J. P.: Impacts of ocean acidification on marine organisms: Quantifying sensitivities and interaction with warming, Glob. Change Biol., 19, 1884–1896, https://doi.org/10.1111/gcb.12179, 2013.

Lenton, A., Matear, R. J., Keller, D. P., Scott, V., and Vaughan, N. E.: Assessing carbon dioxide removal through global and regional ocean alkalinization under high and low emission pathways, Earth Syst. Dynam., 9, 339–357, https://doi.org/10.5194/esd-9-339-2018, 2018.

Lewis, E. and Wallace, D.: Program Developed for CO_2 System Calculations ORNL/CDIAC-105, Carbon Dioxide Information Analysis Centre, Oak Ridge National Laboratory, Oak Ridge, Tennessee, https://salish-sea.pnnl.gov/media/ORNL-CDIAC-105.pdf (last access: 11 June 2024), 1998.

Lueker, T. J., Dickson, A. G., and Keeling, C. D.: Ocean pCO_2 calculated from dissolved inorganic carbon, alkalinity, and equations for K1 and K2: Validation based on laboratory measurements of CO_2 in gas and seawater at equilibrium, Mar. Chem., 70, 105–119, https://doi.org/10.1016/S0304-4203(00)00022-0, 2000.

Marín-Samper, L., Arístegui, J., Hernández-Hernández, N., Ortiz Cortes, J., Archer, S., Ludwig, A., and Riebesell, U.: KOSMOS 2021 Gran Canaria mesocosm study on ocean alkalinity enhancement: phytoplankton metabolic rates, PANGAEA [data set], https://doi.org/10.1594/PANGAEA.964537, 2024.

Meysman, F. J. R. and Montserrat, F.: Negative CO_2 emissions via enhanced silicate weathering in coastal environments, Biol. Lett., 13, 20160905, https://doi.org/10.1098/rsbl.2016.0905, 2017.

Montserrat, F., Renforth, P., Hartmann, J., Leermakers, M., Knops, P., and Meysman, F. J. R.: Olivine Dissolution in Seawater: Implications for CO_2 Sequestration through Enhanced Weathering in Coastal Environments, Environ. Sci. Technol., 51, 3960–3972, https://doi.org/10.1021/acs.est.6b05942, 2017.

Moras, C. A., Bach, L. T., Cyronak, T., Joannes-Boyau, R., and Schulz, K. G.: Ocean alkalinity enhancement – avoiding runaway $CaCO_3$ precipitation during quick and hydrated lime dissolution, Biogeosciences, 19, 3537–3557, https://doi.org/10.5194/bg-19-3537-2022, 2022.

Morse, J. W. and He, S.: Influences of T, S and P_{CO_2} on the pseudo-homogeneous precipitation of $CaCO_3$ from seawater: implications for whiting formation, Mar. Chem., 41, 291–297, 1993.

Nassif, N., Pinna, N., Gehrke, N., Antonietti, M., Jäger, C., and Cölfen, H.: Amorphous layer around aragonite platelets in nacre, P. Natl. Acad. Sci. USA, 102, 12653–12655, https://doi.org/10.1073/pnas.0502577102, 2005.

National Academies of Sciences, Engineering, and Medicine: Negative Emissions Technologies and Reliable Sequestration: A Research Agenda, The National Academies Press, Washington, DC, https://doi.org/10.17226/25259, 2018.

Orr, J. C., Fabry, V. J., Aumont, O., Bopp, L., Doney, S. C., Feely, R. A., Gnanadesikan, A., Gruber, N., Ishida, A., Joos, F., Key, R. M., Lindsay, K., Maier-Reimer, E., Matear, R., Monfray, P., Mouchet, A., Najjar, R. G., Plattner, G. K., Rodgers, K. B., Sabine, C. L., Sarmiento, J. L., Schlitzer, R., Slater, R. D., Totterdell, I. J., Weirig, M. F., Yamanaka, Y., and Yool, A.: Anthropogenic ocean acidification over the twenty-first century and its impact on calcifying organisms, Nature, 437, 681–686, https://doi.org/10.1038/nature04095, 2005.

Paul, A. J. and Bach, L. T.: Universal response pattern of phytoplankton growth rates to increasing CO_2, New Phytol., 228, 1710–1716, https://doi.org/10.1111/nph.16806, 2020.

Paul, A. J., Haunost, M., Goldenberg, S. U., Hartmann, J., Sánchez, N., Schneider, J., Suitner, N., and Riebesell, U.: Ocean alkalinity enhancement in an open ocean ecosystem: Biogeochemical responses and carbon storage durability, EGUsphere [preprint], https://doi.org/10.5194/egusphere-2024-417, 2024.

Pommerening-Röser, A. and Koops, H. P.: Environmental pH as an important factor for the distribution of urease positive ammonia-oxidizing bacteria, Microbiol. Res., 160, 27–35, https://doi.org/10.1016/j.micres.2004.09.006, 2005.

Price, G. D., Badger, M. R., Woodger, F. J., and Long, B. M.: Advances in understanding the cyanobacterial CO_2-concentrating- mechanism (CCM): Functional components, Ci transporters, diversity, genetic regulation and prospects for engineering into plants, J. Exp. Bot., 59, 1441–1461, https://doi.org/10.1093/jxb/erm112, 2008.

Rau, G. H., McLeod, E. L., and Hoegh-Guldberg, O.: The need for new ocean conservation strategies in a high-carbon dioxide world, Nat. Clim. Change, 2, 720–724, https://doi.org/10.1038/nclimate1555, 2012.

Renforth, P. and Henderson, G.: Assessing ocean alkalinity for carbon sequestration, Rev. Geophys., 55, 636–674, https://doi.org/10.1002/2016RG000533, 2017.

Renforth, P., Jenkins, B. G., and Kruger, T.: Engineering challenges of ocean liming, Energy, 60, 442–452, https://doi.org/10.1016/j.energy.2013.08.006, 2013.

Riebesell, U., Wolf-Gladrow, D. A., and Smetacek, V.: Carbon dioxide limitation of marine phytoplankton growth rates, Nature, 361, 249–251, https://doi.org/10.1038/361249a0, 1993.

Subhas, A. V., Marx, L., Reynolds, S., Flohr, A., Mawji, E. W., Brown, P. J., and Cael, B. B.: Microbial ecosystem responses to alkalinity enhancement in the North Atlantic Subtropical Gyre, Front. Clim., 4, 784997, https://doi.org/10.3389/fclim.2022.784997, 2022.

Suzuki, S., Kawachi, M., Tsukakoshi, C., Nakamura, A., Hagino, K., Inouye, I., and Ishida, K. I.: Unstable Relationship Between *Braarudosphaera bigelowii* (= *Chrysochromulina parkeae*) and Its Nitrogen-Fixing Endosymbiont, Front. Plant Sci., 12, 749895, https://doi.org/10.3389/fpls.2021.749895, 2021.

Taucher, J., Bach, L. T., Boxhammer, T., Nauendorf, A., Achterberg, E. P., Algueró-Muñiz, M., Arístegui, J., Czerny, J., Esposito, M., Guan, W., Haunost, M., Horn, H. G., Ludwig, A., Meyer, J., Spisla, C., Sswat, M., Stange, P., Riebesell, U., Aberle-Malzahn, N., Archer, S., Boersma, M., Broda, N., Büdenbender, J., Clemmesen, C., Deckelnick, M., Dittmar, T., Dolores-Gelado, M., Dörner, I., Fernández-Urruzola, I., Fiedler, M., Fischer, M., Fritsche, P., Gomez, M., Grossart, H. P., Hattich, G., Hernández-Brito, J., Hernández-Hernández, N., Hernández-León, S., Hornick, T., Kolzenburg, R., Krebs, L., Kreuzburg, M., Lange, J. A. F., Lischka, S., Linsenbarth, S., Löscher, C., Martínez, I., Montoto, T., Nachtigall, K., Osma-Prado, N., Packard, T., Pansch, C., Posman, K., Ramírez-Bordón, B., Romero-Kutzner, V., Rummel, C., Salta, M., Martínez-Sánchez, I., Schröder, H., Sett, S., Singh, A., Suffrian, K., Tames-Espinosa, M., Voss, M., Walter, E., Wannicke, N., Xu, J., and Zark, M.: Influence of ocean acidification and deep water upwelling on oligotrophic plankton communities in the subtropical North Atlantic: Insights from an in situ mesocosm study, Front. Mar. Sci., 4, 85, https://doi.org/10.3389/fmars.2017.00085, 2017.

Teira, E., Pazó, M. J., Serret, P., and Fernández, E.: Dissolved organic carbon production by microbial populations in the Atlantic Ocean, Limnol. Oceanogr., 46, 1370–1377, https://doi.org/10.4319/lo.2001.46.6.1370, 2001.

Uppström, L. R.: The boron/chlorinity ratio of deep-sea water from the Pacific Ocean, Deep Sea Res. Oceanogr. Abstr., 21, 161–162, https://doi.org/10.1016/0011-7471(74)90074-6, 1974.

Welschmeyer, N. A.: Fluorometric analysis of chlorophyll *a* in the presence of chlorophyll *b* and pheopigments, Limnol. Oceanogr., 39, 1985–1992, https://doi.org/10.4319/lo.1994.39.8.1985, 1994.

Wickham, H., Chang, W., and Wickham, M. H.: Package 'ggplot2,' Creat. elegant data Vis. using Gramm. Graph. Version, 2, Comprehensive R Archive Network (CRAN), 1–189, https://ggplot2.tidyverse.org (last access: 11 June 2024), 2016.

Wittmann, A. C. and Pörtner, H. O.: Sensitivities of extant animal taxa to ocean acidification, Nat. Clim. Change, 3, 995–1001, https://doi.org/10.1038/nclimate1982, 2013.

Wurgaft, E., Wang, Z. A., Churchill, J. H., Dellapenna, T., Song, S., Du, J., Ringham, M. C., Rivlin, T., and Lazar, B.: Particle Triggered Reactions as an Important Mechanism of Alkalinity and Inorganic Carbon Removal in River Plumes, Geophys. Res. Lett., 48, 1–10, https://doi.org/10.1029/2021GL093178, 2021.

State Planet, 2-oae2023, 4, 2023
https://doi.org/10.5194/sp-2-oae2023-4-2023

General considerations for experimental research on ocean alkalinity enhancement

Sam Dupont[1,2] **and Marc Metian**[1]

[1]Radioecology Laboratory, International Atomic Energy Agency, Marine Environment Laboratories, Monaco 98000, Monaco
[2]Department for Biological and Environmental Sciences, University of Gothenburg, Fiskebäckskil 45178, Sweden

Correspondence: Sam Dupont (sam.dupont@bioenv.gu.se)

Received: 13 June 2023 – Discussion started: 26 June 2023
Revised: 7 October 2023 – Accepted: 10 October 2023 – Published: 27 November 2023

Abstract. Ocean alkalinity enhancement (OAE) is proposed as an approach to capture carbon by adding alkaline substances to seawater to enhance the ocean's natural carbon sink. These substances include minerals, such as olivine, or artificial substances, such as lime or some industrial byproducts. Deployment of OAE will lead to complex and dynamic changes in the seawater carbonate chemistry, and in some cases the addition of other compounds and impurities from the minerals. While OAE alters the carbonate chemistry in a very different way, much can be learned from the abundant literature on ocean acidification documenting the impact of changes in the carbonate chemistry on marine life from genes to ecosystems. A vast majority of the experimental work was performed by manipulating the concentration of carbon dioxide in seawater under constant alkalinity (TA) to simulate near-future ocean acidification. Understanding the impact of changes in alkalinity on marine species and the ecosystem is less understood. In the context of OAE, it is critical to resolve such impacts, alone or in combination with other compounds and impurities from the minerals to be co-released during implementation, to ensure that any field manipulation does not translate into damaging biological effects. As for other environmental drivers, this will require an understanding across all the levels of biological organizations from species to ecosystems over relevant time exposure considering the method of deployment (e.g., dilution, repeated exposure) and factors such as local adaptation. Such complex questions cannot be resolved using a single approach, and a combination of monitoring, modeling, laboratory, natural (i.e., proxies or analogs), and field experiments will be required. This chapter summarizes some key general considerations for experimental design. It also compares strengths and weaknesses of the different approaches. We will also consider best practices relevant to OAE such as the need to properly monitor and consider the addition of trace elements and byproducts, as well as potential interactions with other naturally occurring drivers.

1 Identifying a relevant question

A pre-requisite to the selection of a given research approach or strategy is to define a clear question. For a safe and efficient implementation of ocean alkalinity enhancement (OAE) one needs to answer several key questions, including those given below.

- What are the best implementation methods to optimize efficiency and minimize risks?
- Is the implementation of OAE safe for marine species and ecosystems?

These questions are too big and complex to be resolved by a single experiment or approach. Fully addressing these would require a large-scale involvement of the scientific community and strong international and multi-disciplinary collaboration. Specifically, in order to fully understand and project the ecological consequences of OAE, a suite of mechanistic based models will need to be developed and connected

across all levels of biological organization from species to ecosystem. For example, the dynamic energy budget provides a framework to synthesize complex physiological responses and processes at the organism level and allows us to project how key traits (e.g., growth, metabolism, reproduction) respond to environmental changes (Kooijman, 2001). At community and ecosystem levels, data are needed on the response of key ecological traits and processes that structure communities, such as predator–prey relationships, competition, habitat provision, and facilitation. This will require a wide range of different mechanistic experiments that when combined through parameterization of models will provide the holistic view required for forecasting. These models can then be tested against the response in the "real" world, helping validate the model's underlying parameterization and assumptions.

Exposure to elevated alkalinity at different rates and intensity, potentially combined with the other elements such as silicate, calcium, magnesium, and trace metals (e.g., iron, nickel, cobalt, chromium), would expose natural ecosystems to conditions that strongly deviate from the present range of natural variability and thus has the potential to drive negative effects. At present, these impacts are poorly understood. Understanding the impact of multiple environmental changes (alkalinity and the consequence for the carbonate chemistry, as well as other elements) on key marine ecosystems requires research at the crossroad between physiology, ecology, and evolution. As a comparison, after more than 2 decades of research on ocean acidification and the publication of more than 10 000 scientific articles, we are still lacking the full mechanistic understanding that would allow us to bridge chemical and biological changes and the forecasting ability required for science-based management (Cooley et al., 2022).

Regarding the urgency of the climate crisis and the limited resources, it is critical to quickly identify the key subquestions that need to be urgently answered to provide informed guidance to if, how, where, and when OAE should be implemented. These priorities should be identified in the spirit of the United Nation Decade of Ocean Science for Sustainable Development (The science we need for the ocean we want) and focus on the trade-off between the desirable level of understanding to take informed decisions, the time needed to collect such data, and how these data and decisions can lead to concrete actions. Each question can organically translate into a research strategy and the selection of the appropriate approach(es), species and ecosystems, or experimental designs (see Sect. 3).

Examples of key sub-questions to resolve the potential impacts of OAE on marine ecosystems include the following examples.

- What is the best material (e.g., mineral) for a safe implementation of OAE?
- What is the safest deployment method for the surrounding ecosystems?
- What makes a species or an ecosystem sensitive to OAE?

Resolving these questions would allow us to identify the best sites and methods for safe implementation but would require a complex experimental strategy combining laboratory studies, e.g., identifying thresholds for key parameters such as alkalinity or trace element concentrations, resolving the combined effect of multiple drivers, and developing a mechanistic understanding of how species and ecosystem resilience (the inherent ability to absorb various disturbances and reorganize while undergoing state changes to maintain critical functions) to OAE links to factors such as present natural variability, taxonomy, physiology, life-history strategies, trophic levels, and field experimentation, including in mesocosms, to validate mechanistic models. That will require work across the whole range of sizes and complexities and the breaking down of these complex questions into smaller manageable ones within a strategy.

Additionally, it is important to remember that the implementation of OAE will also involve large-scale industrial activity in marine systems. The impacts of these will be additional to the direct chemical changes and any associated additional stressors with the transport and addition of the alkalinity to the marine system should also be considered.

2 Comparison of the different research approaches

Every scientific manipulation experiment, either in the field or in the laboratory, is an abstraction of reality. While best practices, in terms of experimental design, measurements, or monitoring of environmental conditions, are well established (see Riebesell et al., 2011, in the context of ocean acidification), the outcome of any scientific study is strongly dependent on experimental choices (e.g., tested scenarios, duration, level of biological organization, selected species or population) These are often resulting from a compromise between the requested design to test a given hypothesis and practical constraints and limitations. Understanding the impact of OAE on marine ecosystems is a complex question that can be broken down into multiple hypotheses. For each hypothesis, a strong scientific strategy involving multiple approaches and/or experiments is needed. In this section, we will briefly describe and highlight the strengths and limitations of each approach (Fig. 1).

2.1 Laboratory experiments (see Iglesias-Rodriguez et al., 2023, this Guide, for more information and references)

Chemical changes associated with OAE deployment can be easily simulated in laboratory experiments. These includes

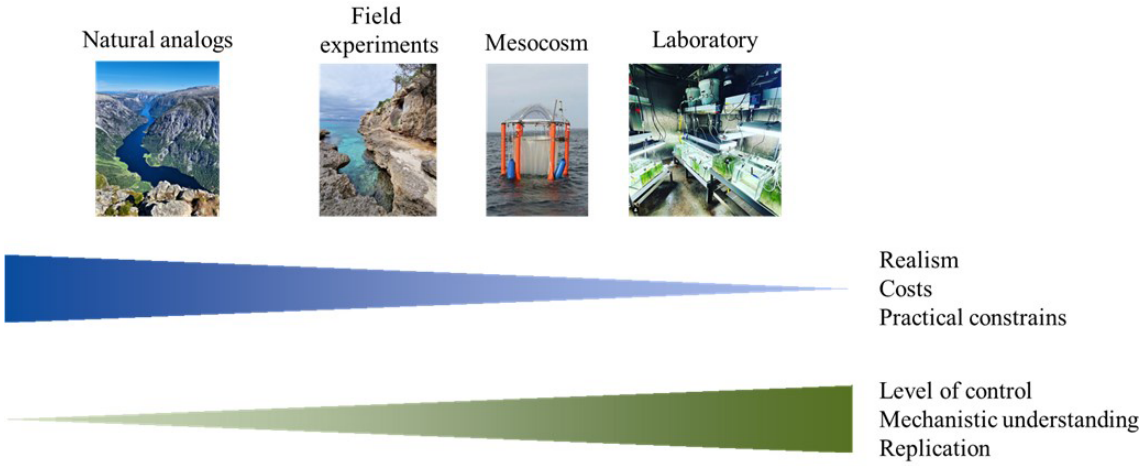

Figure 1. Simplified version of the strengths and limitations of different complementary research approaches. While the level of environmental and ecological realism decreases from natural analogs to laboratory experiments, field-based approaches face other complexities: high costs, legal and practical constraints, lower control and attribution to the tested parameters, and a lower level of replication. The selection of an approach should be based on the question, and most questions requires a strategy combining multiple approaches.

manipulation of alkalinity and/or concentration of the various other compounds or impurities. Different concentrations and dynamic of exposure (e.g., constant vs. fluctuating concentration simulating a dilution or single vs. repeated exposure) can be compared in single- or multiple-driver experimental designs. Laboratory experiments are classically used as a tool to test hypotheses and attribute biological changes to tested variables beyond the correlative approach often used for field observations and manipulations. A wide variety of approaches exist, allowing for small- to large-sized experimental units (from mL to m^3, depending on the model), single and multiple species or life history stages, and short- or long-term exposure, and provide adapted options to work with organisms from bacteria to fish.

- *Strengths*. Experiments in the laboratory offer a wide range of options and have the potential for the highest level of control in the tested parameters (e.g., physicochemistry, food concentration, species composition, density) As such, laboratory experiments, in combination with other approaches, are the best alternative to build a mechanistic understanding of the biological impacts of OAE. While not without limitations, some experimental setups allow for a high level of replication and to test complex questions highly relevant in the context of OAE including the following examples. (What is the biological impact of combined effect of increased alkalinity with trace elements? What is the biological impact of repeated exposures?). As for any experimentation on living organisms, there are some ethical and sometimes legal aspects associated with biological experimentation. However, those are much easier to resolve than with field approaches.
- *Limitations*. While complex laboratory experiments can have some degree of ecological realism, they cannot fully replicate the complexity of a natural ecosystem. For example, it can be highly challenging to include natural variability for all relevant physicochemical parameters (seasonal or associated with OAE deployment) or incorporate the full complexity of an ecosystem. As such, mechanistic models developed from laboratory experiments need to be validated in more realistic settings (e.g., field experiments).

2.2 Mesocosm experiments (see Riebesell et al., 2023, this Guide, for more information and references)

As for laboratory experiments, manipulations in alkalinity and/or other compounds released during OAE deployments can be performed using mesocosms to achieve a greater level of ecological realism. Mesocosms are generally large-scale enclosed bodies of water, with (benthic) or without (pelagic mesocosms) sediments, including biological communities and related processes that can be experimentally manipulated. Depending on the tested communities, the size can vary between 1 L and several cubic meters of seawater.

- *Strengths*. Mesocosm experiments can partially compensate for the limitations of laboratory-based experiments. They sit between laboratory and field experiments and can be used to evaluate the impact of the tested parameter(s) at the ecological level. Working in a closed system minimizes the public concerns and legal requirement when compared to field trials (GESAMP, 2019).
- *Limitations*. While mesocosms allow for a certain level of controls of the environment, some physicochemical

parameters follow natural variability, limiting their ability to attribute the observed effects directly to the tested parameter(s). The size and complexity of mesocosms can also limit the number of replicates and thus their ability to detect significant effects. When limitation occurs in term of replication, either in mesocosm or laboratory experiments, an alternative is to replicate by repeating the same experiment multiple times. However, this can introduce unwanted variability as some biological processes vary between days, seasons, and years and decreasing the probability of detecting significant effects. Some other limitations include unnatural mixing and turbulence (pelagic mesocosms) or unnatural water flows (benthic mecososms) as well as limitation inherent to a closed system.

2.3 Field experiments (see Cyronak et al., 2023, this Guide, for more information and references)

Open-system field experiments consist of a direct manipulation (e.g., addition of alkalinity) in a natural system. This approach can be used to simulate an OAE deployment at realistic spatial scale.

- *Strengths*. This approach allows the evaluation of the potential impacts at the ecosystem level in the real world while other environmental parameters naturally fluctuate.

- *Limitations*. Several logistical (e.g., access) and legal challenges (e.g., permit, public acceptance) can be associated with field experiments. Similarly to mesocosm experiments, the cost of the ecological realism is the complexity in attributing the observed effect to the given treatment. It is complicated by the difficulty of truly replicating the experiment and identifying controls. However, this can be partly resolved by substituting space for time and replicating the experiment in time if no strong year-to-year variability is observed.

2.4 Natural analogs (see Subhas et al., 2023, this Guide, for more information and references)

As for other physicochemical parameters, alkalinity is not constant across the ocean. The natural variability in alkalinity is linked to cycling of carbon dioxide, calcium carbonate, and other minerals. As a consequence, some locations have conditions that can be used as "natural analogs" to OAE deployments. Natural analog sites present environments that resemble the conditions of an OAE implementation and can then be used as a test bed for both sensor deployments and collection of data on feasibility at scale and potential impacts on key species and ecosystems. These include glacial fjords and runoff into the marine system, seafloor weathering of basalts, sites where artificial materials are added to the marine system, river plumes and deltas, and many others (Subhas et al., 2023).

- *Strengths*. Natural analogs provide the opportunity to work in the field at the ecosystem level and provide a test bed for the interpretation and validation of data collected in laboratory and field experiments and models. Different types of analogs can be used to address different space and time processes (Fig. 2 in Subhas et al., 2023) from hours at the deployment site to decades at the global level. Observations of natural analogs also have some practical advantages as they can be less costly than experimental approaches (e.g., mesocosms), logistically risky, and do not require complex permits to implement (e.g., field manipulation).

- *Limitations*. OAE analogs have the same constraints as any natural analog for other environmental parameters. While working in the field provides opportunities for the collection of data at a higher level of complexity, it lacks the control over the tested variable, making it difficult to attribute any observed effect to one or several parameters, and it does not necessarily account for the presence of impurities or the dynamics of exposure associated with some OAE deployments. While some statistical options are available to disentangle the individual effects of the different environmental parameters (e.g., multivariate and regression analyses), a full attribution is not possible as many nonlinear processes and complex interactions are unavoidable when ecology and multiple stressors are involved. This can be partly solved by incorporating mechanistic understanding and theoretical frameworks coming from more controlled laboratory and field studies. Other limitations include the difficulty of replication and identification of control sites. Natural analogs are also open systems with mobile species flowing through the ecosystem and introducing confounding factors and noise in the collected data.

2.5 Modeling considerations (see Fennel et al., 2023, this Guide, for more information and references)

The complex scientific questions associated with OAE will require a combination of approaches to develop the needed mechanistic understanding and field validation. Models are critical tools to bridge the different approaches, generate testable hypotheses, upscale from local to global aspects, and forecast the outcome of different intervention strategies. Developing a fully parameterized model simulating the complexity of the biological response to OAE is extremely challenging. Changes associated with OAE deployment can drive direct effects of each individual driver, including impacts of alkalinity, magnesium, and calcium ions on the calcification or toxic or stimulating effects of trace elements such as iron ions. These can become even more complex and unpredictable when in combination and including the dynamic

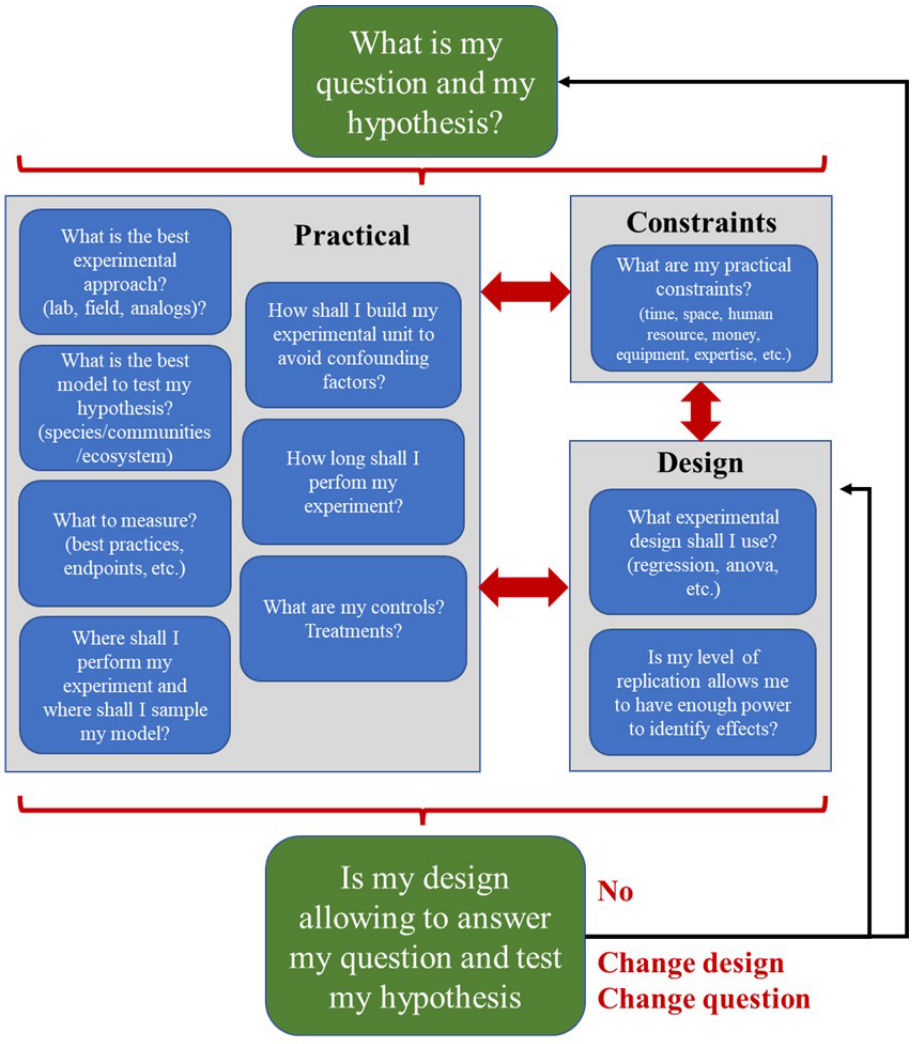

Figure 2. Flowchart guiding decisions for the design of experiments evaluating the impact of OAE. First, start with a question and a hypothesis. The design of the experiment is an array of decisions at the crossroad between constraints (e.g., time, space), experimental choices (e.g., tested biological model, duration), and analytic approaches (e.g., regression, ANOVA). When the final design is fixed, ensure that it would allow for answering the initial question. If not, correct your design or, if this is not possible, change your question.

of exposure. Indirect effects include impacts on the environment properties such as seawater turbidity modulating the propagation of light or cascading ecological processes. A more realistic approach is to use the toolkit of existing models for a fit-for-purpose modelisation associated with specific questions. For example, dynamic energy budget (DEB) is one of the most comprehensive frameworks for bioenergetics, and models based on this theory have been extensively applied to understand the effects of environmental changes, including the ecological consequences (Kooijman, 2001). Ecotoxicological models such as a mechanistically based model can be used to resolve the combined effects of the multiple changes associated with OAE deployment (Schäfer and Piggott, 2018).

3 Best practices: from a scientific question to an experimental strategy

A full consideration of best practices for experimental design is beyond the scope of this chapter. We will summarize some key general and OAE-specific considerations while designing an experimental strategy or experiment. Adapting the famous quote by George Box, we can say that essentially all experiments are wrong, but some are useful (Field et al., 2015). Each research approach is associated with its own set of strengths and limitations (Fig. 1) that, combined with practical and technical constraints, such as time, space, human resources, money, or expertise, lead to decisions that limit experiments that are wrong but that some are useful in terms of the potential of the collected data to answer some com-

plex questions. The full picture can only come from a combination of different approaches and experimental decisions (e.g., Quinn and Keough, 2002).

There are, however, some general best practices that should be followed, including the importance of defining proper controls, monitoring the physicochemical parameters following established procedures, including calibration and use of reference materials, using the appropriate level of true replication, and following best practices for the measured endpoints (e.g., Riebesell et al., 2011).

Following best practices optimizes the chance to identify the impact of a given environmental change. Variability is the rule in any biological data and can have different sources: technical (e.g., quality of the method used for the manipulation of a parameter or the measurement of an endpoint), experimental noise (e.g., confounding factors), and biologically relevance (e.g., genetic diversity or driven by the manipulated parameter). Each experiment should be designed to minimize unwanted variability. This includes randomization of the experimental units, proper training of the person(s) taking care of the experiments, or measuring the endpoints, etc.

For each question and associated experimental design, one must take the following decisions (Fig. 2).

- *What is my model organism or ecosystem?*
  One approach is to follow the Krogh's principle. For such a large number of problems there will be some model of choice (or a few such models) through which it can be most conveniently studied. A given species can be selected for its life history trait, longevity, physiology, phylogenetic position, sensitivity to the tested parameter, or role in the ecosystem. For example, to study the potential for genetic adaptation to OAE, a species with short generation time would be most appropriate. Model species may be considered when specific techniques are needed (e.g., functional genetics). Additional factors also need to be considered, including size, life history stage, age, weight, sex. Different ecosystems, numbers of trophic levels, and levels of complexity (among other factors) can also be considered.

- *Where should I sample or perform the experiment?*
  As a consequence of local adaptation, species and ecosystems evolved different strategies to cope with different locations and environments. For example, different populations of the same species can have contrasting sensitivity to the same changes in the carbonate chemistry (Vargas et al., 2022). In the context of OAE, the physical environment can also influence dilution rates of the alkalinity or the trace elements, the distribution of the particles, or the water turbidity, and the chemistry can also impact the dissolution of the used minerals and modulate other drivers or combined effects. The biological characteristics can also influence the potential sensitivity to changes (e.g., natural variability, redundancy, endangered species).

- *How do I design my experimental unit?*
  To avoid introducing confounding factors, it is critical that the design of the experimental unit (e.g., aquarium, mesocosm) fits the tested species, community, or ecosystem. This includes using the right volume of water, realistic density of biological models, open vs. flow-through design, density of food, water used, aeration, currents, and other physicochemical parameters.

- *How long should I conduct my experiment or observations for?*
  Based on the question, different durations should be considered to ensure that the observed effect can truly be representative of the treatment. For example, this can be short-term, chronic, or dynamic depending on the tested OAE scenario.

- *What is the general experimental design?*
  Two general experimental approaches can be used: the replicated scenario "ANOVA" approach and the gradient "regression" approach (Fig. 3). There are pros and cons to both approaches. The regression approach allows us to identify nonlinear processes, resolve performance curves, and identify potential thresholds. However, there is the risk of not being able to properly analyze the collected data if no obvious trend is present. It is also possible to combine both approaches using a collapsed design (Boyd et al., 2018).

- *Do I have the proper control(s) and treatment(s) to test my hypothesis?*
  All research approaches should consider the proper controls taking into account the present natural variability at the relevant spatiotemporal scale as well as conditions in the context of the implementation of OAE. The treatments can mimic a deployment of OAE and cover a wide range of alkalinity (e.g., 1500 to 4000 µmol kg^{-1}) and other parameters for a more mechanistic approach. The concentrations of alkalinity and trace elements are not the only parameters to consider, as the duration and dynamic of exposure can strongly vary depending on the implementation method. The selection of the experimental approach (laboratory, mesocosm, field, natural analog) and design is highly dependent on the question and will directly inform the selection of treatment(s). The OAE dynamics of deployment over space and time are subjected to a variety of physical forcings. The plume dispersal will be influenced by currents, eddies, seabed topography, and other physical characteristics (Subhas et al., 2023), as well as additional variability from repeated deployments. Any understanding of the biological response to OAE will then need to consider aspects beyond any sensitivity thresholds for alkalinity

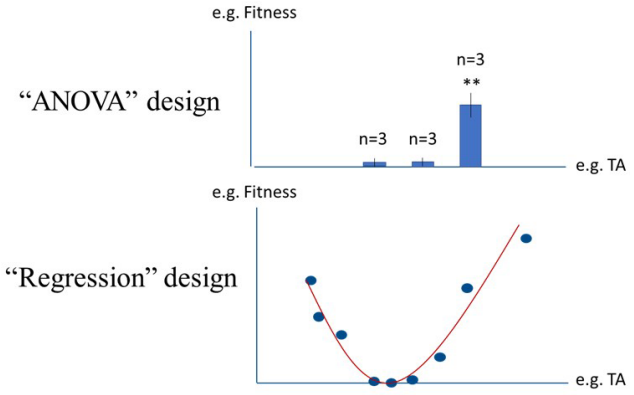

Figure 3. Illustration of two complementary experimental approaches using the same level of replication.

and trace elements and include the dynamic of exposure. Exposure will vary from immediate "shock" responses at the periphery of a plume to longer-term acclimated responses in ecosystems that may sit directly in the outfall of a plume (Subhas et al., 2023). Some experimental methods may be more adapted to simulate such complex dynamics (e.g., field experiments) as they would require complex technologies and high levels of control and monitoring in a closed-systems laboratory or mesocosm experiments. Such complex questions can only be answered through the combination of multiple experimental approaches and a strong communication between fields.

– *What to measure?*
A wide variety of parameters and methods are available to evaluate biological impacts, including indicators of biodiversity, ecosystem health, and individual fitness. A rule of thumb is to use an endpoint that is as close as possible to the process under evaluation. For example, transcriptomic is often used to infer on organismal physiology while there is very poor correlation between these two endpoints (Feder and Walser, 2005). Ultimately, it is critical to evaluate the potential biological impact of OAE deployment on ecosystem functioning. This will require measuring the impacts at several trophic levels and include the higher trophic levels. Evaluating the potential ecological impacts is also critical to build trust with local communities. In April 2023, 300 protesters gathered to voice their concerns regarding an OAE deployment in St Ives Bay and called for greater scientific scrutiny. Specifically, they worried about the impact on the local environment and in particular on the grey seal population. Seals are benthic feeders that could directly and indirectly be impacted by the heavy metals released (Weeks, 2023).

4 Best practices: specificities to OAE

4.1 Manipulation of alkalinity (see Eisaman et al., 2023, this Guide, for more information and references)

The desire to increase the alkalinity of aquatic environments is not new and predates the concept of OAE. For example, aquaculture farmers are using liming agents or sodium bicarbonate to restore pond alkalinity to increase photosynthesis and fish production and to better buffer production water against possible pH changes over time. The so-called "liming" has been used through various materials or chemicals applied in ponds such as agricultural limestone, alkaline slag, agricultural gypsum (calcium sulfate), calcium chloride, slaked lime, quicklime, and lime liquor. While all these compounds mainly neutralize soil acidity before the filling with water, some are more convenient or more effective than others (Boyd and Tucker, 1998). On a smaller scale, aquarists who farm ornamental marine life such as fish, crustaceans, and corals also carefully monitor seawater alkalinity. They use different methods to activate calcium and alkalinity, such as additional water changes, kalkwasser (lime water), "balling", and devices such as calcium reactors containing alkaline material that can produce high-alkalinity liquid upstream of the aquarium (Goemans, 2012).

In the context of OAE, different methods of manipulating alkalinity are proposed. Two main options are generally considered:

– the addition of ground alkaline material or in situ enhanced weathering,

– pre-dissolution of alkaline materials or agents prior to pouring the resulting liquid into studied waters.

These can be directly used in experiments, while a more controlled manipulation of the chemistry (alkalinity and other substances) can be used to resolve the mechanisms and modes of action.

When alkaline materials are used, other compounds or impurities can also be released, such as silicate, calcium, magnesium and various trace metals (e.g., iron, nickel, cobalt, chromium). The main elements released through the use of lime, olivine, or magnesite are magnesium and calcium ions, along with minor elements like iron and trace elements, that occur at relatively low concentrations in seawater. However, their levels could be sufficient to affect marine organisms (e.g., Hauck et al., 2016; Moore et al., 2013). Therefore, the seawater contamination by the compounds and impurities inherent to alkaline materials has to be properly monitored and included in impact studies.

4.2 Monitoring compounds and impurities

There are many analytical methods available for measuring trace metals or other elements. The full process of collecting samples and analyzing dissolved trace elements is time-

consuming and complex. The existence of multiple chemical forms (speciation) and specialized procedures for different elements due to speciation effects and contamination means that such analytical work has to be coordinated with specialized laboratories and chemists. One of the major challenges in determining trace metals is indeed preventing contamination of environmental water samples during sampling and analysis (Benoit et al., 1997). Nevertheless, there are some good procedures available online validated by experts to collect and handle samples for dissolved trace elements analysis (e.g., GEOTRACES, 2017; Noble et al., 2020). Among the different research methods discussed in this section, the survey of dissolved trace metals or other elements inherent in alkaline substances in seawater is easier to plan and to realize in laboratory experiments than in the field as the collection and handling of the samples is more straightforward and the risk of contaminating samples is much lower.

An exhaustive list of analytical equipment available to analyze all possible compounds and pollutants released into the ocean from each candidate alkaline material is outside the scope of this paper. The most suitable approach may be to combine a seawater preconcentration system (automated, such as seaFAST, or non-automated; Hirata et al., 2000; Wuttig et al., 2019) with inductively coupled plasma mass spectrometry (ICP-MS). There are exceptions for some elements, but this approach works for most elements expected to be released. Furthermore, the use of passive samplers has the advantage of better temporal and spatial resolution of marine pollution risks compared to discrete samples (Schintu et al., 2014; samples have then subsequently been analyzed in laboratories).

4.3 Combined effects of increased alkalinity and compounds and impurities inherent to alkaline materials

Many questions remain to be answered to fully address the potential ecological impacts of OAE and understanding the combined effects of increased alkalinity with other compounds and impurities is a tremendous challenge. Such questions require specific best practices and strategies (Boyd et al., 2018; IOC UNESCO, 2022). Parameters of the carbonate chemistry and other dissolved elements are very likely to have different modes of actions and functional changes at the cellular and physiological level. Changes in environmental parameters with different modes of action can lead to complex interactions between these parameters, making it difficult to project their combined impacts. Changes in the seawater chemistry can also directly affect the chemical form and bioavailability of a given element (Millero et al., 2009). Resolving these interactions requires a combination of mechanistic studies, modeling, and complex multi-stressor experiments.

When considering chemicals such as metals as potential stressors, two different aspects need to be considered. One is the dose-specific effects on the organism, and the other is the complexity of maintaining constant realistic metal exposures in the laboratory.

The relationship between organismal metal exposure and internal dose or adverse effects is nonlinear and depends on the metal studied and the organism selected. The accumulation and storage of bioavailable metals varies widely among aquatic organisms and is element specific. In addition, several metals, such as Co, Fe, Mn, and Zn, are essential for the metabolism of organisms and have optimal concentrations in their tissues (the optimal contents vary from species to species). Therefore, depletion or excess of these elements in an organism can have deleterious effects on the organism (e.g., Forstner and Wittmann, 1983), and some high concentrations may also be beneficial to the organism at certain levels.

From a technical point of view, exposing organisms in microcosms or mesocosms to specific levels of dissolved metals (or mixtures of metals) is more difficult than in field experiments. Indeed, the exposure has to be ideally maintained at a certain level in order to provide a more meaningful risk assessment, but at the same time it will not fully mirror the reality of the exposure environment due to fluctuations. Furthermore, there is a high likelihood in the microcosm that the presence of organisms with the ability to bioaccumulate metals will decrease exposure levels; repeated doses or flow-through systems will be required to keep the concentration constant.

Nickel may be one of the most important trace metal pollutants in olivine-based ocean alkalization, but there are other potential bioavailable trace metals (such as Cr, Cu, or Cd; Bach et al., 2019), which all can be bioaccumulated to a certain extent (Metian et al., 2007; Hédouin et al., 2010; Eisler, 2009). There is a large body of literature detailing the toxicity, sub-toxic concentration, or bioaccumulation potential of many of the compounds released by OAE in marine organisms (e.g., the compendium edited by Eisler is one of the most comprehensive sources of information; most elements have an extremely wide range of species from protozoa to vertebrates; Eisler, 2009, 2010). However, the effects of some elements found in rocks have not been studied or are poorly reported (e.g., zirconium).

5 Key recommendations for experimental research relevant to OAE

Resolving the biological impacts of complex and dynamic changes in carbonate chemistry and other compounds and impurities associated with OAE will require a scientific strategy combining different experimental approaches, methods, and collaboration between disciplines. To successfully develop and implement such scientific strategies, we provide the following key recommendations.

- Identify key scientific questions, sub-questions, and associated testable hypotheses.
- For each sub-question, select the most appropriate experimental approach or combination of approaches (laboratory experiments, mesocosms, field experiments, natural analogs, models), locations, biological models, level of biological organization, duration, controls, measured parameters, etc.
- Follow general experimental best practices for experimental design (e.g., replication, analyses)
- Take advantage of existing best practices for each specific field involved (e.g., multiple stressors experiments, manipulation and measurements of the carbonate chemistry and/or impurities).

Data availability. No data sets were used in this article.

Author contributions. SD and MM designed the structure of this manuscript, wrote the initial draft, and performed the needed revisions.

Competing interests. Competing interests are declared in a summary for the entire volume at: https://sp.copernicus.org/articles/sp-oae2023-ci-summary.zip.

Disclaimer. Publisher's note: Copernicus Publications remains neutral with regard to jurisdictional claims made in the text, published maps, institutional affiliations, or any other geographical representation in this paper. While Copernicus Publications makes every effort to include appropriate place names, the final responsibility lies with the authors.

Acknowledgements. We thank the Ocean Acidification and other ocean Changes – Impacts and Solutions (OACIS), an initiative of the Prince Albert II of Monaco Foundation, for its support throughout the project. We extend our gratitude to the Villefranche Oceanographic Laboratory for supporting the meeting of the lead authors in January 2023. We would also like to thank Angela Stevenson for her support in the development and writing of this manuscript. The authors, on the behalf of the IAEA, are grateful for the support provided to IAEA Marine Environment Laboratories by the Government of the Principality of Monaco. Authors also would like to acknowledge the invaluable contribution of Philip Boyd, Steve Widdicombe, and one anonymous reviewer as their thorough review of the first version of the manuscript helped us to make significant improvements.

Financial support. This research has been supported by the ClimateWorks Foundation (grant no. 22-0296) and the Prince Albert II of Monaco Foundation.

The article processing charges for this open-access publication were covered by the Gothenburg University Library.

Review statement. This paper was edited by Jean-Pierre Gattuso and reviewed by Philip Boyd, Stephen Widdicombe, and one anonymous referee.

References

Bach, L. T., Gill, S. J., Rickaby, R. E. M., Gore, S., and Renforth, P.: CO_2 removal with Enhanced Weathering and Ocean Alkalinity Enhancement: potential risks and co-benefits for marine pelagic ecosystems, Front. Clim., 1, https://doi.org/10.3389/fclim.2019.00007, 2019.

Benoit, G., Hunter, K. S., and Rozan, T. F.: Sources of trace metal contamination artifacts during collection, handling, and analysis of freshwaters, Anal. Chem., 69, 1006–1011, https://doi.org/10.1021/ac960798y, 1997.

Boyd, C. E. and Tucker, C. S.: Liming, in: Pond Aquaculture Water Quality Management, Springer, Boston, MA, 178–225, https://doi.org/10.1007/978-1-4615-5407-3_5, 1998.

Boyd, P., Collins, S., Dupont, S., Fabricius, K., Gattuso, J. P., Havenhand, J., Hutchins, D., Riebesell, U., Rintoul, M., Vichi, M., Biswas, H., Gao, K., Gehlen, M., Hurd, C., Kurihara, H., McGraw, C., Navarro, J., Nilsson, G., Passow, U., and Poertner, H. O.: Experimental strategies to assess the biological ramifications of multiple drivers of ocean global changes – a review, Glob. Chang. Biol., 24, 2239–2261, https://https://doi.org/10.1111/gcb.14102, 2018.

Cooley, S., Schoeman, D., Bopp, L., Boyd, P., Donner, S., Ito, S., Kiessling, W., Martinetto, P., Ojea, E., Racault, M. F., Rost, B., Skern-Mauritzen, M., Yemane Ghebrehiwet, D., Bell, J. D., Blanchard, J., Bolin, J., Cheung, W. W. L., Cisneros-Montemayor, A., Dupont, S., Dutkiewicz, S., Frölicher, T., Gaitán-Espitia, J. D., Molinos, J. G., Gurney-Smith, H., Henson, S., Hidalgo, M., Holland, E., Kopp, R., Kordas, R., Kwiatkowski, L., Le Bris, N., Lluch-Cota, S. E., Logan, C., Mark, F. C., Mgaya,Y., Moloney, C., Muñoz Sevilla, N. M., Randin, G., Raja, N. B., Rajkaran, A., Richardson, A., Roe, S., Ruiz Diaz, R., Salili, D., Sallée, J. B., Scales, K., Scobie, M., Simmons, C. T., Torres, O., and Yool, A.: Oceans and Coastal Ecosystems and their Services, in: IPCC AR6 WGII, Cambridge University Press, 379–550, https://doi.org/10.1017/9781009325844.005, 2022.

Cyronak, T., Albright, R., and Bach, L. T.: Field experiments in ocean alkalinity enhancement research, in: Guide to Best Practices in Ocean Alkalinity Enhancement Research, edited by: Oschlies, A., Stevenson, A., Bach, L. T., Fennel, K., Rickaby, R. E. M., Satterfield, T., Webb, R., and Gattuso, J.-P., Copernicus Publications, State Planet, 2-oae2023, 7, https://doi.org/10.5194/sp-2-oae2023-7-2023, 2023.

Eisaman, M. D., Geilert, S., Renforth, P., Bastianini, L., Campbell, J., Dale, A. W., Foteinis, S., Grasse, P., Hawrot, O., Löscher, C. R., Rau, G. H., and Rønning, J.: Assessing the technical

aspects of ocean-alkalinity-enhancement approaches, in: Guide to Best Practices in Ocean Alkalinity Enhancement Research, edited by: Oschlies, A., Stevenson, A., Bach, L. T., Fennel, K., Rickaby, R. E. M., Satterfield, T., Webb, R., and Gattuso, J.-P., Copernicus Publications, State Planet, 2-oae2023, 3, https://doi.org/10.5194/sp-2-oae2023-3-2023, 2023.

Eisler, R.: Compendium of trace metals and marine biota: Volume 1: Plants and Invertebrates, Elsevier, ISBN 9780444534361, 2009.

Eisler, R.: Compendium of trace metals and marine biota: Volume 2: Vertebrates, Elsevier, ISBN 9780444534378, 2010.

Feder, M. E. and Walser, J. C.: The biological limitations of transcriptomics in elucidating stress and stress responses, J. Evol. Biol., 18, 901–910, https://doi.org/10.1111/j.1420-9101.2005.00921.x, 2005.

Fennel, K., Long, M. C., Algar, C., Carter, B., Keller, D., Laurent, A., Mattern, J. P., Musgrave, R., Oschlies, A., Ostiguy, J., Palter, J. B., and Whitt, D. B.: Modelling considerations for research on ocean alkalinity enhancement (OAE), in: Guide to Best Practices in Ocean Alkalinity Enhancement Research, edited by: Oschlies, A., Stevenson, A., Bach, L. T., Fennel, K., Rickaby, R. E. M., Satterfield, T., Webb, R., and Gattuso, J.-P., Copernicus Publications, State Planet, 2-oae2023, 9, https://doi.org/10.5194/sp-2-oae2023-9-2023, 2023.

Field, E.: All Models Are Wrong, but Some Are Useful, Seismol. Res. Lett., 86, 291–293, https://doi.org/10.1785/02201401213, 2015.

Forstner, U. and Wittman, G. T.: Metal Pollution in the Aquatic Environment, 2nd edn., Springer, New York, ISBN 978-3-540-12856-4, 1983.

GEOTRACES: Chapter 5: Trace elements, in: Sampling and Sample-handling Protocols for GEOTRACES Cruises Version 3, 53–106, https://geotracesold.sedoo.fr/Cookbook.pdf (last access: 10 October 2023), 2017.

GESAMP: High level review of a wide range of proposed marine geoengineering techniques, in: IMO/FAO/UNESCO-IOC/UNIDO/WMO/IAEA/UN/UN Environment/UNDP/ISA Joint Group of Experts on the Scientific Aspects of Marine Environmental Protection, edited by: Boyd, P. W. and Vivian, C. M. G., Rep. Stud. GESAMP No. 98, ISSN: 1020-4873, http://www.gesamp.org/publications/high-level-review-of-a-wide-range-of-proposed-marine-geoengineering-techniques (last access: 10 October 2023), 2019.

Goemans, B.: The "living" Marine Aquarium Manual Basic and Advanced Husbandry for the 'Modern' Marine Aquarium, Basic and advances husbrandry for the modern marine aquarium, Salt Corner, ISBN 978-0-615-60306-3, http://www.saltcorner.com/LMAM/ShowChapter.php?ChapterID=17 (last access: 10 October 2023), 2012.

Hauck, J., Kohler, P., Wolf-Gladrow, D., and Völker, C.: Iron fertilization and century-scale effects of open ocean dissolution of olivine in a simulated CO_2 removal experiment, Environ. Res. Lett., 11, 24007, https://doi.org/10.1088/1748-9326/11/2/024007, 2016.

Hédouin, L., Metian, M., Teyssié, J.-L., Fichez, R., and Warnau, M.: Delineation of heavy metal contamination pathways (seawater, food and sediment) in tropical oysters from New Caledonia using radiotracer techniques, Mar. Poll. Bull., 61, 542–553, https://doi.org/10.1016/j.marpolbul.2010.06.037, 2010.

Hirata, S., Honda, K., Shikino, O., Maekawa, N., and Aihara, M: Determination of chromium (III) and total chromium in seawater by on-line column preconcentration inductively coupled plasma mass spectrometry, Spectrochimica Acta Part B At. Spectros., 55, 1089-1099, https://doi.org/10.1016/S0584-8547(00)00169-5, 2000.

Iglesias-Rodríguez, M. D., Rickaby, R. E. M., Singh, A., and Gately, J. A.: Laboratory experiments in ocean alkalinity enhancement research, in: Guide to Best Practices in Ocean Alkalinity Enhancement Research, edited by: Oschlies, A., Stevenson, A., Bach, L. T., Fennel, K., Rickaby, R. E. M., Satterfield, T., Webb, R., and Gattuso, J.-P., Copernicus Publications, State Planet, 2-oae2023, 5, https://doi.org/10.5194/sp-2-oae2023-5-2023, 2023.

IOC-UNESCO: Multiple Ocean Stressors: A Scientific Summary for Policy Makers, edited by: Boyd, P. W., Dupont, S., and Isensee, K., UNESCO, Paris, IOC Information Series, 1404, 20 pp., https://doi.org/10.25607/OBP-1724, 2022.

Kooijman, S. A. L. M.: Quantitative aspects of metabolic organization: a discussion of concepts, Philos. Trans. R. Soc. B, 356, 331–349, https://doi.org/10.1098/rstb.2000.0771, 2001.

Metian, M., Warnau, M., Oberhänsli, F., Teyssié, J. L., and Bustamante, P.: Interspecific comparison of Cd bioaccumulation in European Pectinidae (*Chlamys varia* and *Pecten maximus*), J. Exp. Mar. Biol. Ecol., 353, 58–67, https://doi.org/10.1016/j.jembe.2007.09.001, 2007.

Millero, F. J., Woosley, R., DiTrolio, B., and Waters, J.: Effect of ocean acidification on the speciation of metals in seawater, Oceanography, 22, 72–85, https://doi.org/10.5670/oceanog.2009.98, 2009.

Moore, C. M., Mills, M. M., Arrigo, K. R., Berman-Frank, I., Bopp, L., Boyd, P. W., Galbraith, E. D., Geider, R. J., Guieu, C., Jaccard, S. L., Jickells, T. D., La Roche, J. Lenton, T. M., Mahowald, N. M., Marañón, E., Marinov, I., Moore, J. K., Nakatsuka, T., Oschlies, A., Saito, M. A., Thingstad, T. F., Tsuda, A., and Ulloa, O.: Processes and patterns of oceanic nutrient limitation, Nat. Geosci., 6, 701–710, https://doi.org/10.1038/ngeo1765, 2013.

Noble, A. E., Tuit, C. B., Maney, J. P., and Wait, A. D.: A review of marine water sampling methods for trace metals, Environ. Forensics, 21, 267–290, https://doi.org/10.1080/15275922.2020.1771629, 2020.

Quinn, G. P. and Keough, M. J.: Experimental design and data analysis for biologists, Cambridge University Press, ISBN 9780521009768, 2002.

Riebesell, U., Fabry, V. J., Hansson, L., and Gattuso J.-P.: EUR24872: Guide to best practices for ocean acidification research and data reporting, Publications Office of the European Union, ISBN 978-92-79-20650-4, https://doi.org/10.2777/66906, 2011.

Riebesell, U., Basso, D., Geilert, S., Dale, A. W., and Kreuzburg, M.: Mesocosm experiments in ocean alkalinity enhancement research, in: Guide to Best Practices in Ocean Alkalinity Enhancement Research, edited by: Oschlies, A., Stevenson, A., Bach, L. T., Fennel, K., Rickaby, R. E. M., Satterfield, T., Webb, R., and Gattuso, J.-P., Copernicus Publications, State Planet, 2-oae2023, 6, https://doi.org/10.5194/sp-2-oae2023-6-2023, 2023.

Schäfer, R. B. and Piggott, J. J.: Advancing understanding and prediction in multiple stressor research through a mechanistic basis for null models, Glob. Chang. Biol., 24, 1817–1826, https://doi.org/10.1111/gcb.14073, 2018.

Schintu, M., Marrucci, A., and Marras, B.: Passive Sampling Technologies for the Monitoring of Organic and Inorganic Contaminants in Seawater, in: Current Environmental Issues and Challenges, edited by: Cao, G. and Orrù, R., Springer, Dordrecht, https://doi.org/10.1007/978-94-017-8777-2_14, 2014.

Subhas, A. V., Lehmann, N., and Rickaby, R. E. M.: Natural analogs to ocean alkalinity enhancement, in: Guide to Best Practices in Ocean Alkalinity Enhancement Research, edited by: Oschlies, A., Stevenson, A., Bach, L. T., Fennel, K., Rickaby, R. E. M., Satterfield, T., Webb, R., and Gattuso, J.-P., Copernicus Publications, State Planet, 2-oae2023, 8, https://doi.org/10.5194/sp-2-oae2023-8-2023, 2023.

Vargas, C. A., Cuevas, L. A., Broitman, B. R., San Martin, V. A., Lagos, N. A., Gaitán-Espitia, J. D., and Dupont, S.: Upper environmental pCO_2 drives sensitivity to ocean acidification in marine invertebrates, Nat. Clim. Change, 12, 200–207, https://doi.org/10.1038/s41558-021-01269-2, 2022.

Weeks, J.: Protesters urge caution over St Ives climate trial amid chemical plans for bay, The Guardian, https://www.theguardian.com/uk-news/2023/apr/17/protesters-urge-caution-over-st-ives-climate-trial-amid-chemical-plans-for-bay-planetary-technologies, last access: 2 October 2023.

Wuttig, K., Townsend, A. T., van der Merwe, P., Gault-Ringold, M., Holmes, T., Schallenberg, C., Latour, P., Tonnard, M., Rijkenberg, M. J. A., Lannuzel, D., and Bowie, A. R.: Critical evaluation of a sea*FAST* system for the analysis of trace metals in marine samples, Talanta, 197, 653–668, https://doi.org/10.1016/j.talanta.2019.01.047, 2019.

State Planet, 2-oae2023, 7, 2023
https://doi.org/10.5194/sp-2-oae2023-7-2023

Field experiments in ocean alkalinity enhancement research

Tyler Cyronak[1,★], **Rebecca Albright**[2,★], **and Lennart T. Bach**[3]

[1]Institute for Coastal Plain Science, Georgia Southern University, Statesboro, GA, USA
[2]Institute for Biodiversity Science and Sustainability, California Academy of Sciences, San Francisco, CA, USA
[3]Institute for Marine and Antarctic Studies, University of Tasmania, Hobart, Tasmania, Australia
★These authors contributed equally to this work.

Correspondence: Tyler Cyronak (tcyronak@georgiasouthern.edu) and Rebecca Albright (ralbright@calacademy.org)

Received: 15 June 2023 – Discussion started: 27 June 2023
Revised: 20 October 2023 – Accepted: 24 October 2023 – Published: 27 November 2023

Abstract. This chapter focuses on considerations for conducting open-system field experiments in the context of ocean alkalinity enhancement (OAE) research. By conducting experiments in real-world marine and coastal systems, researchers can gain valuable insights into ecological dynamics; biogeochemical cycles; and the safety, efficacy, and scalability of OAE techniques under natural conditions. However, logistical constraints and complex natural dynamics pose challenges. To date, only a limited number of OAE field studies have been conducted, and guidelines for such experiments are still evolving. Due to the fast pace of carbon dioxide removal (CDR) research and development, we advocate for openly sharing data, knowledge, and lessons learned as quickly and efficiently as possible within the broader OAE community and beyond. Considering the potential ecological and societal consequences of field experiments, active engagement with the public and other stakeholders is desirable, while collaboration, data sharing, and transdisciplinary scientific teams can maximize the return on investment. The outcomes of early field experiments are likely to shape the future of OAE research, implementation, and public acceptance, emphasizing the need for transparent and open scientific practices.

1 Introduction

This chapter addresses considerations for conducting open-system field experiments related to ocean alkalinity enhancement (OAE). We define "field experiment" or "field studies" broadly as the addition or manipulation of alkalinity in a natural system that is relevant to OAE, independent of the spatial and temporal scale. We intentionally exclude spatial and temporal scales from our definition to encompass the wide spectrum of OAE methods and approaches. In fact, field experiments are likely to span spatial scales of squared meters (m^2) to hundreds of squared kilometers (km^2) and last from days to years. Field experiments and studies differ from both "field trials" and "field deployments" in their motivation, as both trials and deployments denote the practical application and usage of a specific product, device, or technology. The scientific focus during field trials is likely to be on the efficacy of carbon dioxide removal (CDR) and fine-tuning operational deployment, while field experiments will encompass a broader range of scientific goals and objectives. The nature, logistics, and objectives of field experiments are likely to make them smaller in scale than operational deployments. This will be advantageous, as field experiments that emulate planned OAE trials and deployments will help create the scientific framework needed to scale operational OAE safely and responsibly.

The benefits of conducting experiments in natural systems include observing complex ecological dynamics and impacts at the ecosystem level, understanding the role of biogeochemical cycles and physical processes that cannot be replicated in other settings, and assessing CDR under real-world

scenarios. The complexity and breadth of some field experiments will necessitate science that transcends disciplinary boundaries, making collaboration a priority. Success in the field faces many challenges due to the inherent complexity of natural systems along with limiting logistical constraints (e.g., permitting, access, social license, infrastructure, life cycle emissions). Despite these challenges, the first OAE field experiments are already underway, many of which are small-scale representations of scalable OAE approaches. There will be much to learn from these early studies, and any knowledge or insights gained should be shared as efficiently and openly as possible within the wider OAE community and beyond.

While some OAE field experiments have been completed or are already in progress, many more are on the horizon. We recommend that three overarching questions be taken into consideration, especially when in the planning stages:

- *What are the main goals of the experiment?*
  Establishing the objectives of a field experiment early in the planning stage will help guide all aspects of the scientific research plan, including site selection, measurement techniques and approaches, data analysis, and measured outcomes. Potential overarching goals of OAE field experiments include demonstrating functionality, efficacy, process, and/or scalability; determining ecological and environmental impacts; developing measurement, reporting, and verification (MRV) protocols; and assessing community engagement. Life cycle assessments (LCAs) may be a critical learning objective for some projects (e.g., Foteinis et al., 2023), especially those that are examining OAE at the scale of operational deployments. This list of overarching goals is not comprehensive, and goals are not necessarily mutually exclusive. For example, larger projects may aim to assess multiple components of an OAE approach, while smaller projects might be highly focused.

- *What is the type of alkalinity perturbation?*
  The type of alkalinity that is added (e.g., aqueous vs. solid, carbonates, hydroxides, oxides, or naturally occurring (ultra)mafic rocks) will ultimately determine many aspects of the scientific research plan. For example, projects adding ground alkaline minerals (e.g., olivine) to the ocean may have different goals and timelines than projects that add aqueous alkalinity (e.g., liquid NaOH) (see Eisaman et al., 2023, this Guide). Priorities for projects adding ground material might include tracking the dissolution of the alkaline material and monitoring the fate of the dissolved alkalinity and its dissolution coproducts (e.g., trace metals), while projects adding aqueous alkalinity will likely be more concerned with the latter. Other important experimental considerations that will be driven by the type of alkalinity perturbation include the concentration of added alkalinity, duration of additions, dilution and advection at the field site, residence time, air–sea equilibration, co-deployed tracers, sampling scheme, and environmental side effects. These and other research considerations are discussed in more detail below.

- *What are the permitting constraints and wider social implications?*
  Addressing the appropriate regulatory requirements is essential before any field experiment can move forward. Permitting requirements will be influenced by the study location, type of alkalinity perturbation, spatial scale, and duration. The use of existing infrastructure (e.g., wastewater discharge sites) and environmental projects (e.g., beach renourishment) may offer ways to facilitate alkalinity perturbations under existing regulatory frameworks. Community engagement and outreach are other areas that will be important to address, especially when the alkalinity perturbation is large and uncontained. Ideally, local communities should be engaged at the earliest possible stage since social license to operate is critical for the success of CDR projects (Nawaz et al., 2023). For a more detailed discussion of legal and social issues, see Steenkamp and Webb (2023, this Guide) and Satterfield et al. (2023, this Guide).

With these overarching questions in mind, we discuss considerations for OAE field experiments in more detail below.

2 Research methods

2.1 Types of alkalinity addition

Field experiments of OAE present many challenges. One of the biggest obstacles to success is tracking alkalinity added to an open system. Methods for adding alkalinity can be divided into two general approaches: (1) in situ or coastal enhanced weathering from the addition of ground alkaline minerals and rocks with the expectation they will dissolve directly in seawater and (2) aqueous alkalinity additions or the addition of "pre-dissolved" alkalinity to seawater that can be generated in numerous ways including through dissolution reactors and electrochemical techniques (Eisaman et al., 2023, this Guide). Tracking the added alkalinity, and subsequent CDR, under each approach comes with its own unique set of challenges and considerations.

Adding ground minerals and rocks to an open system presents two distinct scientific challenges. First, for alkalinity to be considered additional, it needs to be attributed to the dissolution of the solid material. This can be accomplished through a range of techniques including measuring the loss of mass of the added material or using geochemical tracers in the receiving waters. Determining dissolution kinetics in situ will be particularly important, and they are likely to vary between different deployment environments and strategies (e.g., coastal vs. open ocean). For example, the chemistry (e.g., salinity, pH, temperature) of the waters where the mineral is added could vary significantly depending on the envi-

ronment (e.g., beach face, estuary, continental shelf). Chemical (e.g., seawater conditions, such as salinity, pCO_2, and silica concentrations) and physical (e.g., grain size and surface area of the added material) conditions will be critical in determining dissolution rates (Rimstidt et al., 2012; Montserrat et al., 2017; Fuhr et al., 2022). Physical abrasion through wave action and currents is also likely to be an important control on dissolution (Flipkens et al., 2023). Field experiments will help translate dissolution kinetics from laboratory and mesocosm experiments to natural systems, which is not often straightforward due to complicated biogeochemical processes that are hard to replicate ex situ (Morse et al., 2007).

The second major challenge is common to both solid and aqueous approaches and involves tracking the added alkalinity, which becomes a particularly difficult problem in open-system field experiments where water is freely exchanged. Depending on the objectives of the field deployment, this is likely to be a main scientific concern. However, it is important to note that tracking the added alkalinity does not necessarily equate to observing CDR (i.e., an increase in seawater CO_2 stored as bicarbonate or carbonate). Observing an increase in atmospheric CO_2 stored as seawater dissolved inorganic carbon comes with its own set of challenges that are discussed in depth by Ho et al. (2023, this Guide).

Whether or not the alkalinity is derived from in situ mineral dissolution or direct aqueous additions, for OAE to be successful, atmospheric CO_2 needs to be taken up by seawater, or CO_2 effluxes from seawater to the atmosphere need to be reduced. Therefore, understanding the physical mixing and air–sea gas exchange dynamics of the deployment site will be a factor of interest for many field studies. Incorporating physical mixing models with biogeochemical processes will likely be the end goal of many field experiments focused on MRV (Ho et al., 2023, this Guide; Fennel et al., 2023, this Guide). Choosing sites with minimal mixing of different water masses or with well-defined diffusivities could facilitate tracing released alkalinity and subsequent air–sea CO_2 fluxes. While minimal mixing of different ocean water masses may be desired, higher wind speeds and wave action will increase the rate of air–sea gas exchange and may make CDR easier to measure. Background seawater chemistry will also be important in controlling air–sea gas exchange. For example, sites with naturally lower buffering capacities will see greater changes in CO_2 per unit of added alkalinity (Egleston et al., 2010; Hauck et al., 2016). The release of conservative tracers will likely be useful for field experiments that aim to track the added alkalinity and is discussed in more detail below (Sect. 2.5).

Other experimental considerations related to the type of alkalinity perturbation include the duration and location of alkalinity addition, which will be important for environmental and regulatory considerations. Alkalinity can be added once, in timed doses, or continuously. Aqueous alkalinity could be added directly to seawater, but the rate of this addition will likely be important, especially for avoiding secondary precipitation (Hartmann et al., 2023; Moras et al., 2022; Fuhr et al., 2022). Compared to experiments based on one-time additions of aqueous alkalinity or fast-dissolving solid-phase materials (e.g., $Ca(OH)_2$), field experiments adding solid minerals with comparatively slow dissolution rates (e.g., olivine) will likely need to consider longer experimental time frames to incorporate the monitoring of mineral dissolution. However, the timescale of each experiment will ultimately depend on the scientific objectives and could last from weeks to years and even decades. Location is another important factor that will influence logistics. For example, amending beach sand with alkaline minerals will present different challenges compared to the addition of alkaline material to outfalls that discharge into the ocean. Based on these and other considerations, each field experiment will require specific spatial and temporal sampling schemes to be developed. These sampling schemes should be planned well in advance of any perturbation and may require preliminary sampling campaigns to fine tune.

2.2 Alkalinity sources

OAE via coastal enhanced weathering can be accomplished using a variety of naturally occurring and human-made rocks and minerals (Table 1). The addition of these rocks and minerals is done after they have been ground to a desired grain size, with many unique application techniques proposed after the initial grinding step (see Eisaman et al., 2023, this Guide). The simplest application is done via sprinkling the ground material on the ocean surface, although this has many disadvantages including sinking and advection of the material before it dissolves (Köhler et al., 2013; Fakharee et al., 2023), although deployment in boat wakes may be viable (Renforth and Henderson, 2017; He and Tyka, 2023). Other application techniques include spreading material in coastal ecosystems such as on beaches, marshes, riverbeds, and estuaries, which have the potential to enhance dissolution through processes such as physical wave action and favorable water chemistry. However, the complex physical and biogeochemical processes that promote enhanced weathering in coastal ecosystems can make field experimentation more complicated by creating strong spatiotemporal modes of variability in water chemistry. To make results more broadly applicable, field experiments should attempt to mimic real-world alkalinity application scenarios such as those described above.

Any field experiments that add ground material to marine ecosystems may consider tracking the fate of that material from the addition site. Experiments could also artificially contain the material using barriers to avoid rapid loss of the ground material via currents; however, this could make the experiment less comparable to real-world OAE deployments. Sampling should extend from the water column into areas where the material is added, including sediments and pore waters.

Table 1. Types of alkalinity sources and considerations for each.

Alkalinity source	Solid/aqueous	Dissolution kinetics	Dissolution coproducts
NaOH	Aqueous	Instantaneous but can induce brucite ($Mg(OH)_2$) precipitation when NaOH elevates pH > 9. Brucite re-dissolves relatively quickly in most cases.	Alkalinity, Na^+.
Manufactured and natural Mg-derived alkalinity sources (e.g., brucite)	Solid or aqueous slurry	Relatively fast but a combination of dissolution rates both in the receiving and dosing waters.	Alkalinity, limited amounts of nutrients and trace metals (generally less than silicates), Mg^{2+}.
Silicates (e.g., olivine, basalt, wollastonite)	Solid	Relatively slow dissolution kinetics, but rates are different between silicates.	Alkalinity, silicate, trace metals. Materials need to be individually assessed prior to their use.
Manufactured lime-derived alkalinity sources (e.g., quicklime, ikaite)	Solid or aqueous slurry	Relatively fast but different kinetics between lime products.	Alkalinity, limited amounts of nutrients and trace metals (generally less than silicates), Ca^{2+}. Materials need to be individually assessed prior to their use.
Iron and steel slag	Solid	Components within steel slag that provide alkalinity (e.g., CaO) dissolve relatively fast, but different iron and steel slag contains different amounts.	Alkalinity, Ca^{2+}, Mg^{2+}, silicate, phosphate, and trace metals. Materials need to be individually assessed prior to their use.
Natural and synthetic carbonates (e.g., calcite, aragonite)	Solid	They do not dissolve under common surface ocean carbonate chemistry conditions. Dissolution rates can be higher in microenvironments such as corrosive sediment pore waters, where saturation is low due to respiratory CO_2.	Alkalinity, phosphate in some mined sources, dissolved inorganic carbon.

Likely environmental impacts associated with coastal enhanced weathering come from the physical impacts of adding finely ground material or the chemical release of trace elements and other contaminants. Both processes could have associated risks and/or co-benefits for a range of ecological processes and biogeochemical cycles (Bach et al., 2019). For example, the addition of finely ground material could lead to increased turbidity from the initial addition, subsequent resuspension, or secondary precipitation of particulates in the water column. Additionally, any release of nutrients or heavy metals from the dissolving material could alter primary production or cause harm to biological systems. The bioaccumulation of toxic metals in higher trophic level organisms, especially those of commercial importance, is a widespread concern.

Safety criteria should be put in place that can create a pause in the field experiment or prevent future experiments of the same type from taking place. These guardrails should be developed by the broader OAE community but may include obvious damage or health impacts to ecologically important organisms such as primary producers and keystone species, large and unexpected changes in biogeochemical cycles, and the general deterioration of environmental conditions. Risk–benefit analysis may be particularly useful in determining whether projects can or should move forward and may already be included in regulatory requirements through existing frameworks such as environmental impact assessments.

Aqueous and slurry-based additions of alkalinity provide different benefits and challenges compared to solid forms of alkalinity feedstock. One of the primary benefits of aqueous additions is that the alkalinity has been pre-dissolved, avoiding the often slow dissolution kinetics of minerals and rocks in seawater. Aqueous alkalinity can be generated by two main mechanisms: (1) the dissolution of alkaline rocks and minerals in reactors and (2) electrochemical processes that generate alkalinity by splitting seawater or other brine streams into an acid and base (Eisaman et al., 2023, this Guide). For some materials, such as $Ca(OH)_2$ and $Mg(OH)_2$, dissolution slurries are formed, and a combination of particulate and aqueous alkalinity can be dosed into seawater. Any particulates that are dosed from the slurry need to dissolve, meaning dissolution kinetics in seawater will be critical. However, the dissolution of these materials tends to be much quicker than with rocks and minerals (Table 1). There are important processes that need to be considered when adding aqueous alkalinity, including the unintended precip-

itation of calcium carbonates due to locally elevated saturation states (Hartmann et al., 2023; Moras et al., 2022).

Field experiments that use aqueous or slurry-based alkalinity additions will need to assess the impacts on seawater chemistry at the source of addition and across a dilution radius. Depending on the type of experiment and magnitude of additions, this dilution radius could extend upwards of kilometers, but the magnitude of the perturbation to carbonate chemistry would become smaller the further away from the alkalinity source (He and Tyka, 2023). The potential environmental impacts from aqueous type alkalinity additions will be similar to those discussed for coastal enhanced weathering but also include extreme localized changes in carbonate chemistry.

2.3 Considerations for site selection

Careful consideration should be given to site selection and experimental design to make sure the study adequately addresses the specific research questions and goals. Some aspects of the field site that will be important include ecosystem- and site-specific characteristics, the prevailing meteorological and oceanographic conditions, and natural spatiotemporal variability. Logistical considerations for site selection include physical access, permitting, availability of electricity, ship time, and consideration of the local community. These considerations will grow with the scale of field experiments and will likely be first-order determinants of where field experiments take place. For example, proximity to a marine institute (for land-based approaches) or access to a research cruise (for open-ocean approaches) may be desirable. Logistics will ultimately determine where operational OAE deployments take place, and early field experiments will help to elucidate important issues including the impacts of life cycle emissions on CDR.

OAE field experimentation requires careful assessment of the field site prior to alkalinity additions to provide foundational knowledge of the site characteristics. Scientific considerations for site selection can be broken down into three categories, the (1) physical, (2) chemical, and (3) biological properties of each site. Important considerations for each category are provided in Box 1. To facilitate baseline assessments and site selection we propose Table 2 as guidance for relevant parameters to measure. We note that this list is broad; however it is not exhaustive, and specific field sites may require the monitoring of different or additional parameters. Furthermore, some of the listed parameters may be more applicable to specific OAE approaches. Preliminary knowledge of the field site will inform both the experimental design and interpretation of data and experimental outcomes. Due to the large investments in cost and time required to collect baseline data, locations with a wealth of pre-existing scientific data may be considered. These baseline data could be available in the peer-reviewed literature and/or from publicly available coastal and open-ocean time series (e.g., Sutton et al., 2019).

2.4 Measurement considerations

What to measure and the type of instrumentation needed will ultimately depend on the site, scale, and goals of each individual experiment and should be considered on a case-by-case basis. For example, depending on the alkalinity source utilized (Table 1), it may (e.g., in the case of olivine) or may not (e.g., in the case of NaOH) be a priority to measure trace metal or nutrient concentrations. In addition to alkalinity type, the experimental scale will also dictate measurement considerations. For example, if the scale of the perturbation is small or the signal is very dilute, environmental impacts will not likely be measurable far from where the perturbation takes place. If there is a large addition of alkalinity, especially in a semi-enclosed system, both environmental impacts and changes in chemistry will be easier to detect. Ultimately, when OAE is done at a larger scale (e.g., millions of moles' alkalinity), it is likely that large changes in seawater chemistry will need to be avoided to reduce environmental impacts and avoid secondary precipitation. This presents an interesting challenge to conducting field experiments, as the dilution of alkalinity and ultimately CO_2 signal will make MRV more challenging (Ho et al., 2023, this Guide).

Seawater carbonate chemistry measurements will be central to most sampling schemes. To cover the appropriate spatial and temporal scales, traditional bottle sampling will likely have to be combined with state-of-the-art in situ sensors (Bushinsky et al., 2019; Briggs et al., 2020; Ho et al., 2023, this Guide). Bushinsky et al. (2019; their Fig. 1) provide a comprehensive overview of the spatiotemporal capabilities of existing carbonate chemistry sensors and platforms, and care should be taken to make sure sensors are appropriate for measurements in seawater. The appropriate methods and protocols for sampling and analysis are outlined in other chapters in this guide (Schulz et al., 2023, this Guide) and in the Guide to Best Practices (Dickson et al., 2007). Some general considerations for field experiments include appropriately characterizing the natural variability that occurs at the field site through space and time. While total alkalinity (TA) titrations should remain a priority, at least two carbonate chemistry parameters (e.g., total alkalinity, dissolved inorganic carbon, pH, or pCO_2) should be measured for each sample. It is important to note that the combination of pCO_2 and pH is not ideal when calculating CO_2 chemistry (e.g., using CO2SYS) due to the elevated errors when combining those parameters in determining the rest of the carbonate chemistry system in seawater (Lee and Millero, 1995). Currently, commercially available autonomous sensors exist for pH and pCO_2, with sensors in development for both TA and dissolve inorganic carbon (DIC; Fassbender et al., 2015; Briggs et al., 2020; Qiu et al., 2023). While autonomous sensors generally have greater uncertainty than bottle samples coupled with laboratory analysis, they will likely play an important role in sampling schemes to help cover adequate spa-

Table 2. Parameters that could be considered in assessing sites for OAE field experiments. Importantly, some parameters summarized below may require a baseline assessment over sufficiently long time frames to cover the intrinsic variability of physical, chemical, and biological parameters in the studied system. For example, baseline assessment of marine food web structure will likely require a prolonged monitoring effort before (and after) the OAE deployment to have a higher chance of detecting OAE-induced effects on marine biota.

Parameter	Rationale	Potential pathway for assessment
Dilution rate	– Exposure risk to alkalinity and mineral dissolution products. – Detectability of OAE-induced chemical changes.	Tracer release experiment (Sect. 2.5).
Turbulence	– Physical energy input to keep ground particles near the sea surface during dissolution.	Microstructure profiler.
Residence time of perturbed patch in surface ocean	– Determination of residence time of an OAE-perturbed patch in the surface to assess whether there is enough time for air–sea equilibration with the atmosphere.	Risk assessment for incomplete air–sea CO_2 exchange (He and Tyka, 2023; Bach et al., 2023).
Transboundary transport	– Determination of whether there is a high risk for OAE-derived chemicals to be transported into sensitive areas (e.g., marine protected areas, other state territories) in high concentrations. May be useful for residence time as well.	– Tracer release experiment – Virtual Lagrangian particle tracking. – Utilizing natural tracers observable via remote sensing (e.g., CDOM (colored dissolved organic matter) or gelbstoff). – Mixed layer depth.
Light penetration	– Determination of light environment to assess to what extent the addition of particulate alkalinity source could impact turbidity.	Light loggers, turbidity, CTD (conductivity, temperature, and depth) casts.
Carbonate chemistry conditions	– Baseline of mean conditions and variability to assess how much change OAE must induce to become detectable. – Determination if OAE-related changes are likely to affect marine organisms.	Dickson et al. (2007) and ocean acidification literature. Schulz et al., (2023, this Guide)
Macronutrients	– Assessment of whether the designated system is prone to macronutrient fertilization via OAE. (Note that not all OAE approaches would introduce macronutrients into the ocean system.)	Standard photometric approaches (Hansen and Koroleff, 1999). Experimental assessment of limiting elements.
Micronutrients	– Assessment of whether the designated system is prone to micronutrient fertilization via OAE. (Note that not all OAE approaches would introduce micronutrients into the ocean system.)	GEOTRACES cookbook (https://www.geotraces.org/methods-cookbook/, last access: 9 November 2023) Experimental assessment of limiting elements.
Marine food web structure	– Assessment of the planktonic and/or benthic food web structure prior to testing an OAE deployment.	There is a whole range of surveying tools that could be applied depending on the size and abundance of organisms. Applied methods could range from OMICS (including eDNA) to optical observations, acoustics, and flow cytometry.
Risk of damaging organisms by adding ground minerals	– Providing knowledge of whether organisms could be physically harmed, for example, through covering them with mineral powder.	Same range of methods as for the food web assessment.
Endangered species	– Clarification if endangered species could be present at the designated field site.	Same range of methods as for the food web assessment. Plane or drone surveys can help to confirm sightings of larger organisms and there may be online resources to be utilized (e.g., WhaleMap). Furthermore, local knowledge should be sought after from the diverse range of stakeholder groups, for example, consultation with indigenous communities, fishermen, local authorities, and environmental agencies.
Foraging/breeding ground	– Clarification if the designated field site is an important breeding/foraging area for migratory organisms.	Same range as for endangered species assessments.

Physics

- What are the expected dilution rates of the added alkalinity?
- What is the site turbulence, and how will this impact alkalinity additions (e.g., keeping particles in suspension)?
- What is the natural light penetration, and what impacts could increases in turbidity have on this?
- What is the residence time of water in the surface ocean or mixed layer, and how does this relate to the estimated air-sea equilibration time?
- What is driving air-sea gas exchange?
- Will changes in turbidity impact the albedo of the experimental site?
- What is the potential for the lateral export and exchange of alkalinity and other materials?
- Is there the potential for physical disturbance (e.g., impacts of alkalinity additions on physical water mass parameters such as density or the physical impacts of adding undissolved minerals to the benthos)?
- Where will the alkalinity signal be most observable (e.g., pore water vs. water column)?

Chemistry

- What are the natural carbonate chemistry conditions?
- What modes of variability (e.g., daily, seasonal, interannual) impact seawater chemistry?
- How will variations in seawater chemistry impact signal to noise?
- How will seawater chemistry impact mineral dissolution rates?
- Is there potential to disturb the natural concentrations of macro- or micronutrients or toxic metals through dissolution by-products?
- How do anthropogenic sources of alkalinity interact with (and potentially modify) natural sources and sinks of alkalinity?

Biology

- What organisms (benthic and pelagic) are present in the study area, and what are their relative sensitivities to fluctuations in seawater carbonate chemistry (if known)?
- Are there culturally or commercially important species present?
- Are there endangered or rare species present? Is the site a nursery and/or nesting ground? Are there keystone species and/or important primary producers present? These considerations will likely be part of the permitting process.
- Are there times of the day or seasons with elevated species or ecosystem sensitivities?
- What are the trophic dynamics in the environment, and how might the food web be impacted (e.g., shifts in predator–prey relationships)? What are the cascading implications for the ecosystem as a whole? Might effects be transferred beyond the study site via migratory species?
- Could particulates (e.g., ground rock) cause physical damage prior to dissolution?

Box 1. Scientific considerations for field experiments.

tial and temporal resolution in naturally variable marine systems.

While monitoring the background variability and subsequent additions of alkalinity will be critical, scientists may also wish to directly measure fluxes of carbon at the field study site (Ho et al., 2023, this Guide). The direct measurement of carbon fluxes can be accomplished via different methods including benthic and floating chambers, eddy covariance and other benthic boundary layer techniques, and mass balances. These techniques have benefits and drawbacks, including having to enclose the natural system (e.g., chambers) and elevated uncertainty that could be outside of the expected changes due to the perturbation (e.g., eddy covariance). Benthic chamber measurements may be particularly important to quantify the dissolution of minerals and rocks added to sediments. Ultimately, any measurements of fluxes due to OAE activities will likely need to be coupled with numerical modeling to estimate the overall drawdown of atmospheric CO_2 (Fennel et al., 2023, this Guide).

Field experiments should be informed by other scientific studies as much as possible (e.g., studies based on laboratory experiments, mesocosm studies, natural analogs, and numerical modeling). While not necessarily directly translatable to natural systems (Edmunds et al., 2016; Page et al., 2022), these types of studies can provide first-order assessments on safety and efficacy, helping to prevent unintended harmful ecological side effects when conducting large-scale perturbations.

Other measurements that may be useful during OAE field experiments are outlined in Table 2. It is important to note that this list is not meant to be exhaustive, and measurement selection will have to be made on a case-by-case basis. Con-

sidering the difficulties of tracking water masses in an open system, the next section is a more detailed discussion on tracers for monitoring mixing and dilution of water within the OAE field experiment site. Tracking added alkalinity will be critical to determine the impacts and efficacy of alkalinity enrichments and may be one of the biggest challenges facing OAE field experiments.

2.5 Dual-tracer regression technique

If the goal is to track alkalinity additions and measure their effects on carbon fluxes (i.e., net ecosystem production or air–sea exchange), a dual-tracer regression method can be used (e.g., Albright et al., 2016, 2018). This approach uses the change in ratios between an active tracer (alkalinity) and a passive tracer (dye, artificial gas tracer; Table 3) to assess the fraction of added alkalinity taken up or released by biogeochemical processes in the system. Passive tracers do not affect fluid dynamics and are passively advected by the surrounding flow field. The use of passive tracers, such as dye tracers (e.g., rhodamine, fluorescein) or artificial gas tracers (e.g., SF6, CF3SF5), that do not occur in nature helps eliminate background noise. Additional considerations include how many tracers to use and what information each tracer provides (Table 3).

During a dual-tracer experiment, changes in the active tracer (alkalinity) result from mixing, dilution, and biogeochemical activity, whereas changes in the passive tracer are due solely to mixing and dilution. By comparing the alkalinity-to-dye ratios before (e.g., upstream) and after (e.g., downstream) the water mass interacts with a study area, it is possible to isolate the change in alkalinity that is due to biogeochemical processes such as calcium carbonate precipitation and dissolution (Figs. 1 and 2). This technique is an extension of Friedlander et al. (1986) and may have applications in other areas of research pertinent to marine CDR, such as nutrient or pollution assessments and the uptake of industrial or agricultural waste. The primary experimental criteria for the dual-tracer technique are that the active and passive tracers are added in a fixed ratio and at a fixed rate, in areas where there is a dominant flow direction, dispersion, or dilution.

2.6 Detecting change and the importance of controlled experiments

Separating an experimental "signal" from the background "noise" inherent in natural systems can be challenging, especially in field experiments where replication may not be practical (Carpenter, 1990). Gaining baseline knowledge on the physical, chemical, and biological components of the study site should be a priority. There is often considerable natural variability in marine systems, and especially in coastal systems, due to fluctuations in biological activity, hydrodynamics, seasonal and/or interannual influences, and other factors (Bates et al., 1998; Bates, 2002; Hagens and Middelburg, 2016; Landschützer et al., 2018; Sutton et al., 2019; Kapsenberg and Cyronak, 2019; Torres et al., 2021). Fully characterizing this variability could take many years, which may create significant barriers to experimental progress in the field. Therefore, we recommend that any potential modes of spatiotemporal variability be recognized and evaluated while planning field experiments. For instance, in coastal systems with river and groundwater inputs, it will be important to know the impact that freshwater has on carbonate chemistry.

Where possible, conducting controlled experiments will help to maximize the ratio of signal to noise, thereby improving statistical power to detect experimental effects. The pros and cons of replicating experimental controls in space versus time should be taken into consideration. For many field experiments (and natural analogs; see Subhas et al., 2023, this Guide), sample size will be inherently limited (e.g., one, or few study sites); therefore, conducting controls in time (e.g., every third day) may be the best option. For studies with limited (or no) replication, there are statistical methods that can be used to isolate effects pre- and post-treatment (Carpenter, 1990). Numerical simulations and machine-learning-based network design are potentially valuable tools to optimize observational networks to detect experimental change.

3 Additional considerations

Permitting. Addressing regulatory requirements is critical prior to conducting field experiments. The spatial and temporal scale of the field trial, as well as the specific considerations of the deployment site (e.g., protection status), will determine permitting requirements. Engaging with this process early is advised – for example, understanding who the permit-granting authorities are for a given area and timelines for associated regulatory processes. In some cases, the use of existing infrastructure (e.g., wastewater discharge sites) and environmental projects (e.g., beach renourishment) may offer ways to streamline experiments, although permitting will be governed by existing regulations. For a detailed discussion on legal considerations, see Steenkamp and Webb (2023, this Guide).

Community engagement and social considerations of field experiments. The likelihood of harmful ecological consequences from OAE field experiments remains unclear and will ultimately depend on the technology and temporal and spatial scale of the experiment. Field experiments evaluating CDR approaches carry the risk of unintended consequences and impacts over large spatial scales, so appropriate scaling (e.g., starting small) is necessary (NASEM, 2022). In response to these unknowns, researchers should follow the key components for a code of conduct for marine CDR research, e.g., as outlined by Loomis et al. (2022), which details best practices that encourage responsible research amongst both the public and private sectors.

Table 3. Passive tracers that are available and commonly used for use in field experiments and considerations for each. Additional tracers may be useful that are not listed in this table, including helium 3 and tritium.

Tracer	Type	Pros	Limitations	Lifespan
Rhodamine	Fluorescent dye	Sensor-based, high-frequency (> 4 Hz) detection, platform flexibility, detection from space and/or the sky for surface releases.	Optically degrades and absorbs to particles, not good for longer-term studies, not as good signal to noise/detection limits as inert gas tracers.	Several days to weeks
Fluorescein	Fluorescent dye	Sensor-based, high-frequency (> 4 Hz) detection, platform flexibility, detection from space and/or the sky for surface releases.	Degrades optically – not good for longer-term studies (> 24 h).	< 24 h
SF6	Artificial gas	Inert; capable of being measured at very low concentrations; able to quantify mixing and residence time; good for large-scale ocean tracer release experiments.	Lower-frequency detection and less flexibility with platforms, requires discrete measurement. High global warming potential.	years
Trifluoromethyl sulfur pentafluoride (CF_3SF_5)	Artificial gas	Good for large-scale ocean experiments.	Difficult to obtain, lower-frequency detection and less flexibility with autonomous platforms, requires discrete measurement. High global warming potential.	years

Figure 1. Rhodamine dye flowing over a coral reef flat study site during a study in One Tree Island, Australia (Albright et al., 2016). NaOH was used as an active tracer to raise alkalinity, and rhodamine was used as a passive tracer to account for mixing and dilution. Changes in the alkalinity-to-dye ratios were used to isolate the change in alkalinity flux that was associated with an increase in net community calcification on the reef flat.

Social license to operate is critical for the success of CDR projects, and researchers have an obligation to involve the full community of people (public and stakeholders) who may be impacted by the research (Nawaz et al., 2023; Cooley et al., 2023). Therefore, public outreach is important both before and during field experimentation. The study site will determine the potential for community engagement. Coordinating with local and/or regional organizations who are connected to relevant stakeholders (for example, your local Sea-Grant office if in the United States) will be helpful. For additional discussion on social considerations of OAE field trials, see Satterfield et al. (2023, this Guide).

Collaboration and data/information sharing. Considering the inherent challenges to OAE field experiments (cost,

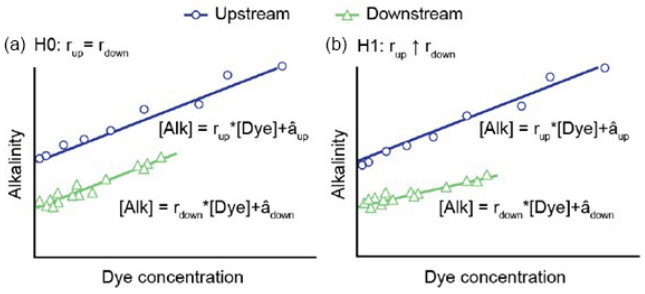

Figure 2. Theoretical representations of the null (H0) and alternative (H1) hypotheses for a dual-tracer regression experiment where NaOH was used as a source of alkalinity and rhodamine dye was used as a passive tracer (from Albright et al., 2016). **(a)** In H0, the benthic community does not take up added alkalinity. Here, the change in alkalinity between the upstream and downstream transects would not be systematically related to the dye concentration, and the ratio of the alkalinity–dye relationship, r, would not be expected to change between the upstream and downstream locations (that is, $r_{up} = r_{down}$). **(b)** In H1, an uptake of added alkalinity occurs by the benthic community. Here, areas with more alkalinity (and more dye) change at a different rate than areas with less alkalinity (and less dye), resulting in a change in the alkalinity–dye slope (that is, $r_{up} > r_{down}$).

permitting, access, logistics, environmental safety), fostering interdisciplinary and collaborative teams will help ensure the greatest return on investment. Examples of ways to foster collaboration include developing test-bed field sites that are open to participation from diverse stakeholder groups (https://oceanvisions.org/highlevelroadmap/, last access: 14 November 2023), making efforts to include groups who may not traditionally have access to and/or the capacity for field campaigns, and including travel support in grant applications to support external collaborators. Making concerted efforts to share information, resources, and ideas will allow researchers to combine knowledge and resources in ways that might not have been possible when working alone, thereby advancing OAE technology and science at a faster pace. When publishing in peer-reviewed literature, uploading data to publicly available data repositories and publishing in open-access journals following best practices should be prioritized (Jiang et al., 2023, this Guide).

Inclusivity and transparency during OAE field trials are crucial to ensure that knowledge gained is fed back into scientific and other communities efficiently, iteratively informing and refining the next generation of experiments. Some field experiments will mimic plans for real-world OAE deployments and should therefore be done in collaboration with relevant stakeholders across science, industry, policy, and communities. To foster collaboration and technology transfer, we advocate for a centralized platform and/or organization to share data and information in this rapidly evolving field. This might look like a centralized, freely accessible platform for early and/or "real-time" information sharing (i.e., before publication) that can facilitate faster information exchange within the research community (e.g., data sharing, permitting issues). Two existing options that could help fill this gap are the Ocean Acidification Information Exchange (https://www.oainfoexchange.org/index.html, last access: 11 November 2023) and the Ocean Visions community (https://community.oceanvisions.org/dashboard, last access: 11 November 2023). It may prove useful to designate core working groups of experts in various aspects of CDR that investigate specific needs and priorities and work to synthesize and share existing knowledge in the context of field experiments. This approach has been adopted by other scientific disciplines in high-priority, rapidly evolving, and highly collaborative fields, greatly benefiting the scientific community at large (e.g., the Coral Restoration Consortium, https://www.crc.world/, last access: 11 November 2023 – and associated working groups). Coordinating field trials with research groups conducting laboratory and mesocosm experiments, studying natural analogs, and undertaking modeling efforts will help strengthen the interpretation and extrapolation of results.

4 Conclusion and recommendations

Given that few OAE field studies have been conducted to date, there is much to learn from the earliest experiments with respect to experimental design, measurement and monitoring, deployment considerations, environmental impact, and more. Early experiments will only engage with a fraction of the temporal and spatial scales involved in full-scale operational OAE, and longer-term and larger-scale studies will become increasingly important to reveal scale dependencies as the field develops. It is important that marine CDR research is hypothesis-driven, structured, deliberate, and well-planned to best inform future decision-making about OAE techniques and deployments. Careful consideration of the physical, chemical, and biological components of the study area will help inform the experimental approach. The use of baseline studies (both previous and contemporary to the OAE deployment) and controls will help to maximize signal-to-noise ratios and identify experimental effects. The timescale of OAE field experiments should not be underestimated, especially when considering permitting, and the data needed to capture the baseline variability in natural systems.

Considering the urgent timeline required for humanity to meet our climate goals, field experiments need to move forward swiftly yet deliberately. To ensure the success of OAE, diverse perspectives from research, industry, policy, and society must converge, demanding transdisciplinary thinking and a commitment to open and transparent science. Central to this ambitious undertaking are the early field experiments, results from which will ultimately determine the successes and failures of OAE projects and technologies.

Key recommendations

1. Ensure inclusivity and transparency (community engagement, data sharing, etc.) for OAE field experiments to both advance the field as quickly as possible and ensure the field progresses in a socially responsible manner.
2. Assess the potential risks and benefits for any perturbation. Proceed according to a code of conduct and precautionary principles.
3. Develop methods to track signal versus noise in highly variable environments, including robust baseline studies to characterize underlying variability (biological, chemical, physical), and include controlled experiments such as chamber incubations to isolate treatment effects.
4. Consider the logistical constraints and opportunities of field locations.
5. Create test-bed field sites that are open to participation from diverse stakeholder groups.

Data availability. No data sets were used in this article.

Author contributions. TC, RA, and LTB all contributed to the conceptualization and writing of this paper.

Competing interests. Competing interests are declared in a summary for the entire volume at: https://sp.copernicus.org/articles/sp-oae2023-ci-summary.zip.

Disclaimer. Publisher's note: Copernicus Publications remains neutral with regard to jurisdictional claims made in the text, published maps, institutional affiliations, or any other geographical representation in this paper. While Copernicus Publications makes every effort to include appropriate place names, the final responsibility lies with the authors.

Acknowledgements. We thank the Ocean Acidification and other ocean Changes – Impacts and Solutions (OACIS), an initiative of the Prince Albert II of Monaco Foundation, for its support throughout the project. We extend our gratitude to the Villefranche Oceanographic Laboratory for supporting the meeting of the lead authors in January 2023. Tyler Cyronak was supported by the Tides Foundation through a Google Carbon Removal Research Award. Lennart T. Bach was supported by the Australian Research Council through Future Fellowship (FT200100846) and by the Carbon-to-Sea Initiative.

Financial support. This research has been supported by the ClimateWorks Foundation (grant no. 22-0296) and the Prince Albert II of Monaco Foundation. It has also been supported by the Tides Foundation through a Google Carbon Removal Research Award, the Australian Research Council through Future Fellowship (grant no. FT200100846), and the Carbon-to-Sea Initiative.

Review statement. This paper was edited by Romany Webb and reviewed by Will Burt, Lester Kwiatkowski, M. Grace Andrews, and Alex Poulton.

References

Albright, R., Caldeira, L., Hosfelt, J., Kwiatkowski, L., Maclaren, J. K., Mason, B. M., Nebuchina, Y., Ninokawa, A., Pongratz, J., Ricke, K. L., Rivlin, T., Schneider, K., Sesboue, M., Shamberger, K., Silverman, J., Wolfe, K., Zhu, K., and Caldeira, K.: Reversal of ocean acidification enhances net coral reef calcification, Nature, 531, 362–365, 2016.

Albright, R., Takeshita, Y., Koweek, D. A., Ninokawa, A., Wolfe, K., Rivlin, T., Nebuchina, Y., Young, J., and Caldeira, K.: Carbon dioxide addition to coral reef waters suppresses net community calcification, Nature, 555, 516–519, 2018.

Bach, L. T., Gill, S. J., Rickaby, R. E., Gore, S., and Renforth, P.: CO_2 removal with enhanced weathering and ocean alkalinity enhancement: potential risks and co-benefits for marine pelagic ecosystems, Frontiers in Climate, 1, 7, https://doi.org/10.3389/fclim.2019.00007, 2019.

Bach, L. T., Ho, D. T., Boyd, P. W., and Tyka, M. D.: Toward a consensus framework to evaluate air–sea CO_2 equilibration for marine CO_2 removal, Limnol. Oceanogr. Lett., 8, 685–691, https://doi.org/10.1002/lol2.10330, 2023.

Bates, N. R.: Seasonal variability of the effect of coral reefs on seawater CO_2 and air–sea CO_2 exchange, Limnol. Oceanogr., 47, 43–52, 2002.

Bates, N. R., Takahashi, T., Chipman, D. W., and Knap, A. H.: Variability of pCO_2 on diel to seasonal timescales in the Sargasso Sea near Bermuda, J. Geophys. Res.-Oceans, 103, 15567–15585, 1998.

Briggs, E. M., De Carlo, E. H., Sabine, C. L., Howins, N. M., and Martz, T. R.: Autonomous ion-sensitive field effect transistor-based total alkalinity and pH measurements on a barrier reef of Kane'ohe Bay, ACS Earth and Space Chemistry, 4, 355–362, 2020.

Bushinsky, S. M., Takeshita, Y., and Williams, N. L.: Observing changes in ocean carbonate chemistry: our autonomous future, Current Climate Change Reports, 5, 207–220, 2019.

Carpenter, S. R.: Large-scale perturbations: opportunities for innovation, Ecology, 71, 2038–2043, 1990.

Cooley, S. R., Klinsky, S., Morrow, D. R., and Satterfield, T.: Sociotechnical considerations about ocean carbon dioxide removal, Annu. Rev. Mar. Sci., 15, 41–66, 2023.

Dickson, A. G., Sabine, C. L., and Christian, J. R. (Eds.): Guide to best practices for ocean CO_2 measurements, North Pacific Marine Science Organization, Sidney, British Columbia, PICES Special Publication 3, 191 pp., https://doi.org/10.25607/OBP-1342, 2007.

Edmunds, P. J., Comeau, S., Lantz, C., Andersson, A., Briggs, C., Cohen, A., Gattuso, J.-P., Grady, J. M., Gross, K., Johnson, M.,

Muller, E. B., Ries, J. B., Tambutte, S., Tambutte, E., Venn, A., and Carpenter, R. C.: Integrating the effects of ocean acidification across functional scales on tropical coral reefs, Bioscience, 66, 350–362, 2016.

Egleston, E. S., Sabine, C. L., and Morel, F. M. M.: Revelle revisited: Buffer factors that quantify the response of ocean chemistry to changes in DIC and alkalinity, Global Biogeochem. Cy., 24, GB1002, https://doi.org/10.1029/2008GB003407, 2010.

Eisaman, M. D., Geilert, S., Renforth, P., Bastianini, L., Campbell, J., Dale, A. W., Foteinis, S., Grasse, P., Hawrot, O., Löscher, C. R., Rau, G. H., and Rønning, J.: Assessing the technical aspects of ocean-alkalinity-enhancement approaches, in: Guide to Best Practices in Ocean Alkalinity Enhancement Research, edited by: Oschlies, A., Stevenson, A., Bach, L. T., Fennel, K., Rickaby, R. E. M., Satterfield, T., Webb, R., and Gattuso, J.-P., Copernicus Publications, State Planet, 2-oae2023, 3, https://doi.org/10.5194/sp-2-oae2023-3-2023, 2023.

Fakhraee, M., Li, Z., Planavsky, N. J., and Reinhard, C. T.: A biogeochemical model of mineral-based ocean alkalinity enhancement: impacts on the biological pump and ocean carbon uptake, Environ. Res. Lett., 18, 044047, https://doi.org/10.1088/1748-9326/acc9d4, 2023.

Fassbender, A. J., Sabine, C. L., Lawrence-Slavas, N., De Carlo, E. H., Meinig, C., and Maenner Jones, S.: Robust sensor for extended autonomous measurements of surface ocean dissolved inorganic carbon, Environ. Sci. Technol., 49, 3628–3635, 2015.

Fennel, K., Long, M. C., Algar, C., Carter, B., Keller, D., Laurent, A., Mattern, J. P., Musgrave, R., Oschlies, A., Ostiguy, J., Palter, J. B., and Whitt, D. B.: Modelling considerations for research on ocean alkalinity enhancement (OAE), in: Guide to Best Practices in Ocean Alkalinity Enhancement Research, edited by: Oschlies, A., Stevenson, A., Bach, L. T., Fennel, K., Rickaby, R. E. M., Satterfield, T., Webb, R., and Gattuso, J.-P., Copernicus Publications, State Planet, 2-oae2023, 9, https://doi.org/10.5194/sp-2-oae2023-9-2023, 2023.

Flipkens, G., Fuhr, M., Fiers, G., Meysman, F. J. R., Town, R. M., and Blust, R.: Enhanced olivine dissolution in seawater through continuous grain collisions, Geochim. Cosmochim. Ac., 359, 84–99, 2023.

Foteinis, S., Campbell, J. S., and Renforth P.: Life Cycle Assessment of Coastal Enhanced Weathering for Carbon Dioxide Removal from Air, Environ. Sci. Technol., 57, 6169–6178, 2023.

Friedlander, S. K., Turner, J. R., and Hering, S. V.: A new method for estimating dry deposition velocities for atmospheric aerosols, J. Aerosol Sci., 17, 240–244, 1986.

Fuhr, M., Geilert, S., Schmidt, M., Liebetrau, V., Vogt, C., Ledwig, B., and Wallmann, K.: Kinetics of Olivine Weathering in Seawater: An Experimental Study, Frontiers in Climate, 4, 831587, https://doi.org/10.3389/fclim.2022.831587, 2022.

Hagens, M. and Middelburg, J. J.: Attributing seasonal pH variability in surface ocean waters to governing factors, Geophys. Res. Lett., 43, 12528–12537, https://doi.org/10.1002/2016GL071719, 2016.

Hansen, H. P. and Koroleff, F.: Determination of nutrients, in: Methods of seawater analysis, edited by: Grasshoff, K., Kremling, K., and Ehrhardt, M., 159–228, https://doi.org/10.1002/9783527613984.ch10, 1999.

Hartmann, J., Suitner, N., Lim, C., Schneider, J., Marín-Samper, L., Arístegui, J., Renforth, P., Taucher, J., and Riebesell, U.: Stability of alkalinity in ocean alkalinity enhancement (OAE) approaches – consequences for durability of CO_2 storage, Biogeosciences, 20, 781–802, https://doi.org/10.5194/bg-20-781-2023, 2023.

Hauck, J., Köhler, P., Wolf-Gladrow, D., and Völker, C.: Iron fertilisation and century-scale effects of open ocean dissolution of olivine in a simulated CO_2 removal experiment, Environ. Res. Lett., 11, 024007, https://doi.org/10.1088/1748-9326/11/2/024007, 2016.

He, J. and Tyka, M. D.: Limits and CO_2 equilibration of near-coast alkalinity enhancement, Biogeosciences, 20, 27–43, https://doi.org/10.5194/bg-20-27-2023, 2023.

Ho, D. T., Bopp, L., Palter, J. B., Long, M. C., Boyd, P. W., Neukermans, G., and Bach, L. T.: Monitoring, reporting, and verification for ocean alkalinity enhancement, in: Guide to Best Practices in Ocean Alkalinity Enhancement Research, edited by: Oschlies, A., Stevenson, A., Bach, L. T., Fennel, K., Rickaby, R. E. M., Satterfield, T., Webb, R., and Gattuso, J.-P., Copernicus Publications, State Planet, 2-oae2023, 12, https://doi.org/10.5194/sp-2-oae2023-12-2023, 2023.

Jiang, L.-Q., Subhas, A. V., Basso, D., Fennel, K., and Gattuso, J.-P.: Data reporting and sharing for ocean alkalinity enhancement research, in: Guide to Best Practices in Ocean Alkalinity Enhancement Research, edited by: Oschlies, A., Stevenson, A., Bach, L. T., Fennel, K., Rickaby, R. E. M., Satterfield, T., Webb, R., and Gattuso, J.-P., Copernicus Publications, State Planet, 2-oae2023, 13, https://doi.org/10.5194/sp-2-oae2023-13-2023, 2023.

Kapsenberg, L. and Cyronak, T.: Ocean acidification refugia in variable environments, Glob. Change Biol., 25, 3201–3214, 2019.

Köhler, P., Abrams, J. F., Völker, C., Hauck, J., and Wolf-Gladrow, D. A.: Geoengineering impact of open ocean dissolution of olivine on atmospheric CO_2, surface ocean pH and marine biology, Environ. Res. Lett., 8, 014009, https://doi.org/10.1088/1748-9326/8/1/014009, 2013.

Landschützer, P., Gruber, N., Bakker, D. C. E., Stemmler, I., and Six, K. D.: Strengthening seasonal marine CO_2 variations due to increasing atmospheric CO_2, Nat. Clim. Change, 8, 146–150, 2018.

Lee, K. and Millero, F. J.: Thermodynamic studies of the carbonate system in seawater, Deep-Sea Res. Pt. I, 42, 2035–2061, 1995.

Loomis, R., Cooley, S. R., Collins, J. R., Engler, S., and Suatoni, L.: A Code of Conduct Is Imperative for Ocean Carbon Dioxide Removal Research, Frontiers in Marine Science, 9, 872800, https://doi.org/10.3389/fmars.2022.872800, 2022.

Montserrat, F., Renforth, P., Hartmann, J., Leermakers, M., Knops, P., and Meysman, F. J. R.: Olivine Dissolution in Seawater: Implications for CO_2 Sequestration through Enhanced Weathering in Coastal Environments, Environ. Sci. Technol., 51, 3960–3972, 2017.

Moras, C. A., Bach, L. T., Cyronak, T., Joannes-Boyau, R., and Schulz, K. G.: Ocean alkalinity enhancement – avoiding runaway $CaCO_3$ precipitation during quick and hydrated lime dissolution, Biogeosciences, 19, 3537–3557, https://doi.org/10.5194/bg-19-3537-2022, 2022.

Morse, J. W., Arvidson, R. S., and Lüttge, A.: Calcium carbonate formation and dissolution, Chem. Rev., 107, 342–381, 2007.

National Academies of Sciences, Engineering, and Medicine (NASEM): A Research Strategy for Ocean-based Carbon Diox-

ide Removal and Sequestration, The National Academies Press, Washington, DC, https://doi.org/10.17226/26278, 2022.

Nawaz, S., Peterson St-Laurent, G., and Satterfield, T.: Public evaluations of four approaches to ocean-based carbon dioxide removal, Clim. Policy, 23, 379–394, 2023.

Page, H. N., Bahr, K. D., Cyronak, T., Jewett, E. B., Johnson, M. D., and McCoy, S. J.: Responses of benthic calcifying algae to ocean acidification differ between laboratory and field settings, ICES J. Mar. Sci., 79, 1–11, 2022.

Qiu, L., Li, Q., Yuan, D., Chen, J., Xie, J., Jiang, K., Guo, L., Zhong, G., Yang, B., and Achterberg, E. P.: High-Precision In Situ Total Alkalinity Analyzer Capable of Month-Long Observations in Seawaters, ACS Sensors, 8, 2702–2712, 2023.

Renforth, P. and Henderson, G.: Assessing ocean alkalinity for carbon sequestration, Rev. Geophys., 55, 636–674, 2017.

Rimstidt, J. D., Brantley, S. L., and Olsen, A. A.: Systematic review of forsterite dissolution rate data, Geochim. Cosmochim. Ac., 99, 159–178, 2012.

Satterfield, T., Nawaz, S., and Boettcher, M.: Social considerations and best practices to apply to engaging publics on ocean alkalinity enhancement, in: Guide to Best Practices in Ocean Alkalinity Enhancement Research, edited by: Oschlies, A., Stevenson, A., Bach, L. T., Fennel, K., Rickaby, R. E. M., Satterfield, T., Webb, R., and Gattuso, J.-P., Copernicus Publications, State Planet, 2-oae2023, 11, https://doi.org/10.5194/sp-2-oae2023-11-2023, 2023.

Schulz, K. G., Bach, L. T., and Dickson, A. G.: Seawater carbonate chemistry considerations for ocean alkalinity enhancement research: theory, measurements, and calculations, in: Guide to Best Practices in Ocean Alkalinity Enhancement Research, edited by: Oschlies, A., Stevenson, A., Bach, L. T., Fennel, K., Rickaby, R. E. M., Satterfield, T., Webb, R., and Gattuso, J.-P., Copernicus Publications, State Planet, 2-oae2023, 2, https://doi.org/10.5194/sp-2-oae2023-2-2023, 2023.

Steenkamp, R. C. and Webb, R.: Legal considerations relevant to research on ocean alkalinity enhancement, in: Guide to Best Practices in Ocean Alkalinity Enhancement Research, edited by: Oschlies, A., Stevenson, A., Bach, L. T., Fennel, K., Rickaby, R. E. M., Satterfield, T., Webb, R., and Gattuso, J.-P., Copernicus Publications, State Planet, 2-oae2023, 10, https://doi.org/10.5194/sp-2-oae2023-10-2023, 2023.

Subhas, A. V., Lehmann, N., and Rickaby, R. E. M.: Natural analogs to ocean alkalinity enhancement, in: Guide to Best Practices in Ocean Alkalinity Enhancement Research, edited by: Oschlies, A., Stevenson, A., Bach, L. T., Fennel, K., Rickaby, R. E. M., Satterfield, T., Webb, R., and Gattuso, J.-P., Copernicus Publications, State Planet, 2-oae2023, 8, https://doi.org/10.5194/sp-2-oae2023-8-2023, 2023.

Sutton, A. J., Feely, R. A., Maenner-Jones, S., Musielwicz, S., Osborne, J., Dietrich, C., Monacci, N., Cross, J., Bott, R., Kozyr, A., Andersson, A. J., Bates, N. R., Cai, W.-J., Cronin, M. F., De Carlo, E. H., Hales, B., Howden, S. D., Lee, C. M., Manzello, D. P., McPhaden, M. J., Meléndez, M., Mickett, J. B., Newton, J. A., Noakes, S. E., Noh, J. H., Olafsdottir, S. R., Salisbury, J. E., Send, U., Trull, T. W., Vandemark, D. C., and Weller, R. A.: Autonomous seawater pCO_2 and pH time series from 40 surface buoys and the emergence of anthropogenic trends, Earth Syst. Sci. Data, 11, 421–439, https://doi.org/10.5194/essd-11-421-2019, 2019.

Torres, O., Kwiatkowski, L., Sutton, A. J., Dorey, N., and Orr, J. C.: Characterizing Mean and Extreme Diurnal Variability of Ocean CO_2 System Variables Across Marine Environments, Geophys. Res. Lett., 48, e2020GL090228, https://doi.org/10.1029/2020GL090228, 2021.